SYNOPTIC CLIMATOLOGY OF THE BEAUFORT SEA COAST OF ALASKA

By
Richard Edward Moritz

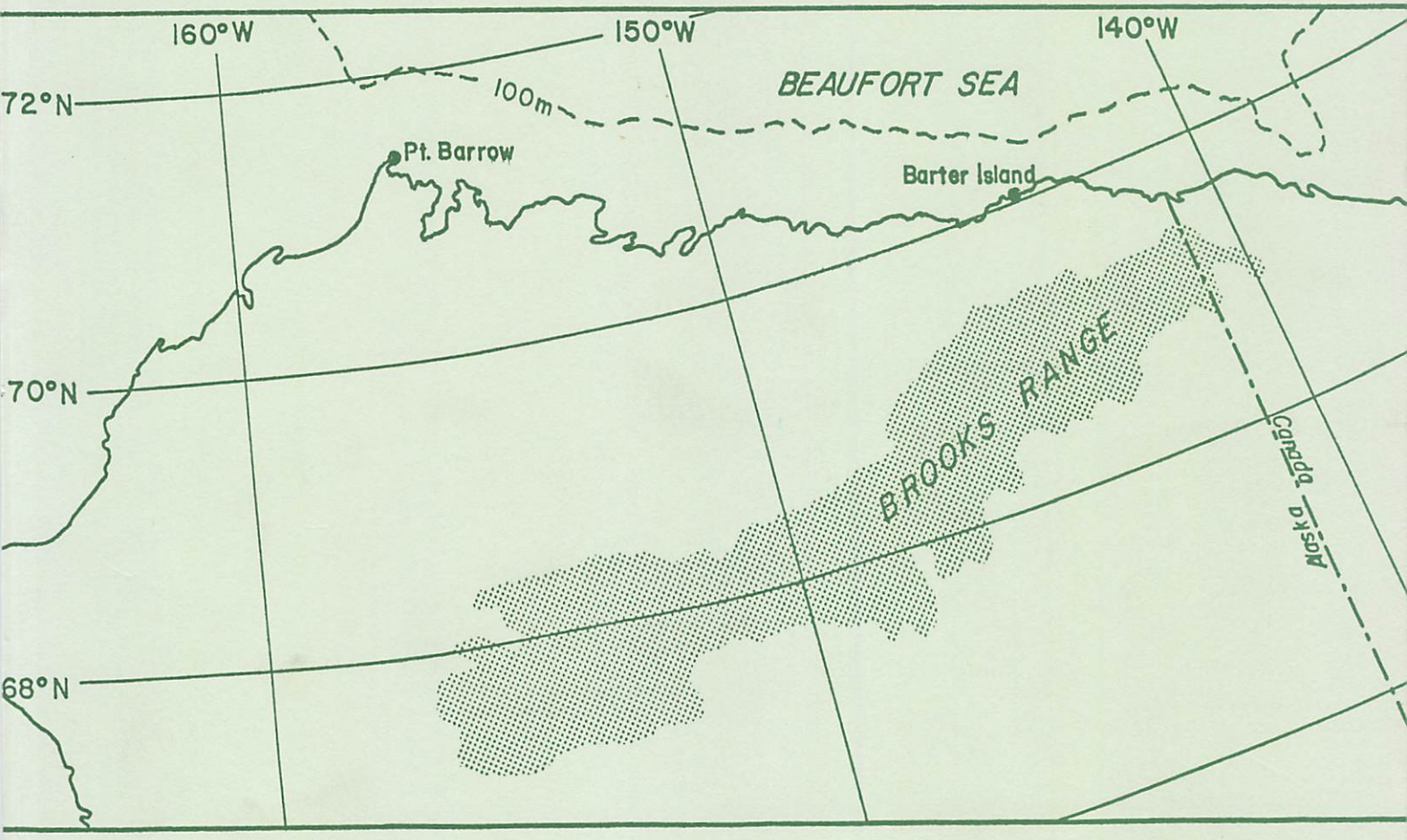

Occasional Paper No. 30
1979

INSTITUTE OF ARCTIC AND ALPINE RESEARCH • UNIVERSITY OF COLORADO

SYNOPTIC CLIMATOLOGY OF THE BEAUFORT SEA COAST OF ALASKA

by

Richard Edward Moritz

Institute of Arctic and Alpine Research
University of Colorado
Boulder, Colorado 80309

1979

University of Colorado
Institute of Arctic and Alpine Research

Occasional Paper 30

ISSN 0069-6145
INSTAAR/OP-30

TABLE OF CONTENTS

LIST OF FIGURES

FIGURE PAGE

FIGURE PAGE

LIST OF TABLES

PREFACE

Many researchers over the years have been interested in the relationships between atmospheric circulation patterns and local weather and climate. Numerous classifications of pressure pattern or airflow types have been formulated and catalogs of their daily occurrence prepared. Until recently, investigators had to use subjectively determined classification categories and the labor involved in preparing catalogs of synoptic types spanning several decades was considerable. Now several "objective" techniques exist which permit long series of such circulation statistics to be prepared rapidly. This study utilizes one of these techniques to classify circulation patterns over Alaska and adjacent ocean areas. The climatic characteristics of the circulation types are documented for stations on the Beaufort Sea coast of Alaska and the results are analyzed in terms of their meteorological reality, as well as statistically.

The study is part of a broader program relating to the effects of both the seasonal climatic regime and synoptic weather events on shorefast ice conditions along the Beaufort Sea coast. The specific climatic information will be of interest to many environmental scientists working on Alaskan problems, while the procedures employed by R.E. Moritz provide a proven systematic approach for application of synoptic-climatological methods in other regions.

Roger G. Barry

Professor of Geography

ACKNOWLEDGEMENTS

I acknowledge with pleasure the guidance and continuing interest of Prof. Roger G. Barry, who directed this research. The helpful comments and criticisms of Harry Van Loon and Dr. David Greenland are also much-appreciated. Dr. T. Nelson Caine provided valuable guidance in formulating statistical hypotheses and tests.

Special thanks go to Mrs. Margaret Eccles, who developed the basic computer programs for the synoptic pressure pattern catalog.

This work was supported by the Bureau of Land Management through interagency agreement with the National Oceanic and Atmospheric Administration, under which a multiyear program responding to needs of petroleum development on the Alaskan continental shelf is managed by the Outer Continental Shelf Environmental Assessment Program (OCSEAP) Office (Contract 03-5-022-91, RU 244, principal investigator: R.G. Barry).

CHAPTER ONE

INTRODUCTION

Requirement for the Study

The 1970's have witnessed sharp increases in man's interest in and awareness of the important role played by climate in shaping the global environment. A number of recent publications illustrate the urgency placed in gaining a better understanding of climate and its fluctuations by the community of atmospheric scientists (S.M.I.C., 1971; U.S. National Academy of Science, 1974; World Meteorological Organization, 1975). Arctic regions, in particular, are subject to relatively large amplitude fluctuations in climatic variables and are thus "sensitive climatic indicators" (Kellogg, 1975, p. v). Although Arctic climatology and meteorology have advanced greatly in the last 20 years (Hare, 1968), much remains to be learned about the interaction between atmospheric circulation systems and the observed surface weather data which form the basis for most climatological analyses.

Alaska's Beaufort Sea Coast is a rapidly developing Arctic frontier region, both in the conventional sense and from a climatological viewpoint. Isolated from mid-latitudes by mountain ranges and in proximity to the polar ice pack, the United States' only Arctic Basin coastline had traditionally occupied a central role in Arctic Research efforts (J. Reed, 1974). Furthermore, the relatively complete time series of weather data at two coastal stations, compiled during the last quarter-century of more reliable Arctic pressure analyses, make the region excellent for synoptic studies of cold climates. Recent economic developments, including oil strikes, pipeline construction and native land claim settlements highlight the practical needs for better knowledge of coastal weather and climate in the short term. Finally, the proposed lease of Beaufort Sea continetial shelf tracts for oil exploration and development in the next few years should be conducted with first-rate knowledge of extreme or hazardous weather conditions, their frequencies of occurrence and their immediate connections with atmospheric circulation systems.

A systematic study of regional weather and climate and their relationships to atmospheric circulation patterns can make a valuable and timely contribution to our knowledge of the Beaufort Sea coastal region. A synoptic climatological approach affords an opportunity to assess the statistical contributions of circulation pattern, persistence and seasonality to the observed time series of weather data. Durst (1951) stresses that climate is a statistical synthesis of daily weather. It follows that a greater understanding of the structure of regional climates can be obtained by investigating associations between daily weather conditions and concurrent circulation patterns over the region. The synoptic climatology can then be built from the statistics of these associations over a number of years. The application of this approach to an Arctic region is both challenging and problematic, because at times the influence of synoptic-scale circulation systems is masked by the snow, ice and temperature inversion conditions at the surface (Wilson, 1967).

To date, there have been several studies which treat aspects of Arctic weather and climate in general (Hare, 1968; Vowinckel and Orvig, 1970; and Bowling, 1975). However, studies of the Beaufort Sea coast region have been somewhat limited in scope. Climatic statistics for the two first order weather stations (Barrow and Barter Island, Alaska) have been compiled and reported (Watson, 1968). The general patterns of mean sea level (msl) pressure in a rather extensive region centered on Alaska have been subjectively identified and catalogged for the period January, 1945 to March, 1963 by Putnins (1966), although the catalog itself is not available. Means and ranges for weather elements at Barrow and Barter Island are stratified by month and pressure pattern type for this catalog in Putnins (1969), but no analyses or tests of significance accompany these raw statistics. A number of studies exist which cover some aspects of the Arctic pressure field and associated weather (Petterssen, 1950; Bodhurtha, 1952; Klein, 1957; Keegan, 1958; Reed and Kunkel, 1960; Wilson, 1967; Selkregg, 1974) but rigorous statistical assessments of pressure pattern-weather relationships are lacking. Case studies of temperature inversions (Bilello, 1966, Vowinckel and Orvig, 1967) and pressure systems associated with low temperature extrema over Alaska (Putnins, 1967) have been reported. Finally, Fahl (1974) presents mean pressure maps for cases of heavy snowfall and high summer temperatures on three of Alaska's glaciers. After examination of this literature, however, it is clear that several basic questions remain to be addressed:

1) What are the climatological regularities in pattern, strength and time evolution of the pressure field over and around Alaska's north coast?

2) To what extent can particular coastal weather characteristics be associated with these pressure patterns?

3) Does the time series of pressure patterns over the region contribute to the explanation and understanding of daily, seasonal and interannual fluctuations in the surface weather and climate?

Synoptic climatological methods can be applied to these questions. The techniques of synoptic climatology, while many and varied, generally address two basic classes of problem:

1) The identification and classification of the principal modes or patterns of regional atmospheric circulation;

2) Assessment of the weather characteristics which obtain over the region under each mode or pattern. (Barry and Perry, 1973, p. 7).

Although highly recommended (Godske, 1959), the decomposition of climatological series into respective compoents due to circulation type and other factors has seen very limited application (Barry and Perry, 1973, p. 290). Such analyses are, however, prerequisite for assessing the statistical significance of between-type weather differences. Thus a synoptic climatological approach allows us to study some basic methodological questions in the discipline, in addition to providing the framework for the regional study.

Statement of the Problem

In this study, daily (1200 GMT) surface pressure pattern in the sector 60° to 80° North latitude, 120° to 170° West longitude are represented as discrete spatial arrays and statistically compared, one with another, to identify characteristic patterns which tend to recur over the region through time. A daily catalog is developed, wherein each daily pattern for the period January, 1946 to August, 1974 is grouped with one or another charactierstic pattern. The grouping is based on the pattern identification process and a numerical index of pattern similarity. From daily sets of coastal meteorological data, the relationships between these pressure pattern groups and surface weather are examined to develop a synoptic climatology for the Beaufort Sea coast region. Conversely, the atmospheric pressure patterns associated with some given weather situations are examined to find recurring associations.

The objectives of this study are:

1) Determine the predominant spatial and temporal modes of the regional surface pressure field

2) Analyze and test the significance of relationships between pressure pattern groups and coastal weather and climate

3) Synthesize the pressure patterns, meteorological data and information from the literature to characterize the regional synoptic climatology.

Definitions and Units

Some inconsistency and overalp seem to exist regarding the meaning of such terms as "weather pattern" and "circulation pattern". In order to avoid ambiguity, pertinent terms are defined below as used in this study:

1) Pressure field--The continuous two-dimensional field of atmospheric pressure at mean sea level and at a given instant of time (1200 GMT in this case)

2) Pressure grid--The discrete representation of (1) in the study sector by a numerical value and unit at each of 36 approximately equidistant grid points, with magnitudes interpolated from standard synoptic pressure charts.

3) Pressure pattern--The shape and spatial configuration of the isobars in the study sector, including curvature, position of low and high pressure center, and direction of the geostrophic surface wind. The pressure field or quantitatively, with some loss of information, from the pressure grid.

4) Characteristic pressure pattern--A single daily pressure grid or pressure field which is taken to represent a large sample of daily grids or fields having similar isobaric configurations, based on standard tests for pattern similarity.

5) Weather element--A numerical value and a unit for a measurement on a meteorological variable at a given observing station.

6) Weather characteristic--A statistical parameter or frequency distribution derived from a time series of weather elements and attributed to some factor (e.g. the season or the characteristic pattern occurring on the days in the series).

The distinction made by the above definitions should be clear. We treat weather as the observed state of the atmosphere measured at a point, while pressure patterns are treated independently as spatial entities. That these two phenomena are, in fact, related is the central theme of synoptic climatology.

The Systeme International (e.g. Shortley and Williams, 1971, p. 9), also known as the mks (meter, kilogram, second) system is used for all physical quantities except two in this study. Temperature (T) is expressed in degrees Celsius (^{o}C) where:

$$(1) \qquad T(^{o}C) = T(K) - 273.15$$

and T(K) is the Kelvin temperature. Pressure is given in millibars (mb) such that:

$$(2) \qquad 1 \text{ mb} = 10^{2}\text{Pa}$$

and the Pascal (Pa) is equal to a force of one Newton acting on an area of one square meter.

Organization of the Presentation

As noted above, the classical problems in synoptic climatology are the determination of atmospheric circulation categories and the assessment of weather characteristics for each category. These problems are the foci of the present study, and the structure of the presentation reflects this approach.

Chapter 2 is devoted to pertinent background information for the study.

In Chapter Three a pressure pattern classification technique is described and applied to a thirty year record of data. The characteristic patterns which result are analyzed and their properties are discussed.

In Chapter Four the time series of daily, nominal pressure pattern types and related statistics are investigated to determine the seasonal nature of pressure pattern occurrence and preferred interdiurnal sequences of pressure pattern types. This information is synthesized with other published work to form a pressure pattern climatology for the Beaufort Sea coast region.

Chapter Five is concerned with the statistical analysis of coastal weather data, particularly insofar as their statistical properties can be attributed to the different characteristic pressure patterns. Analysis of variance and chi-squared tests are applied to weather data stratified by pressure pattern type and month to assess the statistical significance of between-pattern weather differences. For significant cases, the weather characteristics are quantified by measures of central tendency and variability for each characteristic pressure pattern group.

In Chapter Six the derived weather characteristics are discussed and the synoptic climatological interpretations are made. Possible physical mechanisms responsible for the (statistical) weather characteristics of the patterns are discussed. Relationships between the regional patterns and hemispheric circulation processes are also mentioned.

Chapter Seven concludes the thesis with a summary of results and recommendations for further study.

CHAPTER TWO

BACKGROUND

Introduction

This chapter covers a variety of topics which are considered to be relevant background material. The location and regional setting of Alaska's Beaufort Sea coast are briefly described, including certain aspects of the physical environment that may affect meteorological observations at coastal stations. The position of the coast relative to some major features of mean monthly 500 mb patterns is noted, and some characteristics of the atmospheric circulation over and around the region are summarized from existing literature. Finally, the station locations and climatic statistics for Barrow and Barter Island are briefly discussed.

Regional Setting

The Beaufort Sea coast of Alaska extends roughly east-west between Demarcation Point (69° 36' N, 141° W) and Point Barrow (71° 23' N, 156° 27' W) (Figure 1). The entire coast is poleward of the 69th aprallel and bounds uninterrupted Arctic Ocean, which stretches over the pole to Svalbard. Low-lying, level tundra, dotted with numerous shallow lakes, dominates the landscape on Alaska's north coastal plain. From the meteorological station in Barrow it is 145 kilometers south to the nearest elevation in excess of sixty meters and a full 300 kilometers to the foothills of the Brooks Range (about 600 meters high). This mountain chain arcs from southwest to northeast across northern Alaska and, coupled with the slight southeast to northwest trend of the coastline, becomes close enough to affect surface winds and vertical temperature stratification at Barter Island (Reeed, 1959; Dickey, 1961; Schwerdtfeger, 1964). Still, it is over 70 kilometers from Barter Island to the 600 meter elevation contour and, in many respects, ". . . the climate is determined by the surrounding open Arctic water surface", at least during summer (NOAA, 1975, p.1).

A shallow (less than 70 meters deep) continental shelf borders the coast, varying in seaward extent from 110 kilometers in the west to 55 kilometers in the east (Reimnitz and Barnes, 1974; Figure 1). Beyond the shelf break, the sea floor steepens, dropping rapidly to the 3000 meter depths of the Canadian Basin (Sater, 1969). The surface above this Arctic Ocean abyss supports a year-round canopy of thick, multi-year pack ice (Kovacs and Mellor, 1974). By contrast, the sea ice over the continental shelf is usually first year in age. Summer melting and offshore winds create an open waterway or shore lead along the coast for up to two months during favorable years (Figure 2). Mean July surface geostrophic winds trend offshore over much of the shelf (Sater, et al., 1974) but these authors note that the directional variability between years is also large. This variability, coupled with the proximity of the pack ice, means that sea ice can be driven shoreward over the shelf at any time (Kovacs and Mellor, 1974) but these authors note that the directional variability between years is also large. This variability, coupled with the proximity of the pack ice, means that sea ice can be driven shoreward over the shelf at any time (Kovacs and Mellor, 1974). Thus local coastal climates can be affected

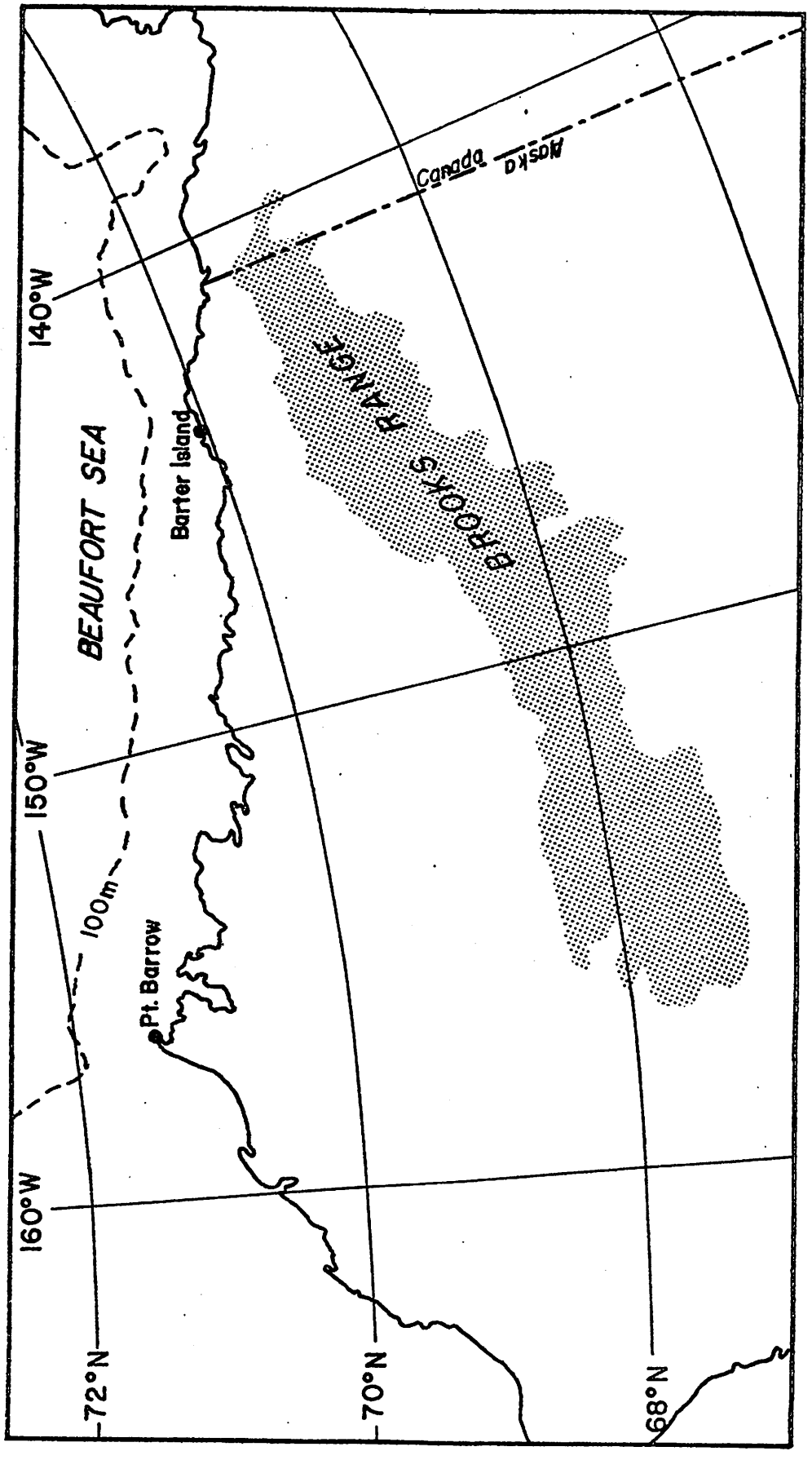

Figure 1: Regional Map of the Beaufort Sea Coast

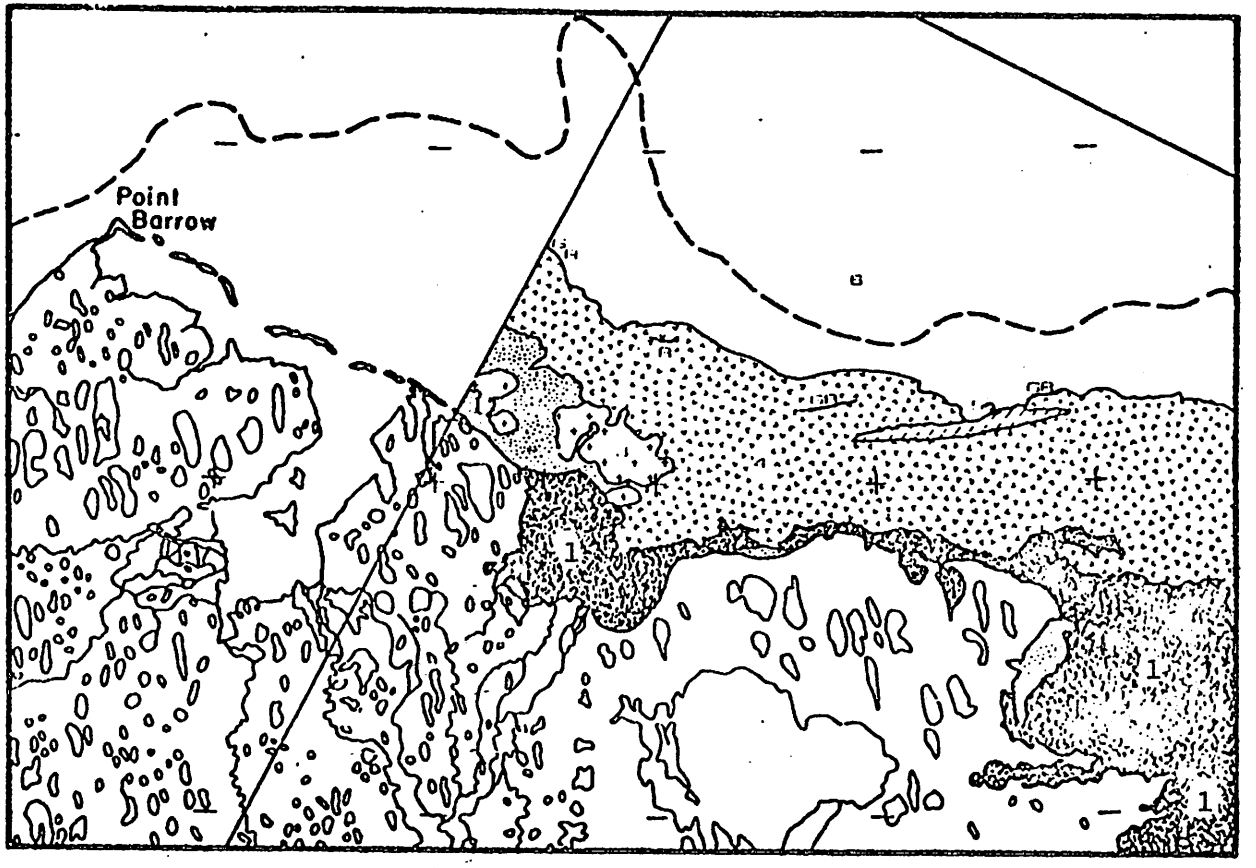

Figure 2: Coastal Ice Map from LANDSAT Scene 2558-21204, August 2, 1976 with Open Water designated as "1"

by either land or sea breezes in summer. The open water near shore is not necessarily at the freezing point, as evidenced by a 12°C water temperature measurement reported by Reimnitz and Barnes (1974) from the inner shelf. Thus northerly summer winds might be expected to bring a relatively cold surface (ice) close to shore in summer, as well ad advecting cooler air off the ocean. During the winter the terrain for tends to hundreds of kilometers in all directions from coastal points is essentially low-lying and snow covered (i.e, sea ice or tundra beneath snow). The state of the sea surface is important in this season also, however, because open leads act as strong local heat and moisture sources (Badgley, 1966; Weller, et al., 1972).

Over the tundra, a dramatic change in surface properties occurs each fall and spring when the snowpack forms and decays, respectively. Albedoes over tundra near Barrow average 0.84 during the snow-covered season, but drop to 0.18 during less than a week in June, on average (Maykut and Church, 1973). This transition occurs when incoming solar irradiance is at maximum near the solstice, so that the tundra is strongly heated during summer. By contrast, the ice at sea, and to a lesser degree on the lakes, persists for about a month after the tundra has cleared of snow, and is close to 0°C (Figure 3). This type of thermal contrast might be expected to set up a strong sea breeze (Walsh, 1977), and it is certain that the temperature conditions will vary strongly with wind direction. For example, Weaver (1970) reports average July, 1966 temperatures of 10.6°C and 2.7°C for winds off the tundra and ocean, respectively, near Barrow. During January, this same author reports a difference of only 1.6°C between such winds, indicating the thermal similarity of snow-covered tundra and sea ice.

Clearly both weather stations in Figure 1 must exhibit characteristics of continental and maritime Arctic climate (Maykut and Church, 1973). The relative importance of each type of influence will depend on the season, the state of the surface and the direction of local airflow. During some seasons the effects of the maountain barrier south of Barter Island must be considered when the observed weather conditions are at variance with the synoptic-scale patterns. All of these factors must be kept in mind when we seek to interpret the weather characteristics of each synoptic pressure pattern group.

Atmospheric Circulation Setting

Regional-scale atmospheric pressure systems which influence the weather at any observing station are vitally connected to the general circulation of the hemisphere and ultimately must be understood in this context. In order to set the stage for our regional analysis we briefly review some of the Northern Hemisphere climatic ciruclation patterns which appear in summer and winter. Also, a summary of studies concerned with the northern Alaska regional circulation is presented.

The primary feature of the free atmosphere in the Northern Hemisphere at all seasons is the circumpolar, westerly vortex (Hare, 1960). Average patterns of this vortex are well represented by the January and July mean 500 mb height contours (Figure 4). The mean "core of the vortex is a cold, nearly-barotropic air mass which overlies the Arctic and lacks organized westerly motions (Hare, 1968, p. 440). South of the core, the strengthening westerlies become highly

baroclinic and are the site of constant cyclonic activity. Synoptic-scale atmospheric motions are quasi-geostrophic in middle and high latitudes (Holton, 1972, p. 28) so that the westerly vortex in the mid-troposphere is a direct consequence of the meridional temperature gradient and the earth's rotation, via the thermal wind mechanism (Hare, 1960). When this temperature gradient decreases (on average) from winter to summer, the mean vortex contracts poleward and weakens, shifting the average baroclinic zones to the north (Palmén and Newton, 1969, p. 74). In both seasons the mean vortices are neither centered on the pole nor circular, but are deformed into eccentric, wave-like patterns which influence the generation and movement of surface pressure systems.

In January, there is a predominantly three-wave structure at high latitudes, with Arctic low centers and major troughs along 140° E and 80° W. A third, lesser trough extends equatorward over eastern Europe. These trough and ridge patterns exhibit preferred locations, even for mean monthly height fields averaged over several decades, which indicates geographical control by features of the earth's surface. Hydrodynamical effects of mountain barriers across the westerlies (Charney and Eliassen, 1949; Bolin, 1950) and thermal effects of ocean-continent distributions (Sutcliffe, 1951; Smagorinsky, 1953) both contribute to the maintenance of these wave patterns. The significance of these effects is that they are geographically stationary and they cooperate in maintaining the east-coast troughs in their climatological positions (Palmén and Newton, 1969, p. 70). Thirty-day mean January trough frequency charts, prepared from a 23-year record of daily 700 mb analyses, show strong frequency maxima which coincide rather well with the mean winter trough locations (Klein and Winston, 1953). This correspondence indicates that the mean winter troughs are persistent and quasi-stationary on a daily basis.

During July the mean 500 mb height gradients are weaker and the mean waves have lesser amplitude than in winter. Although the heating roles of oceans and continents are reversed from winter there is still an indication of mean 500 mb troughs east of Asia and North America, with a ridge over Alaska. These mean troughs also exhibit high daily frequencies in summer, but there are more individual trough and ridge frequency maxima around the hemisphere than in winter (Klein and Winston, 1958). Palmén and Newton (1969, p. 68) point out that the mean July 500 mb contours give the impression of a greater number of waves than the January contours, although the general westerly flow is weaker and the axis of maximum westerlies is shifted northward.

The significance of these hemispheric patterns for our regional study is simple: waves in the upper-troposheric westerlies are physically linked to the genesis and steering of surface cyclones and anticyclones (Bjerknes and Holmboe, 1944; Palmén, 1951; Holton, 1972, p. 116). Thus the nature of the recurring msl pressure patterns in a limited region (for example, Alaska) will be strongly dependent on the relative location of the mean waves. Figures 5 and 6 are two illustrative maps taken from Reed (1959) which emphasize some of these relationships over the Arctic region. The normal tracks of cyclones for the four seasons are shown in Figures 7 and 8 (from Klein, 1956). Inspection of these latter charts indicates that the January map is representative of September through February over our study region. April's chart represents March-April, June's map represents May-June, and the August tracks represent

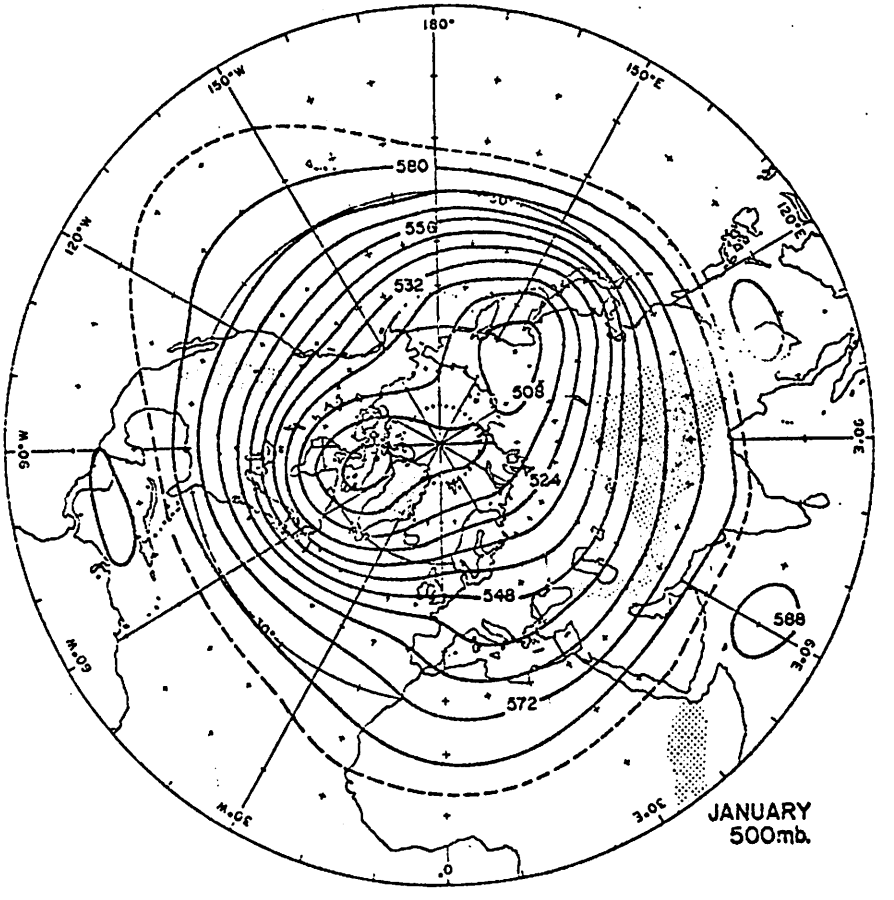

Figure 3: Mean January 500 mb Contours, 80 m interval.

(From: Palmen and Newton, 1969)

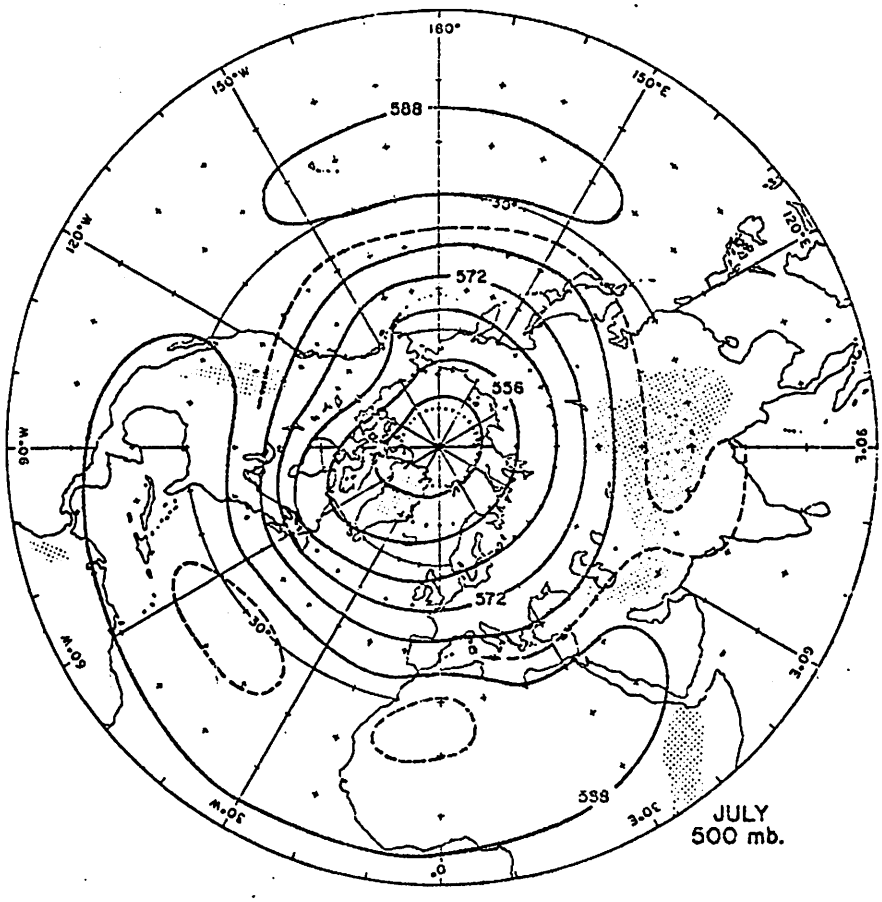

Figure 4: Mean July 500 mb Contours, 80 m interval.
(From: Palmen and Newton, 1969)

July-August situations. We do not imply that this grouping is representative for the Northern Hemisphere outside of the Alaska region. The outstanding feature of Figure 5 which influences Alaska is the pronounced 500 mb trough over Eastern Asia. Using the gradient wind force balance, Bjerknes (1937) showed that there is mid-tropospheric mass divergence downstream from such troughs. In a hydrostatic atmosphere, such divergence implies falling pressure at the surface. The western Pacific air beneath this downstream trough limb is highly baroclinic in winter because of thermal contrasts between the ocean currents and between the contenent and ocean in general. All of these factors favor frequent cyclone developments in the region. The individual short-wave perturbations in the 500 mb contours which are associated with each surface depression (called cyclone waves by Bjerknes, 1937) form on the downstream limb of the long-wave trough and are then steered, roughly speaking, along the large-scale flow by advection (Palmén and Newton, 1969, p. 151). The processes show up on Figure 5 where primary cyclone tracks (large arrows) extend northeastward into the Gulf of Alaska and a secondary track (thin arrow) brings storms along a Bering-Chukchi-Beaufort Sea trajectory. The Guft of Alaska cyclone terminis indicates the stagnation of lows in this region. Klein (1975) and Keegan (1958) attribute this stagnation to the influence of mountain ranges to the north of the Gulf, which mechanically impede the flow. By contrast, Reed (1959) emphasizes the blocking action of the frequent, strong anticyclones which cover northern Alaska during winter. In July (Figure 6) there is a broadly-similar situation, except that the East Asia trough has shifted eastward and, as noted above, the general amplitudes of the troughs and driges are smaller than in winter. Primary cyclone paths terminate in the southern Bering Sea and the Gulf of Alaska, and a secondary track still extends from the Bering Sea into the Beaufort Sea. All of these tracks are shifted somewhat eastward from winter with the mean waves at 500 mb. Cyclonic activity in the central Arctic Basin is more frequent north and west from Alaska, in connection with the Arctic Front baroclinic zone along northern Siberia's coast (Reed and Kunkel, 1960; Barry and Krebs, 1970). Seasonal shifts in these cyclone tracks are illustrated in Figures 7 and 8, where the bold arrows represent primary paths and the dashed arrows are secondary paths of cyclones. The secondary cyclone track from the Bering Sea to the Beaufort Sea does not last into April. Also, cyclones spiralling around the pole north of Alaska becomes less frequent from January to April. The gulf of Alaska remains a center of action during both months, however. One additional primary track appears in April which terminates in the southern Bering Sea. The spring months, then, represent a time of minimum cyclone influence over the central and northern parts of Alaska. This situation changes in May-June (Figure 8) when two additional secondary tracks bring Pacific cyclones over east central Alaska, and Siberian storms over the northern regions, respectively. In August, we see a further northward extension of the Bering Sea primary track, bringing cyclones toward Cape Lisburne, Alaska. A second track takes many of these storms eastward along the Beaufort Sea coastal region. The summer season along the Beaufort coast is clearly the stormy season. The cyclone paths begin to shift back into the winter regime by September.

Maps of winter anticyclone frequencies over the Arctic have been published by Keegan (1958). These charts show that eastern Alaska, Siberia and the Beaufort Sea are under the influence of high pressure systems more frequently than most other Arctic areas. Strong anticyclogenesis, for example, often

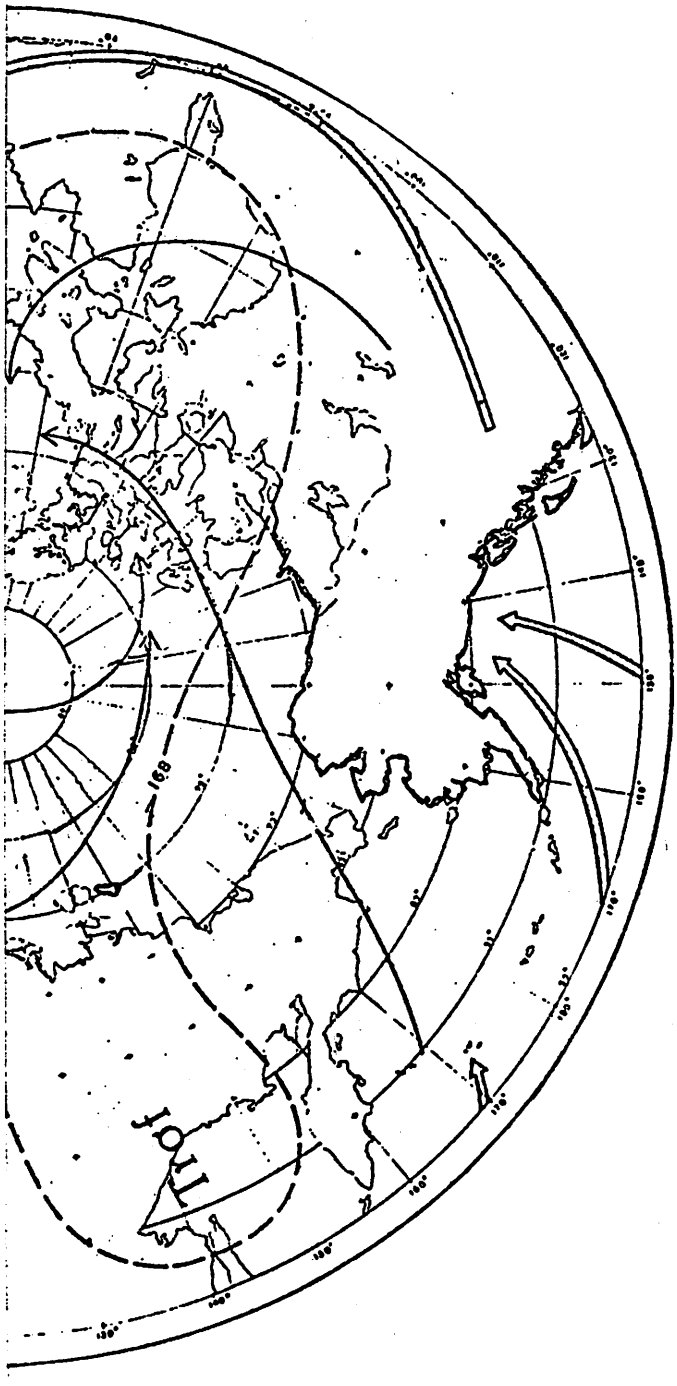

Figure 5: Schematic Cyclone Paths (arrows) and Representative 500 mb Contour (dashed line) for January

(from: Reed, 1959)

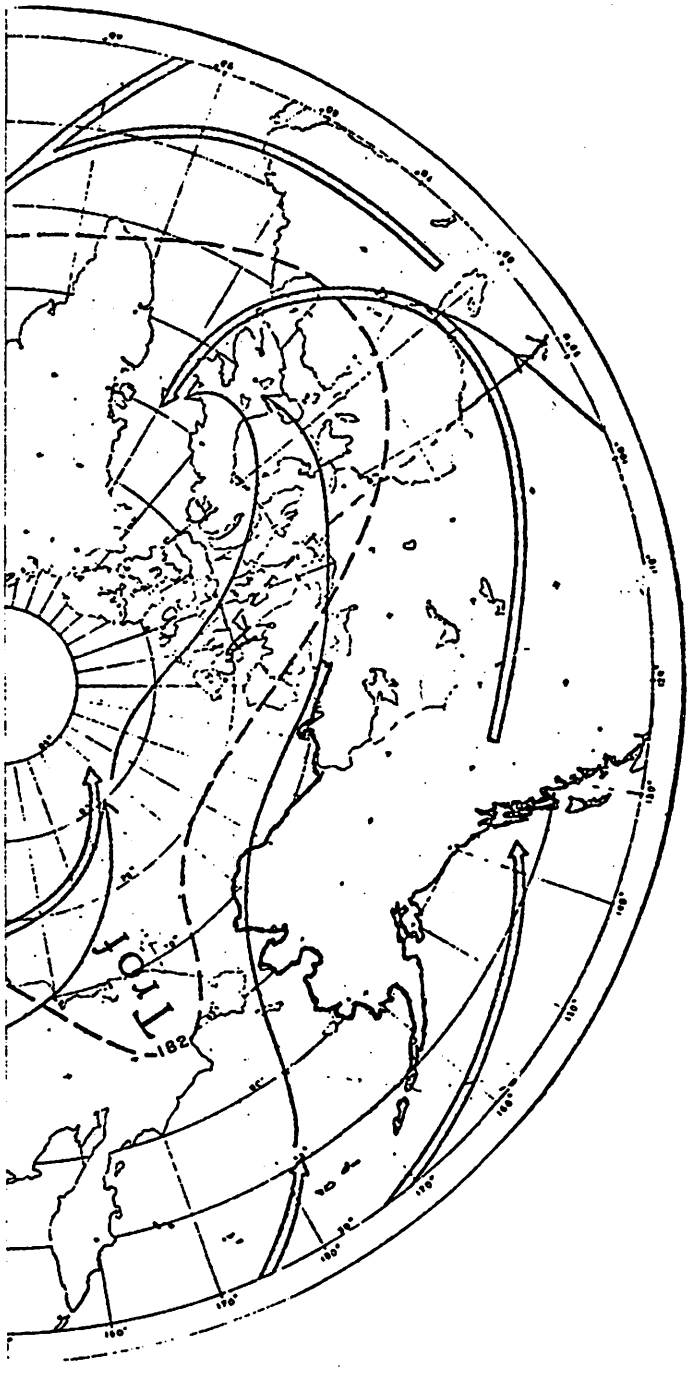

Figure 6: Schematic Cyclone Paths (arrows) and Representative 500 mb Contour (dashed line) for July

(from: Reed, 1959)

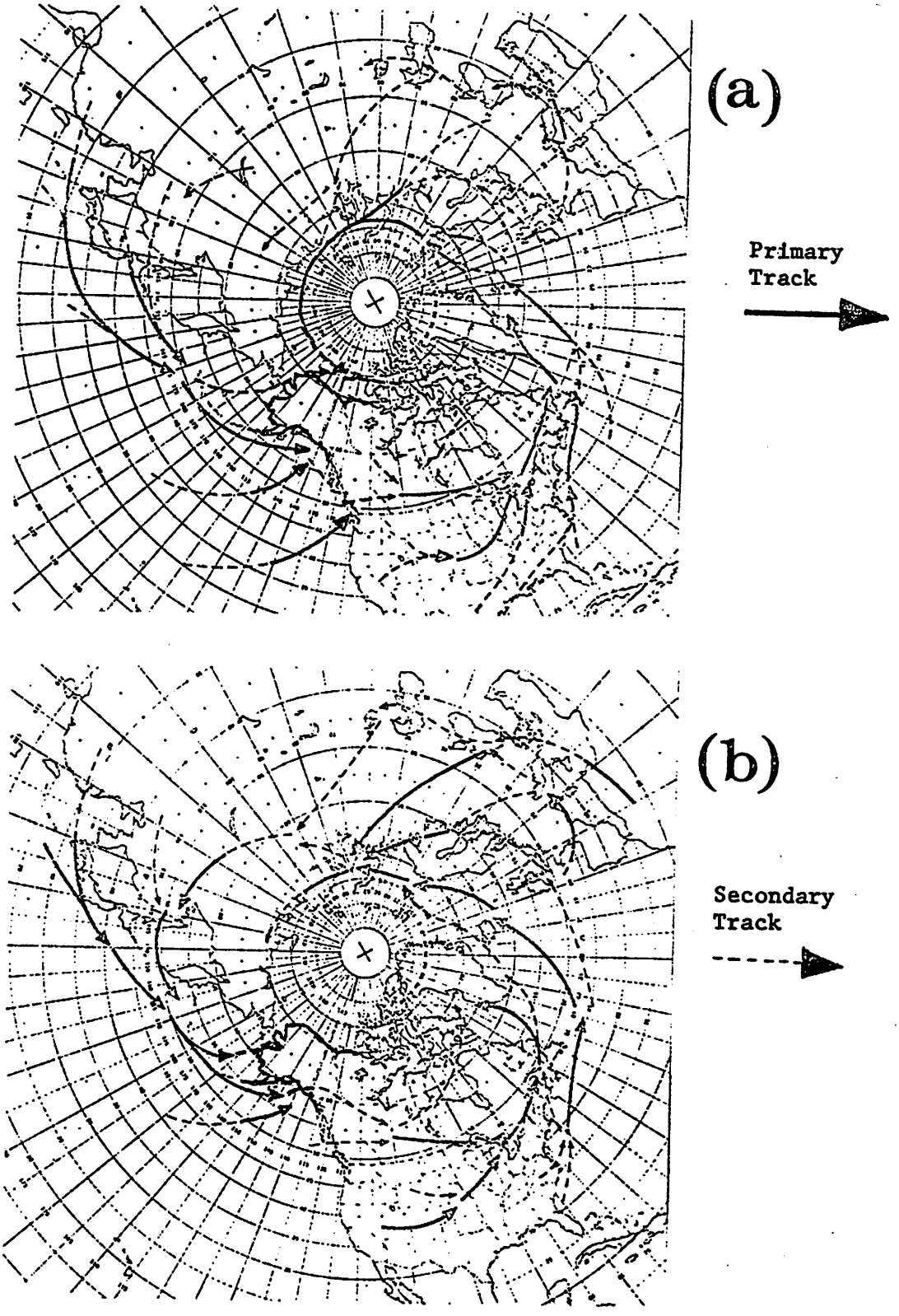

Figure 7: Cyclone Tracks for (a) January and (b) April

(from: Klein, 1957)

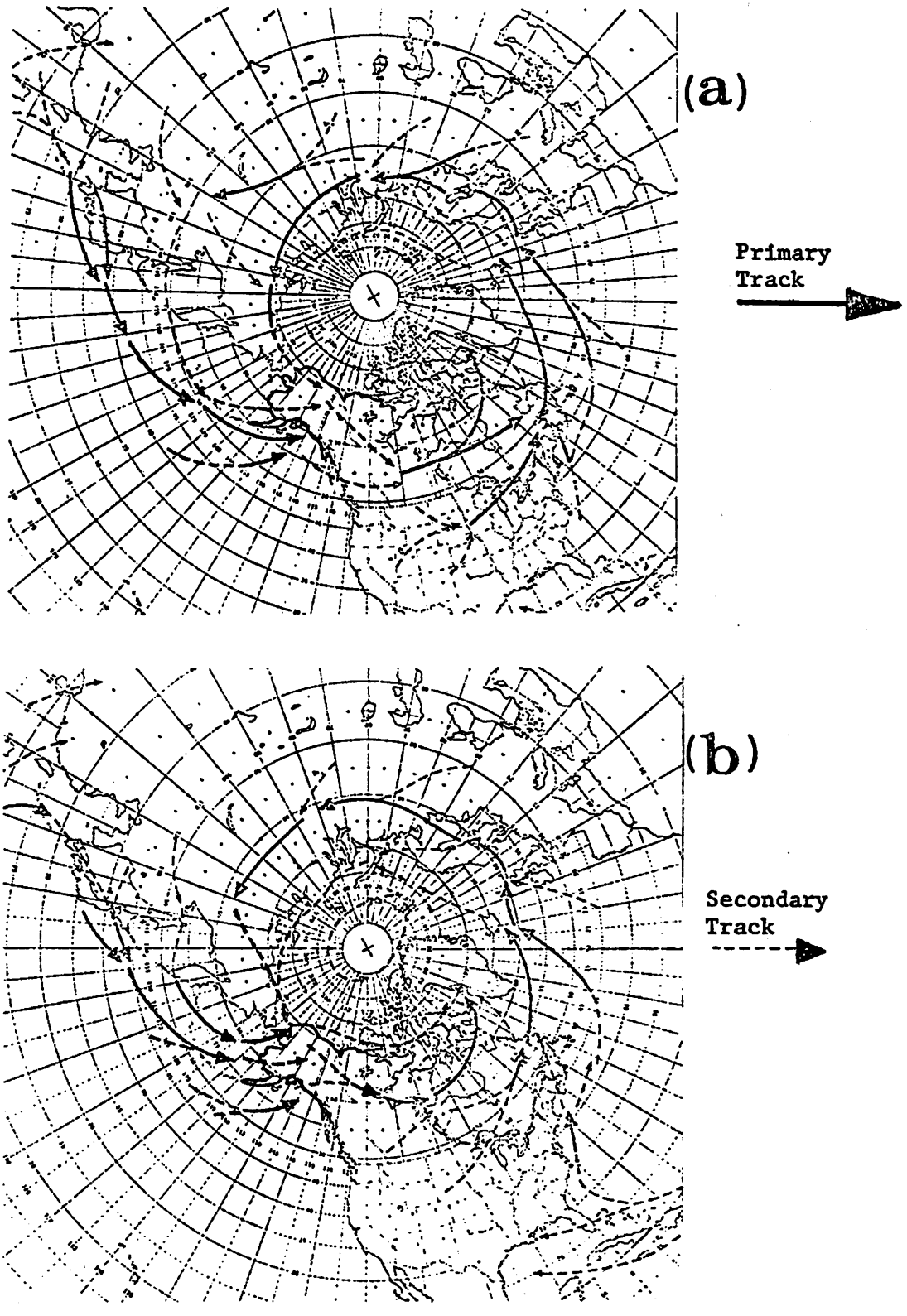

Figure 8: Cyclone Tracks for (a) June and (b) August

(from: Klein, 1957)

takes place over eastern Alaska or the Yukon territory when the mid-tropospheric ridge is well-developed in winter (Bodhurtha, 1952). Klein (1956) identified secondary anticyclone tracks which trend eastward across the Beaufort and Chukchi Seas in January. These tracks become primaries over the eastern Beaufort Sea and the central Brooks range, respectively. Keegan (1958), however, states that Arctic anticyclones tend to change shape and move erratically rather than following well-defined tracks in the majority of cases. His analyses were based on fewer data than Klein's, but more stations were reporting from the Arctic. In general, the anticyclonic systems are weaker and less frequent during summer, but they are still slightly more frequent than cyclones in the Beaufort Sea region (Reed and Kunkel, 1960). In summary, then, it appears that our study sector is bordered by a region of frequent and intense cyclonic activity to the south (Gulf of Alaska) and includes a region of predominantly anticyclonic surface circulation in the northern half. Seasonally, cyclonic storms from the Pacific influence the Beaufort Sea coast from July to February, with a maximum frequency in July-August. Cyclones are largely excluded from northern Alaska and the Beaufort Sea coast during spring. In May-June, cyclones begin to penetrate into Alaska more frequently. In all seasons of the year anticyclones are more frequent than cyclones in the Beaufort Sea region.

In Chapter Three we develop a classification system for daily msl pressure grids over our study region. It is appropriate, then, that we briefly review the study of Putnins (1966) which comprises a subjective classification of the pressure maps in the Alaska region. Putnins' approach to classification involved the subjective grouping of daily pressure maps by inspection of the isobaric patterns and their geographical distribution. From his description of the patterns it appears that a static "pressure pattern" method was applied (see: Barry and Perry, 1973, p. 99). Recurring locations and arrangements of closed lows, closed highs, troughs and ridges are identified by inspection of the map series, and serve to define the pattern types. Twenty-one sea level pressure types were distinguished on this basis, using daily charts for the period January, 1945 through March, 1963.

The most frequent patterns, overall, include low pressure systems south, southwest, and southeast of central Alaska with higher pressure in the Beaufort Sea area. These distributions imply easterly surface geostrophic flow along the Beaufort Sea coast. Major Yukon-Alaska high pressure cells and low pressure systems on the Bering-to-Chukchi Sea trajectory were also represented in Putnins' pattern types. Seasonally, the mean monthly type frequencies shift from a winter regime of lows to the south, highs to the north to a summer regime, comprising frequent ridges across Alaska from the south. During the spring, Putnins' patterns show frequent lows as far north as the southern Brooks Range. The winter-to-summer transition shows a marked decrease in the frequency of patterns with dominant Gulf of Alaska lows. These patterns become more frequent again in October, as the winter regime becomes established once again. On interdiurnal time scales Putnins' patterns showed high persistence in general. In the case of major monthly patterns, they always persisted more often than expected from chance. Several sequences of 10 or more consecutive days of a single pattern type are reported. In summary, then, there is generally good agreement between the mean 500 mb patterns, surface cyclone and anticyclone behaviour, and the more frequent sea

level pressure patterns of Putnins (1966). These regularities in circulation over the study area give us a framework within which to evaluate and compare the results of the present study.

Coastal Stations and Climatic Data

Barrows (71° 18' N, 156° 47' W) and Barter Island (70° 08' N, 143° 38' W) are the only first-order weather stations on the Beaufort Sea Coast of Alaska. These stations are operated and maintained by the National Oceanic and Atmospheric Administration, United States Department of Commerce. Both stations are located close to the shoreline and are representative of conditions at or very near the coast. Barrow, at 9 meters above sea level (asl), is presently located at the Will Rogers-Wiley Post Memorial Airport, which is less than 500 meters ESE (inland) of the Chukchi coast and is 8.5 km SSW of Elson Lagoon on the Beaufort Sea. The Barter Island station is sited at the west end of the local DEW line station, and is less than 500 meters due south of the Beaufort shoreline. The weather data used for synoptic climatological analyses in later chapters come from homogeneous station records with a few minor exceptions. For the periods of record considered in this study, Barter Island's station was never relocated and the Barrow station was moved only 146 meters inland from its initial location, which was more than 250 meters inland of the Chukchi shore (see: NOAA, 1976a; 1976b). The only major instrument change at Barrow involved the height of the wind instruments, which varied from 11.9 meters above ground level (agl) to its present elevation of 9.4 meters agl. This variation is regarded as negligible because the vertical sheer of wind speed is largely confined to the two meters nearest the surface (Holmgren and Weller, 1974, p. 857). At Barter Island, the thermometers and psychrometer were raised from 2.1 to 3.9 meters agl and from 1.8 to 3.6 meters agl, respectively, on September 18, 1972. Holmgren and Weller (1974, p. 860) present typical vertical air temperature profiles for July, July, August, September and February near Barrow. For all cases except February, the 2 meter-to-4 meter temperature difference is much less than 1°C, but in February it is nearly 2°C warmer at the higher level. Therefore, we do not use winter Barter Island temperature data for analysis of trends or fluctuations which overlap the instrument change.

Latitude and the spatial distribution of mountain ranges and oceans lead to zonation in climate-types over Alaska (Watson, 1968). The entire drainage north of the Brooks Range crest is classified as the Arctic Zone, although some moderation of temperature extrema occurs near the coast (e.g. Barrow) as compared to further inland (e.g. Umiat) within this zone (Selkregg, 1974). The climate along the Beaufort coast is qualitatively characterized by low temperatures, strong and persistent surface winds, low precipitation totals, and heavy cloud coverage, particularly in the form of summer-fall stratus and fog (Maykut and Church, 1973; NOAA, 1976a; 1976b). Three major factors which influence climate at high latitude are:

1) The unique radiation regime, with long periods of daylight and darkness during the respective seasons.

2) A snow and ice surface cover for much of the year.

3) A strong positive vertical air temperature gradient (inversion), particularly during winter (Wilson, 1967).

All of these factors contribute to the observed climatic characteristics of the Beaufort Sea coast. A summary of climatic statistics for Barrow and Barter Island is set out in Tables I and II. July is the warmest month at both stations and the coldest month is February. The annual curves of mean monthly temperature are relatively "flat" in mid-winter (Dec-Mar) and in summer (June-Sept) (Figures 9 and 10). By contrast, the temperature rise in spring and the autumn cooling are quite rapid. Overall, the mean monthly temperatures are similar at the two stations, with a maximum difference of only 1.1°C in May, this despite the spatial separation of 485 km. Temperature conditions along the entire coast are thus well-represented by Barrow and Barter Island data (Selkregg, 1974). One interesting aspect of Figures 9 and 10 involves the changes in slope of the mean monthly temperature curves from December to January and from January to February. The annual cooling trend is slowed somewhat in the first interval (-1.5°C at Barter, -1.3°C at Barrow) but increases again in the second interval (-2.4°C and -2.2°C, respectively). Considering only the local effects of the polar night radiative regime, one might expect a more pronounced and symmetrical "trough" in the annual curves of mean monthly temperatures. Possibly there is some recurrent circulation mechanism which temporarily slows the seasonal cooling trend during January. Such processes have been described for Antarctica, where the "coreless winter" regularly occurs (Wexler, 1958). The mean monthly temperature curves at several Antarctic stations actually rise from May to June and fall again from June to July (mid-winter) due to the frequent advection of relatively warm, moist air masses by cyclonic storms at this season (Van Loon, 1967; 1972). The associated high wind speeds also act to sweep away the strong surface temperature inversion, allowing air of relatively high potential temperature to influence the surface. At Barrow and Barter Island we may have a weak analogue to this process which is characterized by a slowed season cooling trend in mid-winter, rather than a full reversal of the trend. The pressure pattern catalog developed in Chapter Three will allow us to investigate this phenomenon as it relates to the atmospheric circulation. The flatness of the summer temperature curves must be related to the proximity of the Arctic Ocean and near-freezing seawater or sea ice. At Umiat, some 125 km inland from the coast, mean July temperatures are much higher than at Barrow and Barter Island (about 12°C), illustrating the important marine influence adjacent to the coast.

Moderately high mean wind speeds are characteristic of both Barrow and Barter Island (Tables I and II). These winds magnify the severity of winter through wind chill effects (Selkregg, 1974). The prevailing directions are mainly easterly, with the notable exceptions of January through April at Barter Island. Easterly flow is in general agreement with the frequent pressure patterns noted above, except perhaps during July-August. Schwerdtfeger (1975) has advanced an explanation for the Barter Island winter westerlies wherein a south-to-north surface pressure gradient is generated when stable air masses move towards the Brooks Range from the north. The winds at Barter Island are somewhat stronger than those at Barrow except in June through August, with maximum speeds (on average) during October through February. At Barrow the strongest mean winds occur from August to November.

Annual precipitation totals for Barrow and Barter Island average 124.1 mm and 179.2 mm, respectively, of which about 40% falls as summer rain (Dingman et al., in press). Conventional precipitation data are inaccurate in this region, however,

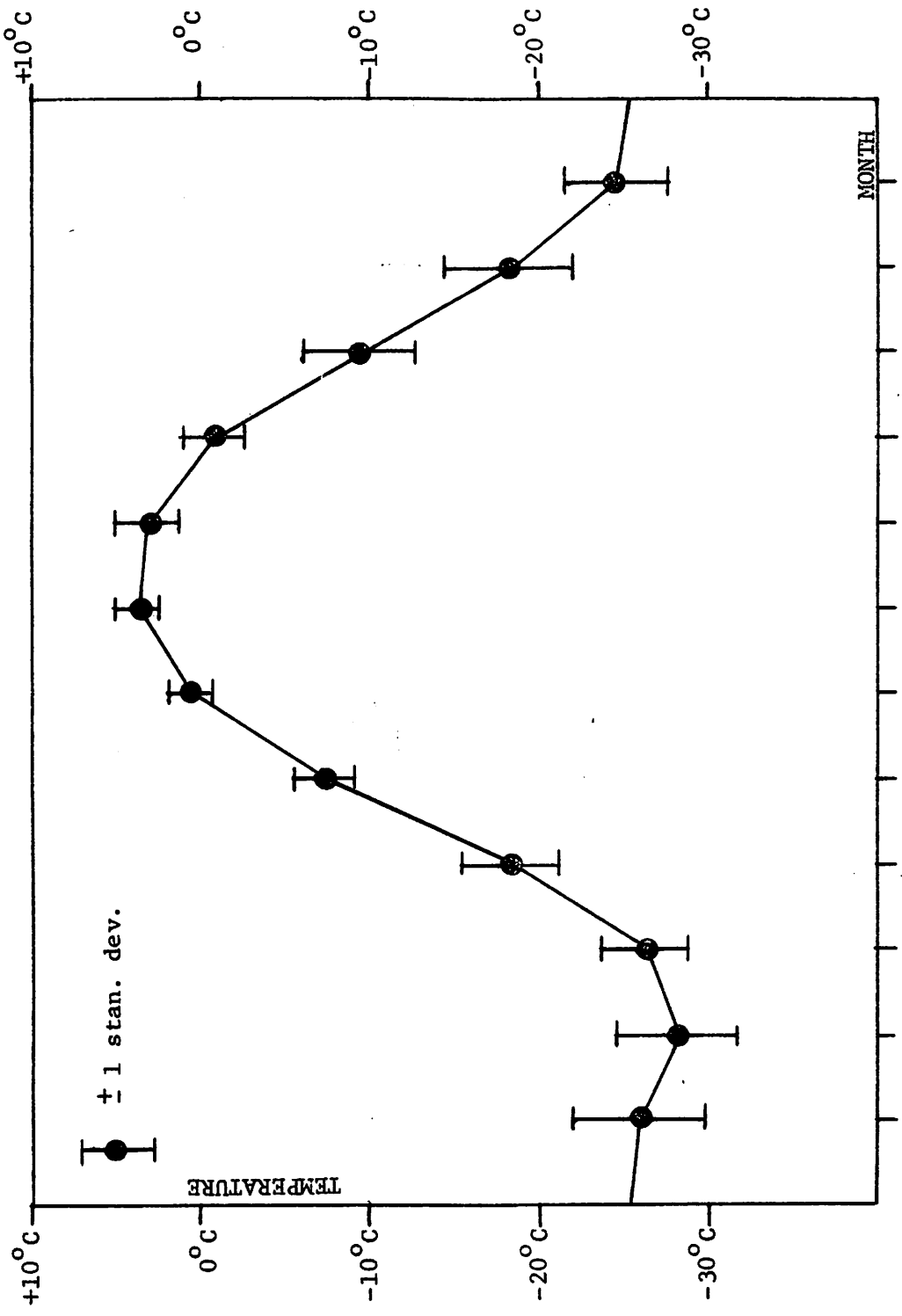

Figure 9: Mean and Standard Deviation of Barrow Monthly Temperatures

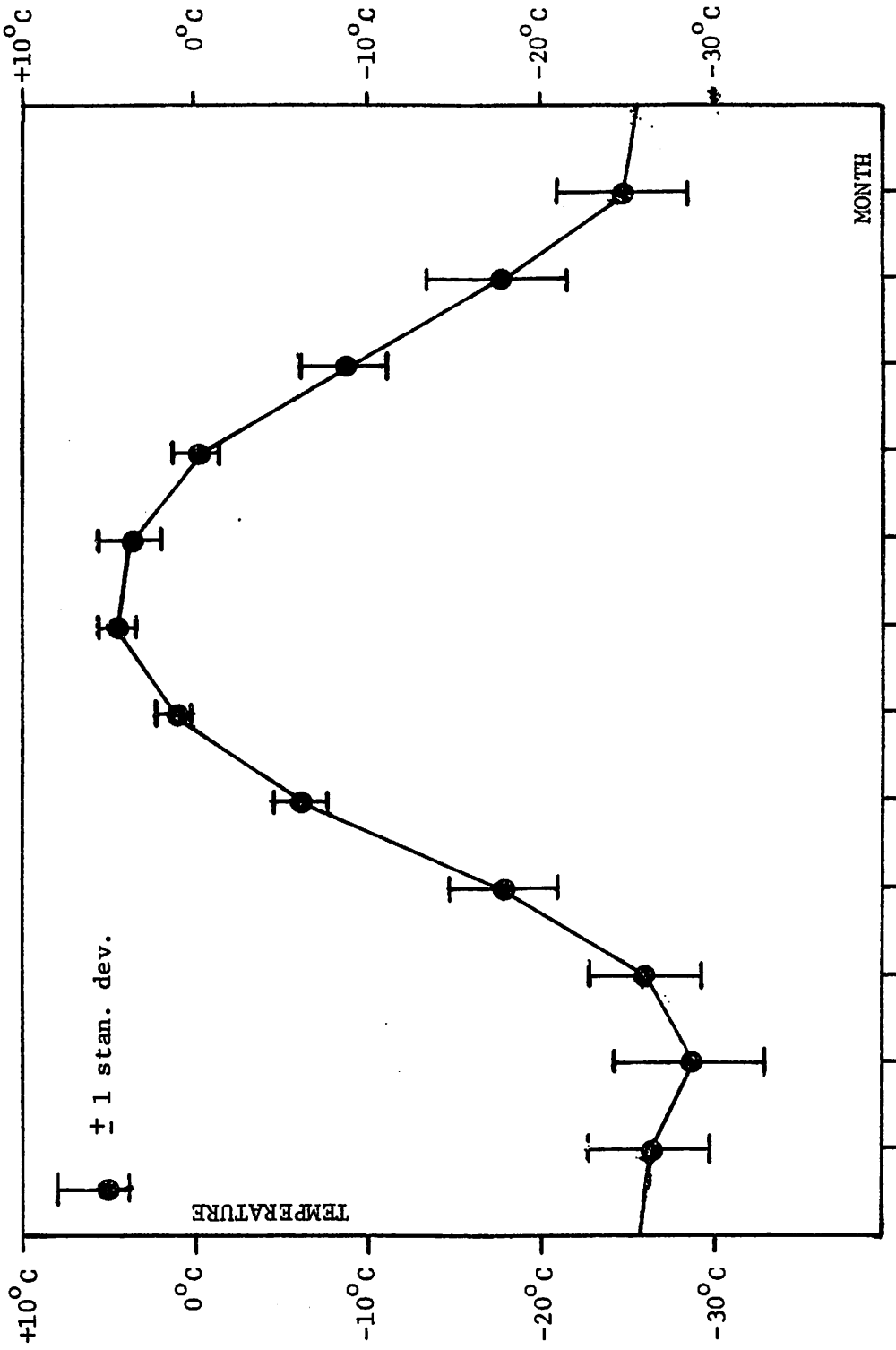

Figure 10: Mean and Standard Deviation of Barter Island Monthly Temperatures

TABLE I

MEAN MONTHLY CLIMATIC DATA FOR BARROW

Month	Wind Speed (ms^{-1})	Temperature (^{o}C)	Prevailing Wind Direc.	Sky Cover (10ths)	Precip. (mm)
Jan.	5.0	-25.9	ESE	5.0	5.8
Feb.	4.9	-28.1	E	5.2	5.1
Mar.	5.0	-26.2	ENE	4.8	4.8
Apr.	5.1	-18.3	NE	5.7	5.3
May	5.2	-7.2	ENE	8.4	4.3
June	5.1	0.6	E	8.0	8.9
July	5.1	3.7	E	8.0	22.4
Aug.	5.5	3.1	E	8.9	26.4
Sep.	5.8	-0.9	E	9.2	14.7
Oct.	5.9	-9.3	E	8.6	14.0
Nov.	5.5	-18.1	E	6.6	7.6
Dec.	5.0	-24.6	E	5.1	4.8

Data from: NOAA (1976a)

TABLE II

MEAN MONTHLY CLIMATIC DATA FOR BARTER ISLAND

Month	Wind Speed (ms^{-1})	Temperature (^{o}C)	Prevailing Wind Direc.	Sky Cover (10ths)	Precip. (mm)
Jan.	6.6	-26.2	W	NA	14.0
Feb.	6.3	-28.6	W	5.4	8.4
Mar.	6.1	-25.9	W	5.4	6.7
Apr.	5.3	-17.8	W	6.0	5.8
May	5.6	-6.1	E	8.3	7.9
June	5.1	1.2	ENE	7.8	13.5
July	4.7	4.4	ENE	7.8	28.4
Aug.	5.2	3.8	E	8.5	32.5
Sep.	5.9	-0.2	E	8.5	22.6
Oct.	6.5	-8.7	E	8.3	20.6
Nov.	6.7	-17.7	E	NA	11.4
Dec.	6.2	-24.7	E	NA	7.4

Data from: NOAA (1976b)

NA: not available

due to turbulence around the precipitation gauges and the frequent "trace" readings which are reported on a daily basis but not included in the numerical totals (Dingman, et al., 1976). These authors estimate that the actual falls are about 1.6 times the amount recorded at the standard observing stations. The average totals are higher at Barter Island than at Barrow in all months, although the previous discussion of regional circulation patterns does not clearly indicate why this is so. The cyclonic storms which pass along the coast generally move west to east (Selkregg, 1974) and should influence both stations. Perhaps the proximity of the Brooks Range adds a component of orographic enhancement at Barter Island. In any case, the summer precipitation maxima coincide with the seasonal increase of coastal cyclone frequency and with the greater availability of local moisture after the tundra thaws and the Arctic Ocean begins to break up. Barter Island records measurable precipitation ($\geq$ 0.254 mm) an average of 91 days per years, compared with 75 days per year at Barrow. Forty-three and 40 of these days occur during July through October, respectively.

Seasonal sky cover variations are primarily related to the local availability of moisture (Barry, 1976). A pronounced increase in mean monthly sky cover takes place between April and May at both stations, and lasts until October, when freezeup normally takes place. Clouds are primarily fog-stratus types, particularly during the summer, although cumuliform clouds occasionally form over the dry tundra under continuous summer insolation. It is important to note that the effects of clouds on the surface energy balance are opposite in summer and winter. In the winter, net radiation at the surface is primarily the result of the difference between the (positive) atmospheric and (negative) surface infrared fluxes. Clouds approximately black body radiators much more closely than does the clear atmosphere (Sellers, 1965), and thus will affect the surface radiation balance in the positive sense during winter darkness. In summer, solar radiation begins to dominate the surface radiation balance. Clouds act to deplete the solar flux and reflect the energy away from the surface, affecting the energy balance negatively at this season. Also, as noted by Vowinckel and Orvig (1962), a given cloud amount (in 10ths) over the Arctic is more opaque to solar irradiance in summer than in winter, due to increased thickness of the cloud layers. Fog, heavy fog and blowing snow conditions comprise the most frequent types of current weather reported (on a daily basis) from both Barrow and Barter Island.

The climatic statistics cited above illustrate the time-average regularities of Beaufort Sea coastal weather. It is also instructive to assess the variability associated with daily and interannual changes in the atmosphere. Table III shows the standard deviations of several daily series of Barrow weather data. For daily wind directions, the standard deviation is given by:

$$s_o = \{-2\ell n(1 - S_o)\}^{\frac{1}{2}} \tag{3}$$

where:

$$S_o = 1 - |\bar{R}| \tag{4}$$

TABLE III

STANDARD DEVIATIONS OF BARROW DAILY WEATHER SERIES

Month	Temperature Departure (^{o}C)	Dew Point Depression (^{o}C)	Wind Speed (ms^{-1})	Wind Dir. (^{o})	Sky Cover (10ths)
Jan.	8.1	2.5	2.6	97	5.0
Feb.	7.2	2.1	2.3	97	3.4
Mar.	6.1	2.1	2.4	88	3.3
Apr.	5.6	1.6	2.1	76	3.5
May	3.6	1.0	2.1	75	2.6
June	2.4	0.9	1.8	80	2.7
July	3.2	1.3	1.7	126	2.4
Aug.	3.4	1.2	2.1	94	1.9
Sep.	2.8	1.0	2.1	86	1.6
Oct.	5.2	1.4	2.4	80	2.1
Nov.	6.3	1.8	2.8	74	3.3
Dec.	7.4	2.2	3.0	101	3.7

Data source same as in Chapter 5

and $|\vec{R}|$ is the magnitude of the mean resultant direction on the unit circle (Mardia, 1972, p.24). For all other weather variables in Table III the standard deviation is:

$$(5) \qquad s = \frac{\{\Sigma(\bar{x} - x)^2\}^{\frac{1}{2}}}{\{ N - 1 \}}$$

where $\bar{x}$ is the mean of the given variable x, calculated from a series of N values. Table III illustrates that a "signal" daily weather fluctuation in one month (say, a temperature departure of $+4^{o}C$ in June) may be "noise" in another month with greatly variability (e.g. January). The variability in daily temperature departures from nomral, for example, is greatest in mid-winter, reaches minima in spring and again in fall, and takes on intermediate, rather low values in the summer. The physical explanations for these standard deviation changes through the year must be, in party, related to the great interdiurnal variability of surface air temperature during formation and breakdown of the inversion in winter. During the transition seasons the temperature variation is damped by effects of snow and ice phase changes acting as heat sink (source) in the spring (fall). It is also worthy of note that the January "kink" in the mean monthly temperature curves (Figures 9 and 10) is associated with the maximum interdiurnal temperature variability, again possibly indicating a "coreless winter" type phenomenon associated with the more frequent incursion of southerly storms. Table III thus illustrates that we must analyze our daily weather data and pressure patterns in relation to the inherent variability changes from season to season for a given weather variable.

The same approach is taken with regard to interannual variability also. Here we may be looking for (practically) significant anomalies in seasonal pressure pattern frequencies which are associated in time with weather departures. In Figures 9 and 10 the bars bracketing each monthly mean temperature are the standard deviations of the monthly mean temperature series. Here again there is a pronounced decrease in variability during spring and fall. The data cited in this section form the background against which we evaluate the weather characteristics of our pressure pattern groups.

CHAPTER THREE

PRESSURE PATTERN CLASSIFICATION

Introduction

In Chapter Two some of the broad-scale, climatological modes of atmospheric circulation over and around Alaska were described. Our primary objective, however, is to characterize the regional pressure patterns on a daily basis, and relate these patterns to daily weather conditions. A pressure pattern classification method is described and the results are reported in this chapter. Analyses of sample daily pressure patterns are presented, followed by a summary of the characteristic patterns, their properties, and frequencies of occurrence.

The Approach

A comprehensive review of the history, approaches and methods of synoptic climatology has been published elsewhere (Barry and Perry, 1973). It suffices to state here that we seek to establish a clear-cut generalization of the regional atmospheric pressure patterns on a daily basis. According to Hare (1955) this is one of the chief values of a synoptic classification approach.

The familiar synoptic models, such as Bjerknes' polar front cyclone (Palmén and Newton, 1969, Ch. 5), illustrate the useful correspondence between local weather and prevailing msl pressure patterns. Dynamical theories of baroclinic cyclone development predict a three-dimensional velocity field which is in general agreement with these models. For example, quasi-geostrophic baroclinic waves which amplify due to the thermal asymmetry of the surface low will generate a secondary circulation with rising motions ahead of the cold front and sinking motions behind it (Holton, 1972, p. 116). This vertical motion field is in agreement with the generalized cloud and precipitation patterns of the Bjerknes model. The horizontal components of trajectories in such a system are southerly behind the warm front and northerly behind the cold front, in agreement with the temperature changes of the Bjerknes model during passage of the low (Palmén and Newton, 1969, p. 310). Finally, decades of successful weather forecasting, based on synoptic models, indicate that there is good reason to treat weather characteristics as some function of msl pressure patterns (Barry and Perry, 1973, p. 97).

From the discussion of cyclone and anticyclone paths and frequencies in Chapter Two, we are justified in assuming that climatologically recurring "types" of pressure patterns should exist over the Alaska region. These characteristic patterns are physically caused by the recurrent, large-scale wave patterns and the regional distributions of oceans, continents, and mountains. By virtue of the dynamical interdependence of the different tropospheric levels, the msl pressure patterns also contain some implicit information about upper-level flow. We stress, however, that no two synoptic systems are exactly alike. A syntoptic climatological approach seeks to define the statistical weather characteristics for independent cases of pressure patterns which are <u>similar</u> but not <u>identical</u>. The identification of characteristic pressure patterns and the classification of daily weather maps into such groups is designed to achieve this objective.

Data and Methods

The time period for our classification is not extremely long, because continuous, reliable synoptic pressure observations over the Arctic Ocean are only available from about 1952 onwards (Reed and Kunkel, 1960). Earlier analyzed charts often include a dominant Arctic high pressure cell over the ocean, which was plotted in the absence of measured data. The resulting mean pan-Arctic high (e.g. U.S. Weather Bureau, 1946) has subsequently been shown to be fictitious in most seasons, since better Arctic analyses have become available (Baur, 1939; Dzerdzeevskii, 1945; Namias, 1958; Keegan, 1958: Reed and Kunkel, 1960). A convenient, readily-available record of Northern Hemisphere msl pressures which roughly corresponds to the period of more reliable Arctic data is archived at the National Center for Atmospheric Research (Jenne, 1975). These data cover the period January, 1946 to August, 1974, and it was decided to use them for the classification experiments. The grids comprise daily, 1200 GMT pressures at each of 1977 grid points (Figure 11) which were interpolated from standard synoptic charts (Jenne, 1975). The data were obtained in magnetic tape format for processing on the CDC 6400 computer. The grid space (Figure 11) is defined by an equidistant, rectangular array of pints, with axes of symmetry along 10° E longitude and 100° E longitude, and is overlaid onto a polar stereographic projection of the hemisphere. The map distance between parallels increases radially from the pole on this projection, so that the grid points have unequal ground spacing at different latitudes. For our study, we use 36 of these grid points in the geographical sector roughly bounded by 60° N latitude, 80° N latitude, 120° W longitude and 170° W longitude (Figure 11). The grid point spacing in this sector is 393 km $\pm$ 13 km. The relatively large number of pints in the southern section of our grid space was used for two reasons:

1) Synoptic pressure analyses are (to this day) much more reliable over central and southern Alaska than over the Beaufort Sea, because there are no permanent stations in the latter area.

2) By including the poleward margin of the Gulf of Alaska, we might identify important changes in the "center of action" which affect the weather further north.

The maximum number of daily grids used to identify characteristic patterns is limited by the extended core storage (ECS) capability of the computer to about 1800 days (about five years). We assume that the most recent daily grids are the most accurate, so the period October, 1969 through August, 1974 was used for identifying characteristic pressure patterns. Finally, it should be noted that the weather data analyzed in later chapters are available only for dates after 1952. Thus the unreliability of pressure analyses between 1946 and 1952 will not affect the study of weather-pressure pattern relationships.

The identification of characteristic pressure patterns (CP's) and the development of a daily catalog are based on techniques adapted from Kirchhofer (1974), who applied the methods to European 500 mb geopotential height fields. Because the pattern similarity tests and criteria are quantitative, the classification procedure is called "objective" (Barry and Perry, 1973, p. 102). However, as discussed below, all such empirical schemes rely on subjective decisions at some stage in the analysis. By using instantaneous, 1200 GMT

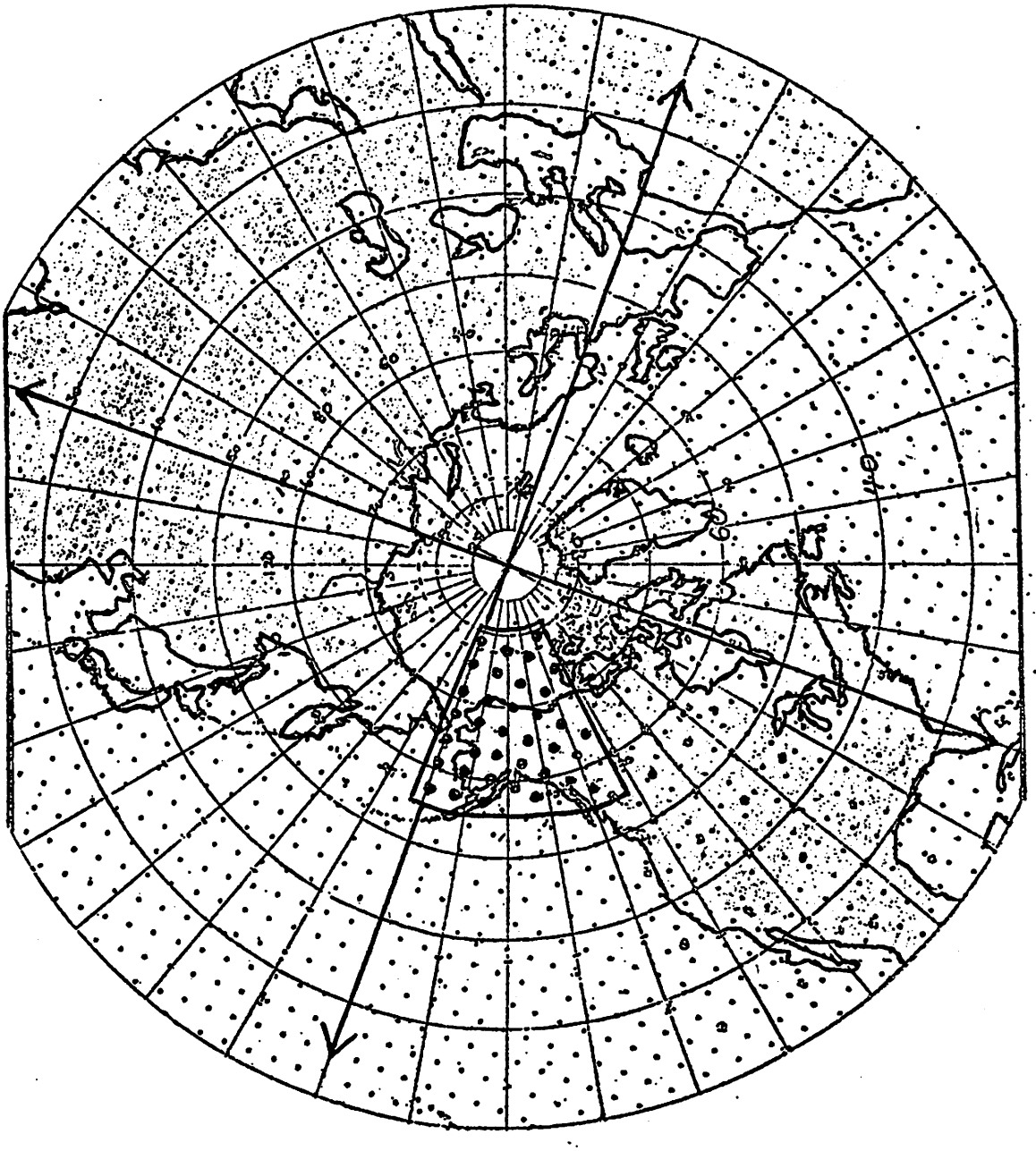

Figure 11: NMC Octagonal Grid, Alaska Sector Outlined

pressure data to represent the atmospheric circulation, we have chosen a "static" approach to the circulation. We shall discuss some of the strengths and weaknesses of this approach after the methods are presented in detail.

Each daily pressure grid is composed of msl pressures at the 36 points in Figure 12. The mean ($\overline{P}$) and standard deviation (s_p) of these 36 pressures are calculated separately for each of the 10470 daily grids in the sample (1946-1974). Each daily grid is then replaced, individually, by its corresponding 36-point standardized grid. This simply means that we replace the pressure at the "Ith" grid point (P(I)) on a given daily grid with P'(I), which is:

$$P'(I) = \frac{P(I) - \overline{P}}{s_p} \tag{6}$$

where I is allowed to take on the values 1 to 36. P'(I) is thus the number of standard deviations by which P(I) differs from the map mean and, as such, is a dimensionless number. For any given daily grid, then, we may express P' as a linear function of P:

$$P' = \alpha + \beta P \tag{7}$$

where:

$$\alpha = \frac{-\overline{P}}{s_p} \tag{8}$$

and:

$$\beta = \frac{1}{s_p} \tag{9}$$

are constants. For each grid, then, the standardized grid will retain the same spatial pattern of lows, highs, troughs, and ridges which was on the pressure map. However, maps where the difference ($P - \overline{P}$) is small over the grid (i.e., weak pressure gradient) will have a correspondingly small s_p, and vice versa for maps with large ($P - \overline{P}$) variations. Thus the standardization process makes the grids comparable, on a quantitative basis, with respect to the spatial pressure pattern, but removes the effects of pressure magnitudes and pressure gradients. The daily catalog listing retains the values of s_p and $\overline{P}$ for each daily grid, because they may represent crucial information at some stage in the analysis. The numerical comparison of any given pair of standardized daily grids is then carried out by calculating the sum of 36 squared differences between the corresponding grid-point values. This quantity is designated as "SCORE" and is given by (comparing days "J" and "K"):

$$SCORE(J,K) = \sum_{1}^{36} \{P'(I,J) - P'(I,K)\}^2 \tag{10}$$

A high SCORE indicates that the two patterns are relatively dissimilar whereas a low SCORE indicates relative similarity. The regional sector is also subdivided into five zonal and six meriodional sections, and the SUBSCORES are calculated for each of these subzones as in (10), but with only five to eight grid points. These numbers are indices of relative similarity for small areas within the total sector. Numerical "threshold" limits are determined such that the SCORE and all SUBSCORES for any pair of daily grids must be less than these limits if the two patterns are to qualify as "similar". The choice of these limits is subjective, although not arbitrary, and is based on short classification tests. These choices are discussed in a later section. It should be noted here that the subzones contain from five to eight grid points, so that the threhold for a given subzone is made proportional to the number of points within it.

The SCORE and SUBSCORE calculations are carried out for all possible pair-wise combinations of daily grids in the 1969-1974 sample. A frequency table is then formed in the computer, such that each of the 1796 days in the five-year sample has a list of dates which passed all similarity tests with its grid. The pressure grid with which the largest number of other grids passed the threshold tests is designated as characteristic pressure pattern number one (CP1). All of the dates within the CP1 frequency list have their own such lists, and these lists are deleted from the frequency table. Also, the dates comprising the CP1 frequency list may appear as entries in the lists of other dates, and these entries are deleted also. The pressure grid which has the largest remaining frequency list is then designated as CP2. This procedure is repeated in an iterative mode until no remaining list exceeds five days in size. Any remaining days are designated as unclassified. The deletion of the dates associated with the previously-defined characteristic patterns is designed to eliminate redundancy among the characteristic patterns and produce distinct pressure pattern groups.

After the CP's have been identified, each of the 10,470 daily grids in the 1946-1974 sample is grouped with one of the CP's based on two criteria:

1) The individual daily grid must pass all threshold tests with the given CP.

2) When a grid passes with more than one CP, it is grouped with the CP with which its SCORE was a minimum.

The second criterion will cause reassignment of a few daily grids in the initial five-year sample. This occurs when a given daily grid is listed with a high-order CP, but has a lower SCORE with a CP identified at a later step. Such a grid would be deleted from the lower-order list, but would be reassigned to that CP under the second criterion above. Again, a small number of daily grids may not pass the similarity tests with any CP, and will be left unclassified.

When all of the calculations are complete, the result is a magnetic tape record which lists each date for the 29 years. The characteristic pattern (CP1, CP2, etc.), SCORE with that CP, mean pressure, standard deviation of the pressures and number of good data points in the grid are also listed after the date. A further datum included for each date is the central pressure (P_c) which is the pressure at the grid point circled in Figure 12.

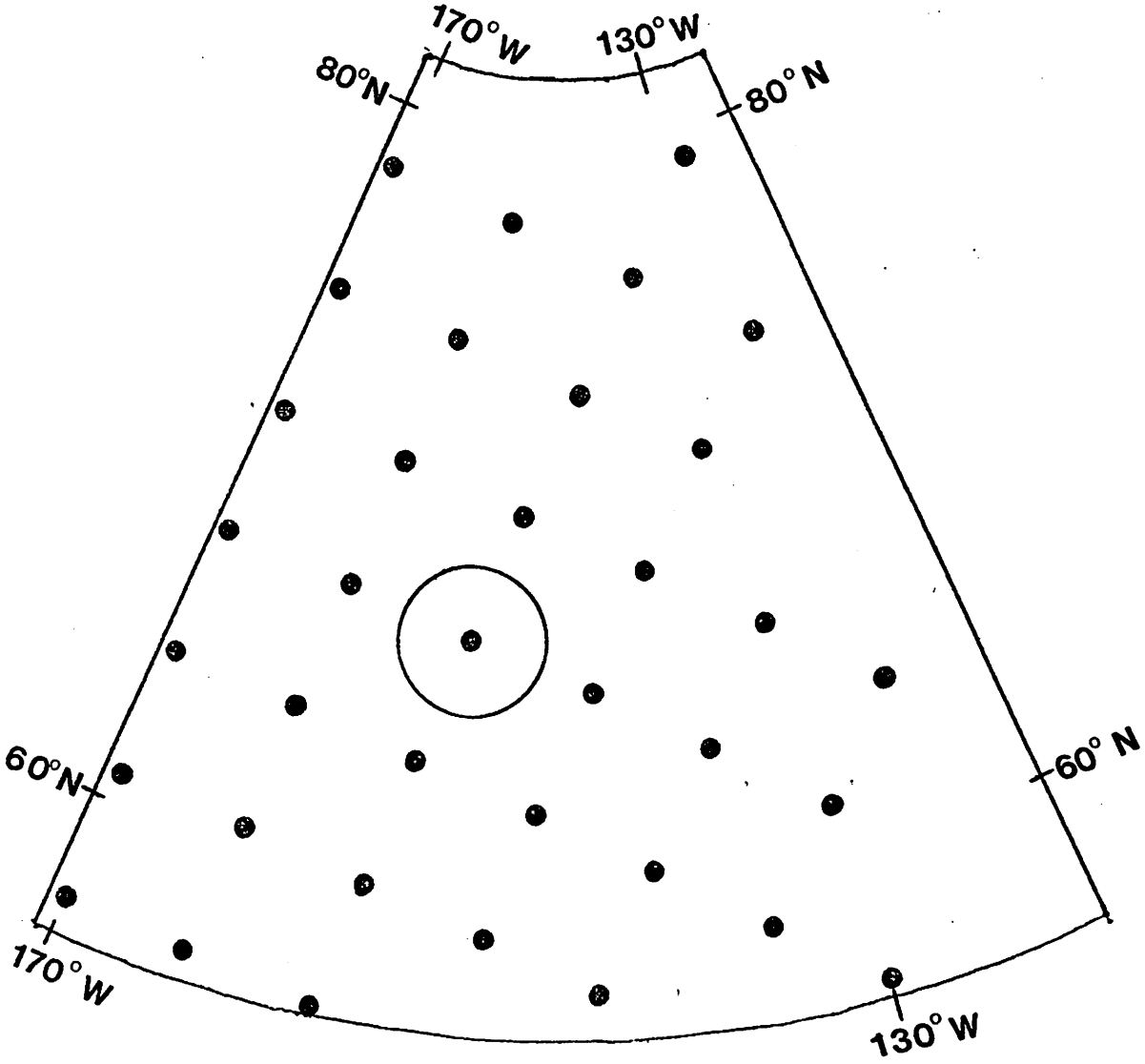

Figure 12: Regional Pressure Grid

Several advantages of this type of classification are:

1) The identification of characteristic patterns and the development of a daily circulation catalog may be programmed for a high-speed, digital computer, using readily-available numerical data.

2) The catalog of nominal characteristic pressure patterns establishes a one-to-one correspondence between a given date and one type of circulation system. This is not the case, for example, when eigenvectors or orthogonal polynomial equations are used to specify the pressure field. In these latter schemes, one daily pattern is characterized by several eigenvector weights or polynomial coefficients, each of which quantified the importance of a distinct spatial pattern (Barry and Perry, 1973, p. 109; Blasing, 1975; LeDrew, 1976, p. 112).

3) Tests for pattern similarity are quantitative and internally consistent for all characteristic patterns, so that a minimum of subjective bias is introduced. This objective property is necessary for a rigorous statistical evaluation of weather-pressure pattern relationships, because a subjective method may be based, in part, on the analyst's prior knowledge of the important weather-pressure correspondences (Barry and Perry, 1973, p. 102).

4) The specific classification techniques used in the present study provide numerical indices of "goodness of fit" of a daily pattern to its corresponding CP (the SCORE) and of the intensity of the pressure pattern (s_p). These two phenomena are sometimes overlooked in studies which focus primarily on the pattern alone (Barry and Perry, 1973, p. 102).

As with any empirical approach, there are also some disadvantages:

1) It is not entirely clear from the classification techniques which features of a daily pressure pattern are most important in determining the CP with which it is grouped. The numerical range of the SCORE from zero to the threshold limit allows for a range of patterns in any CP's group.

2) The actual pattern identification and classification processes do not incorporate the intensities of the patterns involved although, as noted above, this information is retained on the tape. Also, when the pressure field is quite flat (small s_p) the pattern of standardized isobars may be essentially meaningless.

3) Subjectivity must be introduced into the process by selecting appropriate threshold limits (as described below).

4) The static pattern of msl pressure is but one important aspect of the circulation which determines the weather. We are essentially ignoring the upper-levels in the classification process.

5) The statistical patterns are not necessarily related to the important physical patterns in the atmosphere, although previous studies along these lines are encouraging (Sabin, 1974; Scholefield, 1973; Blasing, 1975; Lund, 1963).

Test Classification Results

Preliminary pressure pattern classification tests are necessary in order to determine appropriate threshold limits for the SCORE and SUBSCORE indices. Some previous work with pressure pattern correlation methods (Lund, 1963) may be instructive in this regard. The correlation technique is similar in many respects to our modified Kirchhofer method. The standardization of the daily grids is implicit in the calaculation of the correlation coefficient between two daily grids, because the product of the two grid variances appears in the denominator. Scholefield (1973) reports that the correlation technique classifies the grids on the basis of pattern alone, without regard to pressure magnitudes or pressure gradients, just like the Kirchhofer method. Thus the general results from studies using Lund's technique are qualitatively applicable in this study. Sabin (1974) presents a series of calculations designed to determine an optimal correlation threshold for comparing similar pressure grids. With regard to the development of characteristic patterns and a daily pressure pattern catalog he states that the choice of a threshold must be, at best, a compromise. The tradeoffs involved in this compromise are qualitatively summarized in Table IV. The number of CP's generated should be enough to adequately represent the important pressure systems, but should be small enough so as to include reasonably large samples of daily grids in each group. CP redundancy is an indication of the pattern similarity between characteristic patterns. Obviously we wish these to be distinct, one from the other, for our assessment of weather characteristics. CP-group correspondence indicates the degree of similarity between a given CP and its constituent daily grids in the catalog. Good correspondence is obviously desirable here. The percentage of daily grids which are classified is also important, so that most of the weather of interest can be associated with a definite pressure pattern. The final category in Table IV is the identification of important pressure features. Sabin found that the choice of a correlation threshold influenced the nature of pressure patterns which could qualify as characteristic patterns. Patterns which had pressure centers (lows or highs) near the center of the grid sector were not identified using the stringent threshold. Sabin showed numerically that this is a result of the relatively small grid area over which such a center can range before the threshold criterion is not met. Transitional systems, with the low and high centers near the grid margins, passed the tests more easily. When the threshold criterion was relaxed, however, the central low and high pressure types were recognized in the resulting characteristic patterns. These sorts of analyses illustrate the pragmatic nature of most synoptic classification studies. Often the measure of success for the classification is simply the degree to which it provides useful information for the problem at hand (Barry, 1974). It is clear from Table IV that both stringent and relaxed thresholds have advantages and disadvantages. The stringent thresholds will yield a somewhat large, redundant set of characteristic patterns which will, perhaps, overrepresent the transitional situations. The percentage of days classified will be relatively less than for the relaxed threshold, but a high degree of correspondence exists between the CP and its group of daily grids. The relaxed threholds will produce a relatively small set of distinct CP's with a high percentage of days classified, but the correspondence suffers. Critical considerations, then, are:

TABLE IV

TRADEOFFS BETWEEN SIMILARITY THRESHOLDS

	Status	
Variable	Stringent Threshold	Relaxed Threshold
No. of CP's	Greater	Lesser
CP Redundancy	Greater	Lesser
CP-Group Correspondence	Better	Worse
% of Days Classified	Lesser	Greater
Identification of Important Pressure Features	Worse	Better

Summarized from Sabin (1974).

1) What is the number of CP's which adequately characterizes the important synoptic systems and still provides useful information, both conceptually and in terms of CP sample sizes?

2) At what point does the redundancy between characteristic patterns extend to the associated weather characteristics?

Definite answers to both questions can only be given after a classification has been carried out and analyzed. However, a number of previous studies provide insight into the problem. As noted in Chapter Two, Putnins (1966) subjectively identified 21 different types of msl pressure pattern over the same region that we are studying. It is the present author's opinion that a much larger number of patterns becomes extremely unwieldy and difficult to analyze and conceptualize. Fliri (1965) compared the standard deviations of cloud and temperature series over the Alps as stratified according to four different synoptic classifications, each with a different number of circulation categories. He found that the variability of the unstratified series was reduced by all of the classifications, and this reduction increased with the number of circulation types in the scheme. This result is in agreement with the findings of Sabin (1974). However, beyond about 30 pressure pattern categories, the further variance reduction was very slight. As a point of reference, then, we might expect about 20 to 30 pressure pattern types to be a useful compromise.

The modified Kirchhofer technique described above yielded a manageable number of patterns which, on analysis, appeared to be representative of the important synoptic systems over the western United States with an overall threshold of N_t and SUBSCORE thresholds of 1.8 N_i (Barry, et al., 1977, p. 22). Here N_t is just the total number of grid points in the sector and N_i is the number of points in the "ith" subzone of the grid. We use these values as a point of departure for the present study. For comparative purposes, the stringent threholds $0.5N_t$ and N_i were also tried. The classification procedure was applied to the five-year sample with each of these threshold limits, and the results are shown in Table V. In addition to the usual statistics in Table V, we define R_{20} as the number of inter-CP SCORES less than 20, and R_{40} as the number of inter-CP SCORES less than 40. These are indices of the redundancy of the characteristic patterns. CP-group correspondence was assessed on the basis of the mean SCORE of the constituent grids with their respective CP's, and by comparison of sample weather maps with the corresponding map for the CP. All of the results in Table V are in general agreement with the findings of Sabin (1974). The identification of important pressure features cannot be thoroughly assessed until the entire catalog is generated and analyzed. However, the 51 CP maps included pressure patterns with lows, highs, troughs and ridges in just about every conceivable position and orientation in the grid sector. Also, from our discussion in Chapter Two, it is evident that transitional systems are most frequent over our sector, with lows to the south and highs to the north. Thus the omission of central low and high pressure types may not be such a problem as it was in Sabin's study. Although we have not included the status for the identification variable with the relaxed threshold, a preliminary inspection showed that many of our characteristic patterns looked very similar to Putnins' key pattern, indicating that we may, indeed, have identified the important synoptic systems over the region. Based on the number of CP's (21), the high percentage of days

TABLE V

CLASSIFICATION RESULTS FOR TWO DIFFERENT THRESHOLDS

Variable	Status: Stringent Threshold ($\frac{1}{2}N_t, N_i$)	Status: Relaxed Threshold ($N_t, 1.8N_i$)
No. of CP's	51	21
R_{20}	33	0
R_{40}	244	23
CP-Group Correspondence	Better	Worse
% of Days Classified	85	96
Identification of Important Pressure Features	Good	-

classified, and the success of this threhold reported in Barry, et al. (1977), we shall use the relaxed threshold in our study. It remains to be seen, however (Chapter Five), whether or not this grouping is useful in terms of differentiation of weather characteristics.

Main Classification Results

Table VI is a listing of dates, one for each of the 21 characteristic pressure patterns. The 1200 GMT msl pressure maps for the 21 days are shown in Figures 13 through 16. A description of each pattern is given below.

CP1 is characterized by low pressures in the south, higher pressure to the north, and cyclonic curvature over Alaska south of the Brooks Range. Although our classification procedure removes the effects of pressure gradient variations between daily grids, the standardized isobars will preserve the spatial changes in pressure gradient over a single grid. This is also true of the correlation method (Scholefield, 1973). The strongest gradient for CP1 is over the west-central part of the grid sector, where the isobars are nearly zonal in orientation. The isobars turn almost due south over the southeastern part of the sector.

CP2 has a pressure distribution nearly opposite to that of CP1. High pressures sretch from southeast to northwest across the central grid, with lower pressure in the northwest quadrant.

CP3 has lowest pressure and the most intense gradient in the south-central part of the grid, near Valdez, Alaska. Highest pressures take the form of a relatively weak ridge along the Beaufort Sea coast from the west.

CP4 is characterized by a high pressure center over the southern Yukon which weakens as it extends northwest into the ARctic Ocean. A relatively strong northeast-southwest pressure fall occupies the southwest corner of the grid.

CP5 shows a low center on the southern grid margin, much like CP3. However, the CP5 ridge extends across central Alaska from the WSW, and the pressure drops to a marginal low near Banks Island in the northeast quadrant.

CP6 is dominated by a trough from the WSW which extends over the Brooks Range and into the Yukon. The pressure gradients are relatively constant around this trough, but slacken to the north.

CP7 has a relatively intense low pressure system in the northeast quadrant and a ridge from the west separates this feature from a weak low pressure belt in the southern part of the sector.

CP8 is dominated by a central low pressure cell straddling the Yukon-Alaska border. A ridge of relatively high pressure extends onto the grid sector from the northwest.

CP9 has a zonally-oriented high pressure cell over the Yukon which extends westward towards Seward Peninsula. The steepest pressure gradients on the map are located in the south-central part of the sector.

TABLE VI

DATES OF CHARACTERISTIC PRESSURE PATTERNS

Characteristic Pattern	Year	Month	Day
1	1969	Dec.	03
2	1971	Sep.	20
3	1972	Jan.	15
4	1972	Jan.	24
5	1973	Jan.	24
6	1973	Aug.	06
7	1970	Sep.	29
8	1974	June	02
9	1974	Feb.	25
10	1972	Oct.	25
11	1970	June	14
12	1973	Sep.	01
13	1971	Feb.	28
14	1970	July	02
15	1974	June	12
16	1972	June	22
17	1970	Aug.	17
18	1970	July	07
19	1971	Oct.	25
20	1972	Apr.	02
21	1974	June	18

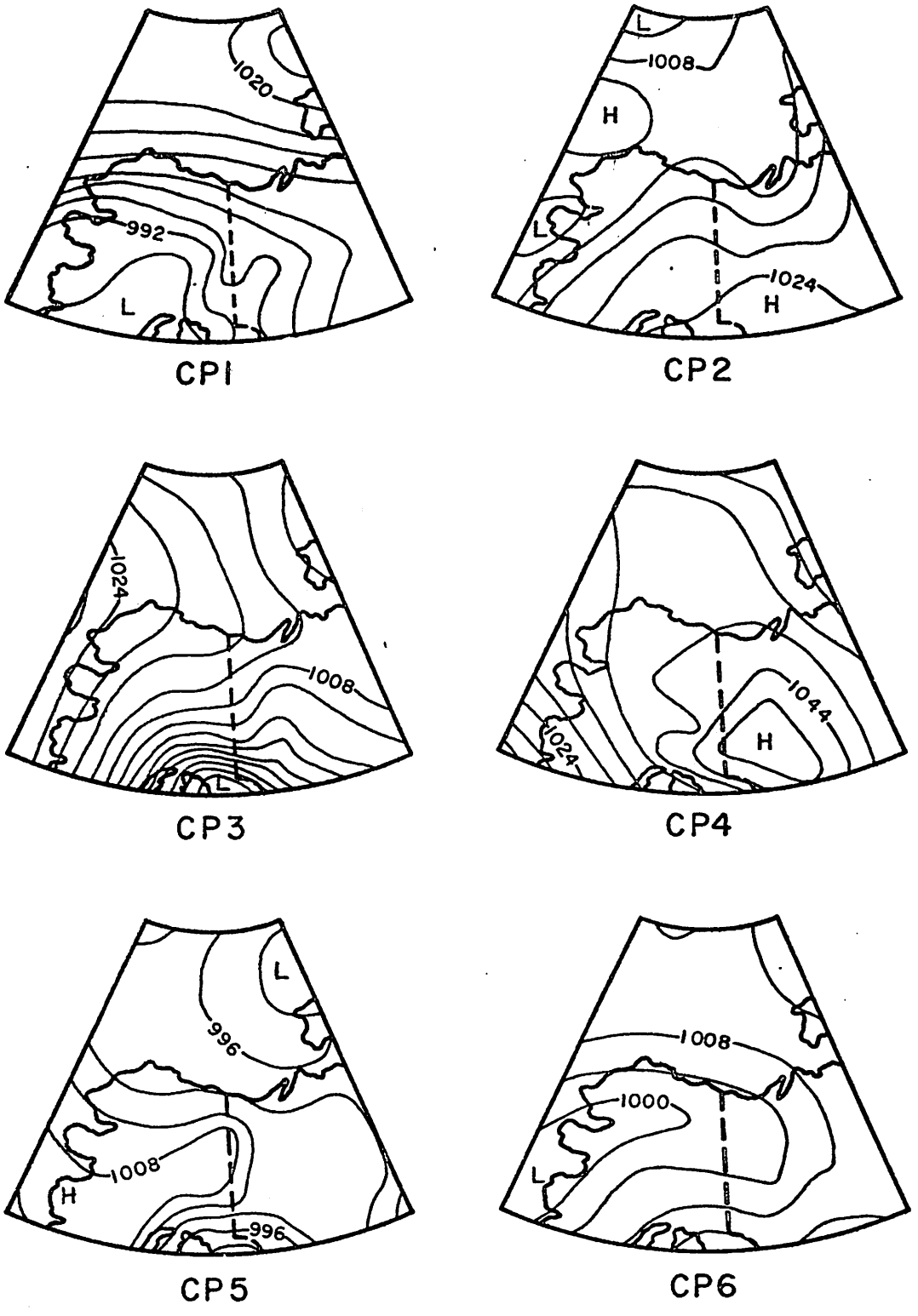

Figure 13: Characteristic Patterns 1-6

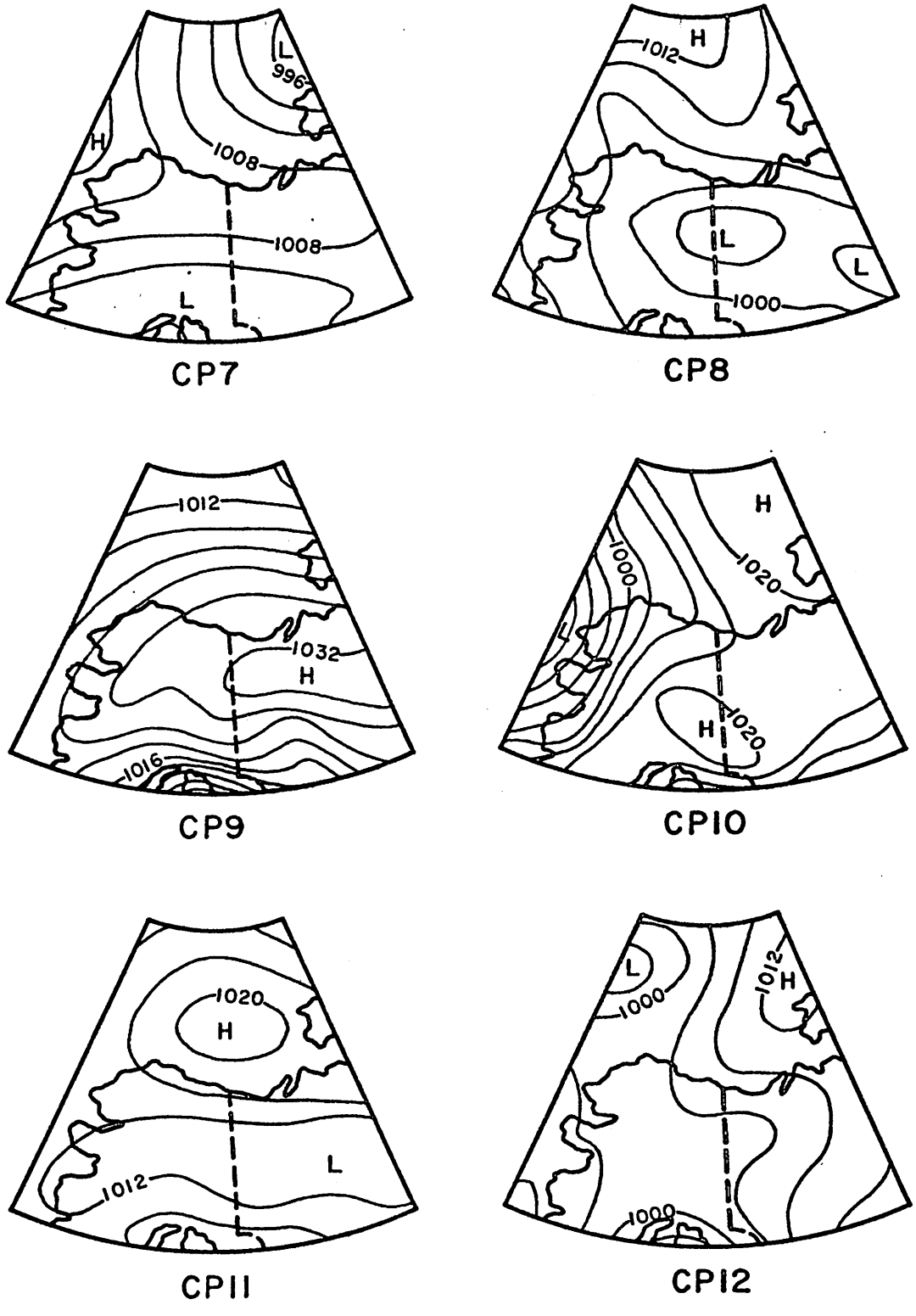

Figure 14: Characteristic Patterns 7-12

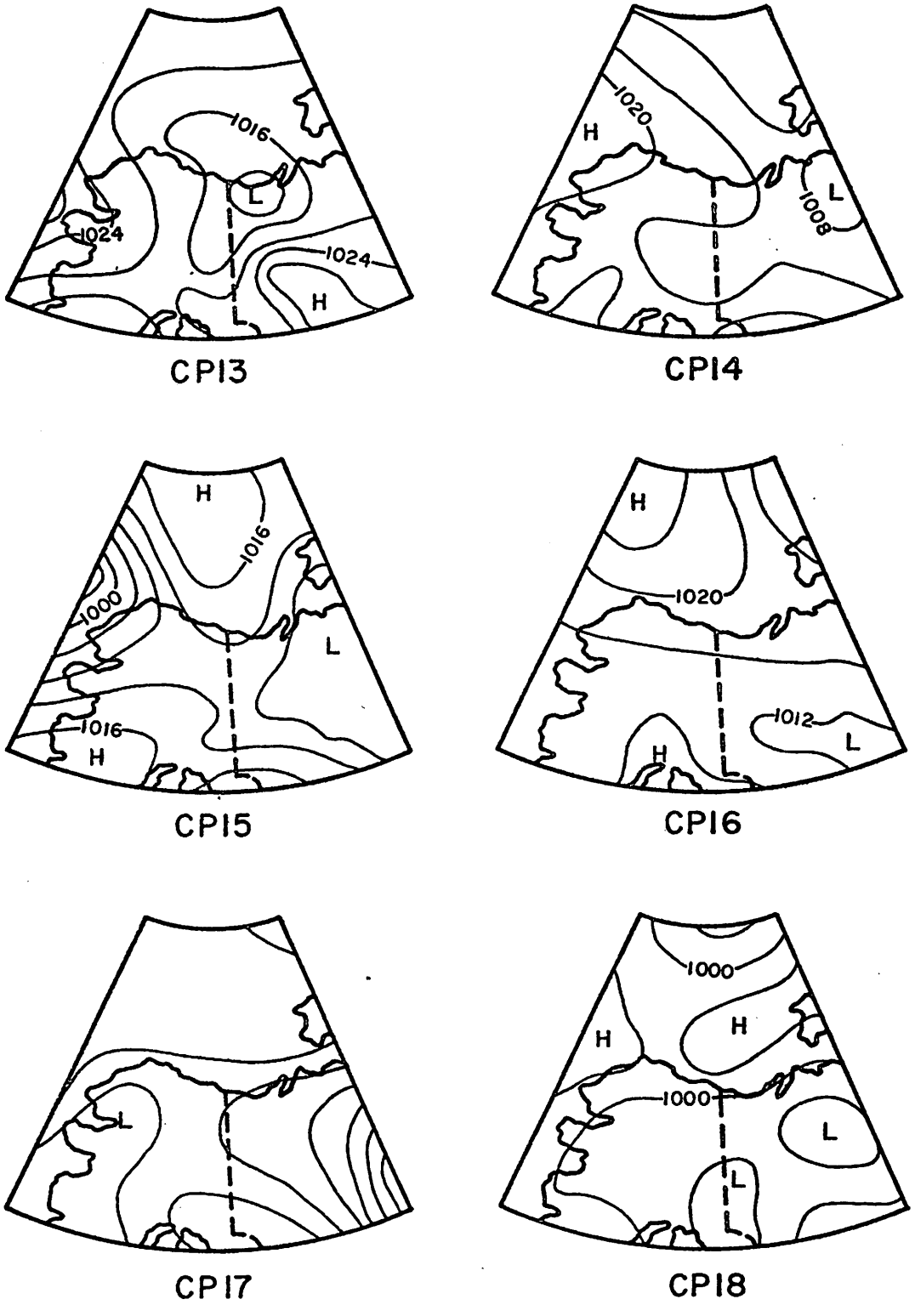

Figure 15: Characteristic Patterns 13-18

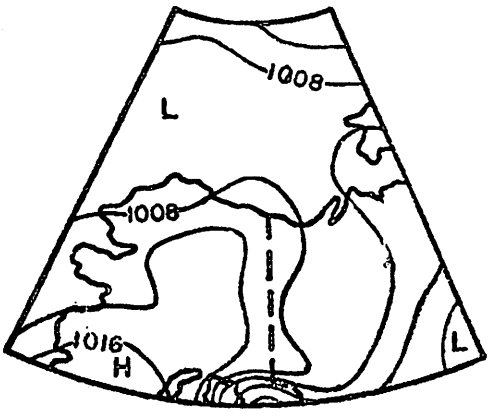

CP19

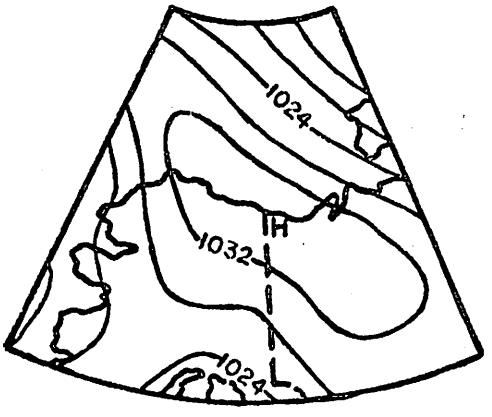

CP20

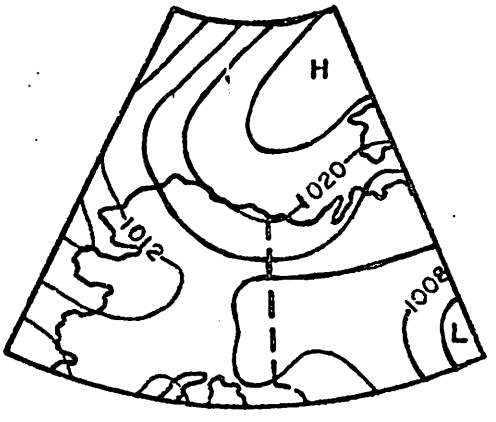

CP21

Figure 16

Sector Pressure Analyses for CP's 19-21

CP10 is characterized by a low pressure cell west of Kotzebue Sound and associated trough extending eastward along the Beaufort Sea coast.

CP11 shows a Beaufort Sea high pressure cell with a belt of low pressure across central Alaska from east to west. Higher pressures are located to the south of this belt.

CP12 has highest pressures along the eastern half of the sector, and a meridional trough in the western part. Low pressure cells near Cook Inlet and in the Beaufort Sea form the endpoints of this trough.

CP13 is characterized by a low pressure cell over the Mackenzie Delta area and a ridge from the southeast across the southern Yukon. The lower pressures on this map extend broadly SW-NE while the higher pressures are approximately E-W oriented.

CP14 has a ridge from the west across the Beaufort Sea coast and a trough from the east across central Alaska.

CP15 shows a low pressure cell in the Chukchi Sea, with high pressures to the northeast and south. The low center is northward from the CP10 low center.

CP 16 shows a high pressure center in the northwest part of the sector, with a low belt from the Yukon across central Alaska to the Bering Sea.

CP17 is dominated by a low system near the southeast margin of the sector which troughs across Alaska to the southwest.

CP18 has a Beaufort Sea ridge separating two low pressure areas in the Arctic Ocean and across Alaska and the Yukon, respectively.

CP19 is characterized by a ridge across central Alaska from the southwest.

CP20 has a high pressure cell extending from the Yukon across the Beaufort Sea coast.

CP21 is dominated by a ridge from the northeast which stretches to the Brooks Range, and a low pressure trough across central Alaska.

Of the 21 characteristic pressure patterns, nine show fairly well defined low systems in the Gulf of Alaska-Bering Sea region, as expected from the discussion in Chapter Two (CP's 1, 3, 5. 6, 7, 12, 13, 16 and 17). Also, 11 CP's have high pressure centers or pronounced high pressure ridges over the Yukon-Beaufort Sea-Arctic Ocean section of the grid (CP's 1, 4, 7, 8, 9, 11, 16, 17, 18, 20 and 21), reflecting the anticyclonic dominance of this area.

Some statistics for each characteristic pattern are presented in Table VII. These data summarize the characteristics of the 1969-1974 sample. The extremely high frequency of CP1 is striking, accounting for 45% of the days in the five-year interval. CP1 also has the lowest mean SCORE of all the CP's, possibly indicating a well-defined mode of surface pressure distribution over the region. The daily CP frequencies drop sharply from CP1 to CP2, and

TABLE VII

STATISTICS FOR 10/1969-8/1974 CLASSIFICATION RUN

Characteristic Pattern	Mean SCORE	SCORE Stan. Dev.	Frequency (Days)	Percent Frequency
1	16.3	8.2	804	45
2	19.4	7.3	202	11
3	17.7	8.3	174	10
4	20.5	7.3	139	8
5	22.1	7.2	69	4
6	22.1	7.7	65	4
7	21.3	8.0	52	3
8	19.8	6.8	52	3
9	20.9	8.0	36	2
10	23.4	7.9	22	1
11	27.9	6.0	18	1
12	21.8	9.0	15	*
13	25.2	7.8	12	*
14	23.8	6.1	11	*
15	23.4	6.6	11	*
16	25.3	6.3	10	*
17	24.6	5.4	9	*
18	27.2	6.8	8	*
19	28.2	8.6	8	*
20	28.4	4.4	5	*
21	24.5	3.0	5	*

* Less than 1%

again from CP4 to CP5. In fact, CP's 1 through 4 account for 74% of all days in the period, while CP's 1 through 9 comprise 90% of the sample. These results indicate that a very limited number of generalized pressure patterns recur frequently over the region, and a rather larger number of less-frequent patterns fill out the sample. The mean scores show some tendency for better correspondence between the first nine CP's and their groups, with no value over 22.1, while somewhat higher mean scores characterize the higher order characteristic patterns.

All of the daily grids in the 1946-8/1974 sample were classified as outlined above. Table VIII shows the frequency statistics for the entire catalog covering this period. The catalog itself is presented in Appendix I, and is available as a magnetic tape record at the Arctic Project Office, Outer Continental Shelf Environmental Assessment Program, National Oceanic and Atmospheric Administration, Fairbanks, Alaska. Table VIII shows that the percentage frequencies of the CP's are more evenly distributed than for Table VII, although CP1 is still most frequent by far. Part of this frequency change is due to the minimum SCORE criterion described in the section on classification methods. We see that CP4 became the second most frequent pattern, and that many of the CP's from 5 upwards gained in percentage frequency of occurrence. An exception to this generalization is CP11, which decreased in percentage frequency. CP's 22 and 23 are unclassified days and missing data, respectively.

As noted earlier, one of the problems with this type of classification approach arises from the range of different patterns which are grouped together when intensity effects are removed (s_p) and a range of SCORES qualify a grid as "similar". It is thus desirable to inspect some individual pressure maps for days grouped with given CP's to determine the necessary and sufficient pressure features which define the given characteristic pattern. Sea-level pressure charts from the U.S. Weather Bureau's Historical Weather Map series (1950-1966) were used for this purpose. Pressure features of interest include lows, highs, troughs and ridges, in addition to isobaric curvature and orientation. For example, Figure 17A shows the plotted positions of the low pressure center for days classified as CP1 during October, 1950-1954. Although these centers appear to cluster near the position of the low on the CP1 may (Figure 13), they clearly range over a large area. All of the CP1 days in the five Octobers had a low pressure center somewhere to the south or southwest of central Alaska but many of the low centers were outside the grid sector. Inspection of individual pressure maps for CP1 days in all months showed that the zonal isobaric orientation over NW Alaska with low pressures to the south and high pressures to the north was almost always present. Figure 17B is a plot of low pressure centers for March, 1950-1954 days grouped with CP3. CP3 is much less frequent, overall, than CP1 (Table VIII), but the few cases presented here show a strong tendency for the low centers to cluster in a small area of the northern Gulf of Alaska. Interestingly, this position is similar to the cluster of center for CP1. The primary feature which distinguishes these patterns was found to be the meriodional isobaric orientation over southwestern Alaska for CP3 cases (Figure 13). This condition implies that CP3 low pressure centers must be east of the Alaska Peninsula. The west-east ridge over the Beaufort Sea coast was also present on most of the daily CP3 cases inspected.

TABLE VIII

FREQUENCY STATISTICS FOR 1946-8/1974 CATALOG

Characteristic Pattern	Frequency (Days)	Percent
1	3541	34
2	779	7
3	981	9
4	1174	11
5	603	6
6	532	5
7	349	3
8	329	3
9	377	4
10	216	2
11	40	*
12	185	2
13	154	2
14	141	1
15	233	2
16	93	1
17	160	2
18	61	1
19	106	1
20	59	1
21	82	1
22	220	2
23	55	*

* Less than 1%

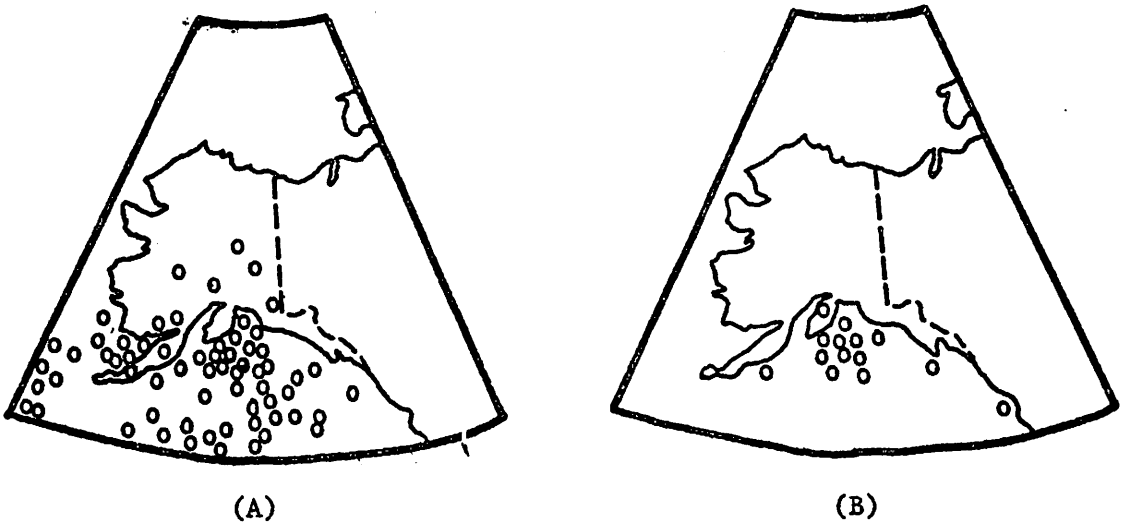

Figure 17: (A) Positions of low pressure centers for days classified as CP1 during October, 1950-1954. (B) Positions of low pressure centers for days classified as CP3 during March, 1950-1954.

Figure 18A shows the locations of high pressure centers for January, 1950-1954 days classified as CP4. A well-defined high pressure center was identified in 24 out of 25 cases. These high centers are fairly closely spaced near the CP4 map position of the high pressure center. The Yukon high pressure system, then, can be taken to be an important characteristic of CP4. Figure 18B shows the location of the low pressure center and trough axis for CP6. The envelope (dashed line) encloses all of the trough axes from 18 individual cases of CP6 during August, 1950-1954. Lows to the west and well-defined troughs with curvature like that on the CP6 map (Figure 13) were identified in all cases, although the actual low center was outside the grid sector in about half of the cases. The four cases cited above serve to illustrate the type of analysis applied to the more frequent CP's. Each daily historical weather map for the period 1950-1966 was inspected for overall similarity to its corresponding CP map. Also, for CP's with identifiable features of circulation on the grid sector, these features were plotted to delimit the variation in their position. The analysis showed that CP's 1, 2, 3, 4, 5, 6, 7, 8, 9, 10 and 15 could be linked with dominant features of circulation and flow directions. The results are listed below.

CP1 is always characterized by low pressures to the south and high pressures to the north, implying easterly surface geostrophic flow along the Beaufort Sea coast. Central Alaska is usually dominated by cyclonically-curved isobars which are zonally oriented over the western part of the grid and meriodional in the southeast.

CP2 has southwesterly surface geostrophic flow across the Beaufort coast, associated with the ridge from the southeast. There is often (not now always) a low pressure center in the northwest part of the grid sector.

CP3 is always associated with the strong Gulf of Alaska low, located east of the Alaska Peninsula. The majority of southern Alaska is under cyclonic curvature around this low. The Beaufort Sea coast is usually influenced by a ridge from the west, although this feature is invariably much weaker than the low.

CP4 is characterized by the Yukon high pressure cell, although in many cases this feature is much weaker than the pressure gradient over the southwestern part of the grid sector, which implies a low pressure center to the southwest of the sector boundary.

CP5 always has a central Alaska ridge from the west or southwest, which separates regions of lower pressures to the north and south. These regions can contain low pressure centers, but the positions of these centers vary greatly from one CP5 case to the next. Westerly flow at the surface is implied for the Beaufort coast.

CP6 is another easterly type along the Beaufort Sea coast. This pattern is always associated with a central Alaska trough from the SW with rising pressures to the north and south of the trough.

The major feature on CP7 days is the pronounced pressure gradient in the northeastern part of the grid sector. The associated low pressure cell is usually off the grid in that direction. A weak ridge along the north Alaskan

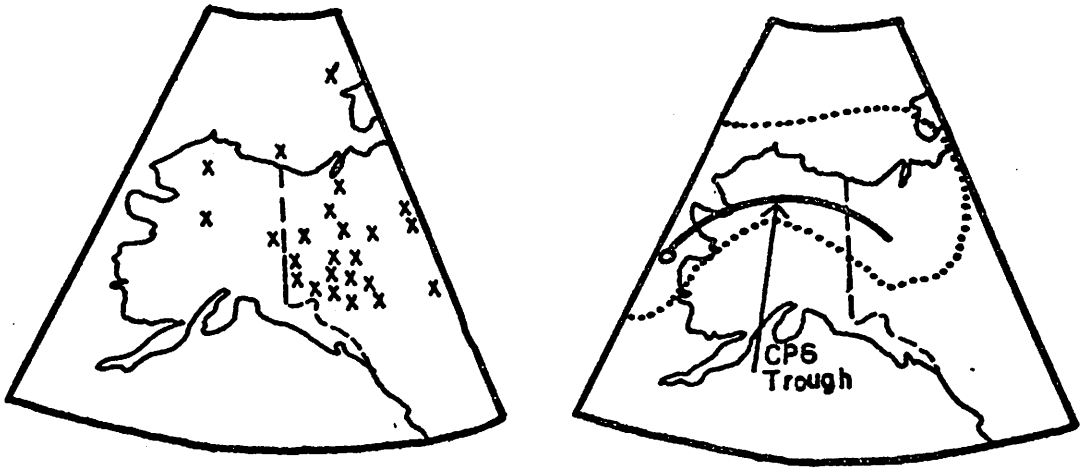

(A) (B)

x - High Pressure Center

••••••••• - Trough Envelope

o - CP6 Low Pressure Center

Figure 18: (A) Positions of high pressure centers for days classified as CP4 during January, 1950-1954. (B) Positions of CP6 low pressure center and trough axis, and envelope containing trough axes for days classified as CP6 during August, 1950-1954.

coastal plain and a weak low system to the south are generally present on CP7 days. Beaufort Sea coast surface geostrophic flow is predominantly NW to W.

CP8 is characterized by a central Alaska-Yukon low pressure system, with rising pressures to the north, west and south. The flow on the Beaufort coast varies from NNW to E. Cyclonic curvature over most of Alaska is another uniquitous CP8 characteristic.

CP9 cases are characterized by a Yukon-Alaska high pressure cell, from which a ridge extends west and southwest across the central part of the state. Pressures are relatively lower north and south from this ridge. Along the Beaufort coast the surface geostrophic flow is predominantly between S and SW.

CP10 always has a low pressure center to the west, although the precise location varies from the Chukchi Sea to eastern Siberia. This feature brings southerly surface geostrophic winds over most of the Beaufort Sea coast.

CP15 is characterized by a Chukchi Sea or East Siberian Sea low pressure cell which troughs eastward over northern Alaska. This feature is generally to the north of the CP10 lows. On the coast the surface geostrophic flow direction is generally S to SW.

Although the remaining CP's may be important for the regional weather variations, their relatively infrequent occurrence and the lack of dominant features of circulation on the CP maps made it difficult to generalize about their characteristics. It was generally found by inspection of the 1950-1966 historical maps that the surface geostrophic flow direction along the Beaufort coast was well represented by the CP maps.

As noted earlier, the magnetic tape listing contains the values of SCORE and s_p for each daily grid. Frequencies of s_p, stratified according to the daily SCORE values, were calculated from the 1946-1974 tape record. From these data the median s_p was determined for each SCORE interval and plotted on a graph (Figure 19). There is clearly a tendency for lower SCORES (i.e., better correspondence between the given daily grid and the CP grid) to be associated with large s_p's, indicative of strong pressure systems. Thus when a given daily pressure grid has a strong pattern of isobars, it tends to bear stronger resemblance to one of the CP's than if it were a relatively weak pattern. From Table VII we saw that first few CP's (in terms of frequency of occurrence) seemed to have lower mean SCORES than the higher order characteristic patterns. Part of this effect is due to the high values of s_p associated with the more frequent CP's. Figure 20 is a plot of median s_p against the CP's, listed in rank order from most frequent to least frequent (for the 1946-1974 catalog). There appears to be a tendency for lower order CP's to have stronger pressure variations over the grid, producing high s_p values.

In summary, we have defined 21 patterns of msl pressures which recur over the study sector through time. Frequencies of occurrence for the patterns show that the great majority of daily patterns are classified with a relatively few CP's. Inspection of 17 years' worth of daily pressure maps and comparison with the corresponding CP maps indicates that a range of patterns is included in each CP group, but that overall the CP maps are good representatives for their constituent daily groups. There is somewhat better pattern definition, pattern strength, and CP-group correspondence for the

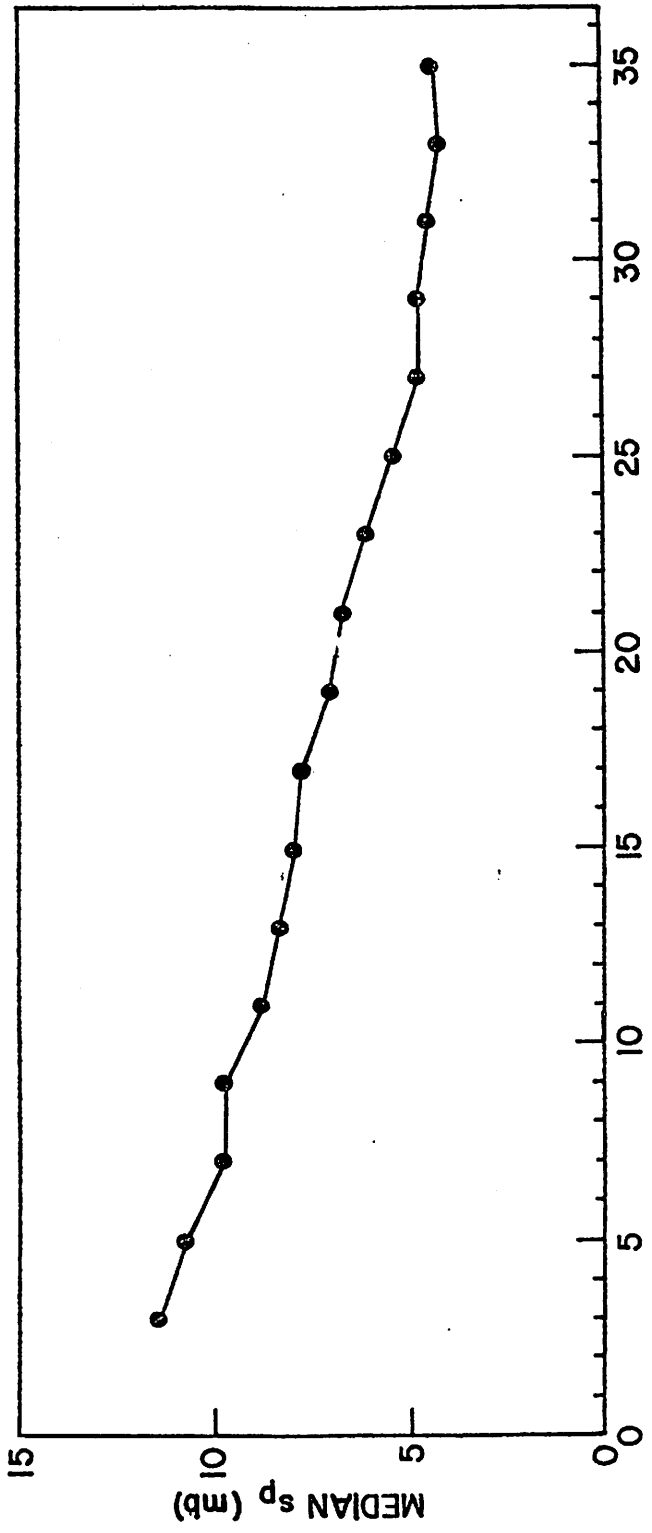

Figure 19: Median Pressure Intensity Index s_p as a Function of SCORE

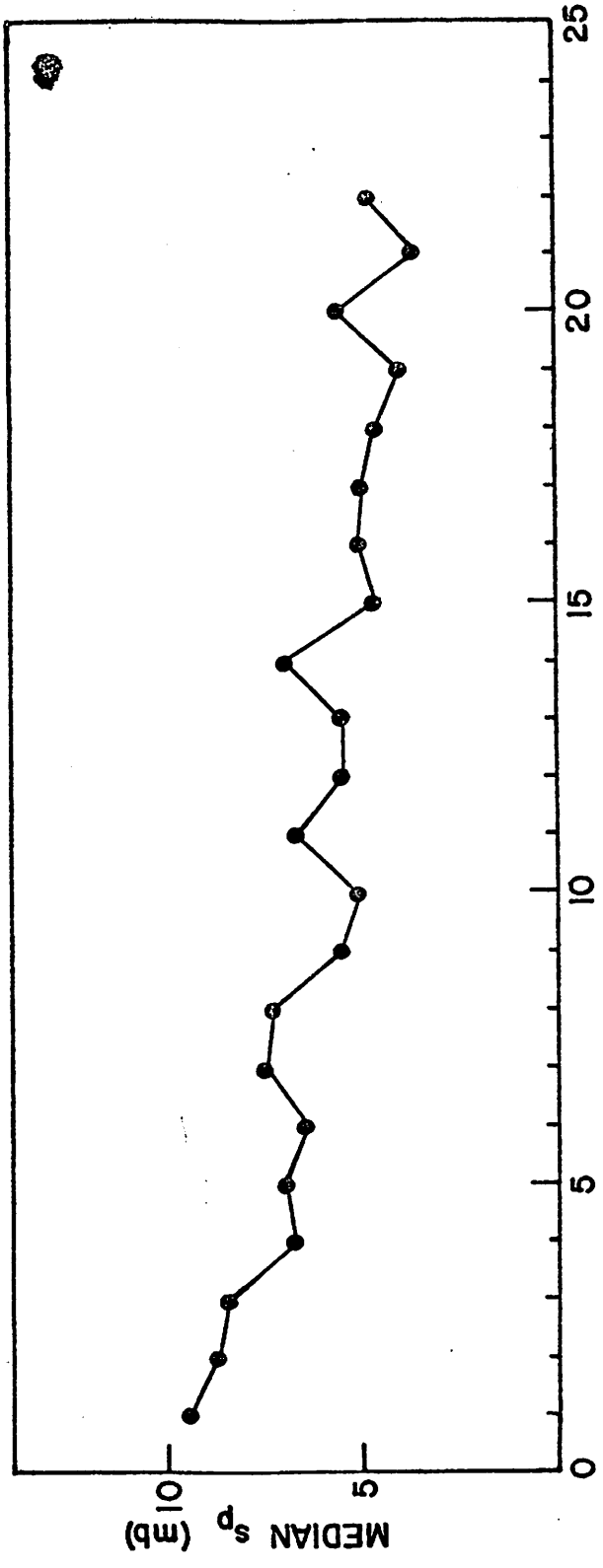

Figure 20: Median Pressure Intensity Index s_p for each CP

first 10 CP's or so as compared to the higher order patterns. Inspection of the CP maps shows that the important pressure features found by other workers, such as Gulf lows, Yukon highs, summer SE ridges, etc. are included in our group of characteristic patterns. The daily catalog of patterns leads naturally to the consideration of seasonal and interdiurnal variations in CP occurrence, which topics are the subject of the following chapter.

CHAPTER FOUR

PRESSURE PATTERN CLIMATOLOGY

Introduction

The daily synoptic catalog developed in Chapter Three leads naturally to consideration of the time series of pressure patterns and related statistics. In this chapter, the temporal characteristics of the regional pressure pattern groups are investigated. Seasonality, persistence and interdiurnal transitions between pressure pattern types are discussed. Seasonal variations in the magnitudes of the pressures and in the intensity of the patterns are also examined. The results are synthesized and compared with previous work to dervive a regional pressure pattern climatology for Alaska's Beaufort Sea coast.

Data

The data for this chapter consist of the 1946-8/1974 daily pressure pattern groups and related statistics on magnetic tape. For each day the list includes date, characteristic pattern, SCORE with the given CP, central pressure, mean pressure, standard deviation of the pressures and number of good data points in the grid. All other data presented in this chapter derive from this source.

Seasonal Pressure Pattern Regime

From the discussion of interseasonal atmospheric circulation changes over the region (Chapter Two) we would expect the monthly frequencies of the CP's to vary between months. From Chapter Three, it is evident that seasonal changes in the overall pressures and pressure gradients in the grid sector could not cause such frequency changes, because the standardizing procedure removes these effects from each daily grid. Therefore, any significant seasonal variations in CP mean monthly frequency must correspond to real shifts in the climatologicasly preferred location and arrangement of the features of circulation. Figure 21 is a plot of mean monthly cumulative percentage frequencies for each characteristic pattern. The expected seasonality shows up clearly on this graph. The months during which the major CP's have relatively constant mean monthly frequencies can be grouped as circulation seasons. Periods of large inter-month changes in CP frequency can be regarded as transitional seasons. In order to accomplish such a grouping of months, an index of intermonth CP frequency change was computed which incorporates the relative frequency of every characteristic pattern (R. Keen, personal comm). The index is given by:

$$(11) \qquad \Delta_{m,n} = \sum_{1}^{23} \left| RF_{i,m} - RF_{i,n} \right|$$

where m and n are the respective months under comparison, $RF_{i,m}$ is the 1946-8/1974 mean monthly relative frequency of occurrence for the "ith" CP in the "mth" month, and the sum is taken over 23 CP's (i=22 for unclassified grids,

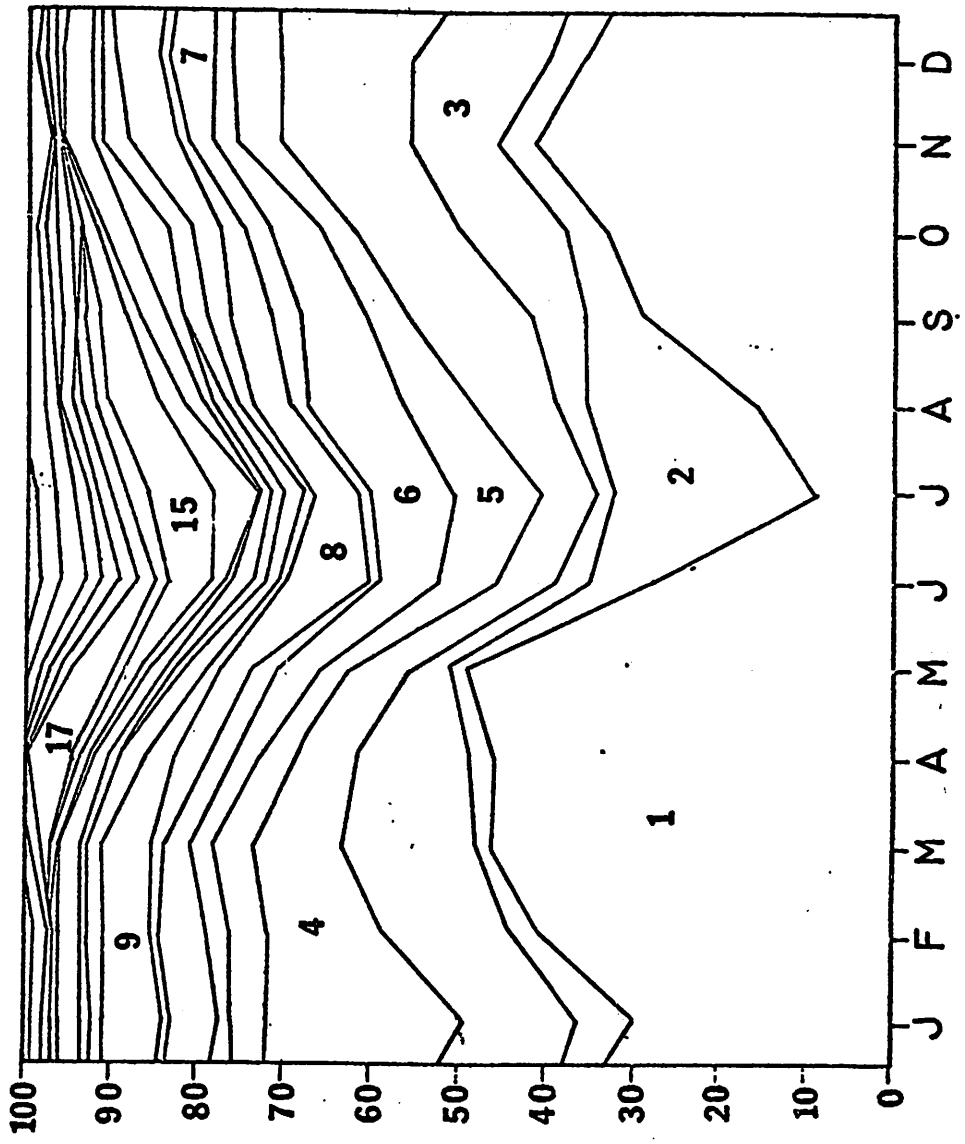

Figure 21: Monthly Cumulative Percent Frequencies of Occurrence for the Characteristic Patterns

i=23 for missing grid data). The index Δ is thus the sum of absolute deviations of relative CP frequencies between months. Relatively large values for these indexes indicate that the two months in question are different with respect to CP occurrence whereas the reverse is true for relatively small values of Δ.

Table IX shows the 12-by-12 intermonthly matrix of the index. The value of Δ for all consecutive monthly pairs (n=m+1) is plotted against month in Figure 22. A first look at Figure 22 shows two periods of strong transition with separate periods of relative stability in CP occurrence frequency. The transitional periods are May through July and August-September. The relatively stable summer circulation season is thus July-August, in accord with the very brief Arctic summer. In fact, the mean monthly temperatures along the Beaufort Sea coast are fairly stable from June to September (Figures 9 and 10), indicating that the summer circulation season is actually shorter than the summer temperature season. A second period of relatively low Δ values occurs for consecutive monthly pairs from September to May, indicating the long duration of the winter circulation regime. The largest values of the index (Table IX) are for between-season monthly pairs (e.g. November-July) which shows that the two stable seasons are very distinct with regard to the mean monthly frequencies of the major CP's. From Figure 21 it is apparent that none of the 10 most-frequent characteristic patterns have pronounced frequency maxima which span the transitional seasons only. The transition seasons, then, seem to be the result of decreasing CP frequencies for patterns of the previous season and increasing CP frequencies for CP's of the following season. Patterns which are distinctly associated with the transition seasons do not appear to be very frequent, with the possible exception of CP17. The monthly pair June-September has the lowest Δ index for all pairs involving June and the second-lowest value for all pairs involving September (Table IX). This fact indicates that the transition seasons are similar to one another with respect to their mean CP frequencies. Both transition seasons, then, appear to be a mix of summer and winter circulation patterns, without distinct patterns of their own. Figures 21 and 22, then, indicate that a fairly stable winter pressure pattern regime obtains between September and May, followed by a transition to more frequent summer types. The summer regime is quite distinct from the winter regime, but lasts only one to two months, followed by another transition where winter types increase and summer types decrease.

Closer inspection of Figure 22 reveals a pronounced spike in the Δ index time series plot in January. December-January and January-February indexes are larger than for adjacent consecutive monthly pairs, so that the month of January may represent a secondary transition season. However, Table IX shows that the mean monthly pressure pattern frequencies of, for example, December and February are more similar to each other than to the adjacent month of January. This is indicated by the relatively higher values of Δ for January-February and December-January than for December-February. Therefore the spike in the time series must represent a brief interruption in the winter pressure pattern regime, rather than a transition from one regime to another. We noted in Chapter Two that the mean monthly temperatures at Barrow and Barter Island showed a slight decrease in the seasonal cooling in January, coupled with greater interdiurnal temperature variability than for surrounding months. The occurrence of a circulation anomaly in this month would also accord with

TABLE IX

VALUES OF $\Delta_{m,n}$

Mo.→	Jan	Feb	Mar	Apr	May	Jun	Jul	Aug	Sep	Oct	Nov	Dec
Jan	0.00	0.33	0.45	0.55	0.77	0.79	1.18	0.95	0.47	0.41	0.37	0.26
Feb	0.33	0.00	0.19	0.28	0.51	0.88	1.26	1.03	0.56	0.38	0.22	0.15
Mar	0.45	0.19	0.00	0.19	0.41	0.89	1.27	1.04	0.63	0.42	0.24	0.26
Apr	0.55	0.28	0.19	0.00	0.32	0.75	1.14	0.93	0.56	0.35	0.29	0.38
May	0.77	0.51	0.41	0.32	0.00	0.56	1.01	0.85	0.52	0.50	0.48	0.59
Jun	0.79	0.88	0.89	0.75	0.56	0.00	0.59	0.50	0.39	0.600	0.78	0.84
Jul	1.18	1.26	1.27	1.14	1.01	0.59	0.00	0.30	0.78	1.00	1.18	1.22
Aug	0.95	1.03	1.04	0.93	0.85	0.50	0.30	0.00	0.55	0.76	0.93	0.99
Sep	0.47	0.56	0.63	0.56	0.52	0.39	0.78	0.55	0.00	0.29	0.45	0.49
Oct	0.41	0.38	0.42	0.35	0.50	0.60	0.99	0.76	0.29	0.00	0.34	0.36
Nov	0.37	0.22	0.24	0.29	0.48	0.78	1.18	0.93	0.45	0.34	0.00	0.22
Dec	0.26	0.15	0.26	0.38	0.59	0.84	1.22	0.99	0.49	0.36	0.22	0.00

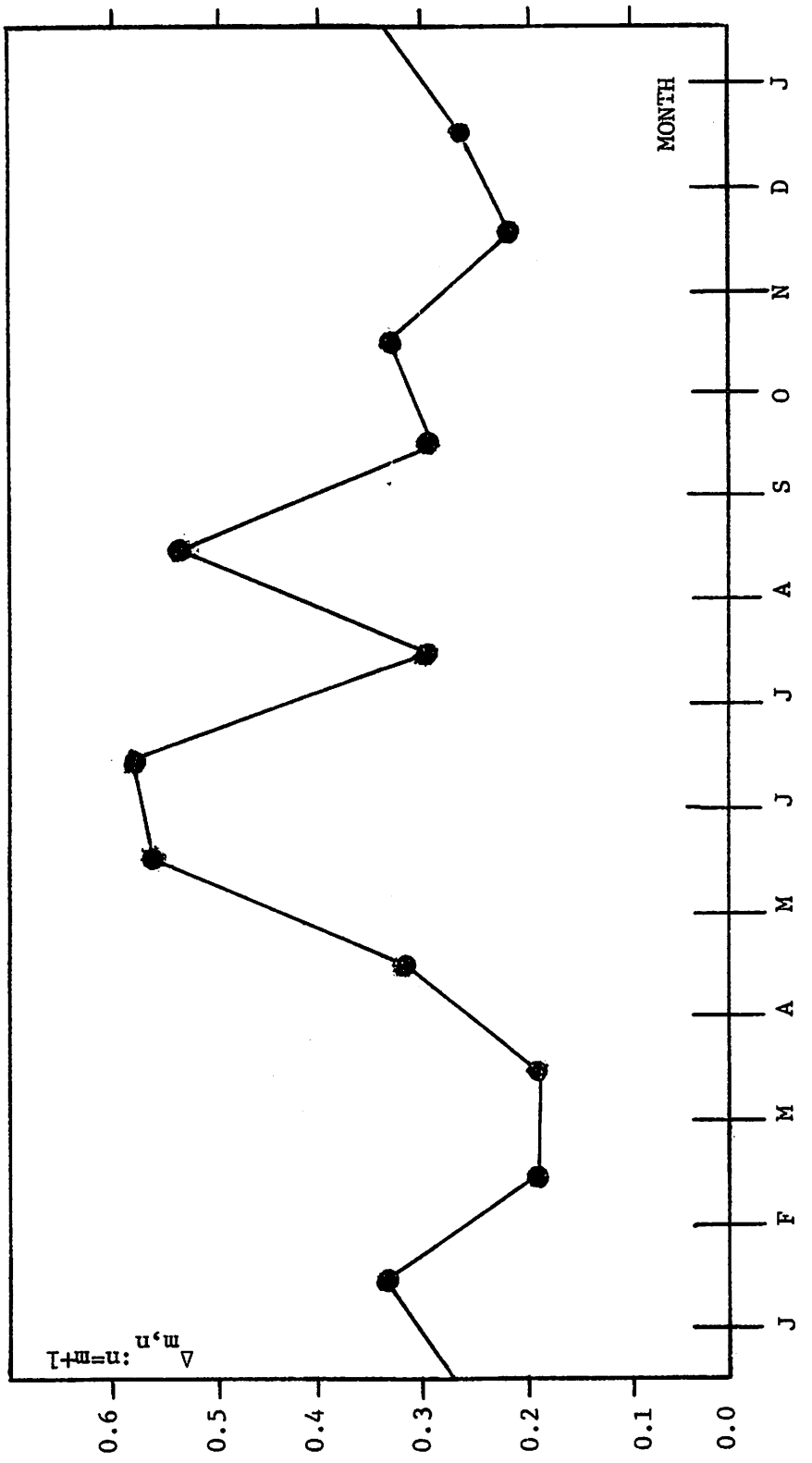

Figure 22: $\Delta_{m,n}$ Index for Consecutive Monthly Pairs

the coreless winter analogy from the southern hemisphere. This possibility is pursued in later sections.

The characteristic patterns which make up the predominant seasonal circulation modes are illustrated by Table X, showing the maximum and minimum monthly mean frequencies of the CP's. Concentrating on those patterns which occur at least five percent of the time in any month, we note that CP1 has its maximum (49%) in May and its minimum (10%) in July. However, these statistics mask the complete dominance of this pattern during most of the winter, which is brought out by Figure 21. The annual oscillation of CP1's mean monthly frequency is the most striking feature of the graph. Between September and May it accounts for a full 39% of the daily pressure patterns, with a secondary maximum in November (42%) and a secondary minimum in January (30%). A set of major characteristic patterns has frequency maxima in the interval December-February, with minima in June and July, including CP's 3, 4, 7, and 9. The major winter pressure patterns consist of these four CP's and CP1 which, taken together, account for 79% of December-February daily patterns. Although all of these CP's are important contributors to the winter regime, their seasonal frequency curves are not identical. Figure 23 illustrates these differences, where mean monthly CP frequency is plotted against month for the winter CP's. CP3 has a similar seasonal frequency curve to that of CP1, except that the pronounced spring frequency decline starts in April-May instead of May-June. Also, CP3 has a slight frequency minimum in November as well as in January. CP4 has a pronounced January maximum (20%) in sharp contrast to CP1. The January interruption in the increase of winter ciruculation patterns, then, is due in part to the CP4 maximum and the CP1 minimum. CP's 7 and 9 are not as frequent as the patterns discussed above, but exhibit a broadly similar seasonal frequency regime. CP7 is less frequent than CP9 during October-January and March-April, but is more frequent during February, May, and August-September. The net result is that CP's 7 and 9 occur almost equally frequently over the entire year (3.3% and 3.6% of days, respectively). Both of these patterns are very infrequent during the summer months. Other characteristic patterns which are important during winter but which do not have frequency maxima at this season are CP's 2 and 5 (about 5% of winter days each).

Table X shows that a second broad group of characteristic patterns has a summer regime, with frequency maxima in June-August and minima between November and March. CP's 2, 5, 6, 8, 14, and 15 are the major patterns in this category, accounting for 51% of the days during June-August and 57% of July-August days. Figure 24 shows the mean monthly percentage frequencies of occurrence for these CP's. CP2 is obviously the dominant summer pressure pattern, with 22% frequency in July and August. CP's 5, 14 and 15 experience their frequency maxima in July, while CP8 is most frequent in June and CP6 in August. CP2 experiences a distinct secondary frequency maximum in January (7%) when it is the fifth-most frequent pattern. Here we have another prominent contributor to the January anomaly. CP5 is also important in winter, occurring on 5% of November-January days. CP's 14 and 15 have frequency curves which are fairly symmetric about their maxima, and are relatively unimportant from September through May.

The only remaining pattern which occurs with at least 5% frequency in any month is CP17, with its maximum in May-June (5%). It is possible that this pattern represents a distinct transition season mode of circulation,

TABLE X

MONTHLY CP FREQUENCY EXTREMA

Month	CP's With Maxima CP#(% Freq.)	CP's With Minima CP#(% Freq.)
Jan	4(20%), 9(7%), 23(1%)	6(2%), 8(1%), 10(1%), 15(1%)
Feb	7(7%)	12(1%), 19(1%)
Mar	none	2(2%), 5(3%), 22(1%)
Apr	10(3%), 19(2%)*	none
May	1(49%), 17(5%)	none
Jun	8(9%), 11(2%), 18(2%), 21(3%)	7(1%), 9(1%)
Jul	2(23%), 5(11%), 14(5%), 15(8%), 16(3%), 20(1%), 22(4%)*	1(10%), 3(2%), 4(6%), 13(1%)
Aug	6(12%), 22(4%)	none
Sep	13(3%)	none
Oct	12(4%), 19(2%)	none
Nov	none	14(1%), 20(1%)
Dec	3(16%)	17(0%)

* indicates a double maximum
CP22=unclassified
CP23=missing data

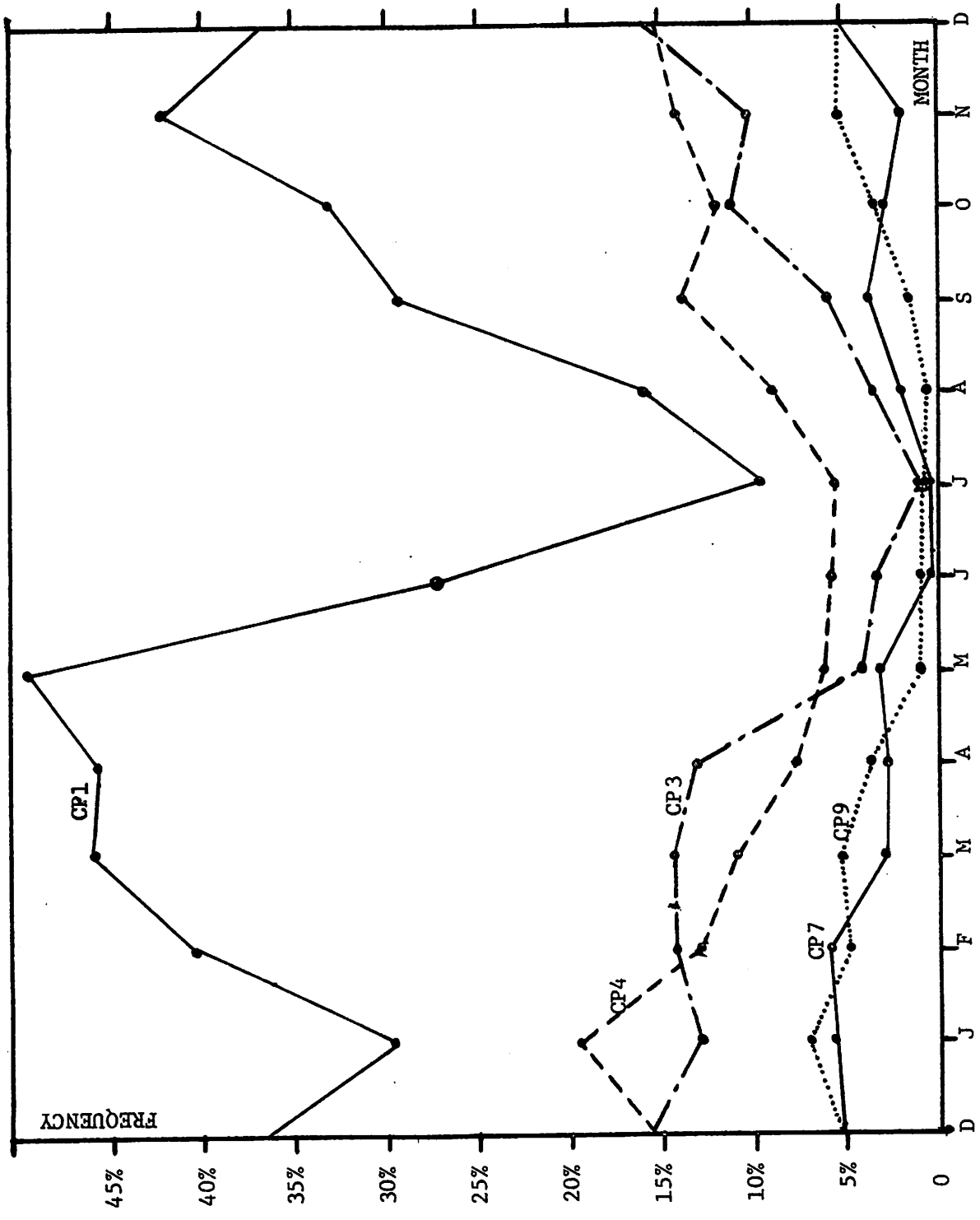

Figure 23: Monthly Percent Frequencies for Major Winter CP's

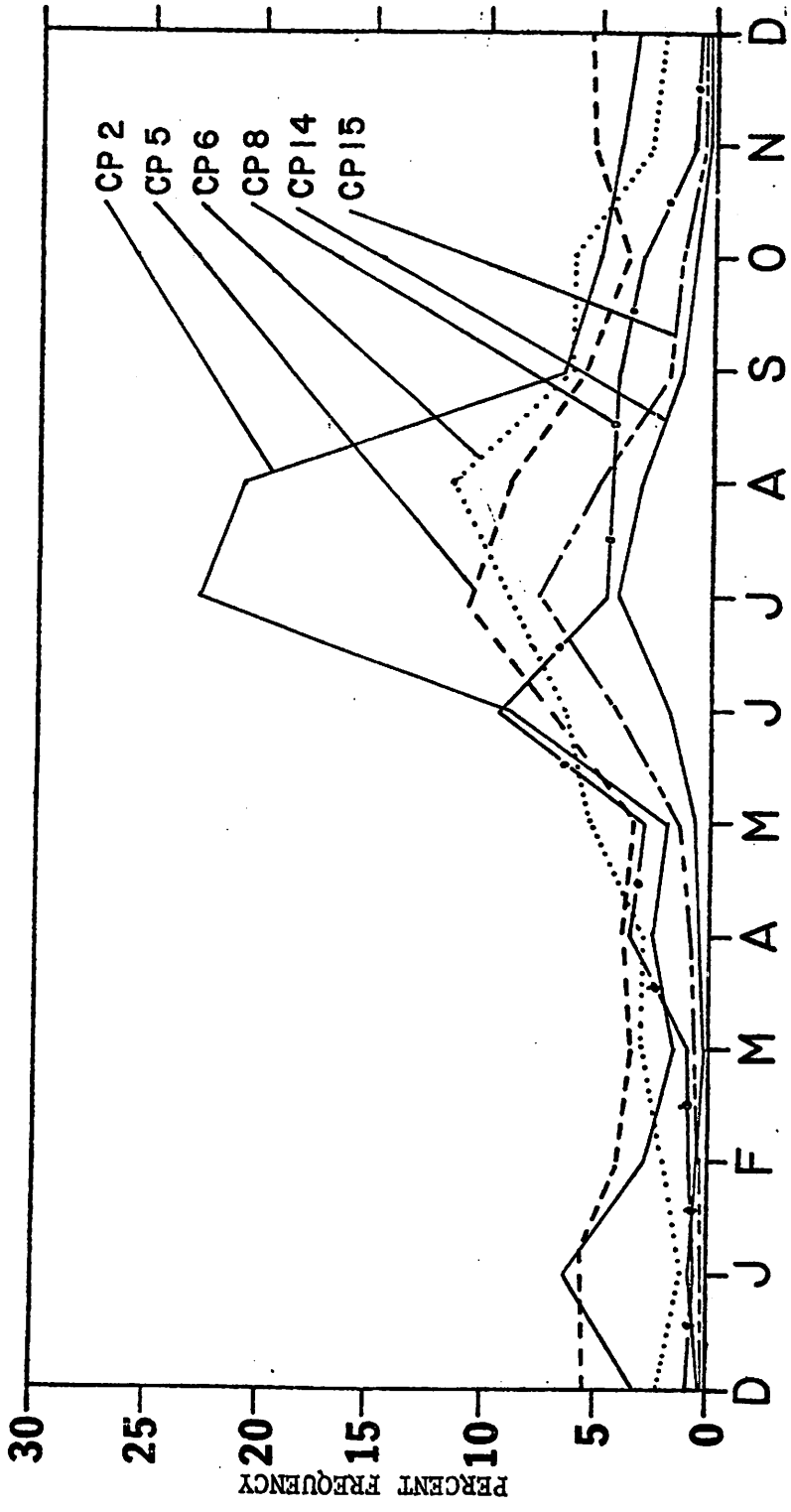

Figure 24: Monthly Percent Frequencies for Major Summer CP's

which occurs as the winter regime shifts to summer. Its relatively low maximum frequency indicates again that the transitional seasons are mainly characterized by decreases in the frequency of CP's from the previous season and increases of following-season CP's, rather than distinct patterns for the transition season only.

In summary, a distinct set of circulation seasons can be defined including winter (September-May), summer (July-August), transition I (May-July) and transition II (August-September). A brief increase of CP's 2, 4, and 5 and a decrease of CP's 1 and 3 create an interruption in the normal winter circulation in January. The transitional seasons are characterized by frequency changes in the patterns of the two main seasons, but do not have distinct patterns of their own. CP17 in transiton I is an exception to this generalization. There are more major summer types (based on 5% minimum frequency) than winter types, but the major winter types account for a higher percentage of days in winter than do the summer types in summer (79% and 57% of days, respectively). The summer circulation season is quite brief, and does not last as long or start as early as the summer temperature season along the Beaufort Sea coast.

Synoptic Aspects of Major Seasonal CP's

Having established the seasonal nature of pressure pattern occurrence, it remains to analyze the major seasonal patterns in terms of the features of circulation on the CP maps. As a first step, we shall attempt to assess the contribution of the major patterns to the mean seasonal pressure fields. In order to do this, the weighted mean standardized grid-point pressures are calculated at each of the 36 points in the study sector for January and July. The variates for the calculation are the respective grid-point values for the four most-frequent CP's in each season, and the weights are the relative frequencies of occurrence for the respective patterns. Figures 25 and 26 show the contoured patterns which result from this procedure. These patterns may be compared with the mean January and July pressure patterns, shown in Figure 27 (from: O'Connor, 1961; Reed and Kunkel, 1960).

The mean January isobars show a striking similarity to our weighted mean map. Both patterns have Gulf of Alaska low pressure centers, zonally-oriented isobars over southern Alaska, and higher pressures to the north. The strongest gradients on both maps are in similar positions also. The only discrepancy in pattern is the northerly location of the high pressure system on the weighted mean map. The four CP's involved in the computations account for 70% of the daily grids in January, and clearly determine the major features of the mean pattern.

The correspondence between the two July maps is good, but perhaps somewhat poorer than the January case. The major reversal of high and low pressure positions from winter to summer was reproduced quite well. Also, the low pressure system on the NNW margin of the grid sector is found on both charts. The importance of CP2 in determining the characteristics of the mean maps is evident in the fact that the southeast high and northwest low are in almost identical locations on the mean July pressure map, the CP2 map and the weighted mean map of July standardized isobars. The relatively weak trough on the weighted mean map is contributed by CP6, and is in agreement

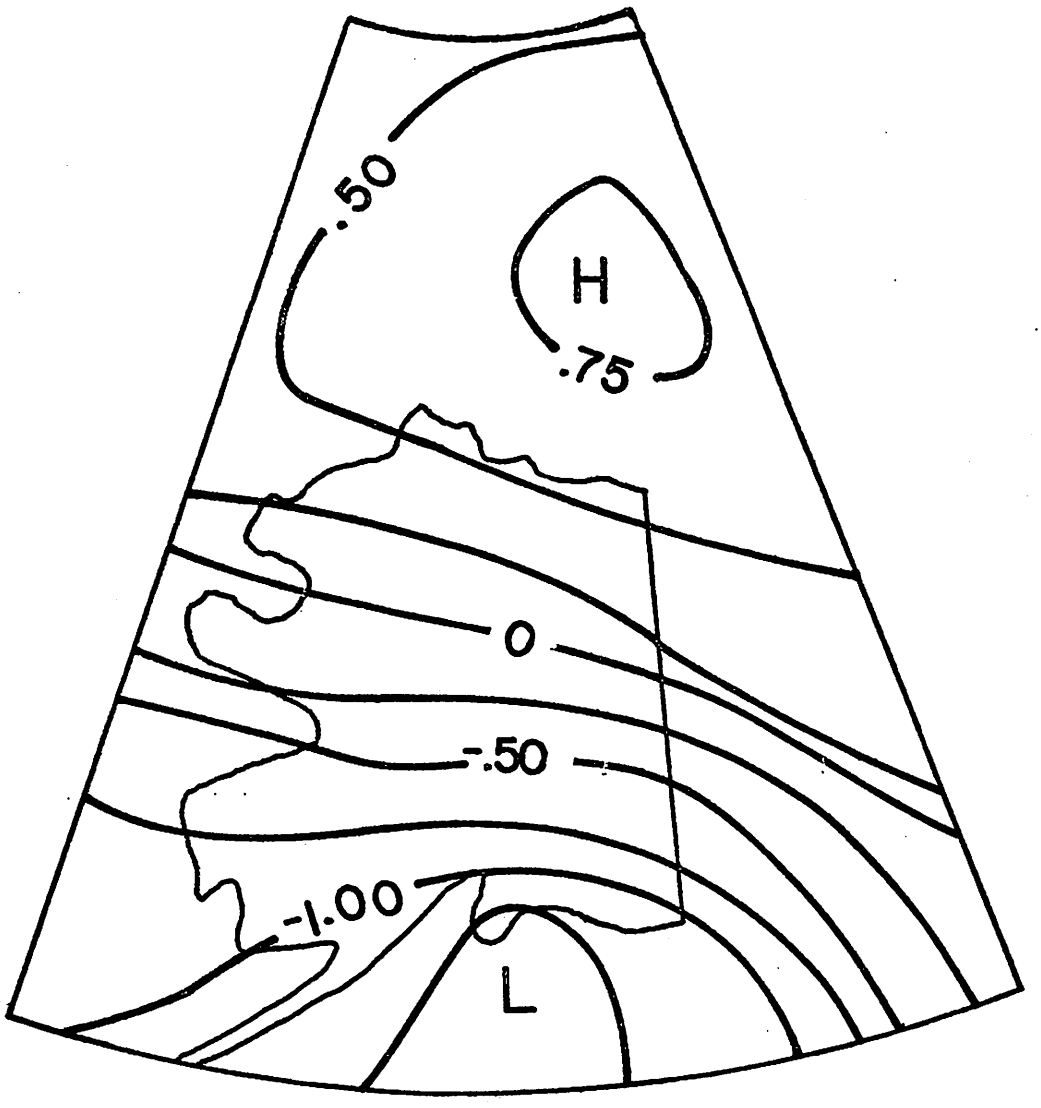

Figure 25: Weighted Mean Standardized

Isobars for CP's 1, 3, 4 and 9

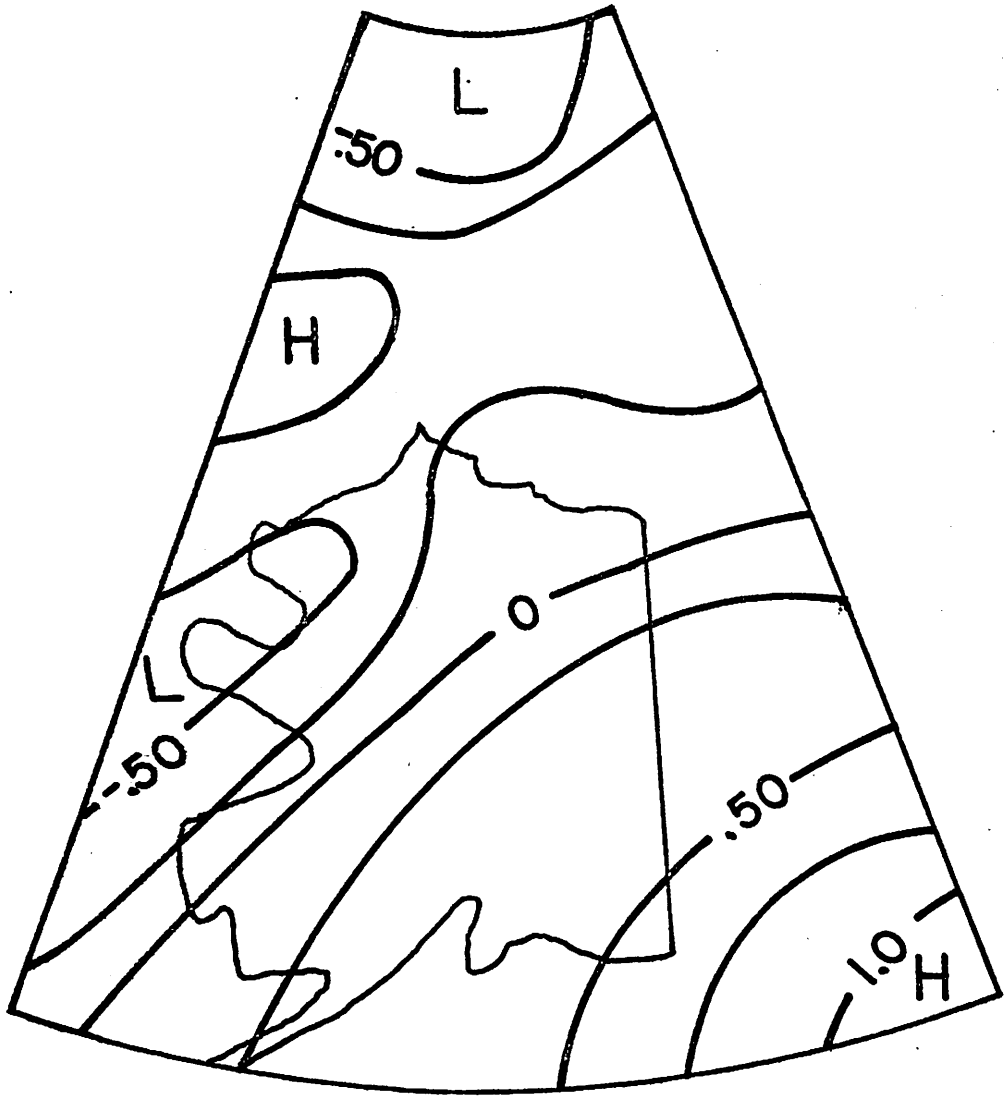

Figure 26: Weighted Mean Standardized

Isobars for CP's 1, 2, 5 and 6

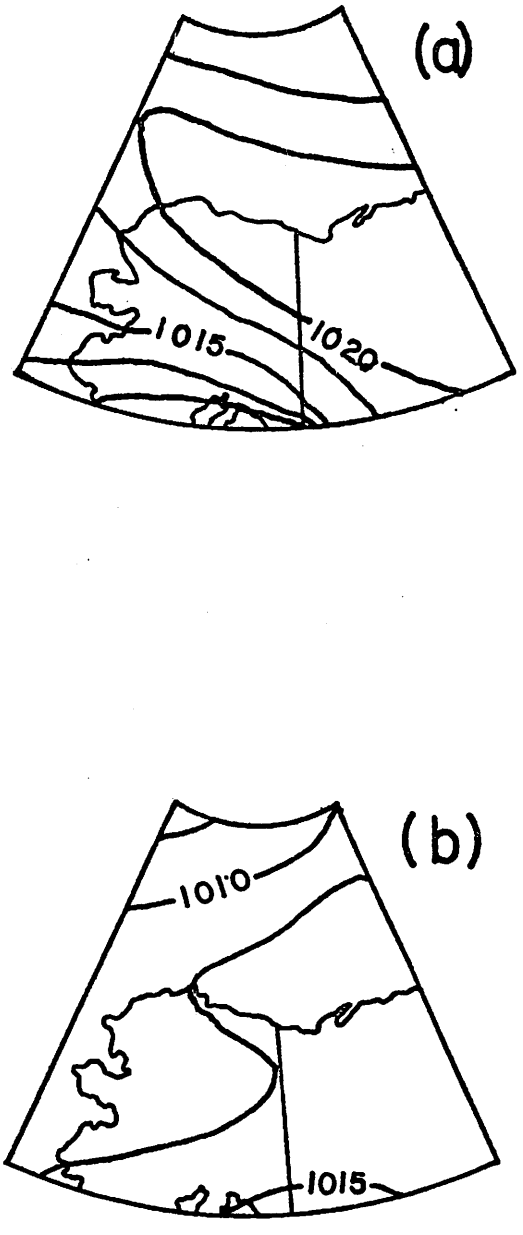

Figure 27: Mean Monthly Sea Level Pressure (mb)

for (a) January and (b) July

with the actual mean July chart. The weak ridge, extending from the southeast across Alaska to Barrow is indicated on both maps also. In summary, it is concluded that a relatively limited number of characteristic patterns which occur frequently determine the broad features of the mean regional pressure field in winter and in summer.It is also worthy of note that CP1 is itself a fair approximation to the mean January isobars, and CP2 compares faborably with the mean July chart. These facts indicate that there are a large number of individual daily patterns which look similar to the mean pattern. Thus the mean January and July isobaric patterns are not mere statistical artifacts.

The major winter CP's include patterns 1, 3, 4, 7, and 9. All of these patterns have low pressure centers or falling pressures to the southwest, south or southeast in the grid sector. This fact is in substantial agreement with the findings of Reed (1959) and Keegan (1958) who noted the frequent arrival and stagnation of cyclonic storms in the Bering Sea-Gulf of Alaska region during winter. Keegan's belt of maximum anticyclone frequency arcs from the Yukon across the Beaufort Sea toward Siberia (see Chapter Two). These areas are occupied by high pressure centers or ridges on CP's 3, 4, 7, and 9 while CP1's influence can be either cyclonic or anticyclonic along the coast, but highest pressures are always in the northern half of the sector. Thus the major winter patterns result from the frequent and often persistent anticyclone/ridge features in the north and the continuous train of cyclones moving through the southern half of the grid sector. Keegan also stressed that cyclones influenced the Arctic Basin much more frequently in winter than was previously though. Patterns 2, 5, and 7 all occur with at least 5% frequency in winter, and all are associated with decreasing pressure to the north, northwest or northeast in the grid sector. These patterns, then, represent the circulation modes within which polar lows influence the northern part of the sector, at least in winter. We note, however, that CP7's northeastern low pressure area is generally cut off from the Beaufort Coast by a ridge from the west.

The broad scale, qualitative similarity between the major winter CP's (lows SW, S or SE, highs and ridges NW, N, NE) illustrates one of the principle advantages of our classification technique over eigenvector or principal component methods. As Blasing (1975, p. 99) states: "Principal component eigenvectors are constrained to be orthogonal to (uncorrelated with) each other, while natural modes of atmospheric behaviour are not necessarily so constrained." Clearly the winter pressure patterns over the study sector exhibit distinct, recurrent modes, but these are far from mutually orthogonal.

The major summer characteristic patterns include CP's 2, 5, 6, 8, 14 and 15. There is considerable variety in the location of circulation features among these major patterns. However, certain features common to some of these CP's are worth mentioning. For example, CP's 2, 6, 8, 14, and 15 have increasing pressures to the south along the southeast margin of the grid sector. These higher pressures may result from the northward shift of the subropical anticyclone during the summer season. Comparison of the mean July msl pressure maps presented by Reed and Kunkel (1960) and O'Connor (1961) for Arctic regions and the northern hemisphere, respectively, shows that the mean ridge from the southeast on Figures 26 and 27 is a northward extension of the Pacific high pressure cell. Bryson and Lahey (1958) have presented a set of climatologically recurring events which define the natural circulation seasons

over North America. They note the disappearance of the Aleutian low during July to late August, in accord with our increase in summer patterns and decrease in winter types. In an earlier study, Bryson and Lowry (1955) noted that this shift is often associated with a rather abrupt transition of the Pacific high from its winter position to its summer position, further north, which occurs around late June. It appears that these large scale shifts cause the summer types to have higher pressures in the southeast section of the grid and a decrease in the frequency of patterns with low pressures over the southern part of the grid sector.

CP's 2, 5, and 14 all have low pressure systems somewhere to the north. These patterns are all at maximum frequency during summer and represent the frequent cyclone passages through the Arctic Basin as presented by Reed and Kunkel (1960) and discussed in Chapter Two. Low pressure cells to the west of Alaska and troughing eastward across the state are indicated for summer by the frequency maxima of CP's 6 and 15 (also CP10 occurs at this season). Recall that CP4 contributes about 6% of the daily patterns in summer, despite the fact that it has a frequency minimum at this season. This fact indicates that lows in the north Pacific-Bering Sea region are also important during the warm season. CP8 is quite distinct from the other summer CP's and is characterized by a pronounced low pressure cell over the Alaska-Yukon border and dyclonic isobaric curvature over much of Alaska. The strong summer maximum and pronounced winter minimum in CP8 frequency indicate the tendency for low pressure systems to decay on the margins of Alaska or to move around the interior in winter. This tendency is in agreement with the review of circulation studies in Chapter Two. Penetration of low systems into central Alaska is much more common in summer. Also, as noted by Streten (1974) and Krebs and Barry (1970), the northern coasts of Alaska and Siberia can be cyclogenetic regions in summer, due to the baroclinicity along the land-ocean boundary. Such cyclogenesis would also be expected to contribute to the more frequent patterns with low pressure systems over central or northern Alaska in summer.

The only characteristic pattern with 5% frequency in some month which is not a dominant winter or summer pattern is CP17, which has its maximum frequency during transition I. It is interesting to note several features of the CP17 map. A southern Bering Sea low is located near the southwest grid margin but higher pressures form a meridional ridge from the southern edge of the sector. CP17 may represent a pattern which illustrates the increasing importance of the Pacific high pressure cell as summer approaches, but which still experiences the influence of Pacific lows from the west. The Beaufort Sea high pressure cell is well represented on the CP17 map. Also, the northern third of Alaska is dominated by a trough connecting the southwest low with another low to the southeast. This type, then, may signal the seasonal shift, when lows begin to penetrate the interior of the state on a more frequent basis. The SCORE between the standardized grids for CP's 1 and 17 is a relatively low 37. The redundancy between these two patterns indicates that CP17 is a modification of the CP1 pattern, wherein the Pacific high pressure cell begins to influence the southern part of the grid sector.

In summary, the synoptic aspects of the major seasonal characteristic patterns are in general agreement with previous work on the circulation over the study region. The circulation regime seems to be remarkably simple in

the first approximation, with northern high pressure features and lows to the south in winter, and a seasonal reveral with a ridge to the southeast and lows to the west, northwest, north and northeast during summer. These seasonal shifts are apparently caused by the large scale wave adjustments between summer and winter, which shift the semi-permanent high pressure cells and the major cyclone tracks.

Interdiurnal Pattern Transitions

A description of the regional circulation should include the major modes of pressure pattern evolution on a day-to-day basis. In this section the interdiurnal transitions of the CP's are examined. An interdiurnal transition sequence is defined by the ordered pair $(I \rightarrow J)$ where I is the characteristic pattern which occurred on a given day and J is the CP which occurred on the following day. Note that $(I \rightarrow J)$ can be any of the 23^2 permutations (CP22= unclassified, CP23=missing grid data), and that there are $N_t - 1$ such ordered pairs for a sample of N_t daily patterns. Thus the frequency of a given transition has units of days. We shall treat the general case of all such transitions, and the special cases of persistence (I=J) and non-persistence ($I \neq J$). A statistical model is developed with which to test the significance of a given transition frequency when compared to a random transition sequence.

In order to assess the day-to-day changes among our CP groups we simply count the number of $I \rightarrow J$ transition sequences and express the frequencies in a 23 x 23 matrix. These matrices were generated for all data and for transitions stratified by month, respectively. The number of $I \rightarrow J$ transitions is $N(I \rightarrow J)$, $N(I)$ is the number of occurrences of CP"i", and N_t is the total number of days for the entire catalog or for a given month over the catalog period, depending on the case under consideration. It is necessary to define certain probabilities in order to assess these transiton sequences. The probability of occurrence for CPI is taken to be its relative frequency of occurrence over the catalog period:

$$(12) \qquad P(I) = \frac{N(I)}{N_t}$$

The conditional probability of occurrence for CPJ, given CPI on the previous day is just:

$$(13) \qquad P_c(J/I) = \frac{N(I \rightarrow J)}{N(I)}$$

Equation (13) can be used for all transitions, including persistence cases when I=J. We also considere cases with the additional condition Φ that I did not persist ($I \neq J$). The conditional probability is:

$$(14) \qquad P_c(J/I,\Phi) = \frac{N(I \rightarrow J)}{N(I) - N(I \rightarrow I)} \quad , \quad I \neq J$$

These probabilities were calculated and printed out in matrix form. They are discussed later in this section.

The occurrence of a given CP or CP transition sequence may be treated as an elementary event with probability π, corresponding, for example, to P in (12). In a given trial, then, we have a "success" if the event occurs. A mutually exclusive elementary event can then be defined which o-curs with probability:

$$\gamma = 1 - \pi \tag{15}$$

For example, the mutually exclusive event which complements "occurrence of CPI" is simply "occurrence of any CP other than I". The sampling distribution which corresponds to such a model is the binomial distribution, where the successive terms of the binomial expansion of $(\gamma + \pi)^n$ give the probabilities of 0, 1, 2, ..., n-1, n successes in a sample of n trials taken from a population wherein π is the probability of a successful trial. For large n this distribution approaches the normal (Gaussian) distribution with mean:

$$\mu = n\pi \tag{16}$$

and standard deviaion:

$$\sigma = \sqrt{n\gamma\pi} \tag{17}$$

(Wonnacott and Wonnacott, 1969, p. 121). Thus σ quantifies as variability in the number of successes we obtain in samples of n trials from a population with known probability π. For our CP transitions the number of successes is in units of days, so we may divide by n to covert to relative frequency or probability:

$$\sigma n = \frac{\sqrt{n\pi\gamma}}{n} = \frac{\sqrt{\pi\gamma}}{\sqrt{n}} \tag{18}$$

If we take a sample of n transition sequences and calculate some probability P from the sample, we can now test the statistical significance of the difference between P and a given probability π by using σ_n. Formally, we may state a null hypothesis, where the sample with probability P was drawn from some population with probability π':

$$H_o : \pi = \pi' \tag{19}$$

Equation (19) is taken to be false if, with greater than 95% probability, P came from a population with probability $\pi' \neq \pi$. Mathematically this may be expressed by the inequality:

$$|\zeta| \equiv \left| \frac{P - \pi}{\sigma_n} \right| \geq 2.0 \tag{20}$$

Now, two characteristic patterns I and J occur independently of one another (interdiurnally) if the conditional probability $P_c(J/I)$ is equal to the unconditional probability P(J) (Wonnacott and Wonnacott, 1969, p. 45). For case I, then, π in Eq. (20) is given by P(J) and we compare with with P(J/I) to assess statistical independence. From (13) P(J/I) is calculated from a sample of N(I) days, which corresponds to n in equation (18). Case I allows

us to treat all cases and persistence cases. For non-persistence cases, the sample probability is given by (14), and the denominator of this equation is substituted for n in (18). The random probability for this case is:

$$(21) \qquad P(J/\Phi) = \frac{N(J)}{N_t - N(I)}$$

which corresponds to π in (20). Case 2, then treats the probability that a given day will be CPJ, given that the previous day was CPI and that I did not persist. If the quantity ζ is less than -2.0 then CPJ tends not to follow I as often as we would expect for a random sequence and the reverse is true for ζ greater than 2.0. For values between these endpoints the observed transition frequency is too close to the random expectation to imply any preferred tendency.

Inspection of the 23 x 23 ζ matrix for case I, all data, showed that persistence is the dominant process on interdiurnal time scales. The null hypothesis (19) was rejected with greater than 99% confidence for all I→I CP sequences and ζ was positive in every case. When stratified by month, all of the major monthly CP's persisted more often then for a random process, again at better than 99% confidence levels. These facts indicate that the case II model should be used to examine transitions between different CP's. Frequency histograms of the duration (in days) of spells of a given CP were generated for inspection. Figures 28 and 29 shows these plots for CP's 1 and 2. The rapid falloff of frequency as duration increases is indicative of an autoregressive process, and may be approximated by a first order Markov chain (Barry and Perry, 1973, p. 239). In such a model, P_o is the conditional probability for a given event, such as the occurrence of CPI, given CPI on the previous day (as calculated in (13)). Assuming that P_o remains constant throughout some sequence of days beginning with CPI then:

$$(22) \qquad P(\geq n) = P_o^{(n-1)}$$

where $P(\geq n)$ is the probability of a consecutive sequence of $\geq n$ CPI days. When $P(\geq n)$ equals 0.5 then 50 percent of the Markov distribution is less than n so the median duration of spells for a given CP is just n days. If we set $P(\geq n)$ equal to 0.5 in (22), take the natural logarithm of both sides and solve n, we get:

$$(23) \qquad n_{0.5} = \frac{\ln 0.5}{\ln P_o} + 1$$

which is a measure of persistence based on the lag-one probability of persistence. Table XI shows the probability $P_c(I/I)$, the median duration $n_{0.5}$, and the case I ζ value for all CP persistences. Also shown are the mean and maximum duration of spells for each CP. The great persistence of CP1 is very striking, as well as the 34 consecutive CP1 days which occurred once in the period of record. There is a considerable drop in the mean, median and maximum durations from CP1 to CP2, but CP's 2-5 are still quite persistent on a day-to-day basis. For the higher order patterns, especially beyond CP9, persistence is less important although still highly significant in a statistical sense (note the ζ's). In Chapter Two the tendency for Pacific low pressure

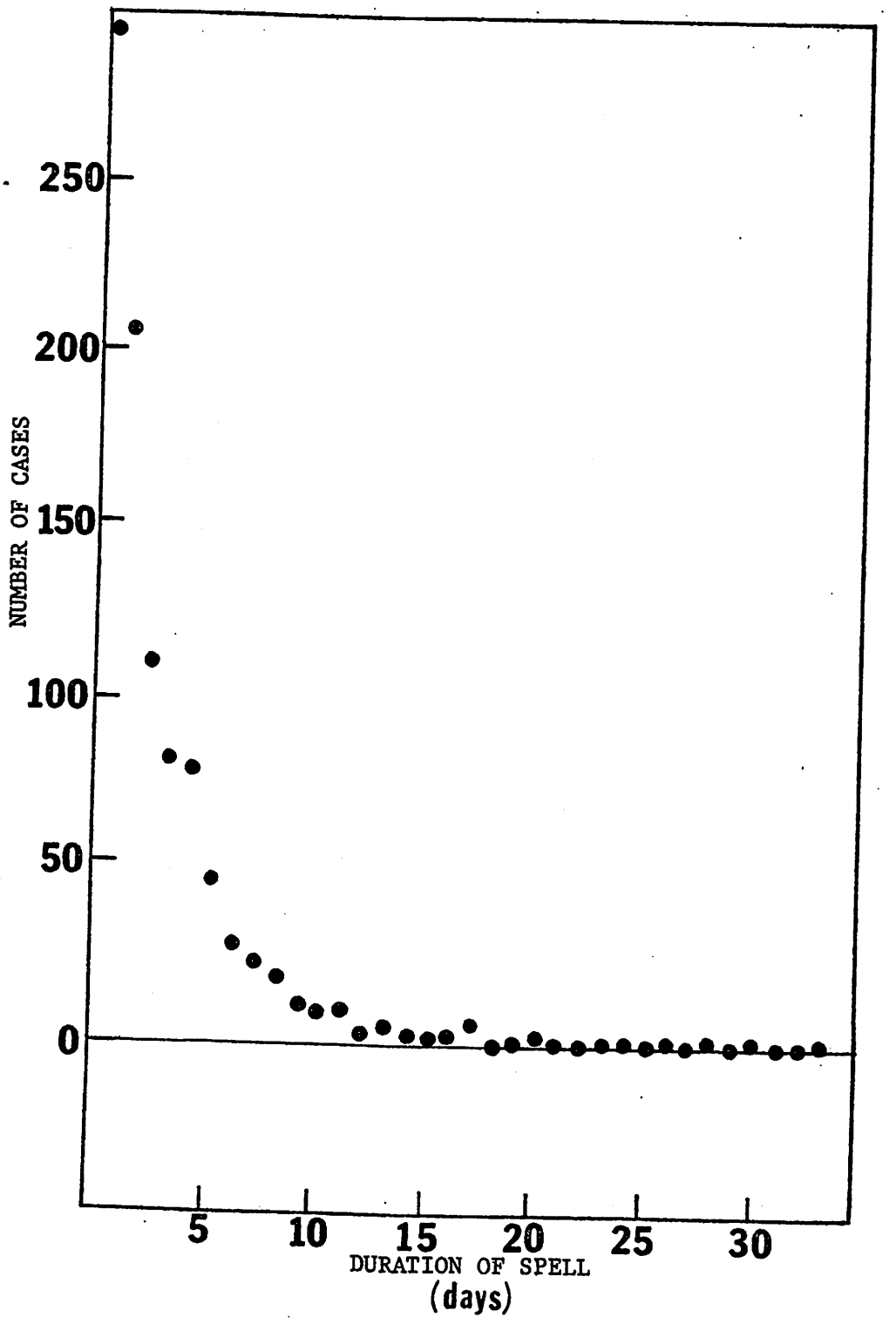

Figure 28: Frequency of Spells: CP1

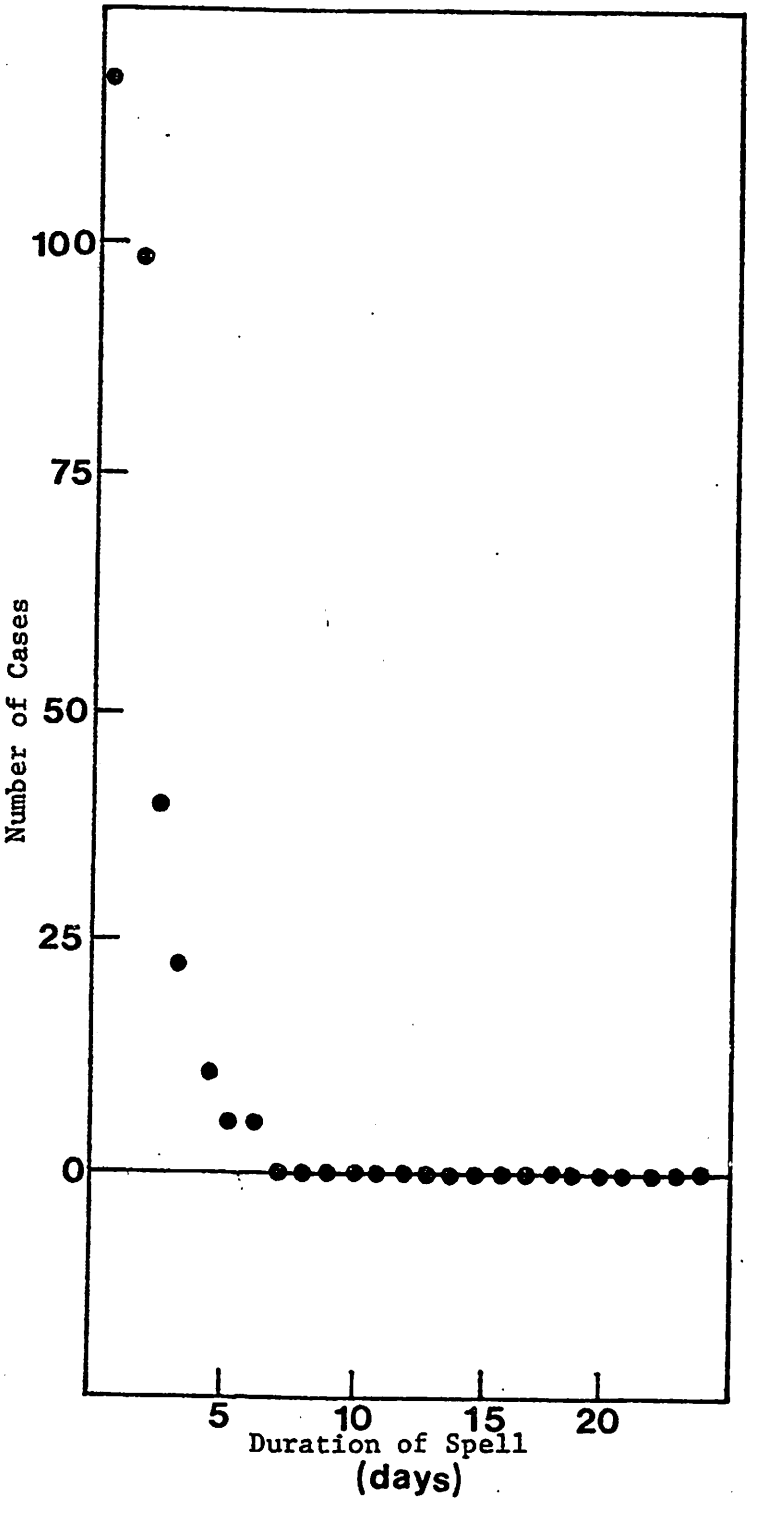

Figure 29: Frequency of Spells: CP2

TABLE XI

PERSISTENCE STATISTICS FOR CHARACTERISTIC PATTERNS

CP	$P_c(I/I)$	Median $n_{0.5}$(days)	Mean Spell Duration (days)	Max. Spell Duration (days)	ζ
1	72%	3.1	3.9	34	48.1
2	46%	1.9	1.9	7	41.2
3	43%	1.8	1.8	8	36.6
4	38%	1.7	1.6	11	28.9
5	40%	1.8	1.7	11	36.6
6	28%	1.5	1.4	5	24.1
7	29%	1.6	1.4	5	26.9
8	27%	1.5	1.4	5	24.5
9	27%	1.5	1.4	5	24.7
10	18%	1.4	1.2	4	16.1
11	13%	1.3	1.1	2	12.4
12	14%	1.4	1.2	3	12.7
13	6%	1.2	1.1	2	5.2
14	16%	1.4	1.2	3	15.4
15	20%	1.4	1.3	5	18.6
16	11%	1.3	1.1	2	10.1
17	14%	1.4	1.2	4	12.6
18	11%	1.3	1.1	3	11.2
19	9%	1.3	1.1	2	8.7
20	10%	1.3	1.1	3	9.9
21	26%	1.5	1.3	4	25.5
22	9%	1.3	1.1	2	7.2
23	25%	1.5	1.3	8	25.6

systems to stagnate after their arrival in the Gulf of Alaska was noted, along with the persistence of northerly anticyclone cells over the study area. The persistence of CP1 clearly supports this picture of the msl circulation evolution. On a seasonal basis, the persistence of the CP's closely parallels their frequency of occurrence. For example, $P_c(1/1)$ is 75% in May during maximum CP1 frequency but falls to 46% in July. By contrast, $P_c(2/2)$ is greatest in July (52%) at CP2 maximum and is reduced to 45% in January. The major summer pattern is thus less persistent, even during summer, than is the major winter pattern during winter. The persistences of all the CP's indicates that a time unit greater than one day might be useful when characterizing the patterns of msl pressure over the Alaska region. However, all of our pressure data and weather observations are in a daily format, so we continue to analyze the climate using the daily time unit.

The great persistence of the first few characteristic patterns complicates the treatment of non-persistence transitions, although the case II model removes persistence effects. The case II transition probabilities for the most probable case with a given initial CP are generally less than 30 percent. Rather, the major seasonal patterns appear to change to two to four other major CP's with about equal frequency, leading to transition probabilities which are so small as to be essentially useless in a forecasting scheme. There are a few notable exceptions to this however, and these are noted below. The transition probabilities do provide some insight into the preferred modes of pressure pattern evolution. Our case II ($I \neq J$) probabilities are calculated from (14) and are compared (using ζ) with the random expectation (21). Figures 30 and 31 are the transition diagrams for all major seasonal patterns ($\geq$ 5% frequency in at least one month). All case II transition probabilities of ten percent or greater are shown by directed arrows, and statistically significant cases with $\zeta \geq 2.0$ are denoted by "s". The most frequent transition from CP4 is to CP1, indicating an eastward displacement of the low pressure center from the Bering Sea region towards the Gulf of Alaska. The $4 \rightarrow 1$ transition sequence occurs significantly more often than at random. Although CP's 7, 3, 6, and 17 do not change to CP1 more often than at random, these transitions are nonetheless quite probable (20%-30%). It is noteworthy that all four of these CP's have low pressure cells or troughs in the Gulf of Alaska-Central Alaska area, indicating that they are somewhat similar to CP1. This concentration is supported by the fact that the mean SCORE between CP1 and these four CP's is 46.2 wheres the mean SCORE between CP1 and all other CP grids is 64.4. It is important to note that CP1 frequently occurs both before and after CP's 3, 4, and 6, which fact, together with the high CP1 persistence, indicates the very limited variability of msl pressure patterns over our study sector for much of the year. It is also noted that the CP4-CP1-CP3 sequence is significantly non-random (and preferred) under case II, and is associated with the eastward progression of a low pressure cell from the Bering Sea to the northeast Gulf. During such a sequence the progressive displacement of the low and accompanying change of isobaric orientation over the southwest-central part of Alaska serve to cut off the Beaufort Sea region from the influence of the southern low pressure systems. A beaufort Sea coast ridge from the west occurs on CP3, indicating dominance by air of Siberia or Arctic Basin origin. Despite statistical significance for the 4-1-3 sequence, the product of $P_c(1/4,\Phi)$ and $P_c(3/1,\Phi)$ is only eight percent, indicating the steadily-diminishing forecast value which characterizes such transition triplets. In general, then, CP1 is associated with the normal persistence of highs or ridges to the north and the stagnation of lows in the

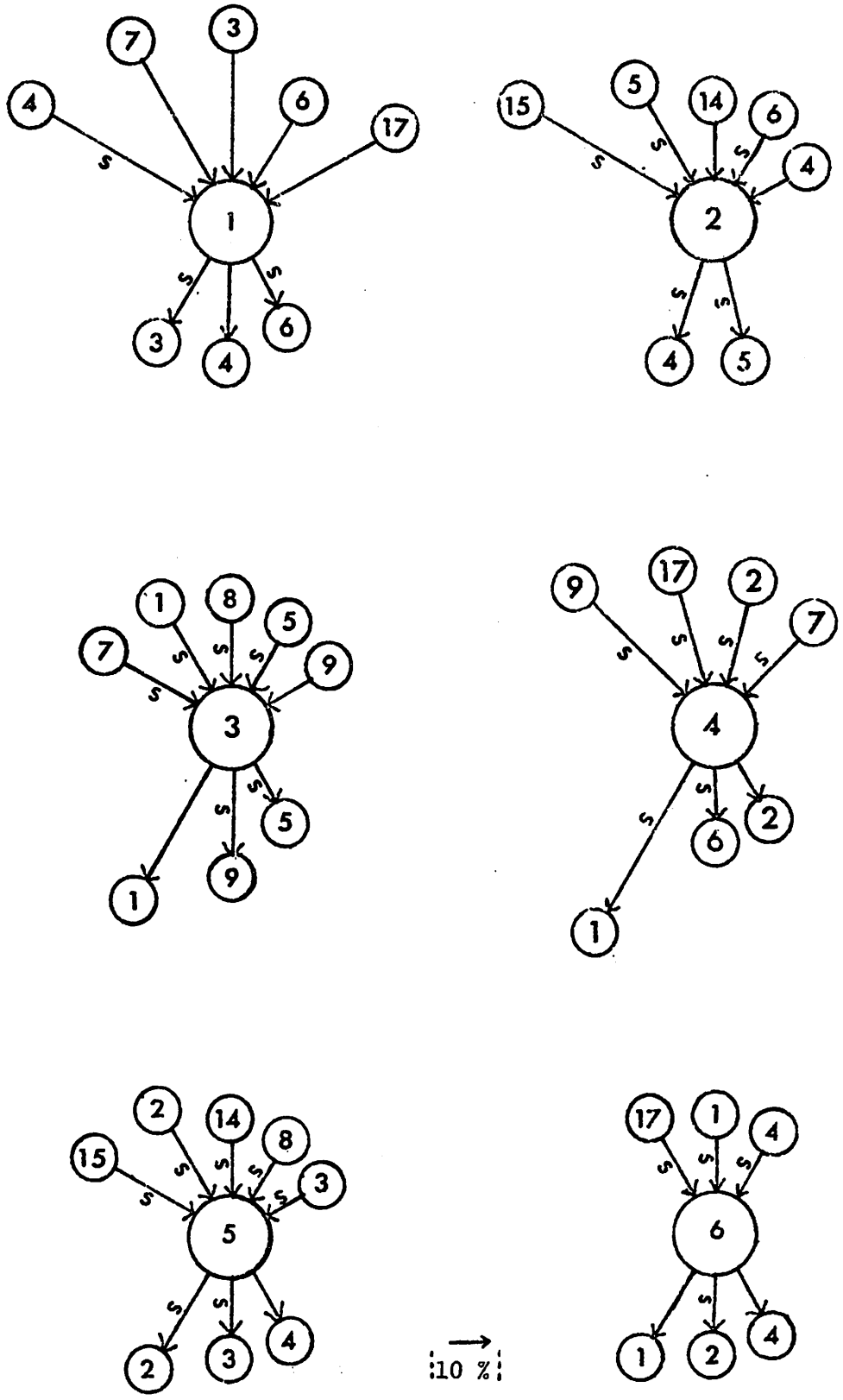

Figure 30: Case II transition probabilities P(J/I,Φ) for all data. Length of arrow is proportional to transition probability. "s" indicates statistical significance: $\zeta \geq 2.0$.

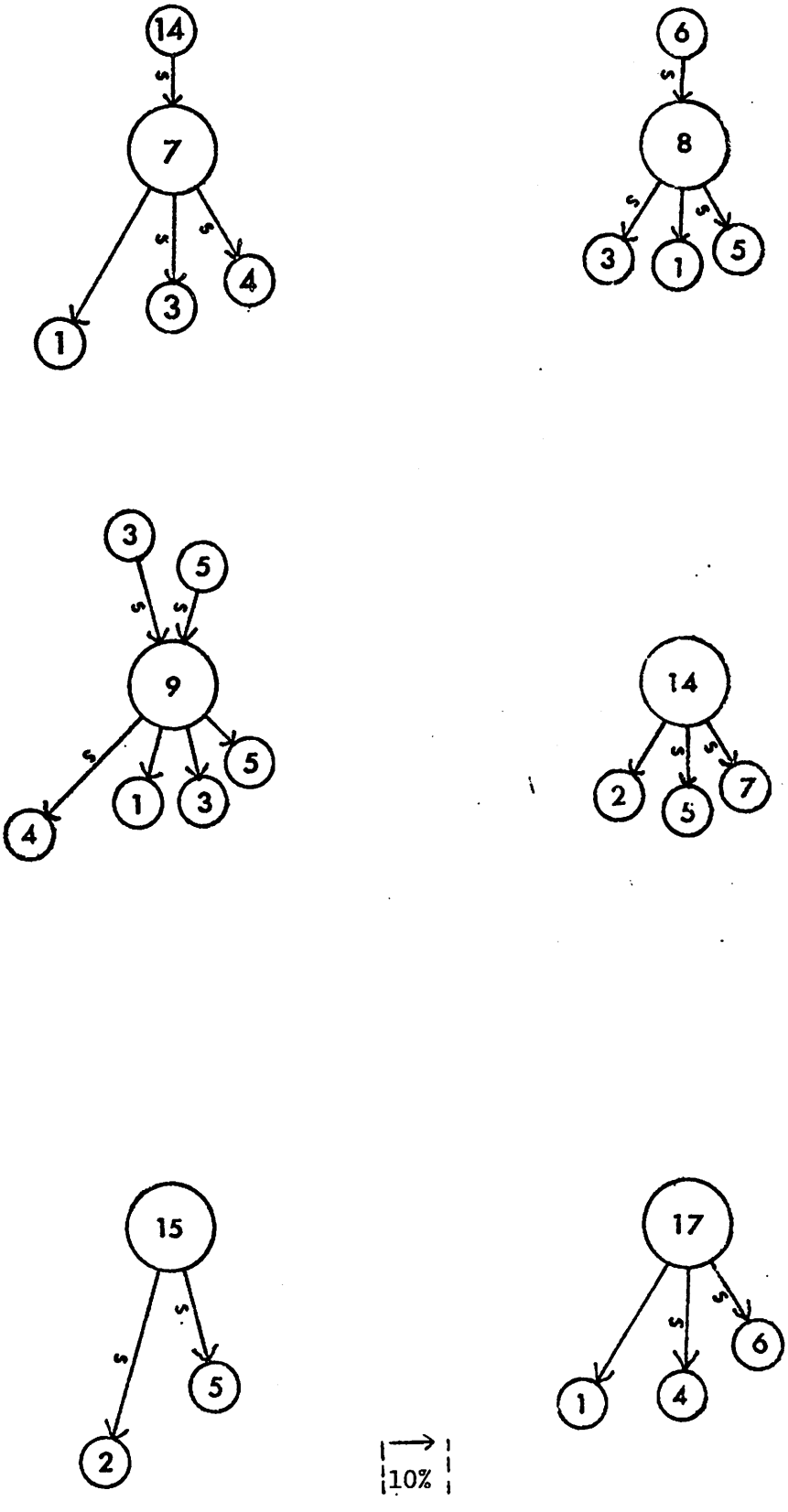

Figure 31: Case II transition probabilities P(J/I,Φ) for all data.

Gulf. A normal sequence consists of CP4, with a low to the southwest, followed by CP1 and then CP3, where the low moves to the northeastern Gulf and a ridge from the west dominates the Beaufort coast. The fact that CP1 frequently leads to CP's which frequently transition back to CP1 indicates the almost cyclic nature of the pressure changes over the region when CP1 is most frequent (winter). Interruptions in this normal chain of transitions (e.g. occurrence of CP's 2 or 5) are not predictable on the basis of our pressure pattern classification alone, although we can specify their relative frequency for the sample. Variations within each CP group (over the range of SCORE) and in the upper atmosphere must determine whether a given CP6 in winter, for example, will change to CP1 or CP2.

CP2 follows CP's 15, 5, and 6 more frequently than expected from random transitions, and also follows CP's 4 and 14 more than 10% of the time that these patterns change to another CP. CP2 is usually characterized by relatively low pressures in the Arctic Ocean north of Alaska and a ridge from the southeast over the state. The northern lows appear to move into the Arctic Basin along the west coast. For example, CP's 4, 6, 14, and 15 have lowest pressures off the southwest or west coasts of Alaska. These transitions to CP2, then, represent the storms on the Bering-Chukchi-Beaufort Sea trajectory. CP2 is highly persistent, but when it changes it is usually to CP's 4 and 5, although not often enough to be useful for forecasting (21% and 20% for case II, respectively).

CP3 transitions to CP1 most often, as do several other CP's. The statistically significant transition from CP3 to CP9 indicates the development of the CP9 high pressure cell from the CP3 ridge. The transition from CP8 to CP3 is characterized by a southward displacement of the central Alaska low. Again, however, we see several major CP's (1, 5, and 9) which occur both before and after CP3, making it difficult to define any specific direction of pressure pattern evolution.

CP4 follows CP9 quite frequently (33%) which change is characterized by a weakened high pressure system being displaced to the south from its CP9 position. A Bering Sea low pressure system begins to influence the southwestern part of the grid sector for this change also. The transition from CP2 to CP4 may indicate that the CP2 ridge exerts a blocking action on the Pacific low pressure systems, so that they enter the southern Bering Sea region and influence the grid sector from that quadrant under CP4. CP4 is somewhat interesting in that it leads to two opposite patterns; CP1 and CP2. The case II probabilities for each month show that CP4 changes to CP1 55% of the time in May but only 15% of the time in July-August. By contrast, the probability of CP2 after CP4 changes from 4% to 18% for these months. This probability change must be related to the shift in the baroclinic zones from winter to summer, as well as adjustments in the mean upper waves. For example, during May the areas north of the Bering Strait are covered by either snow or ice, but in July there is a thermal boundary between the warm coast and cool ocean. The baroclinicity at this boundary may be causing a more frequent transition of lows up the west coast in summer, instead of eastward into the Gulf as in winter. CP6 also follows more frequently from CP4 in July (25%) than in May (9%), supporting this picture of the development. The January circulation interruption mentioned earlier also arises in this regard, because CP4 changes to CP2 18% of the time in January, which is higher

than for any other winter month. Some mechanism, then, causes the southwest lows to move up the west coast more frequently in January than in the other winter months, when the lows move eastward.

CP5 follows from all of the major summer patterns except CP6, and all of these transitions are significant. The fact that CP3 occurs before and after CP5 indicates west-east ridges across Alaska shift erratically north and south, but do not exhibit preferred directions of motion.

CP6 transitions to but not from CP2, indicating a northward movement of the low pressure cell. Since both of these patterns are major summer types, this mode is in agreement with our earlier interpretations of the shift in baroclinic zones from winter to summer. CP6 can also transition to CP1 indicating a displacement of the low to the southeast.

CP7 is primarily associated with the major winter patterns with lows to the southwest, south or southeast and highs or ridges to the north. Accordingly, it changes most often to CP's 1, 3, and 4. The northeastern low pressure area is the main characteristic which distinguishes CP7 from these other winter patterns, and is apparently not as frequently associated with the normal winter pattern as are the southern low and northern high. Thus only CP14, oddly a summer pattern, leads to CP7 more often than at random and more than 10% of the time.

CP8 has a tendency to develop from lows to the west (CP6) which indicates an eastward progression of the low center. CP8 is most frequent in June, and perhaps the low pressure cells which enter the Gulf in winter and the Chukchi Sea in summer are steered in an intermediate trajectory across central Alaska at this season. When CP8 changes to another pattern, it is usually with a southward displacement of the low center, as in CP's 3, 1, and 5.

CP9 frequently develops from CP3, indicating the intensification and eastward displacement of the CP3 ridge from the west. CP9 usually changes to CP4 with a southerly displacement of the high center and a relative weakening of the high compared to other features on the grid.

The final transition sequence of note is the CP15→CP2 system. Given that CP15 occurred and that it changed to another CP, there is better than a 40% chance a CP2 will result over the whole year and a 61% chance in July! This transition is thus quite probable, and further emphasizes the important role of the west coast storm track in summer. However, the situation wherein a low is moving up the west coast is probably easily predicted by dynamical models as well. The real forecast value of the pressure patterns, then, must lie in their associations (as yet unproved) with surface weather in the study region. The sequences of characteristic patterns do, however, provide us with a good descriptive understanding of some of the major modes of pressure pattern evolution on a daily basis.

Pressures and Pressure Gradients

As explained in Chapter Three, our pressure pattern classification routine is designed to compare patterns without taking the pressure magnitudes or gradients into account. From equation (7) it follows that the actual

pressure gradient between any two given grid points I and J is proportional to s_p, the standard deviation of the 36 pressures, as long as the standardized different (P'(I)-P'(J) is constant. This difference varies within CP groups, of course, because of the range of SCORE, but s_p is nonetheless an appropriate index of the pressure gradient intensity for each pattern. Table XII shows the mean values of s_p for each CP in January, May, July and October. The maximum values occur near mid-winter and drop steadily to a summer minimum. Thus the summer pressure patterns are, in general, weaker than those of winter, in addition to being somewhat more variable as noted previously. The winter CP's (e.g. CP1) undergo this weakening as well as the summer patterns. The msl pressure patterns are stronger in early winter (October) than in late winter (May). Kovacs and Mellor (1974) note that "fall" storms are the most severe along the Beaufort Sea coast, in agreement with our pattern intensities. Table XII again brings out the tendency for more intense systems in the first few CP's and weaker patterns among the higher order types. It is also worth mentioning that the most frequent seasonal patterns (CP's 1 and 2) are the most intense CP's during their respective seasons of maximum frequency. This fact again indicates that the two main seasonal patterns are indeed "real" and not a statistical artifact of the calculations.

In Table XIII we present the mean values of the central grid-point pressures p_c (see Figure 12), again listed by CP for January, May, July and October. There is a broad seasonal tendency for the mean pressures of the major CP's to decrease from January through October. The mean January and July msl maps (Figure 27) show a five millibar drop between these months over central Alaska. Of particular interest are the strong pressure drops from July to October for CP's 6 and 8, indicating deeper lows during this season of more intense storms. Note that CP's 6 and 8 occur only rarely in January and May. Inter-CP comparisons in Table XIII show that CP's 2, 3, 4, 5, 7 and 9 are associated with relatively high central pressures, indicating dominance by their respective high pressure cells and ridges over the central part of Alaska. The main winter pattern, CP1, has somewhat intermediate pressure, except during October, when the southern low pressure cell dominates the state. On the Beaufort Sea coast the curvature may be either cyclonic or anticyclonic under this CP. CP's 6 and 8 are apparently the major "low pressure" types over the central part of Alaska.

Summary of Patterns and their Climatology

It has been demonstrated that the sector patterns of msl pressure exhibit pronounced seasonality. Seasonal changes in the system intensities and pressure magnitudes are also evident. The main seasons of the pressure patterns are winter, from September to May, and summer, during July-August. These main seasons are separated by transitional seasons during May-July and August-September. The main seasons are characterized by distinct pressure pattern regimes. In winter the regime consists of lows to the southwest, south and southeast of Alaska with highs or ridges in the northern regions. The summer patterns are more variable than those of winter, but are characterized in general by the northward extension of the Pacific high over the southeast part of the grid sector. The movement of low pressure cells up the west coast of Alaska or into the interior are also very important at this season. The transition seasons are primarily due to the increase of patterns characteristic of the following main season and a corresponding decrease of previous

TABLE XII

MEAN PRESSURE INTENSITY INDEX BY SEASON AND PATTERN

Characteristic Pattern	Mean s_p (mb)			
	January	May	July	October
1	12.2	7.6	5.4	9.3
2	11.2	5.9	5.9	8.4
3	9.8	6.1	4.6	7.9
4	10.7	6.4	5.6	9.0
5	8.1	6.0	5.6	6.8
6	10.8	5.7	4.7	8.2
7	9.1	5.4	4.3	6.3
8	----	5.9	4.2	7.2
9	8.8	5.1	3.4	6.5
10	9.5	5.0	3.3	7.9
11	----	3.4	3.1	----
12	8.4	4.7	3.9	6.1
13	7.9	6.3	4.8	6.6
14	8.7	4.8	4.4	5.8
15	----	6.2	4.8	6.9
16	----	5.0	3.6	----
17	----	5.3	4.7	5.9
18	----	5.5	3.6	5.6
19	6.7	4.5	3.3	5.8
20	----	----	3.6	7.2
21	----	4.2	3.3	4.9
22	4.5	3.5	3.9	4.1

---- insufficient frequency of occurrence.

TABLE XIII

MEAN CENTRAL PRESSURE BY SEASON AND PATTERN

Characteristic Pattern	Mean P_c (mb)			
	January	May	July	October
1	1011	1011	1011	1003
2	1025	1021	1014	1013
3	1022	1020	1017	1009
4	1024	1016	1015	1013
5	1027	1020	1015	1018
6	1005	1009	1007	998
7	1025	1019	1015	1013
8	990	1008	1008	999
9	1032	1026	1018	1021
10	1019	1017	1018	1011
11	----	1015	1012	----
12	1012	1012	1011	1001
13	1010	1011	1010	1006
14	1021	1010	1010	1012
15	1010	1013	1012	1009
16	1005	1016	1016	1016
17	1021	1013	1011	1007
18	----	1006	1004	1008
19	1026	1020	1020	1018
20	1044	1026	1016	1013
21	----	1015	1013	1011
22	1018	1016	1016	1012

---- insufficient frequency of occurrence.

season types. The main interplay between patterns involves CP's 1 (winter) and 2 (summer). CP17 is the only major pattern which occurs mainly in a transition season, with its maximum in May-June, Indexes of inter-month CP frequency change show that the progressive increase of winter patterns is interrupted in January, when CP's 2, 4, and 5 occur more frequently than in adjacent winter months. CP's 1 and 3 show corresponding frequency decreases in January. During the transition from winter to summer low pressure patterns can move into central Alaska more frequently than during winter. This is evidenced by the (CP6→CP8) transitions and the frequency maximum of CP17 which has lowest pressures to the north of the CP1 low. Spring is marked by the increase in the influence of the Pacific high pressure cell, corresponding to the "high jump" phenomenon described by Bryson and Lowry (1955) and the disappearance of the Aleutian low during early summer (Bryson and Lahey, 1958). The more frequent movement of storms over central Alaska and the increasing importance of the west coast cyclone track may be due to the blocking action of this high as well as the baroclinicity of the coastal zone after the sea ice breaks up. The mean January and July msl pressure fields over the sector show patterns which are quite similar to the patterns generated by a weighted mean of the first four CP's in each season. The similarity between the mean fields and the CP1 (in winter) and CP2 (in summer) patterns is fairly good also. These facts indicate that the day-to-day variation of the pressure patterns is not extremely great and that the mean monthly patterns are similar to a large number of individual daily patterns.

Interdiurnal transitions for persistence and inter-CP cases are not random. All major patterns persist, but particularly CP1. In winter the characteristic patterns which frequently precede CP1 (CP's 3, 4, and 6) also follow CP1 frequently, indicating the cyclic, invariant nature of the dominant winter pattern. CP's 2 and 5 do not enter this regular sequence and can be considered to be winter "anomalies". These patterns occur more frequently during January than during other winter months. CP4 often transitions to both CP1 and CP2, so that our model of the msl pressure patterns seems inadequate in terms of distinguishing the pattern precedents to these two major types. Variations in the upper atmosphere, in the msl pressure field outside of our grid, and within the CP4 group (because of the range of SCORE) are all factors which our model does not take into account, but which could determine whether a given CP4 will evolve into CP1 or CP2. The transitional probabilities for our CP's are, in general, too low to be of use in an operational forecasting scheme, but they do provide a better understanding of the pressure pattern evolution than was previously available. The climatological regularities of pattern evolution include the transitions from Beaufort Sea coast ridges to Yukon high pressure cells and the movement of lows from the Pacific through the southern Bering Sea and into the northeastern Gulf of Alaska. These lows exhibit the greatest persistence when located in the central Gulf. During the spring transition season lows move from the southwest into central Alaska. In summer, the paths turn northward up the west coast of the state and into the Arctic Basin.

The static patterns of msl pressure contain implicit information about the weather, including geostrophic wind flow direction, curvature of the isobars, and origin of the systems (most of our lows are from the Pacific, for example). In the following chapter we shall examine the statistical weather characteristics of the pressure pattern groups. Statistical tests are applied to determine whether or not significant weather differences exist between the several CP's.

CHAPTER FIVE

STATISTICAL ANALYSIS OF WEATHER ELEMENTS

Introduction

In this chapter we investigate the daily weather data in relation to the pressure patterns discussed previously. The data are described in the first section. A conceptual model of a weather element as a function of time, space and pressure pattern type is then outlined. A form of the model is applied to dialy local climatological data from Barrow and Barter Island to aid the analysis of the weather characteristics within each characteristic pressure pattern group. The statistical significance of inter-CP weather characteristic differences is tested and measures of central tendency and dispersion are calculated for significant cases.

Data

The data analyzed in this chapter were abstracted from the NOAA publication Local Climatological Data (LCD) for Barrow and Barter Island. The weather variables are listed in Table XIV. To insure accuracy, the data were keypunched and verified, directly from the LCD sheets. The data cards were then listed on the line printer and a random sample of three percent of daily observations was inspected and compared with the original data sheets. Less than one percent of the sample data were in error. The data were then written onto a magnetic tape with all of the daily synoptic pressure pattern information described in previous chapters. All subsequent programs contained data checking statements to eliminate unrealistically large departures from typical values, so that our sample statistics, such as the mean and variance, would not be unduly influenced by any large errors in the bad data. When such anomalous values are encountered in the programs, the variable and the data are printed for inspection so that the original LCD sheet can be consulted. In this manner we decided whether very extreme data are due to punching errors or represent actual weather anomalies. The Barrow LCD cover the period 1/1955-8/1974 while the Barter Island record extends from 12/1961 to 8/1974. The end dates were determined by the availability of the pressure grid data and the lengths of record were determined by the funds for keypunching.

Conceptual Model of Weather Elements

The treatment of climatological time series must begin with the recognition that the variables are intrinsically stochastic or random rather than deterministic in nature (Thom, 1970). That is, such variables conform to the model:

$$x_\nu = (w_\nu + \varepsilon_1) + \varepsilon_2 \qquad (24)$$

where x is a particular measurement or prediction on the weather variable ν, w is the model value of the variable, ε_2 is the error associated with the measurement of ν and ε_2 is a stochastic error term introduced by the (simplified) physical model w. The parentheses in (24) emphasize that w and ε_1 are

TABLE XIV

WEATHER VARIABLES FOR SYNOPTIC CLIMATOLOGY

Variable	Symbol	Units
Maximum Temperature	T_{mx}	^{o}C
Minimum Temperature	T_{mn}	^{o}C
Mean Temperature	$\overline{T}$	^{o}C
Mean Temp. Departure	$\delta\overline{T}$	^{o}C
Mean Dew Point	$\overline{T}_d$	^{o}C
Fog	F	+
Heavy Fog	HF	+
Blowing Snow	BS	+
Precipitation (w.e.)	r	mm
Snowfall	s	cm
Wind Direction*	WD	Degrees**
Resultant Wind Speed	U_r	ms^{-1}
Mean Wind Speed	$\overline{U}$	ms^{-1}
Fastest Mile Speed	U_f	ms^{-1}
00-24 LST Sky Cover	SC	10ths

*Prevailing before 1965, resultant thereafter.

**Clockwise from north, for direction from which the wind blows.

+Occurrence or non-occurrence of the given weather condition.

"... inseparably bound together and cannot be disjoined by the observation process" because both parameters are intrinsic properties of the physical model (Thom, 1970, p. 208). For example, one might wish to predict tomorrow's daily maximum temperature T_{mx} at Barrow, using the long term mean for the date as a prediction. The physical model is simply the annual march of average daily maximum temperatures (w) and the stochastic error term might be the standard deviation of the series of Tmx for the given date. The latter term accounts for the myriad of factors which determine daily maximum temperature but which are not included in the simple physical model. A proper forecast statement for this model is: with probability P, tomorrow's daily maximum temperature at Barrow will be $\overline{T}_{mx}$, plus or minus $\varepsilon_1(T_{mx})$ degrees (we neglect the measurement error). With P=95% we have ε_1 equal to twice the standard deviation of the series, assuming a normal distribution. Thus ε_1 allows for a range of daily maxima which will satisfy the forecast. We note that the entire statement must be couched in probability terms, indicating that we are never certain that the forecast interval will be satisfied (except for the trivial case where ε_1 covers all possible values). All realistic climatological and meteorological investigations which utilize observed data must deal with such stochastic variables, because all of the physical models are simplified versions of reality to some degree. In particular, we treat the variation of weather elements within our CP groups as random processes.

In this study of synoptic pressure patterns, we wish to construct a model which allows for the quantification of CP weather characteristics and for tests of statistical significance of such characteristics. Such a model was proposed schematically by Godske (1959) and forms the basis for many of our computations. Godske recognized the stochastic property of meteorological and climatological variables, but outlined a series of time and space terms which expresses some of the deterministic components. The function may be written as follows:

$$(25) \qquad x_\nu = \phi_\nu(g,s,a,d) + \psi_\nu(g,s,a,d) + \chi_\nu(g,s,a,d) + \varepsilon_\nu(g,s,a,d)$$

for a particular observation x on the variable ν. The terms ϕ, ψ, and χ represent the time dependence of ν on secular, annual and diurnal scale, respectively. ε is again the stochastic error function. The variables g, s, a, and d denote geographical location, secular time (unit: one year), annual time (unit: one day) and diurnal time (unit: one hour), respectively. That space is regarded as one-dimensional need not concern us so long as we realize that each location has its own ensemble of functions for each variable ν. The function ϕ characterizes the trend of ν over some series of years, ψ describes the annual march of daily normals for the variable, χ gives the diurnal cycle of ν and ε accounts for the random scatter of the actual measurements about these expected values. Godske goes on to point out that a fifth function Θ_ν could be added to equation (25) in order to characterize the regular variation in ν according to a system of well-defined circulation patterns. If this fifth term is really a useful addition to (25) then the new stochastic error term ε_ν' should be less than ε_ν. Also, significant differences between the several circulation functions should exist regarding their different effects on ν. Long time series of hourly data would be necessary to carry out a complete analysis according to equation (25). Fortunately, several simplifications may be introduced which allow us to consider some of the climatological problems for the Beaufort Sea coast. In

the first approximation, as suggested by Godske, it is acceptable to ignore the secular function compared to the other terms in (25), particularly if the series is not too long. One longest series (Barrow) is twenty years, so we take it that the secular trend is negligible compared to seasonal and CP differences. The diurnal function may be removed by considering all variables as daily values (mean, maxima, total, etc.). The regular annual function might be expressed as a series of sine and cosine terms, but it is simpler to stratify the data by month, thus removing most of the seasonal variation. Such a stratification has the added advantage that it groups periods of more homogeneous variability than does an harmonic fit. Particularly sensitive variables (e.g. temperature) can be treated as departures from normal for each of the 365 dates, further damping any residual annual variability between the beginning and end of a month. Our weather element model now takes on the very simplied form:

$$x_\nu = \psi_\nu(a) + \Theta_\nu(a,CP) + \varepsilon_\nu'(a,CP) \tag{26}$$

where ψ converts a departure from normal into its real magnitude, Θ accounts for the effects of the month and the characteristic pattern, and ε' is the random variation. The variable a denotes the annual time expressed in months, so we have 12 functions Θ and ε' for each weather element and characteristic pattern. Including cases of missing grid point data and unclassified patterns we have 23 such functions for each month and weather element. In summary, we have removed diurnal effects by considering daily values. The annual variation has been damped by stratifying the data by month and considering sensitive variables as departures from normal. The data are then further stratified according to the occurrence of the characteristic pattern on the corresponding date. The secular trend is assumed equal to zero. If this startification is useful, there should be some significant differences between the several functions Θ in a given month. In the following section we undertake the practical application of this conceptual model to the climate of our study region.

Statistical Analyses

When we consider a given set of 30 daily weather observations in some month we hope to increase the amount of information over the format: one hourly observation per year, which might be used with equation (25). In fact, by considering the day as a zero-order time unit and the month as a sample grouping unit, we have increased our sample size significantly. However, we have no increased our independent cases by a factor of 30, because meterological variables are serially correlated on interdiurnal time scales (Panofsky and Brier, 1968). It has been suggested that the number of degrees of freedom which can be assigned to 30 consecutive daily observations is between about six (Godske, 1959) and ten (Panofsky and Brier, 1968). In order to investigate the effects of persistence in reducing our degrees of freedom, we calculate the linear coefficient of serial correlation for several lags ℓ (in days after the day zero) and for several weather variables ν:

$$r(\ell) = \frac{\Sigma\{(x_\tau - \bar{x})(x_{\tau+\ell} - \bar{x}\}}{\sqrt{\Sigma\{x_\tau - \bar{x}\}^2 \Sigma\{x_{\tau+\ell} - \bar{x}\}^2}} \tag{27}$$

where x_τ is the weather element at time τ, $x_{\tau+\ell}$ is the value at time $\tau+\ell$, and $\bar{x}$ is the mean for the series. The coefficient of determination is defined as the square of the correlation coefficient (Alder and Roessler, 1972, p. 210):

$$d(\ell) = (r(\ell))^2 \tag{28}$$

and is the proportion of the total variance in the series of x that is explained by a least-squares linear relationship with the value of x, ℓ days previously. Multiplying $d(\ell)$ by 100 allows us to express this dependence as a percentage of the total variance, so that we have a good index of the importance of serial correlation in reducing the independence of the daily observations. The quantity:

$$t = \frac{r}{\frac{\sqrt{1 - r^2}}{\sqrt{N - 2}}} \tag{29}$$

satisfies a "student's" t-distribution with N - 2 degrees of freedom, for a correlation coefficient r calculated from N pairs of variates (Alder and Roessler, 1972, p. 213). This statistic allows us to assess the signficance of the difference between $r(\ell)$ and zero, under the null hypothesis that the sample was taken from a population with correlation $\rho(\ell)=0$. Of course, if the serial correlation is zero then no linear relationship exists between the paired variates at the given lag. Tables XV through XXIV shows these statistics for several daily weather variables at Barrow. The sample period is 1968-1973, inclusive, and has been divided into two-month groups (January-February, April-May, July-August, and September-October). The highest serial correlations occur for the several measures of temperature. At lag one over 50% of the variance in daily temperature departures is typically accounted for by autocorrelation effects. Clearly our monthly degrees of freedom must be substantially reduced from 30 in this case. It is also of interest to note that some of the correlations drop off quite rapidly after lag one (e.g. U_r in September-October) while others remain large and highly significant up to and including lag ten (e.g. $\delta\overline{T}$ in September-October). This variation indicates that we cannot assign a single number of degrees of freedom to several different variables in a given month. Seasonal variations for a given variable are also evident in the tables. For example, the northerly component of the daily resultant wind speed $U_r(N)$ is quite persistent in winter but not in other seasons. By contrast, $U_r(E)$, the easterly component, is more persistent in summer and fall than in winter. Several interesting meteorological aspects of these tables will be examined in a later section. For the present, it is clear that the number of independent daily observations in a month depends on the season and the weather variable under consideration, but is definitely less than 30. Godske (1966) has presented an equation for calculating the degrees of freedom for a series of N daily observations with known serial correlation coefficients for lags 1 through N - 1. The modified degrees of freedom N' is:

$$N' = \frac{N}{1 + 2\{\frac{N-1}{N}\rho_1 + \frac{N-2}{N}\rho_2 + \ldots\frac{1}{N}\rho_{N-1}\}} \tag{30}$$

TABLE XV

SERIAL CORRELATION OF BARROW WEATHER DATA: $\delta\overline{T}$

ℓ (days)	r(ℓ)	d(ℓ)	N	t	t(.01)*
(January-February)					
1	.81	66%	350	26.1	2.6
2	.59	35%	344	13.4	2.6
3	.47	22%	338	9.7	2.6
4	.36	13%	332	6.9	2.6
5	.25	6%	326	4.7	2.6
6	.16	3%	320	2.9	2.6
(April-May)					
1	.80	64%	360	25.2	2.6
2	.57	33%	354	13.1	2.6
3	.40	16%	348	8.1	2.6
4	.29	9%	342	5.7	2.6
5	.24	6%	336	4.5	2.6
6	.18	3%	330	3.4	2.6
(July-August)					
1	.73	53%	366	20.4	2.6
2	.54	29%	360	12.2	2.6
3	.45	20%	354	9.4	2.6
4	.39	15%	348	7.9	2.6
5	.31	10%	342	6.0	2.6
6	.25	6%	336	4.7	2.6
7	.21	5%	330	4.0	2.6
8	.16	3%	324	2.9	2.6
9	.19	4%	318	3.5	2.6
10	.22	5%	312	4.0	2.6

*If: $|t| \geq t(.01)$, then there is greater than 99% probability that r(ℓ) comes from a population with $\rho(\ell) \neq 0$.

TABLE XV (continued)

SERIAL CORRELATION OF BARROW WEATHER DATA: $\delta\overline{T}$

ℓ (days)	$r(\ell)$	$d(\ell)$	N	t	$t(.01)^*$
(September-October)					
1	.84	71%	360	29.7	2.6
2	.66	43%	354	16.4	2.6
3	.54	29%	348	12.0	2.6
4	.46	21%	342	9.5	2.6
5	.39	15%	336	7.8	2.6
6	.34	12%	330	6.6	2.6
7	.35	12%	324	6.6	2.6
8	.37	14%	318	7.1	2.6
9	.40	16%	312	7.7	2.6
10	.39	15%	306	7.3	2.6

*If: $|t| \geq t(.01)$, then there is greater than 99% probability that $r(\ell)$ comes from a population with $\rho(\ell) \neq 0$.

TABLE XVI

SERIAL CORRELATION OF BARROW WEATHER DATA: T_{mx}

ℓ (days)	r(ℓ)	d(ℓ)	N	t	t(.01)*
(January-February)					
1	.80	64%	350	24.6	2.6
2	.59	35%	344	13.6	2.6
3	.47	22%	338	9.9	2.6
4	.38	14%	332	7.4	2.6
5	.27	8%	326	5.1	2.6
6	.18	3%	320	3.2	2.6
(July-August)					
1	.67	45%	366	17.3	2.6
2	.49	24%	360	10.5	2.6
3	.41	17%	354	8.5	2.6
4	.37	14%	348	7.5	2.6
5	.29	8%	342	5.6	2.6
6	.19	4%	336	3.5	2.6
7	.18	3%	330	3.2	2.6
8	.13	2%	324	2.3	2.6
9	.16	3%	318	3.0	2.6
10	.20	4%	312	3.7	2.6

*If: $|t| \geq t(.01)$, then there is greater than 99% probability that r(ℓ) comes from a population with $\rho(\ell) \neq 0$.

TABLE XVII

SERIAL CORRELATION OF BARROW WEATHER DATA: T_{mn}

ℓ (days)	r(ℓ)	d(ℓ)	N	t	t(.01)*
(January-February)					
1	.77	59%	350	22.6	2.6
2	.56	31%	344	12.4	2.6
3	.46	21%	338	9.5	2.6
4	.36	13%	332	6.9	2.6
5	.26	7%	326	4.9	2.6
6	.20	4%	320	3.6	2.6
(July-August)					
1	.76	57%	365	22.0	2.6
2	.58	34%	359	13.4	2.6
3	.50	25%	353	10.7	2.6
4	.45	20%	347	9.4	2.6
5	.41	17%	341	8.3	2.6
6	.40	16%	335	8.1	2.6
7	.35	12%	329	6.8	2.6
8	.29	8%	323	5.4	2.6
9	.28	8%	317	5.2	2.6
10	.27	8%	311	5.0	2.6

*If: $|t| \geq t(.01)$, then there is greater than 99% probability that r(ℓ) comes from a population with $\rho(\ell) \neq 0$.

TABLE XVIII

SERIAL CORRELATION OF BARROW WEATHER DATA: $\delta\overline{T}_d$*

ℓ (days)	r(ℓ)	d(ℓ)	N	t	t(.01)**
(January-February)					
1	.55	30%	284	11.0	2.6
2	.51	26%	277	9.8	2.6
3	.38	15%	267	6.7	2.6
4	.39	15%	259	6.8	2.6
5	.34	12%	252	5.8	2.6
6	.40	16%	248	6.8	2.6
7	.34	11%	243	5.6	2.6
8	.34	12%	239	5.6	2.6
9	.39	15%	234	6.4	2.6
10	.26	7%	227	4.1	2.6
(April-May)					
1	.71	51%	346	18.9	2.6
2	.63	39%	339	14.8	2.6
3	.61	37%	332	13.9	2.6
4	.59	34%	325	13.0	2.6
5	.55	30%	318	11.6	2.6
6	.49	24%	311	9.8	2.6
7	.45	21%	304	8.8	2.6
8	.44	20%	297	8.5	2.6
9	.40	16%	290	7.5	2.6
10	.38	15%	283	7.0	2.6
(July-August)					
1	.47	22%	347	10.0	2.6
2	.32	10%	338	6.2	2.6
3	.24	6%	329	4.5	2.6
4	.19	3%	324	3.4	2.6
5	.19	4%	320	3.5	2.6

*$\delta\overline{T}_d \equiv (\overline{T} - \overline{T}_d)$, the daily dew point depression.

**If: $|t| \geq t(.01)$ then there is greater than 99% probability that r(ℓ) comes from a population with $\rho(\ell) \neq 0$.

TABLE XVIII (continued)

SERIAL CORRELATION OF BARROW WEATHER DATA: $\delta\overline{T}_d$*

ℓ (days)	r(ℓ)	d(ℓ)	N	t	t(.01)**
(September-October)					
1	.31	9%	360	6.1	2.6
2	.22	5%	354	4.1	2.6
3	.17	3%	348	3.1	2.6

*$\delta\overline{T}_d \equiv (\overline{T} - \overline{T}_d)$, the daily dew point depression.
**If: $|t| \geq t(.01)$ then there is greater than 99% probability that r(ℓ) comes from a population with $\rho(\ell) \neq 0$.

TABLE XIX

SERIAL CORRELATION OF BARROW WEATHER DATA: $U_r(N)$*

ℓ (days)	r(ℓ)	d(ℓ)	N	t	t(.01)**
(January-February)					
1	.65	42%	308	14.8	2.6
2	.38	14%	300	7.0	2.6
3	.31	10%	292	5.5	2.6
4	.31	10%	285	5.5	2.6
5	.30	9%	279	5.2	2.6
6	.30	9%	273	5.3	2.6
7	.22	5%	268	3.8	2.6
(April-May)					
1	.51	26%	346	11.0	2.6
2	.13	2%	339	2.5	2.6
(July-August)					
1	.51	26%	347	11.0	2.6
2	.21	4%	338	3.9	2.6
(September-October)					
1	.52	27%	360	11.4	2.6
2	.18	3%	354	3.4	2.6

*$U_r(N) \equiv U_r\{COS(WD)\}$, the northerly component of the daily resultant.

*If: $|t| \geq t(.01)$ then there is greater than 99% probability that r(ℓ) comes from a population with $\rho(\ell) \neq 0$.

TABLE XX

SERIAL CORRELATION OF BARROW WEATHER DATA: $U_r(E)$*

ℓ (days)	r(ℓ)	d(ℓ)	N	t	t(.01)**
(January-February)					
1	.60	36%	308	13.2	2.6
2	.32	10%	300	5.8	2.6
3	.28	8%	292	4.9	2.6
4	.17	3%	285	3.0	2.6
(April-May)					
1	.67	45%	346	16.8	2.6
2	.28	8%	339	5.4	2.6
(July-August)					
1	.70	49%	347	18.3	2.6
2	.46	21%	338	9.5	2.6
3	.37	13%	329	7.1	2.6
4	.33	11%	324	6.2	2.6
5	.32	10%	320	6.1	2.6
6	.30	9%	316	5.5	2.6
7	.23	5%	311	4.1	2.6
8	.19	3%	304	3.1	2.6
9	.16	3%	297	2.8	2.6
10	.16	3%	290	2.8	2.6
(September-October)					
1	.67	44%	360	17.0	2.6
2	.45	20%	354	9.3	2.6
3	.34	12%	348	6.8	2.6
4	.25	6%	342	4.8	2.6
5	.20	4%	336	3.6	2.6
6	.18	3%	330	3.2	2.6
7	.15	2%	324	2.8	2.6

*$U_r(E) \equiv U_r\{SIN(WD)\}$, the easterly component of the daily resultant.

*If: $|t| \geq t(.01)$ then there is greater than 99% probability that $r(\ell)$ comes from a population with $\rho(\ell) \neq 0$.

TABLE XXI

SERIAL CORRELATION OF BARROW WEATHER DATA: COS(WD)

ℓ (days)	r(ℓ)	d(ℓ)	N	t	t(.01)*
(January-February)					
1	.55	30%	308	11.4	2.6
2	.24	6%	300	4.3	2.6
3	.14	2%	292	2.4	2.6
4	.17	3%	285	2.9	2.6
5	.18	3%	279	3.0	2.6
6	.20	4%	273	3.4	2.6
7	.17	3%	268	2.8	2.6
8	.16	2%	263	2.6	2.6
(April-May)					
1	.44	20%	348	9.2	2.6
2	.12	1%	341	2.1	2.6
(July-August)					
1	.36	13%	347	7.2	2.6
2	.14	2%	338	2.6	2.6
(September-October)					
1	.41	16%	360	8.4	2.6
2	.14	2%	354	2.6	2.6

*If: $|t| \geq t(.01)$ then there is greater than 99% probability that r(ℓ) comes from a population with $\rho(\ell) \neq 0$.

TABLE XXII

SERIAL CORRELATION OF BARROW WEATHER DATA: SIN(WD)

ℓ (days)	r(ℓ)	d(ℓ)	N	t	t(.01)*
(January-February)					
1	.51	26%	308	10.4	2.6
2	.27	7%	300	4.8	2.6
3	.24	6%	292	4.1	2.6
(April-May)					
1	.53	28%	348	11.5	2.6
2	.17	3%	341	3.2	2.6
(July-August)					
1	.57	33%	347	13.0	2.6
2	.43	18%	338	8.6	2.6
3	.32	10%	329	6.1	2.6
4	.26	7%	324	4.8	2.6
5	.27	7%	320	5.0	2.6
6	.28	8%	316	5.2	2.6
7	.16	2%	311	2.8	2.6
8	.15	2%	304	2.6	2.6
(September-October)					
1	.61	38%	360	14.7	2.6
2	.46	21%	354	9.8	2.6
3	.38	14%	348	7.6	2.6
4	.25	6%	342	4.8	2.6
5	.20	4%	336	3.8	2.6
6	.16	2%	330	2.9	2.6
7	.15	2%	324	2.7	2.6

*If: $|t| \geq t(.01)$ then there is greater than 99% probability that r(ℓ) comes from a population with $\rho(\ell) \neq 0$.

TABLE XXIII

SERIAL CORRELATION OF BARROW WEATHER DATA: U_r

ℓ (days)	r(ℓ)	d(ℓ)	N	t	t(.01)*
(January-February)					
1	.53	28%	308	10.8	2.6
2	.30	9%	300	5.4	2.6
3	.22	5%	292	3.8	2.6
(April-May)					
1	.54	29%	346	12.0	2.6
2	.20	4%	339	3.8	2.6
(July-August)					
1	.42	17%	347	8.5	2.6
2	.15	2%	338	2.7	2.6
(September-October)					
1	.31	10%	360	6.2	2.6
2	.01	<1%	354	0.2	2.6
3	-.08	<1%	348	-1.6	2.6
4	-.14	2%	342	-2.6	2.6

*If: $|t| \geq t(.01)$ then there is greater than 99% probability that r(ℓ) comes from a population with $\rho(\ell) \neq 0$.

TABLE XXIV

SERIAL CORRELATION OF BARROW WEATHER DATA: SC

ℓ (days)	r(ℓ)	d(ℓ)	N	t	t(.01)*
(January-February)					
1	.44	20%	350	9.2	2.6
2	.17	3%	344	3.1	2.6
(April-May)					
1	.63	40%	357	15.4	2.6
2	.38	15%	351	7.7	2.6
3	.29	8%	345	5.6	2.6
4	.25	6%	339	4.8	2.6
5	.24	6%	333	4.6	2.6
6	.21	4%	327	3.9	2.6
7	.16	3%	321	2.9	2.6
(July-August)					
1	.60	35%	366	14.1	2.6
2	.33	11%	360	6.5	2.6
3	.20	4%	354	3.8	2.6
4	.18	3%	348	3.4	2.6
5	.22	5%	342	4.1	2.6
6	.20	4%	336	3.7	2.6
7	.19	3%	330	3.4	2.6
8	.14	2%	324	2.5	2.6
9	.18	3%	318	3.3	2.6
10	.16	2%	312	2.8	2.6
(September-October)					
1	.48	23%	360	10.2	2.6
2	.29	8%	354	5.7	2.6
3	.24	6%	348	4.7	2.6
4	.16	3%	342	3.0	2.6

*If: $|t| \geq t(.01)$ then there is greater than 99% probability that r(ℓ) comes from a population with $\rho(\ell) \neq 0$.

where ρ_i is the serial correlation coefficient at the "ith" lag. The data for these computations were available from the previous tables. N' for the monthly groups and variables are presented in Table XXV, as computed from (30).

We are now in a position to apply some tests in order to determine whether or not our pressure pattern grouping provides a statistically significant discrimination of the weather elements. It has been pointed out (Thom, 1966) that a statistically significant result is not necessarily of any practical significance. However, Thom also stresses that a practically significant result must be substantiated by a statistical test that discriminates the real from the happenstance. At this stage, then, our tests can save us considerable time and effort if it happens that no significant relationships exist between the CP groups and the weather elements. Our conceptual model (equation (26)) gives us some 23 functions θ and ε' for each weather elements and month. These functions should describe the deterministic and random components of weather element variation for each CP. For a continuous variate with a normal distribution, the mean and variance are just such functions. Furthermore, for a set of K stratified samples with sample means and variances $\bar{x}_i^2$ and s_i for i=1,K, the techniques of analysis of variance (ANOVA) are appropriate for assessing the existence and statistical significance of group differnces in the means (Godske, 1959; Godske, 1966). Although these techniques are suited to the second basic problem addressed in synoptic climatology (page 4), their application has been quite limited (Barry and Perry, 1973, p. 290). Qualitatively, the ANOVA procedure is quite simple. The weather element series are divided into sample groups defined by the characteristic pressure pattern which occurs on the corresponding day. For each CP group we calculate the mean $\bar{x}$ and variance s_i^2 of the stratified sample variates about the corresponding group mean (for CP "i"). These quantities s_i^2 are averaged over all of the CP groups to obtain the pooled variance s_p^2. This term is the stochastic variation inherent in our model. The variance of the group means about the total (unstratified) mean $\bar{X}$ is then calculated from the K group means. This term, $s_{\bar{x}}^2$ represents the variation among the several deterministic components of our model (i.e., the CP groups). If our group means $\bar{x}_i$ are very different from one another (large $s_{\bar{x}}^2$) and the pooled (within CP group) variance s_p^2 is comparatively small, then we have identified an important source of variation in the weather element series by grouping the pressure patterns into CP groups. If, on the other hand, s_p^2 is large relative to $s_{\bar{x}}^2$, then the between-group differences are insignificant. Formally, ANOVA involves the estimation of the population variance by two independent methods and the comparison of these estimates (Wonnacott and Wonnacott, 1969, p. 200). The first estimate is just s_p^2, the pooled variance. It can be shown (Wonnacott and Wonnacott, 1969, p. 108) that the variance of the mean for a sample of n variates with sample variance s^2 is:

$$(31) \qquad s_{\bar{x}}^2 = \frac{s^2}{n}$$

We have, in effect, calculated the variance of sample means as our between-groups value $s_{\bar{x}}^2$ so that:

$$(32) \qquad s^2 = n s_{\bar{x}}^2$$

TABLE XXV

PER-MONTH DEGREES OF FREEDOM FOR WEATHER VARIABLES

	N' (days per thirty)			
Variable	Jan-Feb	Apr-May	Jul-Aug	Sep-Oct
$\delta\overline{T}$	5.9	6.2	5.7	4.7
T_{mx}	5.9	---	7.9	---
T_{mn}	6.0	---	5.0	---
$\delta\overline{T}_d$	5.7	4.4	9.0	12.6
COS(WD)	8.7	11.6	13.8	13.5
SIN(WD)	10.2	12.3	6.9	7.0
U_r(N)	6.6	10.8	11.3	12.4
U_r(E)	8.8	10.5	6.0	6.9
U_r	9.8	12.5	13.4	17.3
SC	13.6	7.1	7.7	10.0

---Serial correlation not calculated because of within-month trend for the variable at this seasnn.

is a second estimate of the population variance. If all of our sample groups come from the same population with mean μ and variance ρ^2, then s^2 from (32) and s_p^2 are estimates of the same quantity. Since our groups are all from the same population we have:

$$(33) \qquad H_o: \mu_1 = \mu_2 = \ldots = \mu_k = \mu$$

as a null hypothesis. For such a set of k samples the ratio:

$$(34) \qquad F = \frac{s^2}{s_p^2} = \frac{n s_{\bar{x}}^2}{s_p^2}$$

satisfied an F-distribution with k - 1 degrees of freedom for the numerator and N - k degree of freedom for the denominator (Wonnacott and Wonnacott, 1969, p. 201), where N is the total number of variates for all of the groups. If our null hypothesis (33) about the population is true, F should be about one. For F sufficiently larger than one we must reject H_o in favor of the alternative hypothesis H_1 that some of the group means are different. The equations used in this study are of different computational form than described above because of unequal sample sizes for the CP groups and the necessity of computer programming. However, the resulting F-ratio is identical to (34). The complete equations as programmed were taken from Alder and Roessler (1972, pp. 294, 303). Tables XXVI-XXX show the results of the ANOVA calculations for some of our weather variables. Not all of our variables are consistent with the requirements of ANOVA (normal distribution, homogeneous variances, continuous variates). Alder and Roessler (1972, p. 307) note, however, that ANOVA is a fairly robust statistical test, giving adequate results for data which do not depart radically from the first two requirements above. Precipitation measurements characteristically exhibit a "J-shaped" distribution wherein frequency drops off for progressively larger totals on a daily basis. Sky cover often exhibits a "U-shaped" distribution, with maximum frequencies for clear and overcast conditions. Wind direction is a circular variable, requiring special methods of statistical analysis. Thus other, non-parametric, methods of analysis must be applied to data which do not meet the requirements of ANOVA. With these remarks in mind, it is immediately obvious from the ANOVA tables that our characteristic pressure pattern groups contain statistically significant weather element information.

The F-ratio for mean and maximum daily temperature departures indicates that some highly-significant inter-CP differences exist in all months. The largest F statistics are for mid-winter months, while the minima occur in June or September. Highly significant differences between CP's exist in all months with regard to mean daily wind speed $\bar{U}$, although the distinctions between CP's are not as good as for temperature. The month of best wind-CP correspondence is June, in contrast to the temperature data. Dew point depressions do not correspond to the CP's as well as the other variables. Highly significant differences between CP mean dew point depressions occur in April and July through September, but not during other months. In summary, then, the tables show that:

1) The pressure pattern classification yields highly significant differences between weather element means, stratified by CP groups. The best

TABLE XXVI

ANOVA RESULTS FOR BARROW DATA: $\delta\overline{T}$

Month	Number of CP's	N	N'	s^2	s^2_p	F	F(.01)*
January	19	620	103	665.3	48.3	13.8	2.3
February	18	565	92	403.3	42.0	9.6	2.3
March	20	620	102	221.6	32.3	6.9	2.3
April	21	600	102	269.9	23.3	11.6	2.3
May	22	620	105	78.1	11.5	6.8	2.3
June	22	600	97	26.3	5.5	4.8	2.3
July	22	620	95	81.4	8.2	9.9	2.3
August	21	620	96	66.6	10.0	6.6	2.3
September	21	570	66	40.5	7.3	5.6	2.3
October	21	589	70	142.7	23.2	6.2	2.3
November	18	570	76	210.8	35.8	5.9	2.3
December	18	589	89	495.0	41.6	11.9	2.3

*If: $F \geq F(.01)$ then there is greater than 99% probability that some of the sample means for the CP groups come from populations with different means.

TABLE XXVII

ANOVA RESULTS FOR BARTER ISLAND DATA: $\delta\overline{T}$

Month	Number of CP's	N	N'	s^2	s_p^2	F	F(.01)*
January	18	403	67	680.7	47.0	14.5	2.5
February	19	367	60	239.0	50.2	4.8	2.5
March	22	403	67	216.5	33.8	6.4	2.5
April	22	390	66	192.3	26.2	7.3	2.5
May	23	403	68	92.0	12.0	7.7	2.5
June	23	390	63	16.5	4.9	3.4	2.5
July	23	403	62	49.5	6.7	7.4	2.5
August	22	403	62	41.4	6.7	6.2	2.5
September	21	360	42	31.9	5.9	5.4	2.5
October	22	372	44	104.9	22.0	4.8	2.5
November	18	360	48	156.6	29.7	5.3	2.5
December	19	372	56	472.5	42.5	11.1	2.5

*If: $F \geq F(.01)$ then there is greater than 99% probability that some of the sample means for the CP groups come from populations with different means.

TABLE XXVIII

ANOVA RESULTS FOR BARROW DATA: δT_{mx}^{*}

Month	Number of CP's	N	N'	s^2	s_p^2	F	F(.01)**
January	19	620	103	920.3	55.1	16.7	2.3
February	19	565	92	556.7	49.9	11.2	2.3
March	22	620	102	278.1	36.2	7.7	2.3
April	22	600	102	343.3	30.1	11.4	2.3
May	23	620	105	109.0	14.5	7.5	2.3
June	23	600	97	78.2	12.4	6.3	2.3
July	23	620	95	176.1	18.1	9.8	2.3
August	23	620	96	113.1	16.5	6.9	2.3
September	23	570	66	54.5	11.2	4.9	2.3
October	22	589	70	192.3	24.9	7.7	2.3
November	19	570	76	291.5	42.9	6.8	2.3
December	19	589	89	626.4	44.8	14.0	2.3

*$\delta T_{mx} \equiv (T_{mx} - \overline{T}_{mx})$, where $\overline{T}_{mx}$ is the monthly mean maximum of daily temperatures.

**If: $F \geq F(.01)$ then there is greater than 99% probability that some of the sample means for the CP groups come from populations with different means.

TABLE XXIX

ANOVA RESULTS FOR BARROW DATA: $\bar{U}$

Month	Number of CP's	N	N'	s^2	s_p^2	F	F(.01)*
January	20	620	183	32.1	5.8	5.5	2.0
February	18	565	164	26.9	4.8	5.6	2.0
March	22	620	185	18.5	5.3	3.5	2.0
April	22	600	228	20.0	4.0	5.0	2.0
May	23	620	235	14.7	4.0	3.7	2.0
June	23	600	227	16.9	2.7	6.3	2.0
July	23	620	254	7.8	2.8	2.8	2.0
August	23	620	254	16.0	4.0	4.0	2.0
September	23	570	306	12.2	4.3	2.9	2.0
October	22	589	318	20.1	5.5	3.7	2.0
November	19	570	209	26.4	7.2	3.7	2.0
December	19	589	217	31.7	6.1	5.2	2.0

*If: $F \geq F(.01)$ then there is greater than 99% probability that some of the sample means for the CP groups come from populations with different means.

TABLE XXX

ANOVA RESULTS FOR BARROW DATA: $\delta\overline{T}_d$

Month	Number of CP's	N	N'	s^2	s^2_p	F	F(.01)*
January	15	310	43	11.9	5.8	2.0	2.5
February	18	280	35	6.0	4.1	1.5	2.6
March	20	310	39	7.9	4.2	1.9	2.4
April	18	300	26	7.0	2.5	2.8	2.8
May	22	310	23	1.2	1.0	1.1	2.8
June	23	300	37	1.4	0.8	1.6	2.3
July	23	310	70	3.9	1.4	2.8	2.2
August	21	310	72	3.3	1.2	2.8	2.2
September	20	270	93	2.3	1.0	2.4	2.1
October	22	279	95	2.8	1.8	1.5	2.1
November	17	270	64	6.8	3.2	2.1	2.3
December	19	279	53	8.4	4.6	1.8	2.4

*If: $F \geq F(.01)$ then there is greater than 99% probability that some of the sample means for the CP groups come from populations with different means.

discriminations are for temperatures, especially in mid-winter, and for wind speeds in June and in winter. For these two variables, however, all months have some significant cases. Dew point depressions do not exhibit such good correspondence, but highly significant differences exist in four of twelve months.

2) Seasonal variations are evident in the amount of the total weather element variation accounted for by inter-CP differences. For example, the within-groups variance s_p^2 decreases dramatically from January to June for $\delta\bar{T}$, but the between-means variance decreases by a greater proportion, leading to a smaller (but still highly significant) F statistic.

Wind direction, sky cover and precipitation are variables which, for reasons already stated, are not adaptable to standard ANOVA procedures. All three variables are, however, easily subjected to chi-square contingency tests for association. These tests are applicable when an elementary event has K possible outcomes (e.g., six directional intervals of 60^o for wind directions). For a given sample, the frequency with which each of these K outcomes occurs is counted for each of J separate criteria (e.g. the 23 CP's). These frequencies are then cast in a J by K contingency table, and represent the observed frequencies o. Each cell in the table can be assigned an expected frequency e, based on the null hypothesis that the two criteria of classification (WD and CP's in our example) are independent (Alder and Roessler, 1972, p. 232). For a given cell, e is simply the product of row and column frequency totals divided by the total frequency for the entire table, for the row and column which intersect at the cell. Chi-square is then calculated as:

$$\chi^2 = \Sigma \frac{\{o - e\}^2}{e} \tag{35}$$

where the sum of the quotients is taken over all cells in the table. If all of the observed values are close to the expected frequencies, then chi-square will be small and our two criteria are independent. If the observed frequencies differ greatly from the expected, then it is likely that a non-random relationship exists between the two criteria. Formally, χ^2 for a J by K contingency table satisfies a chi-square distribution with (J - 1) X (K - 1) degrees of freedom. Furthermore, this statistic is independent of the frequency distribution of the variable. Chi-square was calculated as in (35) for wind directions, sky cover and precipitation. In each case there were 23 columns corresponding to the CP's. The wind direction criterion was divided into six 60^o intervals. Sky cover was expressed in ten 1/10th coverage intervals. Precipitation intervals were 0-trace, .01 inches, .02 inches, .03 inches, and greater than .03 inches, respectively. Based on "Cochran's relaxation" (Cochran, 1954), Siegal (1956) states that fewer than 20% of the cells in a chi-square contingency table should have expected frequencies less tahn five, for a valid test. However, Maxwell (1967) showed that reliable results can be obtained with less than 2% of the cells meeting this criterion. In any event, it is desirable to treat contingency tables limited to the more frequent CP's in a given month or season, in order to minimize the cells with a low expectation. The number of CP's in any given calculation, then, is always less than 23. The wind direction and sky cover calculations were carried out by month, while groups of adjacent, within-season months were analyzed for precipitation characteristics, in order to increase the number of chases with measurable precipitation. The results of the chi-square tests are shown in Tables XXXI-XXXIII. The wind directions are

TABLE XXXI

CHI-SQUARE RESULTS FOR BARROW DATA: WD

Month	Number of* CP's (J)	Number of WD Intervals (K)	J X K	Cells e<5	χ^2	$\chi^2(.01)$**
January	7	6	42	16	351.9	51
February	6	6	36	15	212.3	44
March	6	6	36	14	206.9	44
April	6	6	36	17	220.7	44
May	9	6	54	36	270.0	64
June	10	6	60	37	323.3	70
July	9	6	54	21	248.7	64
August	9	6	54	20	303.4	64
September	7	6	42	22	205.6	51
October	9	6	54	27	215.3	64
November	6	6	36	15	273.3	44
December	7	6	42	14	243.2	51

*Always the most frequent types for the month.

**If: $\chi^2 > \chi^2(.01)$ then there is greater than 99% probability that a non-random association exists between WD and the CP's.

TABLE XXXII

CHI-SQUARE RESULTS FOR BARROW DATA: r*

Months	Number of** CP's (J)	Number of r Intervals (K)	J X K	Cells e<5	χ^2	$\chi^2(.01)$***
Jan-Mar	11	5	55	30	214.9	64
Apr-May	10	5	50	33	104.0	57
June	8	5	40	29	41.8	48
Jul-Aug	11	5	55	21	132.9	64
Sept	7	5	35	18	82.1	43
Oct	6	5	30	12	55.7	38
Nov-Dec	9	5	45	25	85.3	53

*r intervals in inches rather than mm for χ^2 tests.

**Always the most frequent types for the period.

***If: $\chi^2 > \chi^2(.01)$ then there is greater than 99% probability that a non-random association exists between r and the CP's.

TABLE XXXIII

CHI-SQUARE RESULTS FOR BARROW DATA: SC

Month	Number of* CP's (J)	Number of SC Intervals (K)	J X K	Cells e<5	χ^2	$\chi^2(.01)$**
January	6	10	60	27	73.1	70
February	4	10	40	12	24.3	47
March	4	10	40	12	38.8	47
April	4	10	40	20	25.7	47
May	6	10	60	46	66.7	70
June	8	10	80	60	81.2	90
July	8	10	80	55	140.6	90
August	7	10	70	51	76.5	82
September	7	10	70	55	64.9	82
October	6	10	60	40	48.8	70
November	5	10	50	24	21.6	57
December	7	10	70	40	72.3	82

*Always the most frequent types for the month.

**If: $\chi^2 < \chi^2(.01)$ then there is greater than 99% probability that a non-random association exists between SC and the CP's.

very clearly associated with the characteristic patterns in a non-random fashion. This is to be expected because the direction of geostrophic surface flow is one of the phenomena which we attempted to classify. It is nonetheless encouraging to see such a high degree of correspondence between directional intervals and characteristic patterns. The precipitation categories are also associated with the CP's except perhaps during June. Late winter and mid-summer associations seem to be strongest for this variable. There appears to be a highly significant association between CP's and sky cover in January and July, but in no other months. This fact is somewhat surprising, because the good association with precipitation might imply a link with sky cover also. However, the SC variable takes no account of the type of clouds.

In summary, we have demonstrated in this chapter that the pressure pattern classification produces stratified weather element populations with highly significant differences. The best distinctions are for various temperature measures. Wind speeds, wind directions, andprecipitation variables are also related to the CP's at a high level of significance. The distinctions are not so clear for sky cover and dew point depressions, varying seasonally from non-significant to highly significant. In the following chapter, we shall examine the particular weather characteristics associated with each major CP, and attempt to interpret the weather characteristics in terms of the synoptic scale patterns.

CHAPTER SIX

SYNOPTIC CLIMATOLOGY

Introduction

In this chapter we investigate the weather characteristics of the frequent pressure patterns in each season. The spatial and temporal properties of the pressure patterns are used to make processual inferences about the observed weather characteristics. Associations among the different weather variables for a single CP group are also discussed. The chapter concludes with a summary of the major synoptic controls on the climate of Alaska's Beaufort Sea coast.

Presentation of Weather Data

Weather data used in calculating the CP weather characteristics are from the Barrow and Barter Island series described in Chapter V (Table XIV). The data were stratified into CP/month groups, and the mean and standard deviation were computed for each stratum. The stratified sets are summarized on frequency histograms (Figures 32-57). (Table XXXVI provides a key.) The wind direction histograms are plotted in polar coordinates, with each cell extending towards the direction from which the wind was blowing. Note that the length, not the area, of each cell is proportional to the relative frequency of winds from the corresponding direction. Means and standard deviations of wind directions were calculated as in Mardia (1972, pp. 20-25). The histograms for non-directional data have the standard format, with frequency as the ordinate and the measured variable as the abcissa. Below each histogram in the first column are listed the month, characteristic pattern, station and variable name which correspond to the data presented. In column two, "sample" gives the total number of (daily) data points on the histogram. on the cartesian plots, the ordinate ranges from zero to "SAMPLE". The average and standard deviation of each distribution are designated by "MEAN" and "SD", respectively.

January, June, July and September were chosen to represent the main seasonal variations of CP weather characteristics. Any important within-season variations in the characteristics of a given pattern are noted where relevant.

Winter

The mean January weather data for important winter CP's are set out in Table XXXV. Table XXXIV is a key for the variable names in the weather element tables. The most frequent pattern in winter is CP1, and its January histograms are shown in Figure 32. CP1 surface winds are from ENE inJanuary at Barrow, in agreement with the surface flow expected from the CP1 synoptic map. In general, the Barrow prevailing winds are between easterly and east-northeasterly in winter (Table I) and it is clear that the winter frequency of CP1 (40%) is the immediate cause of this flow regime. In this respect, then, CP1 represents the "normal" winter mode of surface air flow, as well as the normal mode of pressure distribution. Mean daily temperature departures are slightly below normal at Barrow and Barter Island throughout the winter, but the distributions

TABLE XXXIV

KEY FOR WEATHER CHARACTERISTIC TABLES

Symbol	Explanation
CP	Characteristic pattern
$\overline{dT1}$	Mean of the daily temperature departures at Barrow
$\overline{dT2}$	Mean of the daily temperature departures at Barter Island
$\overline{WD}$	Mean of the daily wind directions at Barrow
$\overline{U}$	Mean of the daily wind speeds at Barrow
$\overline{SC}$	Mean of the daily sky covers at Barrow
$\overline{dT_D}$	Mean of the daily dew point depressions at Barrow
r	Total precipitation catch (water equivalent) at Barrow 1956-1974, for the given season and CP
%-1	r as a percentage of the unstratified seasonal catch at Barrow, 1956-74
%-2	Number of days with measureable precipitation at Barrow, as a percentage of the number of daily occurrences of the given CP

TABLE XXXV

JANUARY CP WEATHER CHARACTERISTICS

CP	$\overline{dT1}$ (°C)	$\overline{dT2}$ (°C)	$\overline{WD}$ (°)	$\overline{U}$ (m/s)	$\overline{SC}$ (1/10)	$\overline{dT_D}$ (°C)	r* (mm)	%-1 (%)	%-2 (%)
1	-1.8	-2.4	73	5.6	5.2	4.5	66.3	20	11
2	+13.5	+15.1	226	7.5	7.9	2.3	46.2	14	58
3	-3.6	-3.4	304	4.0	5.2	4.1	19.0	6	11
4	+3.0	+2.8	104	5.4	5.9	3.9	46.5	14	19
5	+2.7	+5.6	267	6.9	6.1	5.3	29.5	9	29
6							16.0	5	46
7	-2.5	-3.3	315	3.2	4.1	3.8	0.5	0	2
8							8.1	2	53
9	+1.4	-1.5	154	5.6	6.4	3.5	26.2	8	23
10							41.9	13	44

*Precipitation data are for season I (January-March) rather than for January.

TABLE XXXVI

KEY FOR WEATHER CHARACTERISTIC HISTOGRAMS

Variable	Histogram symbol	Coordinates	Abcissa endpoints	Cell Interval
Daily temperature departure	T-DEP	Cartesian	$-30^{\circ}C$, $+30^{\circ}C$	$2^{\circ}C$
Daily wind direction	WIND DIR	Polar	0°, 360°	30°
Daily wind speed	WIND-1	Cartesian	0m/s, 30m/s	2m/s
Daily sky cover	CLOUD	Cartesian	0/10ths, 10/10ths	1/10th

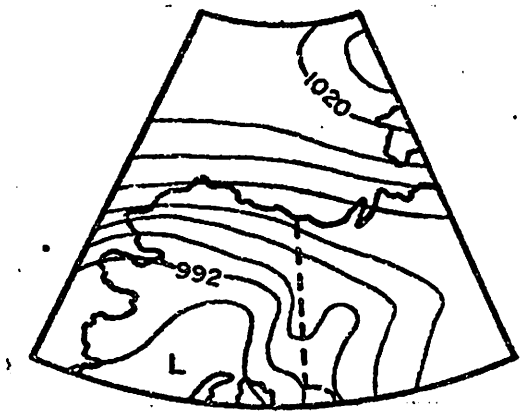

CP1

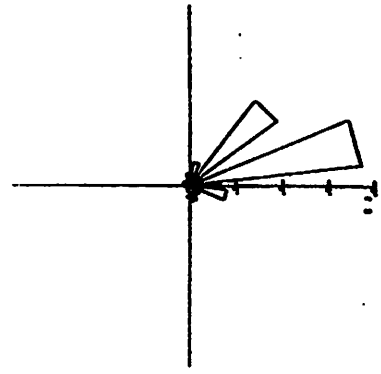

MONTH 1 SAMPLE 175
PATTERN 1 MEAN 72.6
STATION BARROW SD 41.4
VARIABLE WIND DIR

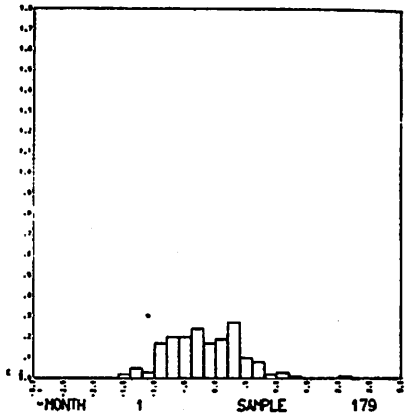

MONTH 1 SAMPLE 179
PATTERN 1 MEAN -1.8
STATION BARROW SD 5.8
VARIABLE T-DEP

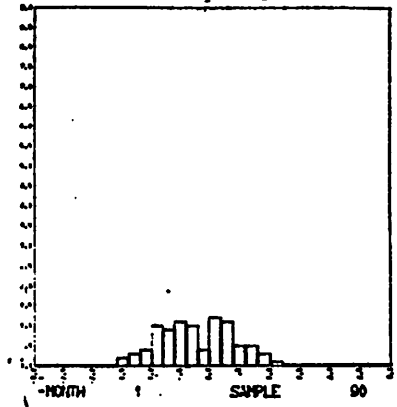

MONTH 1 SAMPLE 90
PATTERN 1 MEAN -2.4
STATION BARROW SD 6.2
VARIABLE T-DEP

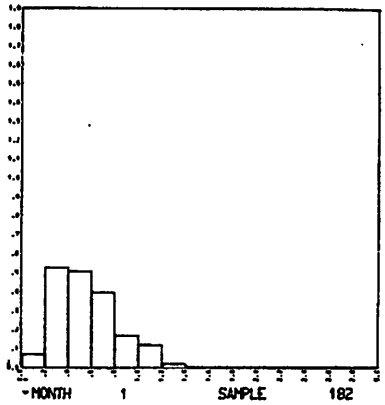

MONTH 1 SAMPLE 182
PATTERN 1 MEAN 5.6
STATION BARROW SD 2.6
VARIABLE WIND-1

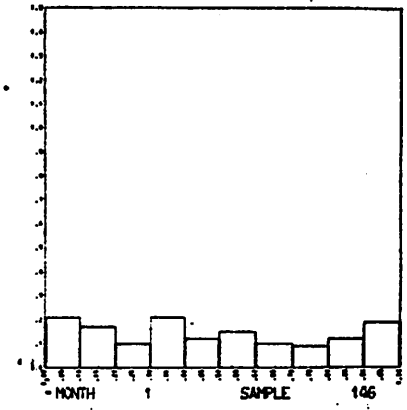

MONTH 1 SAMPLE 146
PATTERN 1 MEAN 5.2
STATION BARROW SD 3.0
VARIABLE CLOUD

Figure 32: Histograms for January: CP1

(Figure 32) show that positive departures occur quite frequently. Indeed the modal temperature departure at Barrow is +3°C. With more than 80% of the CP1 temperature departures between -10°C and +4°C, we see that this pattern is not usually associated with large-magnitude temperature departures in winter. The January average wind speed is 5.6 ms^{-1} for CP1 at Barrow, exceeding the mean monthly speed by 0.6 ms^{-1}. Notice that 80% of the wind speed distribution lies between 2 ms^{-1} and 8 ms^{-1}, indicating again that CP1 is the climatic normal pattern in winter. A few extreme readings, up to 14 ms^{-1}, have pulled the average speed somewhat above the overall January mean. CP1 has a remarkably flat distribution of daily sky coverage at Barrow, with an average of 5.2 tenths and no clear mode. Again, this mean value lies quite close to the January mean of 5.0 tenths at Barrow. This pattern is the largest Season I (Jan.-Mar.) contributor of precipitation at Barrow, with 66.3 mm, which is 20% of the 1955-1974 total catch for Season I. However, measureable precipitation ($\geq$ 0.254 mm) occurred in only 11% of the CP1 cases, indicating that this is really a dry pattern. The high frequency of occurrence of CP1, coupled with the low overall seasonal precipitation in the region, is responsible for its dominant contribution to the seasonal catch.

The second-most frequent January pattern is CP4, which occurs on about 20% of January days and 15% of the time during all winter months. Figure 33 presents the weather characteristics for this pattern. CP4 winds come from the ESE on average. Recall from Chapter IV that CP4 has its frequency maximum in January while CP1 experiences a secondary minimum (29%). The prevailing January wind direction at Barrow is ESE, compared with E to ENE for all other winter months. CP4's increase in frequency is partly responsible for the southerly component. CP2 is the other major pattern involved in the January wind shift. We note that the CP4 winds are not in total agreement with the geostrophic direction on the CP4 synoptic map (roughly southerly). We saw in Chapter IV that the southwest low pressure area on the CP4 map can extend over much of the Arctic slope in individual cases, which may explain the easterly orientation of the Barrow surface winds. Daily temperature departures for this pattern have a very broad distribution, ranging from -16°C to +20°C at Barrow. The standard deviation of this series ($\pm$ 7.6°C) is almost as large as the unstratified January value at Barrow ($\pm$ 8.1°C, see Table III), indicating that CP4 did not contribute substantially to the variance reduction in the ANOVA calculations. The scatter is CP4 temperature departures may also be attributed to the variable extent of the southwest low pressure area versus the central high among individual cases. As we shall see presently, Pacific low pressure systems tend to bring above-normal temperatures to the Beaufort coast during winter. Despite the scatter, however, the mean departures are about 3°C above normal at both stations in winter. The mean CP4 wind speed is a near-normal 5.4 ms^{-1} in January, but on rare occasions this pattern brings winds up to 16 ms^{-1}. These extreme values indicate once again the potential influence of the southwest low. The cloud distribution is flat, much like that of CP1, with an average value of 5.9 tenths. From Table XXXVI we see that 14% of the Season I precipitation comes from CP4, and 19% of cases are associated with measurable precipitation at Barrow. With regard to winter temperatures, at least, CP4 provides a rather unsatisfactory grouping of weather data.

CP3 accounts for 10 to 15% of winter days and is the third major pattern in January. In Figure 34 we see that the wind directions at Barrow are quite variable for this pattern, having a standard deviation of $\pm$96°. We might

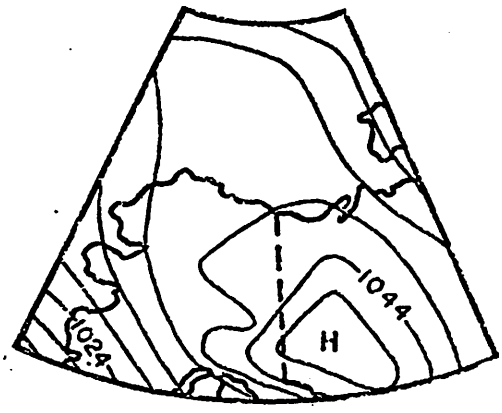

CP4

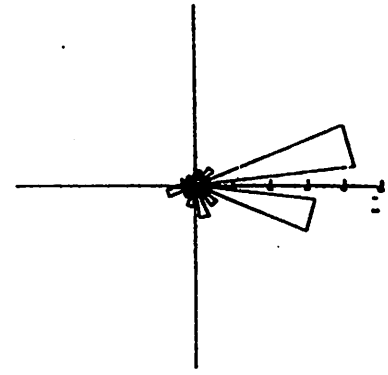

MONTH 1 SAMPLE 127
PATTERN 4 MEAN 104.1
STATION BARROW SD 65.9
VARIABLE WIND DIR

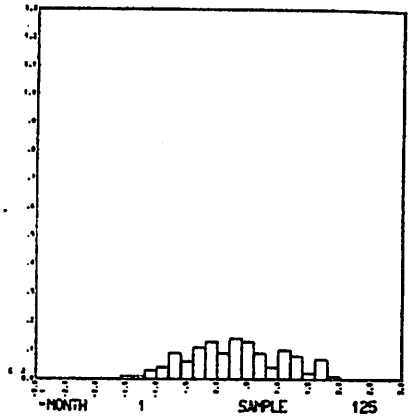

MONTH 1 SAMPLE 125
PATTERN 4 MEAN 3.0
STATION BARROW SD 7.6
VARIABLE T-DEP

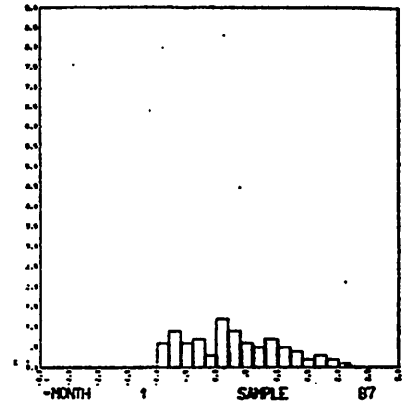

MONTH 1 SAMPLE 87
PATTERN 4 MEAN 2.8
STATION BARTER SD 7.8
VARIABLE T-DEP

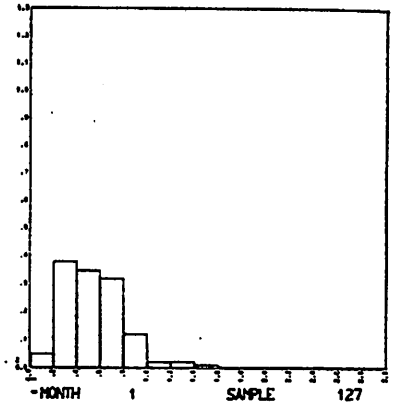

MONTH 1 SAMPLE 127
PATTERN 4 MEAN 5.4
STATION BARROW SD 2.5
VARIABLE WIND-1

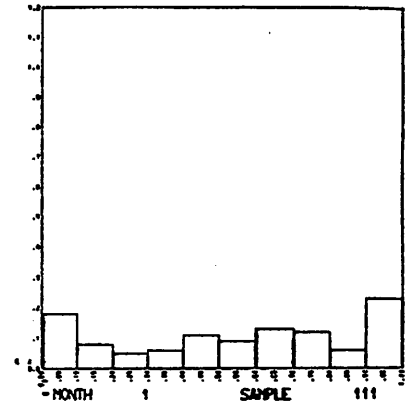

MONTH 1 SAMPLE 111
PATTERN 4 MEAN 5.9
STATION BARROW SD 3.2
VARIABLE CLOUD

Figure 33: Histograms for January: CP4

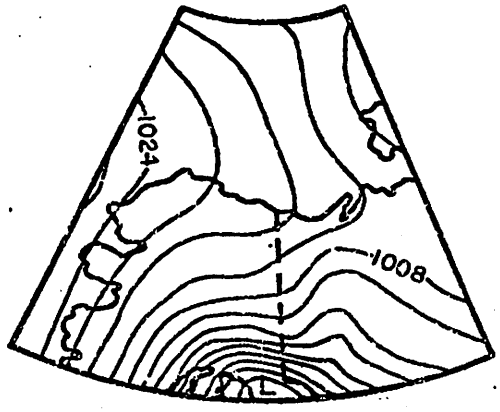

CP3

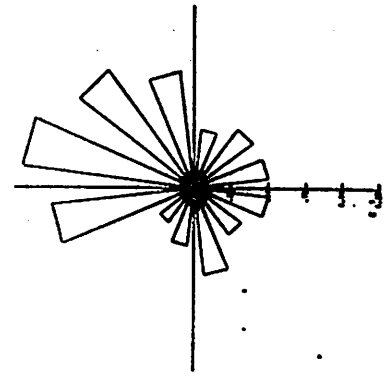

MONTH	1	SAMPLE	76
PATTERN	3	MEAN	304.2
STATION	BARROW	SD	96.0
VARIABLE	WIND DIR		

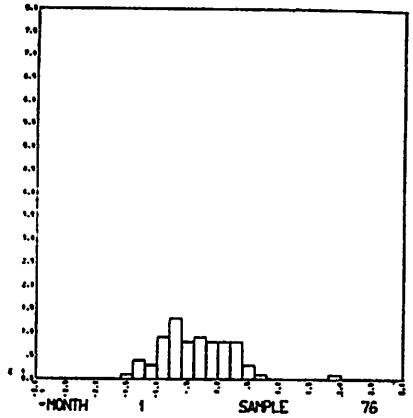

MONTH	1	SAMPLE	76
PATTERN	3	MEAN	-3.6
STATION	BARROW	SD	5.7
VARIABLE	T-DEP		

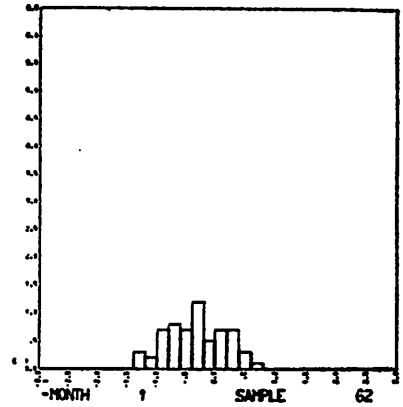

MONTH	1	SAMPLE	62
PATTERN	3	MEAN	-3.4
STATION	BARTER	SD	4.9
VARIABLE	T-DEP		

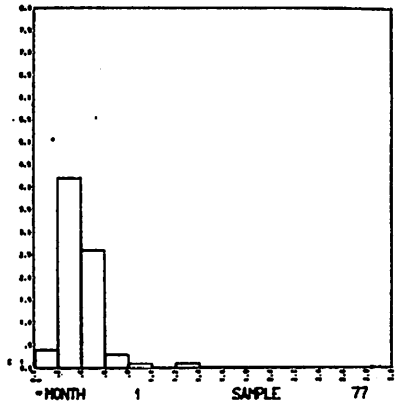

MONTH	1	SAMPLE	77
PATTERN	3	MEAN	4.0
STATION	BARROW	SD	1.7
VARIABLE	WIND-1		

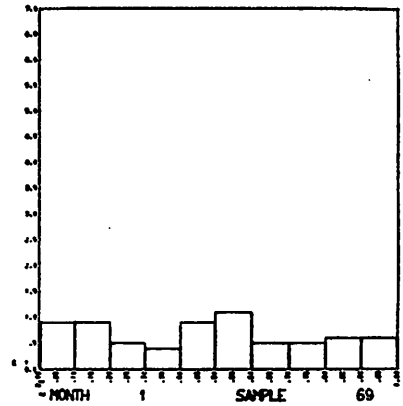

MONTH	1	SAMPLE	69
PATTERN	3	MEAN	5.2
STATION	BARROW	SD	2.9
VARIABLE	CLOUD		

Figure 34: Histograms for January: CP3

expect this sort of variability for CP3 because the high-pressure ridge from the west (over Barrow) is the weakest feature on the CP3 synoptic map. Also, a slight north or south displacement of the ridge axis corresponds to a large shift in the surface geostrophic wind direction along the Beaufort Sea coast. Such variation is to be expected between individual cases of CP3, because a range of SCORES can pass the similarity test thresholds. The CP3 temperature departures are strongly negative at both Barrow ($-3.6^{o}C$) and Barter Island ($-3.4^{o}C$), and remain so throughout the winter. In fact, the average CP3 temperature departure for 97 daily cases in December was $-6.0^{o}C$ at Barrow! This CP is the coldest of all major winter patterns. Over 70% of the January departures for CP3 were negative at Barrow. Barrow wind speeds give an indication of the processes responsible for the negative temperature departures. The average speed is only 4.0 ms^{-1} and the modal value is 3 ms^{-1}. Such light and variable winds are a characteristic of diffuse Arctic high pressure cells and ridges (Wilson, 1967, p. 60). When the winds are light, vertical mixing of air parcels by mechanical turbulence is strongly inhibited, particularly when the surface layers are statitically stable, as they are over Barrow in winter. Such conditions can lead to intense radiative cooling at the surface and low air temperatures in the boundary layer. Another factor of possible importance is the ridge orientation, which indicates surface geostrophic streamlines from the norhtwest over Barrow. The lowest mean winter temperatures in the northern hemisphere occur over northeastern Siberia, and the CP3 ridge often represents an eastward extension of the flow from this cold source. The mean CP3 sky cover is an unremarkable 5.2 tenths in January. Also, only 6% of Barrow's season-I precipitation catch results from CP3 occurrences, despite its 13% frequency in winter. These facts indicate the dry nature of this pattern. Evidently the Beaufort coast is completely cut off from the surface circulation of the Pacific region when the CP3 ridge occurs. Low temperatures, light and variable winds, partly cloudy skies and very little precipitation and all characteristics of this pressure pattern.

The major "weather-producing" pattern in winter is, paradoxically, the most frequent summer CP. CP2 has a secondary frequency maximum in January (7%) and accounts for slightly less than 5% of winter patterns overall. Figure 35 shows that the Barrow winds come from the southwest under this pattern in January, almost directly opposite to the CP1 and prevailing monthly winds. This direction is in substantial agreement with the large scale, surface geostrophic flow on the CP2 synoptic map. Clearly CP2 is a major contributor to the highly-significant χ^2 association between CP's and wind directions in January. The most striking weather characteristics of this pattern are its January temperature departures at Barrow ($+13.5^{o}C$) and Barter Island ($+15.1^{o}C$). Large positive temperature departures are a property of CP2 throughout the other winter months as well. We noted in Chapter IV that CP2 often occurs at the end of a transitional sequence involving the movement of low pressure cells from the Pacific-Bering Sea region into the Arctic Basin. Clearly the scenario is consistent with the large, positive temperature departures, as such storms can sweep away the surface temperature inversion and bring relatively warm marine air into the area (e.g. Wilson, 1967, p. 60). A number of other CP2 weather characteristics support this picture, including a mean wind speed of 7.5 ms^{-1}, largest of any major winter CP. Note also that the modal speed is 9 ms^{-1}. In Table XII we saw that CP2 has the second-largest pressure pattern intensity index (s_p = 11.2 mb) in January, indicating the relative strength of these cyclonic incursions, which leads to high wind speeds. Mean

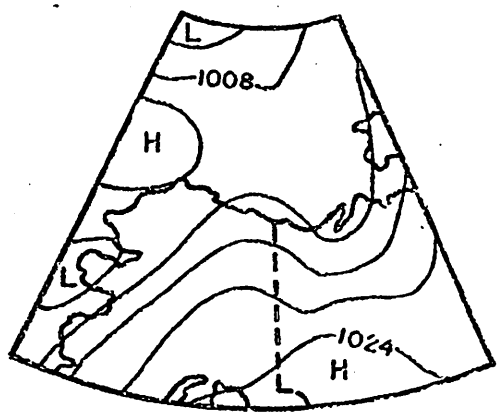

CP2

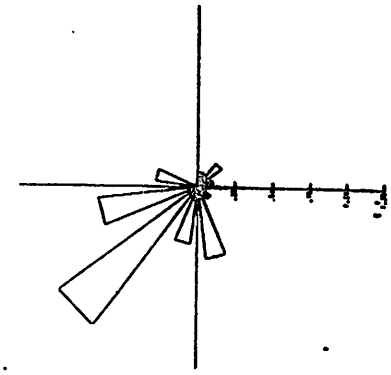

MONTH 1 SAMPLE 56
PATTERN 2 MEAN 225.7
STATION BARROW SD 55.1
VARIABLE WIND DIR

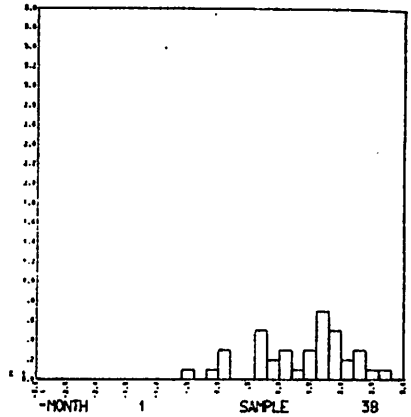

MONTH 1 SAMPLE 38
PATTERN 2 MEAN 13.5
STATION BARROW SD 7.6
VARIABLE T-DEP

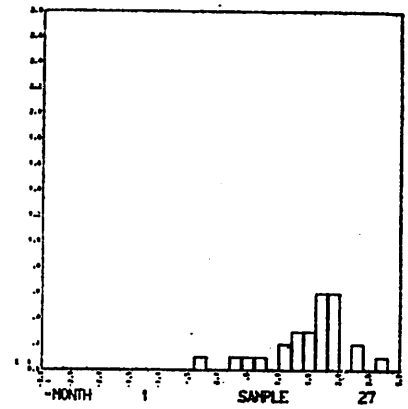

MONTH 1 SAMPLE 27
PATTERN 2 MEAN 15.1
STATION BARTER SD 6.4
VARIABLE T-DEP

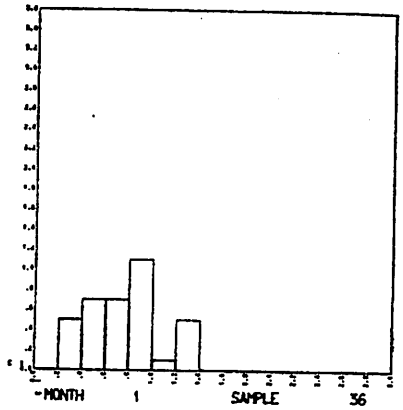

MONTH 1 SAMPLE 36
PATTERN 2 MEAN 7.5
STATION BARROW SD 3.1
VARIABLE WIND-1

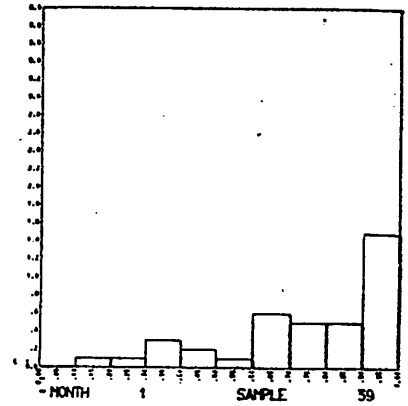

MONTH 1 SAMPLE 39
PATTERN 2 MEAN 7.9
STATION BARROW SD 2.5
VARIABLE CLOUD

Figure 35: Histograms for January: CP2

CP2 sky cover at Barrow (7.9 tenths) is also the largest of any January pattern, and again suggests the influx of moister air from the Pacific area. The cyclonic flow around the northwest CP2 low pressure area should produce rising motions in the vicinity of Barrow, hence the cloudiness. Although this pattern occurs on less than 5% of days during Season I, it contributes 14% of the seasonal precipitation at Barrow. Indeed, 58% of all occurrences of CP2 had measurable precipitation at Barrow during Season I, 1955-1974. The precipitation characteristics point up the moist, cyclonic nature of this pattern once again. We also note that the warm, moist, cloudy air associated with CP2 would be expected to decrease the net losses of infrared radiation from the surface duirng winter, which is also in accord with the positive temperature departures.

It is worthwhile to note at this stage that CP2 occurs on about 3% of days during December, February, March and April. Thus the increase in frequency to 7% in January is largely responsible for the interruption in the mean seasonal cooling trend at Barrow and Barter Island (Chapter II). In this respect, then, the coreless winter analogy is valid, because the January warmings are characterized by incursions of warm, marine air masses associated with cyclonic systems, much like the June warmings in Antarctica (Van Loon, 1967). The major differences are the greater magnitude and regularity of these effects in the Antarctic as compared to Alaska. The overall (unstratified) distribution of January temperature departures is noticeably right-skew at Barrow, unlike any of the other winter months, again due primarily to the increase in CP2 frequency.

CP7 is a second major winter pattern characterized by a ridge from the west extending along the coast, but the intense low pressure cell is to the northwest, unlike CP3 (Figure 36). The mean January winds come from the northwest under CP7 at Barrow, in substantial agreement with the surface flow expected from the synoptic map. Again the ridge brings negative temperature departures to Barrow (-2.5°C) and Barter Island (-3.3°C) in January. This characteristic obtains during all winter months for CP7, with a minimum value at Barrow of -4.6°C in February. CP7 has the lighest winds of any major winter CP, as evidenced by a mean speed of only 3.2 ms^{-1} at Barrow. The mean January sky coverage is only 4.1 tenths, with a mode at zero tenths. These conditions are conducive to radiative cooling at the surface, much like CP3. The anticyclonic curvature associated with the CP7 ridge leads to bery dry air over the Beaufort coast. Despite the 5% frequency of CP7 in season I, it contributed but 0.5 mm of precipitation at Barrow during 1955-1974 (less than 1% of the seasonal total). Thus this pattern has rather well-defined weather characteristics in winter, including relatively clear skies, low temperatures, slight, northwesterly winds and no significant precipitation.

CP9 accounts for 6% of the daily winter pressure patterns, and is dominated by a high pressure belt stretching from the northern Yukon to Norton Sound. In Table XIII we saw that the mean January CP9 pressure in the center of the grid is 1032 mb. highest for any major winter CP. This high leads to southeasterly surface flow over Barrow (Figure 37). Despite the southerly component of the surface wind, the mean CP9 temperature departures are only +1.4°C at Barrow and -1.5°C at Barter Island. Indeed the sign of the CP9 departures changes from month to month at Barrow during winter. We also note the large standard deviations for the January temperature departure distributions. These facts

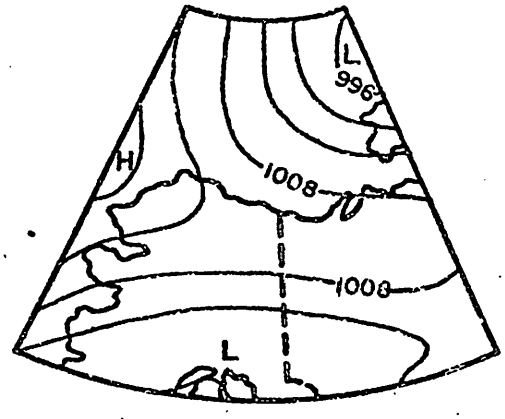

CP7

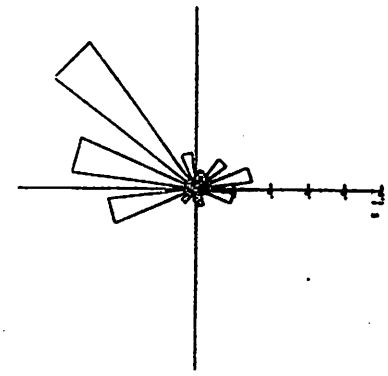

MONTH 1 SAMPLE 34
PATTERN 7 MEAN 314.7
STATION BARROW SD 66.7
VARIABLE WIND DIR

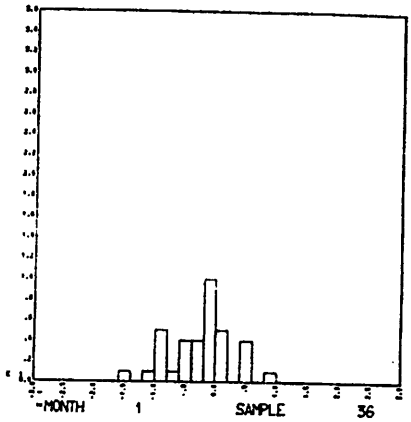

MONTH 1 SAMPLE 36
PATTERN 7 MEAN -2.5
STATION BARROW SD 5.2
VARIABLE T-DEP

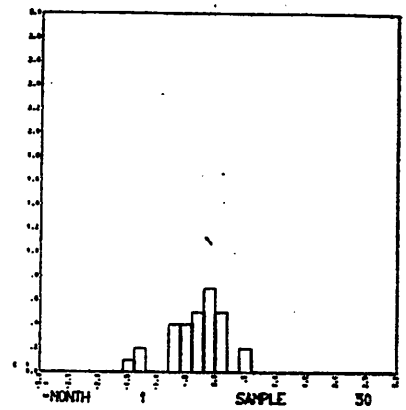

MONTH 1 SAMPLE 30
PATTERN 7 MEAN -3.3
STATION BARTER SD 4.9
VARIABLE T-DEP

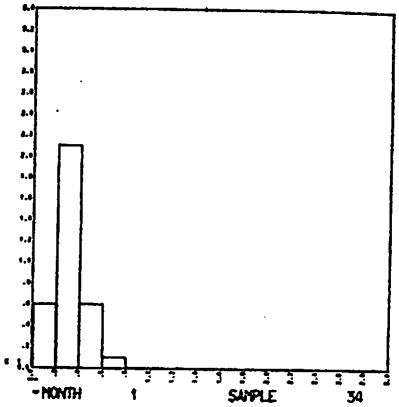

MONTH 1 SAMPLE 34
PATTERN 7 MEAN 3.2
STATION BARROW SD 1.4
VARIABLE WIND-1

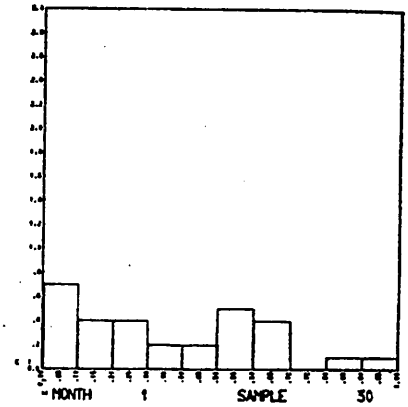

MONTH 1 SAMPLE 30
PATTERN 7 MEAN 4.1
STATION BARROW SD 2.6
VARIABLE CLOUD

Figure 36: Histograms for January: CP7

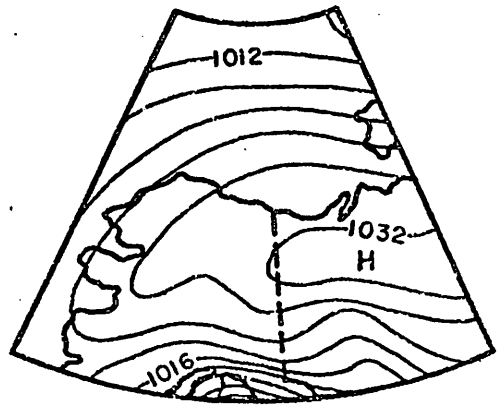

CP9

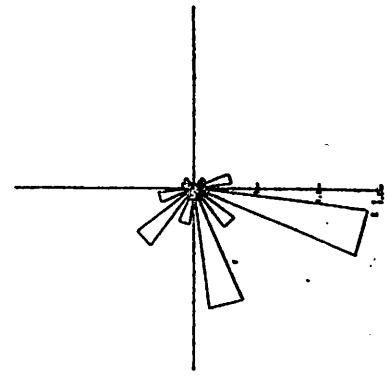

MONTH 1 SAMPLE 46
PATTERN 9 MEAN 153.5
STATION BARROW SD 62.8
VARIABLE WIND DIR

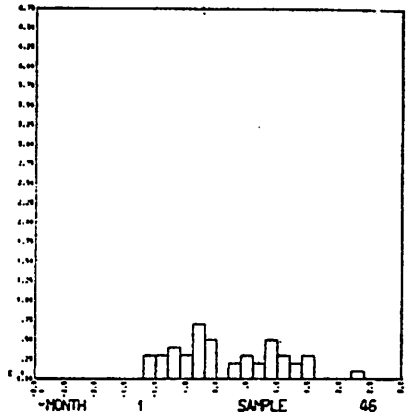

MONTH 1 SAMPLE 46
PATTERN 9 MEAN 1.4
STATION BARROW SD 8.6
VARIABLE T-DEP

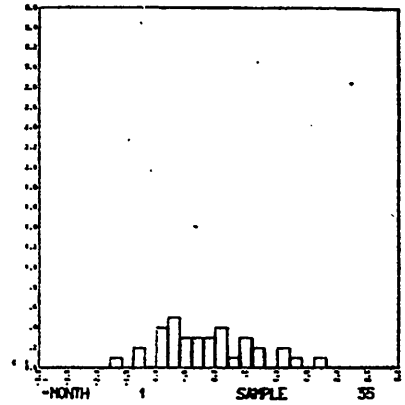

MONTH 1 SAMPLE 35
PATTERN 9 MEAN -1.5
STATION BARTER SD 7.8
VARIABLE T-DEP

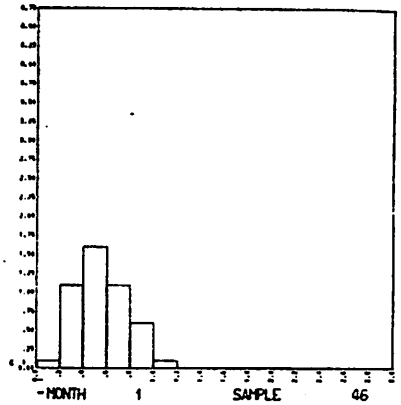

MONTH 1 SAMPLE 46
PATTERN 9 MEAN 5.6
STATION BARROW SD 2.3
VARIABLE WIND-1

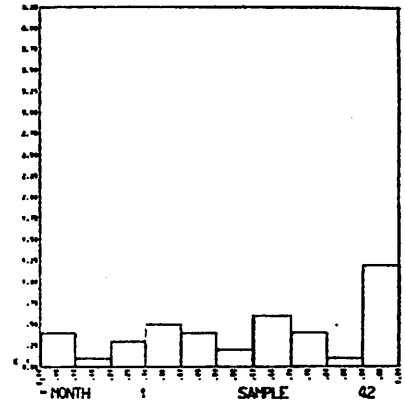

MONTH 1 SAMPLE 42
PATTERN 9 MEAN 6.4
STATION BARROW SD 3.1
VARIABLE CLOUD

Figure 37: Histograms for January: CP9

indicate that CP9 is not a highly-deterministic pattern with regard to winter temperatures. The mean wind speed (5.6 ms^{-1}) is close to the monthly normal at Barrow, but seems rather large for a high pressure, anticyclonic pattern. Despite the locally anticyclonic curvature, CP9 is associated with cloudy conditions at Barrow. In short, CP9 has weather characteristics which do not lend themselves to interpretation in terms of the CP9 synoptic map.

The final pattern with at least 5% frequency in winter is CP5 which, like CP2, is most frequent during the summer. From Figure 38 we see that this pattern has a ridge across central Alaska from the southwest, which separates the low pressure areas to the south and northeast. Westerly surface geostrophic wind flow is indicated, and is corroborated by the CP5 surface wind direction at Barrow (267°). This pattern brings above-normal temperatures to Barrow and Barter Island throughout the winter, on average, but the scatter in the distributions is large. High mean daily wind speeds accompany this pattern at Barrow, and are probably responsible for the positive mean temperature departures. As we noted previously, such high winds can mix air of relatively high potential temperature downward into the surface layers, when the mechanical turbulence is capable of overcoming the static stability in the air column. However, a static pressure pattern classification such as the present one cannot adequately distinguish the origin and trajectory of an air mass, except indirectly through the analysis of transition sequences. The fact that CP's 15 and 2 most frequently precede CP5 (Figure 30) implies that this pattern is associated with the west coast cyclonic systems. However, these transition probabilities cover less than 50% of the total CP5 cases. Clearly the origin of the air circulating around the northeast low pressure cell is crucial in determining the sign of temperature departures over Barrow. Thus the scatter in the CP5 temperature departure distributions presents a deficiency of our static description of the circulation. CP5 brings relatively cloudy conditions to Barrow in January, and accounts for 9% of the season I precipitation there. 29% of the CP5 cases had measurable precipitation, again illustrating a relationship between above-average temperatures, high winds, cloud and precipitation in winter.

Of the less-frequent patterns in winter, CP's 6 and 10 are characterized by above-normal wind speeds, large positive temperature departures, and frequent measurable precipitation at Barrow. Both of these patterns have low pressure cells on the west coast of Alaska, with troughs extending to the east. These characteristics support the contention that cyclonic storms of Pacific origin are the main source of warm weather fluctuations on the Beaufort Sea coast at this season. CP8, a central low pattern, brought measurable precipitation in over 50% of its cases also.

In summary, it is clear that practically-important, as well as statistically-significant, associations exist between the pressure pattern groups and their weather characteristics in winter. At least three major types of winter weather regime can be identified on the Beaufort Sea coast. Near-normal conditions are associated with CP1 occurrence, having low pressures to the south and highs or ridges to the north. These conditions include easterly to northeasterly surface winds at 2 to 8 ms^{-1}, temperatures between -20°c and -35°C, infrequent, light precipitation, and about five tenths average sky cover. Evidently the advection of relatively warm, moist air from the Pacific and Gulf of Alaska is limited in most winter cases of CP1. The temperature regime is determined mainly by the negative surface net radiation (about -2431 Wm^{-2}, on average, Maykut and Church, 1973). The second winter weather regime is associated with

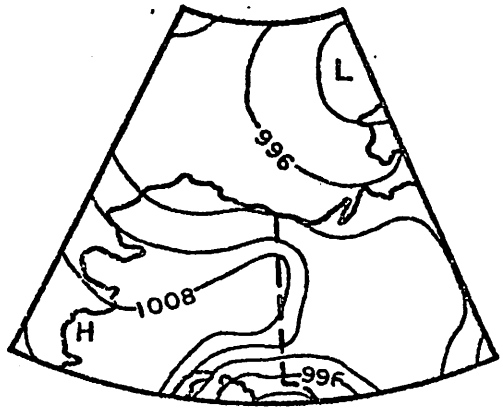

CP5

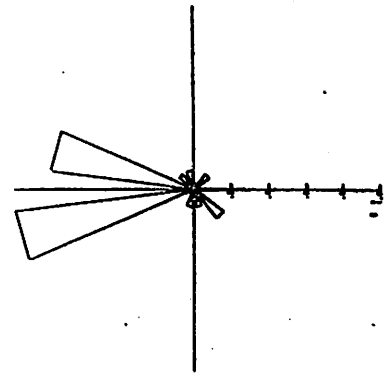

MONTH 1 SAMPLE 25
PATTERN 5 MEAN 267.1
STATION BARROW SD 50.8
VARIABLE WIND DIR

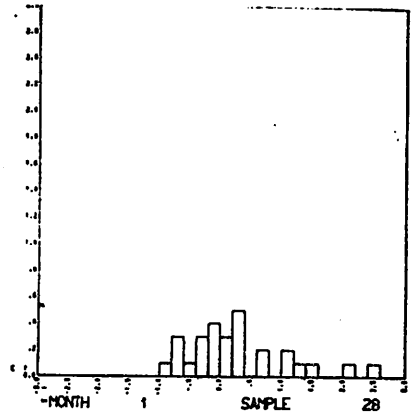

MONTH 1 SAMPLE 28
PATTERN 5 MEAN 2.7
STATION BARROW SD 8.4
VARIABLE T-DEP

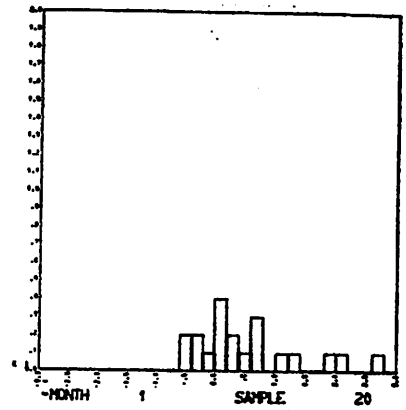

MONTH 1 SAMPLE 20
PATTERN 5 MEAN 5.6
STATION BARTER SD 8.9
VARIABLE T-DEP

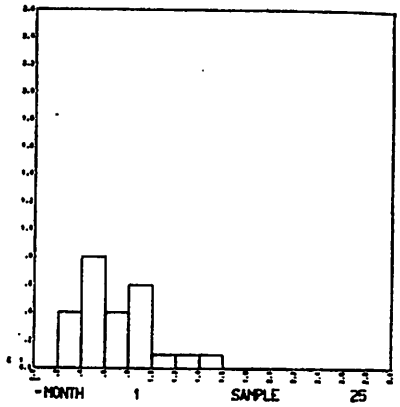

MONTH 1 SAMPLE 25
PATTERN 5 MEAN 6.9
STATION BARROW SD 3.1
VARIABLE WIND-1

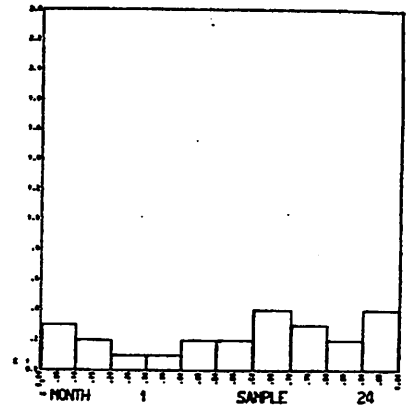

MONTH 1 SAMPLE 20
PATTERN 5 MEAN 6.1
STATION BARROW SD 3.1
VARIABLE CLOUD

Figure 38: Histograms for January: CP5

ridges from the west, which extend eastward along the Beaufort coast. This flow pattern cuts off the area from Pacific circulation influences, and brings light, variable winds, slightly clearer skies than CP1, and almost no significant precipitation. Such conditions lead to maximum surface net radiation losses in winter, producing average temperatures around -30°C in mid-winter, with extremes below -40°C. CP's 3 and 7 are the major patterns which define this regime of surface circulation. The wind directions vary considerably from case to case when these ridge patterns occur, but are northwesterly, on average. The geostrophic surface streamlines and northwesterly surface winds suggest that some of the CP7-CP3 cooling may be a result of temperature advection from the area of the Siberian high pressure cell. The third major type of winter weather is associated with the occurrence of CP2 and other, less-frequent patterns having low pressure off the west or northwest Alaska coasts. These patterns bring unseasonably warm air over the region, with occasional temperatures above the freezing point. Strong winds, frequent and relatively heavy precipitation, and overcast skies are all characteristics of these patterns in the cold season. The winds for CP2 are predominantly southwesterly, as are the surface geostrophic streamlines over the study region. Depsite the warmings associated with CP2 in winter, it should be observed that the combination of high winds, relatively moist air, and blowing snow may make surface conditions more undesirable than the calm, clear, -35°C weather associated with, say, CP3. CP's 4, 5, and 9 are frequent winter patterns which do not fit neatly into the weather regimes discussed above. The wind direction distributions associated with each of these patterns show relatively little scatter, but the temperature, sky cover and wind speed data are not to clear cut. In the case of CP4 we speculate that the circulation around the southwestern low pressure cell extends over our study region by variable amounts in different cases, leading to the variable weather characteristics. With CP5 it seems that the origin and trajectory of the Arctic Basin low pressure cell is crucial in individual cases. In any event, further work on such "program patterns" should lead to a better understanding of just which features of the surface pressure field are most important in determining the weather characteristics. Finally, the coreless winter phenomenon described in Chapter II appears to result from more-frequent CP2 occurrence in January than in other winter months. The January maximum in CP4 occurrence may also enhance this effect.

Spring

Table XXXVII contains the weather characteristics for the frequent June pressure patterns. It is noteworthy that more CP's occur with 4% to 10% frequency in June than in January, and the most-frequent CP occurs in only 23% of cases, indicating a more variable dirculation regime than in winter. Nonetheless, CP1 remains the number one pattern, and its weather characteristics are shown in Figure 39. The Barrow surface winds continue to blow from the east-northeast under this pattern, with even less scatter than the corresponding January distribution. Although the average CP1 temperature departures are -0.6°C at Barrow and -0.5°C at Barter Island, such small departures can be significant, in a statistical sense at least, because of the low overall variability for weather elements in the month of June. For example, we saw in Chapter II that the unstratified standard deviation of the June daily temperature departures at Barrow was ±2.4°C, which may be compared with ±8.1°C in January. At any rate, CP1 brings temperatures just slightly below normal in June, much as it did in January. The average wind speed associated with this

TABLE XXXVII

JUNE CP WEATHER CHARACTERISTICS

CP	$\overline{dT1}$ (°C)	$\overline{dT2}$ (°C)	$\overline{WD}$ (°)	$\overline{U}$ (m/s)	$\overline{SC}$ (1/10)	$\overline{dT_D}$ (°C)	$\overline{r^*}$ (mm)	$\overline{\%-1}$ (%)	$\overline{\%-2}$ (%)
1	-0.6	-0.5	73	6.2	8.2		16.5	9	9
2	+1.8	+1.2	201	4.0	7.5		30.5	16	29
4	+0.2	+0.9	88	4.9	7.1		10.9	6	11
5	+0.1	+0.8	254	4.8	8.2		25.4	14	27
6	0.0	+0.9	82	5.3	8.8		38.1	20	20
8	-2.0	-1.8	30	4.4	9.2		10.9	6	17
12	+0.9		130	4.1	7.2		11.7	6	23
14	-1.9	-1.1	314	4.4	9.6		4.6	2	22
15	+1.1	+0.8	219	5.3	8.6		8.1	4	36
17	-0.1	-0.7	90	4.8	7.9		11.4	6	19
21	+1.6	-1.0	112	5.1	7.3		5.3	3	32

*Precipitation data are for Season III (June).

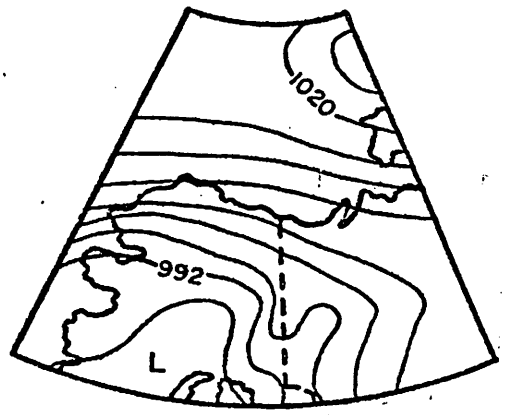

CPI

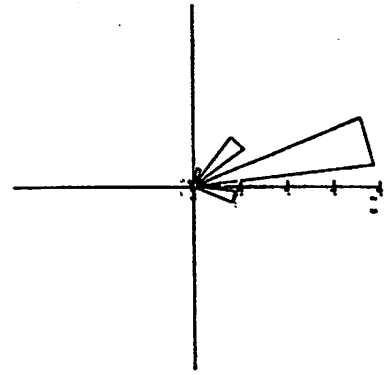

MONTH	6	SAMPLE	138
PATTERN	1	MEAN	72.5
STATION	BARROW	SD	31.1
VARIABLE	WIND DIR		

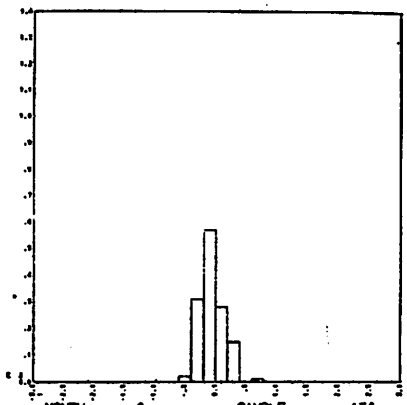

MONTH	6	SAMPLE	134
PATTERN	1	MEAN	-.6
STATION	BARROW	SD	2.0
VARIABLE	T-DEP		

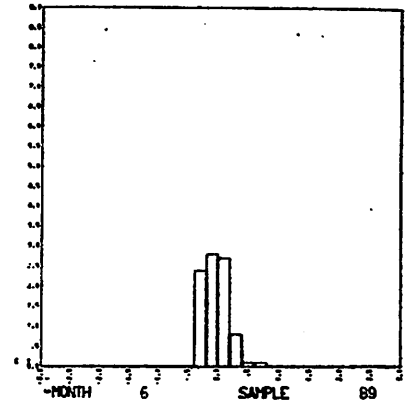

MONTH	6	SAMPLE	89
PATTERN	1	MEAN	-.5
STATION	BARTER	SD	2.1
VARIABLE	T-DEP		

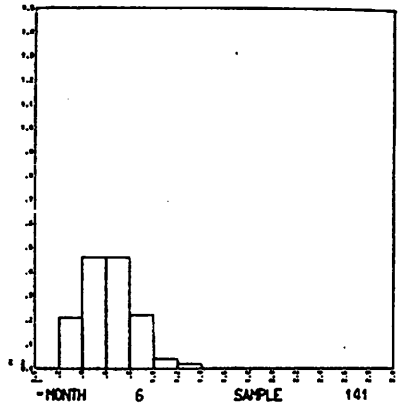

MONTH	6	SAMPLE	141
PATTERN	1	MEAN	6.2
STATION	BARROW	SD	2.0
VARIABLE	WIND-1		

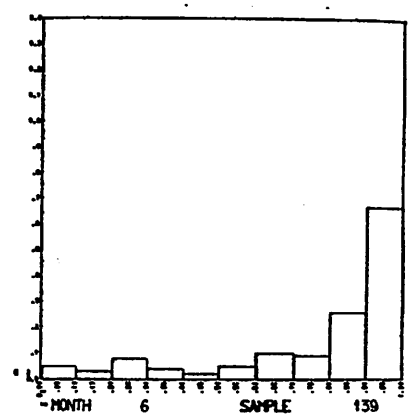

MONTH	6	SAMPLE	139
PATTERN	1	MEAN	8.2
STATION	BARROW	SD	2.6
VARIABLE	CLOUD		

Figure 39: Histograms for June: CP1

pattern at Barrow is 6.1 ms^{-1}, and is one to two ms^{-1} higher than all of the other major June CP's except CP16. This weather characteristic is largely responsible for the ANOVA F-ratio of 6.3 for Barrow's mean wind speed in June, which is the largest value for this variable in any month. This high wind speeds of CP1 are somewhat puzzling, because the pressure pattern intensity index (s_p, see Chapter IV) drops to about half of its January value during June, but the surface winds become stronger. This discrepancy may indicate the inadequacy of the land-based synoptic station network for representing the large-scale pressure gradients normal to the coast. Also, it is quite plausible that large-scale sea breeze effects begin to systematically accelerate the synoptic-scale easterlies as summer approaches (Moritz, 1977). In any case, CP1 stands out as a windy pattern in June. In Tables I and II it was shown that the overall cloudiness increases markedly from April to May at both Barrow and Barter Island. Such increases occur across all of the CP groups, leading to a non-significant χ^2 test for the June inter-CP sky cover differences (Table XXXIII). CP1, for example, has 8.2 tenths mean sky coverage and a modal value of ten tenths. Only 2 of 14 CP's had modes other than ten tenths in June, and all of the mean values were in the range 7.1 tenths to 9.6 tenths. It appears, then, that the local availability of moisture (probably from melting snow and ince and leaks in the pack ice) is more important in determining the June cloudiness than is the type of pressure pattern. Again, the inter-CP precipitation differences were not highly-significant in June (Table XXXII). CP1 contributed 16.5 mm, which is 9% of the 1955-1974 total for June at Barrow, and had measurable precipitation in 9% of cases. Overall, CP1 brings fairly normal weather conditions over the coast during the transition season, except for rather high mean wind speeds.

CP8, with a low pressure center over east-central Alaska and cyclonic flow over the Beaufort coast, is the second most-frequent CP in June, accounting for 10% of the daily patterns. From Figure 40 we see that this pattern is associated with north-northeasterly winds at Barrow, bringing air directly off the ice-covered ocean during June. These winds are associated with mean temperature departures of -2.0°C (Barrow) and -1.8°C (Barter Island). These data make CP8 the coolest June pattern. The mean wind speed for CP8 is 4.4 ms^{-1}, or 0.7 ms^{-1} below the overall June average at Barrow. It is perhaps worthwhile to note that the juxtaposition of high to the north, low to the south, as with CP1, is absent in this pattern, leading to rather light winds. This characteristic occurs with other patterns as well. Despite the non-significant χ^2 results, the CP8 sky cover distribution is strongly weighted towards the overcast end, indicating the tendency for the cyclonic surface flow to produce vertical motions in the already-moist air. It is during June that the clouds begin to affect the surface radiation balance in a negative sense, because of the dominance of the solar radiation term as summer approaches. Such effects might be expected to lead to negative mean temperature departures such as those of CP8. Measurable precipitation was produced by CP8 in only 17% of cases at Barrow, despite the cyclonicity of the pattern. The main distinguishing characteristic of the central low, then, is its tendency to bring northerly winds and below-average temperatures over the northern coast.

The frequency of CP2 increases from May to June, heralding its brief dominance as the major summer pattern. In Figure 41 it is evident that a great deal of scatter characterizes the June wind direction distribution for CP2. However, the mean value remains somewhat west of south, as in winter. It is

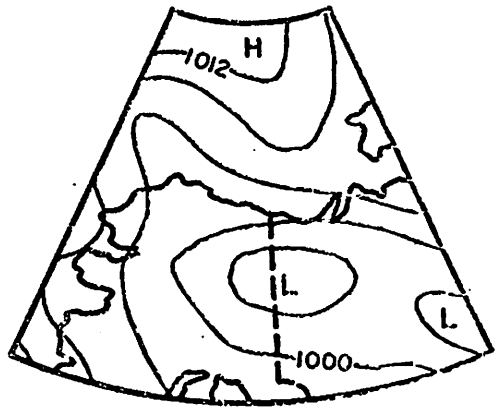

CP8

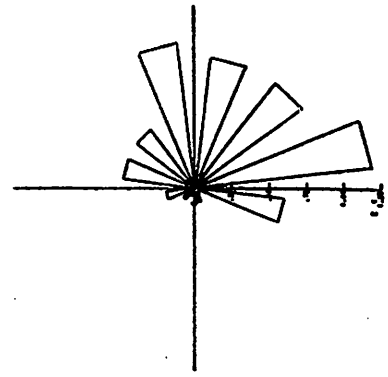

MONTH	6	SAMPLE	60
PATTERN	8	MEAN	29.6
STATION	BARROW	SD	63.5
VARIABLE	WIND DIR		

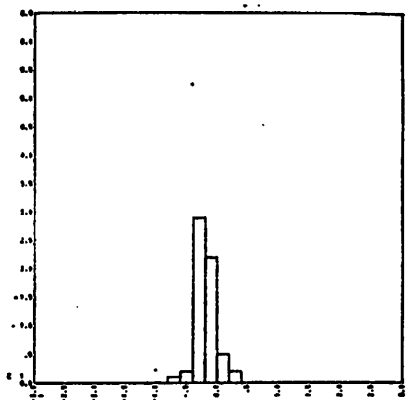

MONTH	6	SAMPLE	61
PATTERN	8	MEAN	-2.0
STATION	BARROW	SD	1.7
VARIABLE	T-DEP		

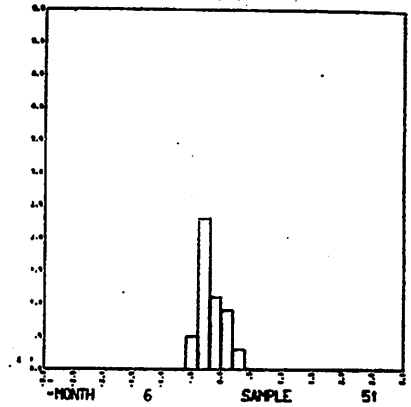

MONTH	6	SAMPLE	51
PATTERN	8	MEAN	-1.8
STATION	BARTER	SD	2.0
VARIABLE	T-DEP		

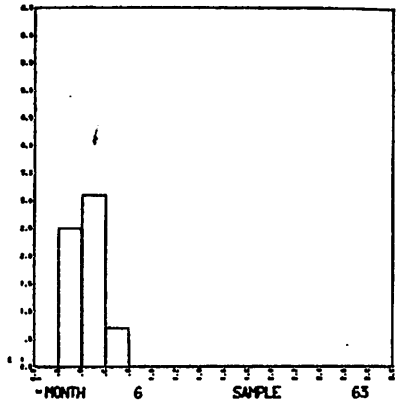

MONTH	6	SAMPLE	63
PATTERN	8	MEAN	4.4
STATION	BARROW	SD	1.3
VARIABLE	WIND-1		

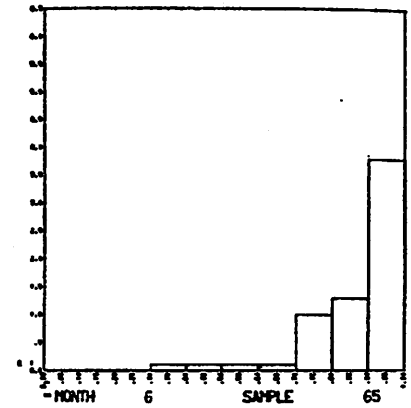

MONTH	6	SAMPLE	65
PATTERN	8	MEAN	9.2
STATION	BARROW	SD	1.2
VARIABLE	CLOUD		

Figure 40: Histograms for June: CP8

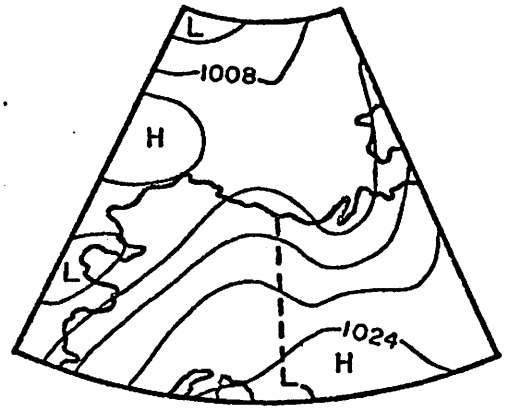

CP2

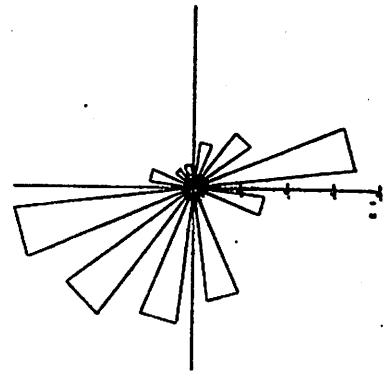

MONTH 6 SAMPLE 45
PATTERN 2 MEAN 200.7
STATION BARROW SD 93.0
VARIABLE WIND DIR

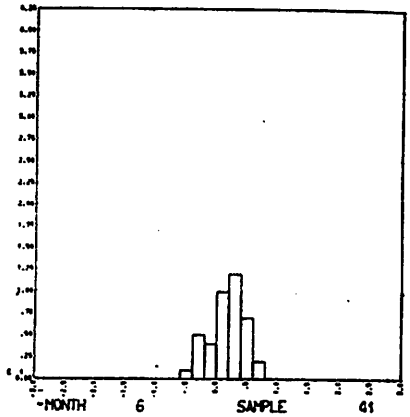

MONTH 6 SAMPLE 41
PATTERN 2 MEAN 1.8
STATION BARROW SD 2.9
VARIABLE T-DEP

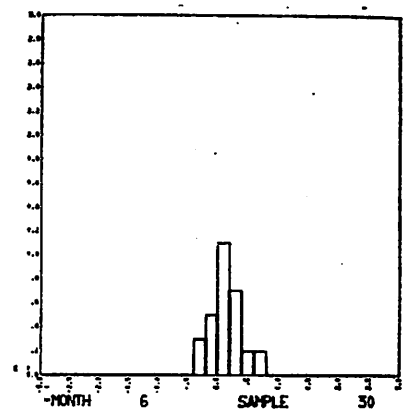

MONTH 6 SAMPLE 30
PATTERN 2 MEAN 1.2
STATION BARTER SD 2.6
VARIABLE T-DEP

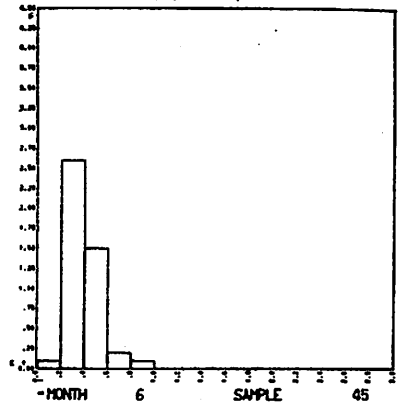

MONTH 6 SAMPLE 45
PATTERN 2 MEAN 4.0
STATION BARROW SD 1.2
VARIABLE WIND-1

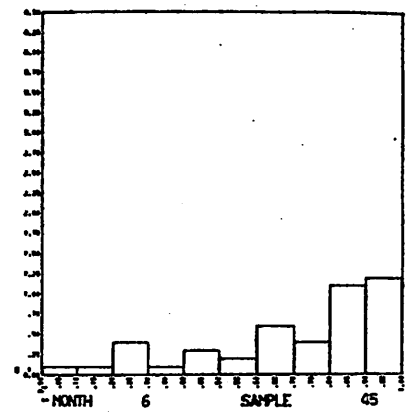

MONTH 6 SAMPLE 45
PATTERN 2 MEAN 7.5
STATION BARROW SD 2.6
VARIABLE CLOUD

Figure 41: Histograms for June: CP2

also interesting to notice that CP2 is the warmest pattern in June, just as it was in January. The associations of CP2 with cloudy skies, high winds and frequent, relatively heavy precipitation do not exist in the transition season, however. In fact, CP2 has the lowest mean wind speed of all major June patterns, and the fourth-lowest mean sky cover out of the 15 most-frequent June CP's. The lack of these associations implies a different warming mechanism than in winter. This is not surprising, because the surface temperature inversion weakens considerably from January to June, and the overall mean temperature gradient from the north Pacific to the Arctic coast is much weaker at this season. Therefore, the incursion of air from the south does not represent so large a change in spring. Also, since the overall regional baroclinicity is decreased, the cyclonic systems do not develop such intense pressure gradients in spring, leading to weaker surface winds. If, as suggested in Moritz (1977), the coastal easterlies are accelerated by the land-ocean heating differences, then synoptic patterns with southwesterly flow will oppose the sea breeze flow, and may have lower mean wind speeds as a consequence. We also note that, once the snow cover starts to disappear from the tundra, the continuous solar irradiance heats the surface. Thus winds with a southerly component may be expected to lead to horizontal enthalpy flux convergence near the coast, which indicates rising temperatures. These local advection effects should become progressively more important in comparison to the synoptic-scale advection as the summer proceeds and the heating contrasts between tundra and ocean intensify. Measurable precipitation accompanies 29% of the CP2 occurrences in June, about half the corresponding value for January. Much of the fall-off may be attributed to the lesser intensity of the patterns in spring and the decreased thermal contrasts between the Arctic Coast and the Bering Sea region. Both of these changes should lead to less-vigorous vertical motions in spring. CP2 is, however, second only to CP6 in its contribution to the monthly catch at Barrow (16%).

CP6 occurs on 7% of June days, and is characterized by low pressure off Alaska's west coast with a trough extending eastward over the state (Figure 42). The temperature departures are unremarkable at Barrow ($0^{o}C$) and slightly positive at Barter Island ($+0.9^{o}C$). Barrow winds come from the east under CP6 in June, in agreement with the geostrophic flow expected from the synoptic map. The average June CP6 wind wpeed is 5.3 ms^{-1} at Barrow, which is roughly normal for the month. CP6 mean sky cover is somewhat heavier than for most other June patterns. Precipitation turns out to be the most prominent weather characteristic of this pattern in June. 20% of the monthly catch results from CP6 despite its 7% frequency. This is another pressure pattern associated with the west coast cyclone trajectory, indicating that the origin of the participating air mass may be an important factor in causing spring precipitation, as is the cyclonic curvature of the surface isobars. It is worth pointing out that the near-continuous overcast for most June patterns may well be a thin, local layer of stratus, while a few patterns could be associated with thicker cloud layers, related to a deep vertical circulation. Such differences are not resolved by our mean sky cover variable, which takes no account of the cloud type.

CP5 is another summer pattern whose frequency increases from May to June, accounting for over 5% of days. Winds are from the west under CP5, as they were in winter (Table XXXVII). CP5 is not associated with systematic, large-magnitude temperature departures in June. Similarly, Barrow mean sky cover and wind speed are near normal for CP5. This pattern does, however, contribute 14% of the June precipitation, with measurable falls in 27% of cases.

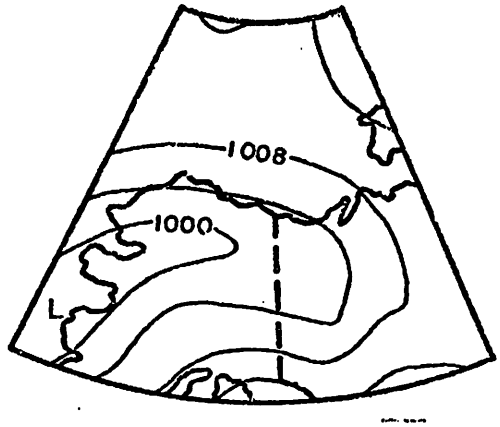

CP6

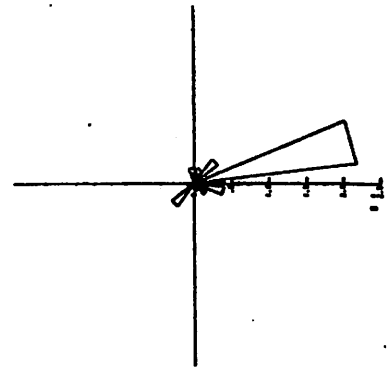

MONTH	6	SAMPLE	42
PATTERN	6	MEAN	82.0
STATION	BARROW	SD	54.5
VARIABLE	WIND DIR		

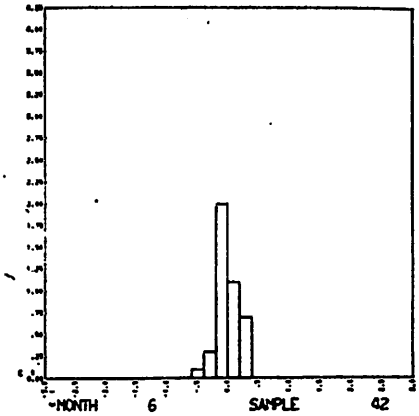

MONTH	6	SAMPLE	42
PATTERN	6	MEAN	.0
STATION	BARROW	SD	1.7
VARIABLE	T-DEP		

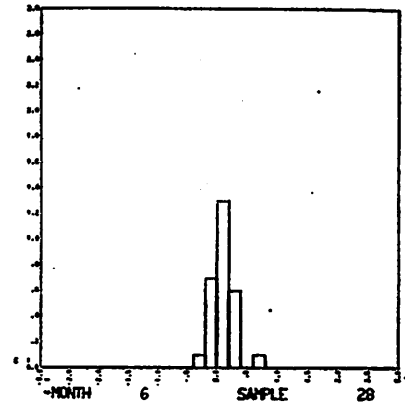

MONTH	6	SAMPLE	28
PATTERN	6	MEAN	.9
STATION	BARTER	SD	1.9
VARIABLE	T-DEP		

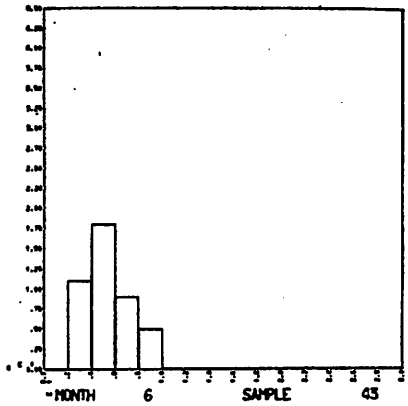

MONTH	6	SAMPLE	45
PATTERN	6	MEAN	5.3
STATION	BARROW	SD	1.8
VARIABLE	WIND-1		

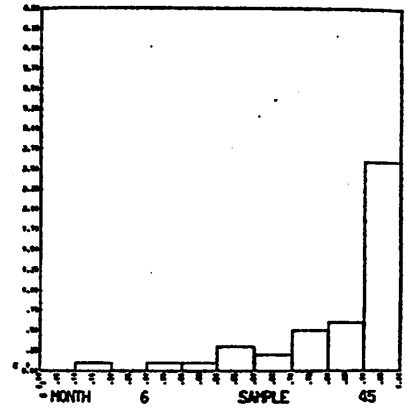

MONTH	6	SAMPLE	45
PATTERN	6	MEAN	8.8
STATION	BARROW	SD	1.9
VARIABLE	CLOUD		

Figure 42: Histograms for June: CP6

CP4 accounts for 6% of the daily June patterns, bringing tempratures slightly above normal at both Barrow and Barter Island. The winds come from almost due east at Barrow, which indicates a large-scale trajectory right along the coastline (Table XXXVII). These winds tend to be about 5 ms^{-1}, on average. Precipitation is rather infrequent (11% of CP4 cases). This pattern has the lowest mean sky cover of all June CP's at Barrow (7.1 tenths), which may suggest a connection between incident solar radiation and screen temperature departures, but the clouds still cover a substantial fraction of the sky.

CP14 is a rather infrequent, but interesting, June pattern (Figure 43). The weather characteristics of CP14 include negative temperature departures at Barrow (-1.9°C) and Barter Island (-1.1°C), which are the second-lowest among all June CP's. The relatively low temperatures are associated with northwesterly surface winds, indicating outflow from the central Arctic Basin. CP14 is characterized by high pressures in the Chukchi Sea and northeasterly surface geostrophic flow on the Beaufort coast. We also note that this pattern has the highest mean sky cover (9.6 tenths) of all June patterns. Given the anticyclonic curvature of the isobars in this case, we might expect thin stratus, advected from the ice-covered ocean, rather than thick, precipitation-bearing clouds associated with the cyclonic storms on the west coast.

CP15, with a strong low pressure cell in the Chukchi Sea, brings relatively warm air to Barrow and Barter Island in June (Table XXXVII). Barrow's winds are from the southwest, on average, for CP 15, indicating large-scale warm advection and local flow from the tundra surface in most cases. 36% of the CP15 cases brought measurable precipitation to Barrow in June. Mean sky cover (8.6 tenths) and wind speed (5.7 ms^{-1}) are slightly above the monthly normals.

Finally, CP21 is of interest because of the contrasting temperature departures at Barrow (+1.6°C) and Barter Island (-1.0°C). Notice from Figure 44 that Barter Island's surface geostrophic winds are northeasterly for this pattern, while Barrow's flow is from the southeast. Indeed, the observed surface winds at Barrow are from the east-southeast. Again we see a positive association between termperature departures and flow from the tundra surface and interior of Alaska, and vice versa. The 32% occurrence of measurable precipitation for CP21 is surprising, given the strong anticyclonic curvature of the isobars.

The month of June is one of transition, in terms of the atmospheric circulation as well as the local climate on the Beaufort Sea coast. The strong winter circulation regime, dominated by CP's 1, 3, and 4 gives way to more frequant northward excursions of low pressure cells (CP's 2, 5, 6, and 8) and a generally greater variety of patterns. Coastal weather is less variable in June than in any other month. The sky is usually overcast, winds blow steadily at about 5 ms^{-1} and temperatures seldom stray more than 3 of 4°C from normal, which is just slightly above the freezing point. Patterns with a southerly component to their mean surface winds are associated with positive temperature departures (CP's 2, 21, 15 and 12). In June the southerly flow implies local advection of warm air from the tundra as well as macroscale advection from low latitudes. Patterns with a northerly mean wind component are coolest, including CP's 8, 14 and 1. CP's 6, 2, 5, and 15 contribute over half of the June precipitation at Barrow and are associated with the movement of low pressure cells from the Bering Sea area to the Arctic Basin. All of the major

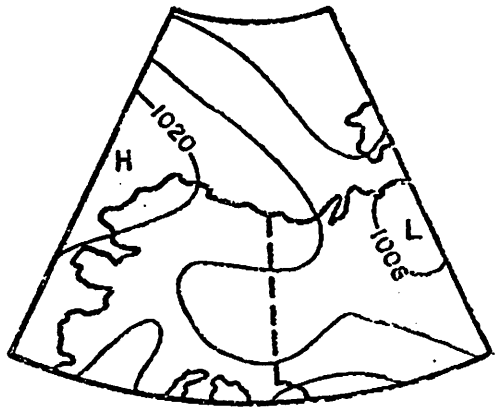

CP14

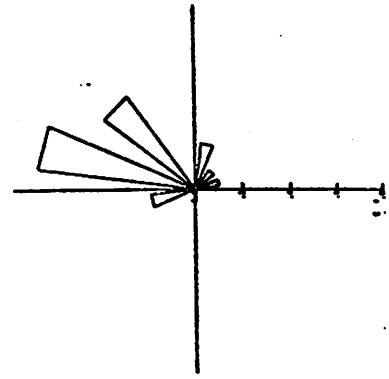

MONTH	6	SAMPLE	18
PATTERN	14	MEAN	313.6
STATION	BARROW	SD	47.0
VARIABLE	WIND DIR		

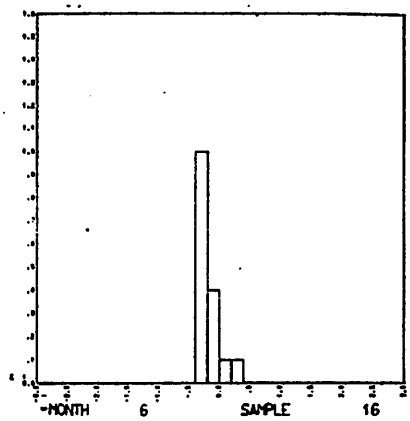

MONTH	6	SAMPLE	16
PATTERN	14	MEAN	-1.9
STATION	BARROW	SD	1.7
VARIABLE	T-DEP		

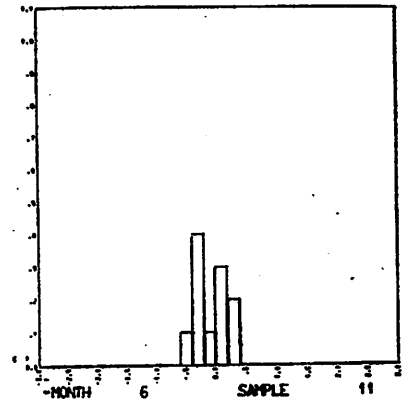

MONTH	6	SAMPLE	11
PATTERN	14	MEAN	-1.1
STATION	BARTER	SD	2.4
VARIABLE	T-DEP		

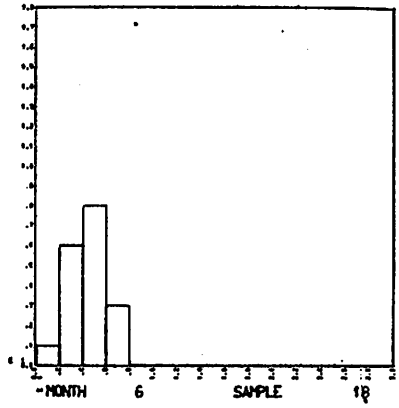

MONTH	6	SAMPLE	18
PATTERN	14	MEAN	4.4
STATION	BARROW	SD	1.4
VARIABLE	WIND-1		

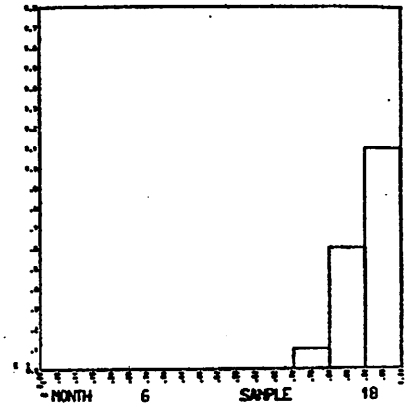

MONTH	6	SAMPLE	18
PATTERN	14	MEAN	9.6
STATION	BARROW	SD	.6
VARIABLE	CLOUD		

Figure 43: Histograms for June: CP14

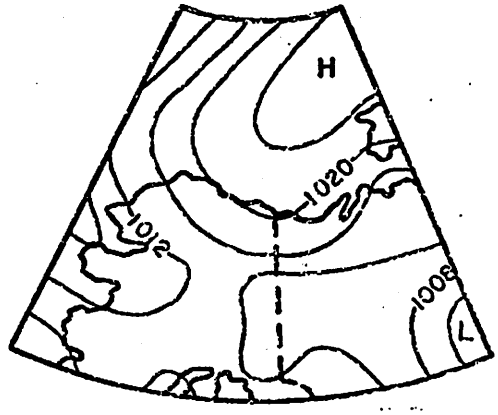

CP21

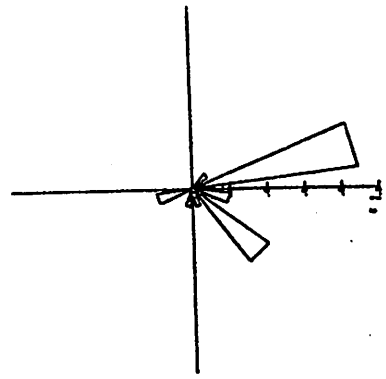

MONTH	6	SAMPLE	21
PATTERN	21	MEAN	111.8
STATION	BARROW	SD	53.7
VARIABLE	WIND DIR		

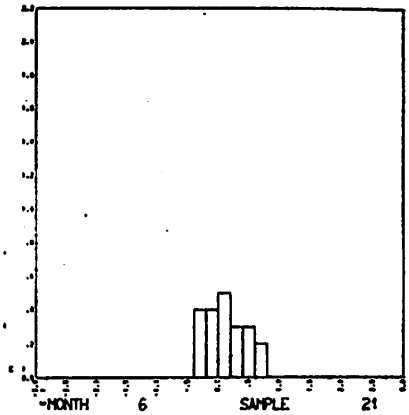

MONTH	6	SAMPLE	21
PATTERN	21	MEAN	1.6
STATION	BARROW	SD	3.1
VARIABLE	T-DEP		

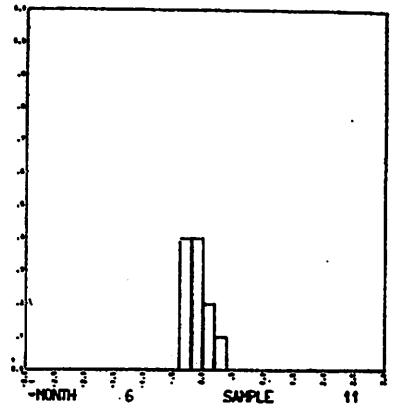

MONTH	6	SAMPLE	11
PATTERN	21	MEAN	-1.0
STATION	BARTER	SD	1.6
VARIABLE	T-DEP		

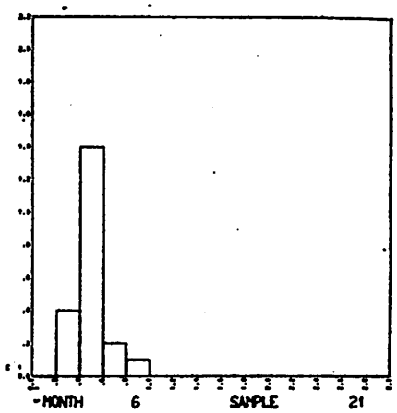

MONTH	6	SAMPLE	21
PATTERN	21	MEAN	5.1
STATION	BARROW	SD	1.2
VARIABLE	WIND-1		

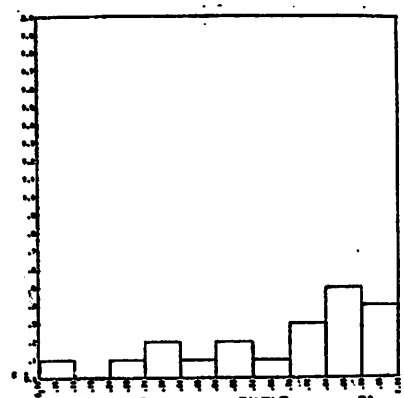

MONTH	6	SAMPLE	20
PATTERN	21	MEAN	7.3
STATION	BARROW	SD	2.7
VARIABLE	CLOUD		

Figure 44: Histograms for June: CP21

June patterns bring cloudy conditions to the Beaufort coast, and differences in cloud type and thickness cannot be resolved with the Local Climatological Data sets.

Summer

The summer circulation regime is fully developed in July and the Beaufort Sea coast. CP1 reaches its annual minimum frequency (9%) while CP2 dominates (22%), indicating a full reversal of the most-frequent CP's surface geostrophic wind direction from winter. The weather characteristics for major summer pressure patterns are set out in Table XXXVIII. Figure 45 shows the distributions for CP2. The center of the wind direction distribution is southwesterly, again in agreement with the geostrophic direction on the CP2 synoptic map. This flow brings temperature departures of +1.0°C to Barrow and +1.6°C to Barter Island, making CP2 the third-warmest July pattern. Interestingly, the respective departures in August are only +0.1°C and +0.2°C. Inter-CP sky cover and dew-point depression differences are highly significant in July, and these weather characteristics help us identify some of the salient processes which occur with each CP. For example, CP2 is associated with a relatively large mean dew point depression of 2.1°C at Barrow. This relatively dry air corresponds to frequent winds off the tundra, in agreement with the CP2 surface flow and temperature departures. CP2 also has the second-lowest mean sky cover of any major July pattern (6.9 tenths). Despite this relatively low sky cover, measurable precipitation accompanies 46% of July-August CP2 occurrences at Barrow. This pattern accounts for a full 35% of the seasonal precipitation catch in summer. Thus the summer circulation's main mode is a warm, southwesterly pattern, frequently associated with precipitation, but with relatively large surface dew point depressions, on average. Recall that CP2 is often the final pattern in transition sequences involving low pressure systems on a Bering Sea-to-Arctic Basin trajectory. Also, the southeast high pressures on the CP2 map are often northward extensions of the quasi-permanent Pacific high pressure cell in summer. It should appear that interannual variations in the date at which the Pacific high establishes its more-northerly summer location may correspond to systematic temperature anomalies on the margins of the Arctic Ocean, because the west coast cyclone patterns bring relatively warm air over the region. These patterns, in turn, occur more frequently after the northward displacement of the Pacific high. The positive feedback potential between June temperature departures, the albedo of sea ice, and the solstitial maximum in solar radiation has been emphasized by Fletcher (1969, p. 10). We have noted already, however, that our static pressure pattern classification cannot reliably establish the origin and trajectory of the air masses associated with each CP. For example, Reed and Kunkel (1960) state that low pressure systems over the Beaufort Sea often originate in the baroclinic zone along the Siberian Coast, rather than moving up the Bering Straits. It is clear that the large-scale connections between Beaufort Sea ice conditions and May-June shifts in the Pacific high need to be investigated further in this connection. Our analysis does indicate that earlier-than-normal incursions of cyclonic storms in spring and early summer lead to positive temperature departures along Alaska's north coast, in agreement with the argument of Fletcher (1969, p. 11, 47).

CP5 (Figure 46) accounts for 11% of July's pressure patterns in the region. As in winter this pattern brings surface westerlies to Barrow, which indicates advection directly off the Chukchi Sea. The associated temperature

TABLE XXXVIII

JULY CP WEATHER CHARACTERISTICS

CP	$\overline{dT1}$ (°C)	$\overline{dT2}$ (°C)	$\overline{WD}$ (°)	$\overline{U}$ (m/s)	$\overline{SC}$ (1/10)	$\overline{dT_D}$ (°C)	$\overline{r^*}$ (mm)	$\overline{\%-1}$ (%)	$\overline{\%-2}$ (%)
1	-1.7	-1.5	68	6.3	6.4	1.7	49.5	5	15
2	+1.0	+1.6	227	5.1	8.5	2.1	329.7	35	46
4	+2.0	+0.2	89	5.5	6.9	2.5	28.4	3	21
5	-2.1	-1.4	262	5.0	8.9	1.8	115.6	12	46
6	-0.3	-1.2	71	5.4	8.0	1.8	77.7	8	34
8	-2.5	-3.0	9	4.6	8.9	0.9	64.3	7	39
14	-3.2	-2.6	308	3.9	8.2	1.4	15.0	2	30
15	+1.3	+0.1	196	5.0	8.9	2.1	156.0	17	54
21	+0.6	-1.8	91	5.3	8.0		1.5	0	23

*Precipitation data are for season IV (July-August) rather than for July.

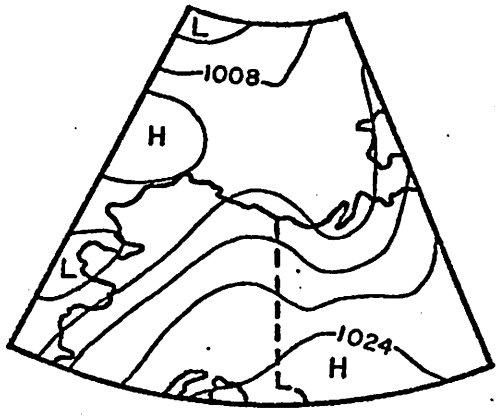

CP2

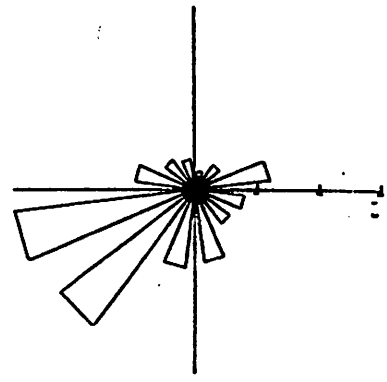

MONTH 7 SAMPLE 139
PATTERN 2 MEAN 226.8
STATION BARROW SD 80.2
VARIABLE WIND DIR

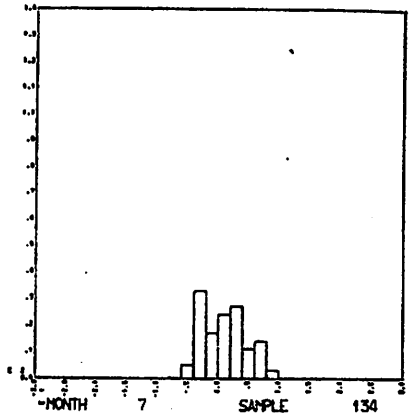

MONTH 7 SAMPLE 134
PATTERN 2 MEAN 1.0
STATION BARROW SD 3.6
VARIABLE T-DEP

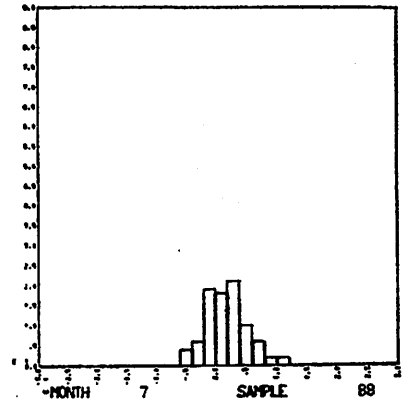

MONTH 7 SAMPLE 88
PATTERN 2 MEAN 1.6
STATION BARTER SD 3.4
VARIABLE T-DEP

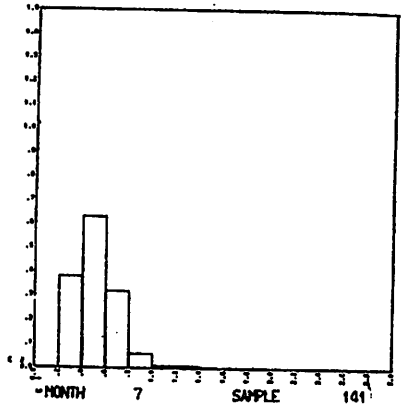

MONTH 7 SAMPLE 141
PATTERN 2 MEAN 5.1
STATION BARROW SD 1.7
VARIABLE WIND-1

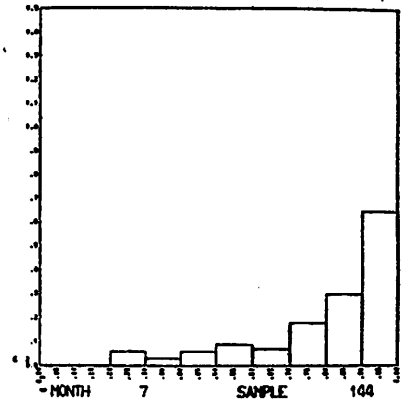

MONTH 7 SAMPLE 144
PATTERN 2 MEAN 8.5
STATION BARROW SD 2.0
VARIABLE CLOUD

Figure 45: Histograms for July: CP2

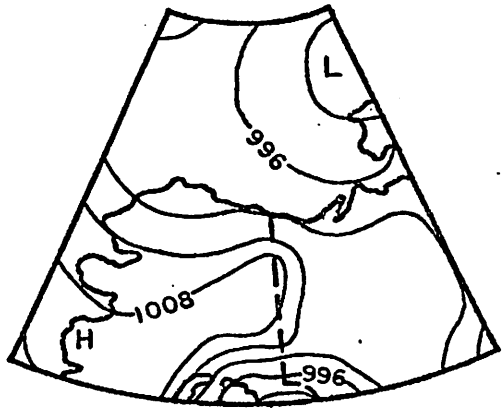

CP5

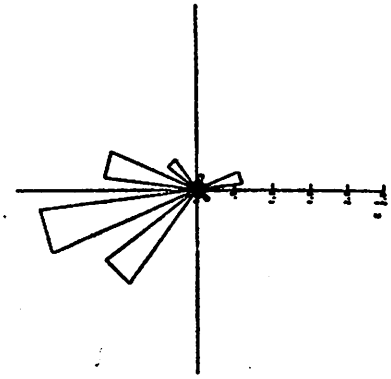

MONTH	7	SAMPLE	71
PATTERN	5	MEAN	262.2
STATION	BARROW	SD	59.8
VARIABLE	WIND DIR		

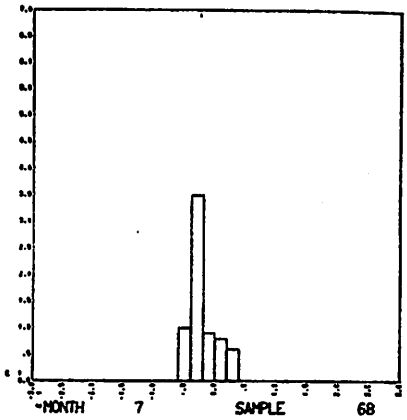

MONTH	7	SAMPLE	68
PATTERN	5	MEAN	-2.1
STATION	BARROW	SD	2.3
VARIABLE	T-DEP		

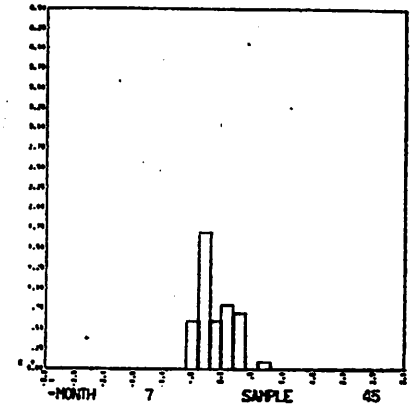

MONTH	7	SAMPLE	45
PATTERN	5	MEAN	-1.4
STATION	BARTER	SD	2.9
VARIABLE	T-DEP		

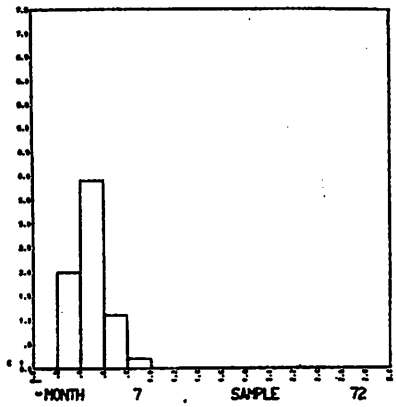

MONTH	7	SAMPLE	72
PATTERN	5	MEAN	5.0
STATION	BARROW	SD	1.5
VARIABLE	WIND-1		

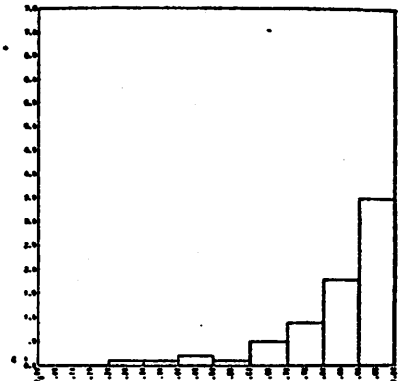

MONTH	7	SAMPLE	72
PATTERN	5	MEAN	8.9
STATION	BARROW	SD	1.5
VARIABLE	CLOUD		

Figure 46: Histograms for July: CP5

departures are negative at both Barrow (-2.1°C) and Barter Island (-1.4°C). At the latter station the surface geostrophic flow is from west-northwest, again indicating advection from the ocean. CP5 wind speeds average 5.0 ms^{-1} in July and are similar to the mean monthly speed (5.1 ms^{-1}) and the CP2 speed (5.1 ms^{-1}). Relatively cloudy skies (8.9 tenths) are frequent precipitation (46% of cases) also accompany this pattern. 12% of Barrow's July-August precipitation falls during occurrence of CP5. Despite the fact that CP5 usually occurs in a sequence of northward-moving pressure features, it has negative temperature departures, pointing up the importance of local advective effects near the sea-tundra boundary in summer.

CP1 is the third major summer pattern and brings northeasterly winds and negative temperature departures to the region (Figure 47). Perhaps the most interesting CP1 characteristic is its high surface wind speed at Barrow (6.3 ms^{-1}). As in June, this value is substantially higher than one would expect from the pressure intensity indexes in Table XII. In fact, although the CP1 value is 12.2 in January and only 5.4 in July, the corresponding surface wind speeds at Barrow are 5.6 ms^{-1} and 6.3 ms^{-1}, respectively. Since the geostrophic surface wind speed is (roughly) proportional to the index s_p, the winds must be either highly ageostrophic or driven by pressure gradients normal to the coast which are not recorded on the NMC pressure grids. As shown in Mortiz (1977), the latter explanation is more plausible, wherein the local gradient is enhanced by an offshore pressure gradient due to ocean-tundra heating contrasts. As we shall see in this section, the easterly patterns have higher mean wind speeds than the westerly patterns in July. CP1's northeasterly winds come from the Beaufort Sea, bringing relatively moist air over Barrow as indicated by the dew point depression of only 1.7°C. This pattern is, however, the least cloudy of the major July CP's, with mean sky cover of 6.4 tenths. Precipitation occurs in only 15% of CP1 cases in July-August, accounting for 5% of the seasonal catch. This statistic makes CP1 the driest summer pattern.

CP15 is another frequent summer pattern associated with the west coast cyclone track (Figure 48). The low pressure cell in the Chukchi Sea area brings winds from the south-southwest at Barrow, but considerable scatter is evident on the directional histogram. Again these southerlies are associated with positive temperature departures at Barrow in July (+1.3°C) and August (+1.7°C), although the Barter Island values are more modest (+0.1°C and +0.8°C, respectively). Note from the CP15 synoptic map that Barter Island is somewhat east of the strongest southerly flow. The mean CP15 wind speed is 5.0 ms^{-1} in July, which is about normal for the month. The dew point depressions for this pattern averaged 2.1°C, which value is relatively large, again in association with southerly wind flow. The strong cyclonic curvature of CP15's isobars brings frequent precipitation (54% of cases) and cloudy skies (8.9 tenths) to Barrow in July. Despite CP15's position as the fourth-most frequent pattern in summer, it accounts for 17% of the season precipitation, ranking second behind CP2 in this respect.

Another west coast low pressure pattern is CP6 (Figure 49) with 7% frequency in July. Barrow winds are from east-northeast with this pattern, most frequently bringing temperatures 2 to 3°C below normal. However, the temperature departure distributions are right-skew, and a few, relatively warm cases bring the mean value up to -0.3°C at Barrow and -1.2°C at Barter Island. The

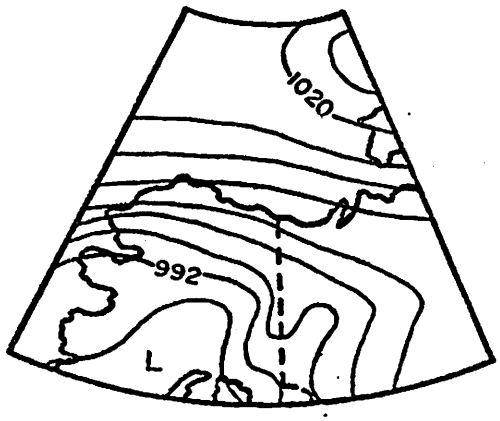

CP1

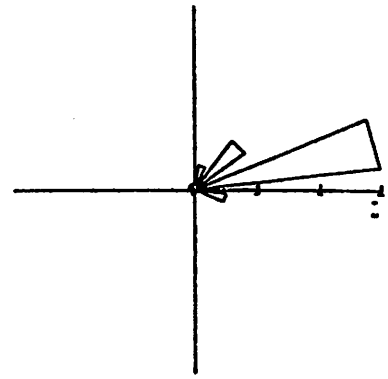

MONTH	7	SAMPLE	52
PATTERN	1	MEAN	67.6
STATION	BARROW	SD	32.4
VARIABLE	WIND DIR		

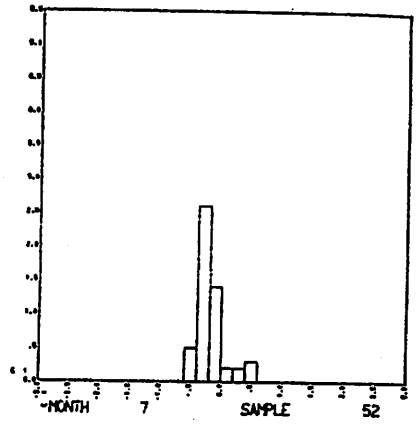

MONTH	7	SAMPLE	52
PATTERN	1	MEAN	-1.7
STATION	BARROW	SD	2.4
VARIABLE	T-DEP		

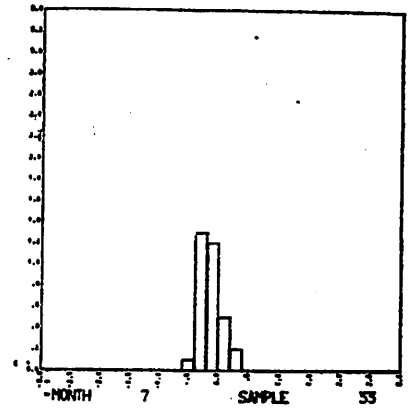

MONTH	7	SAMPLE	53
PATTERN	1	MEAN	-1.5
STATION	BARTER	SD	2.0
VARIABLE	T-DEP		

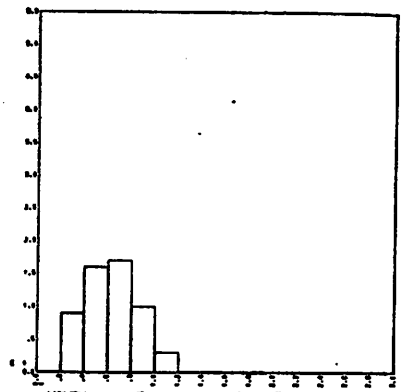

MONTH	7	SAMPLE	55
PATTERN	1	MEAN	6.3
STATION	BARROW	SD	2.2
VARIABLE	WIND-1		

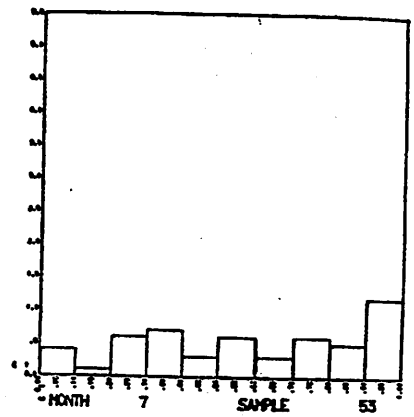

MONTH	7	SAMPLE	53
PATTERN	1	MEAN	6.4
STATION	BARROW	SD	3.0
VARIABLE	CLOUD		

Figure 47: Histograms for July: CP1

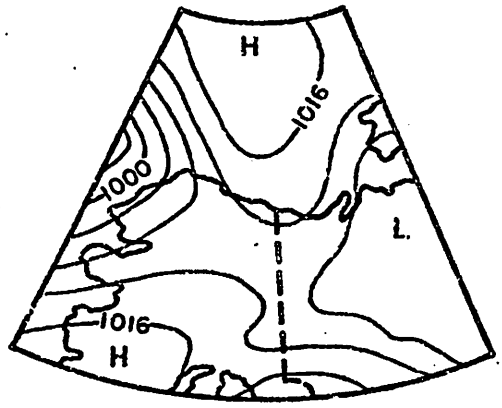

CP15

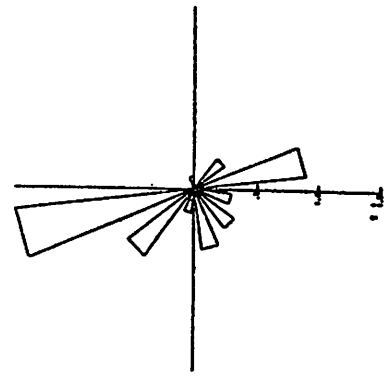

MONTH	7	SAMPLE	49
PATTERN	15	MEAN	195.6
STATION	BARROW	SD	89.9
VARIABLE	WIND DIR		

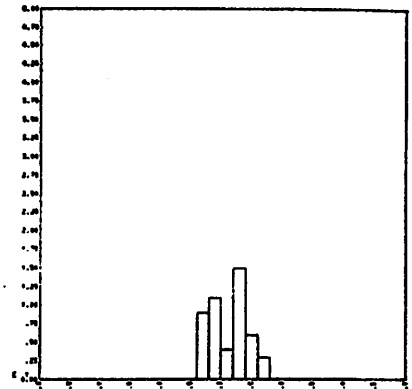

MONTH	7	SAMPLE	48
PATTERN	15	MEAN	1.3
STATION	BARROW	SD	3.1
VARIABLE	T-DEP		

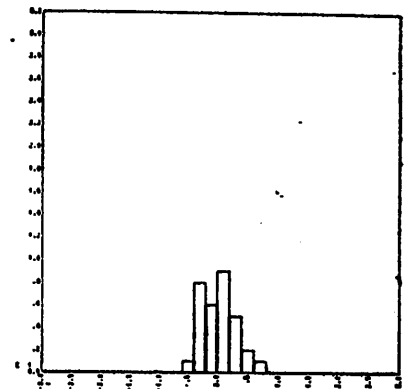

MONTH	7	SAMPLE	52
PATTERN	15	MEAN	.1
STATION	BARTER	SD	2.8
VARIABLE	T-DEP		

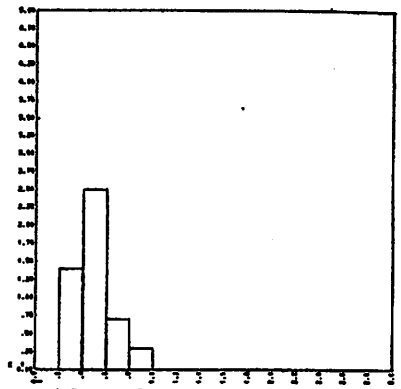

MONTH	7	SAMPLE	49
PATTERN	15	MEAN	5.0
STATION	BARROW	SD	1.6
VARIABLE	WIND-1		

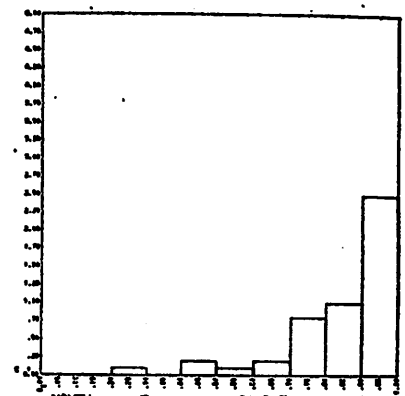

MONTH	7	SAMPLE	49
PATTERN	15	MEAN	8.9
STATION	BARROW	SD	1.6
VARIABLE	CLOUD		

Figure 48: Histograms for July: CP15

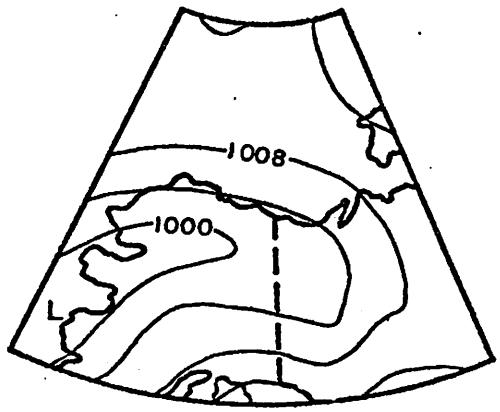

CP6

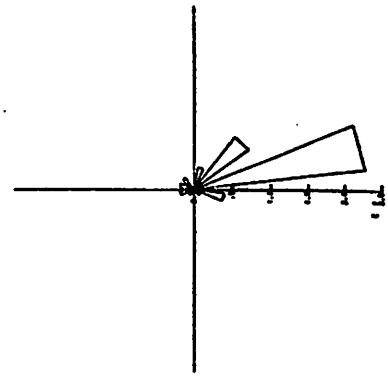

MONTH	7	SAMPLE	47
PATTERN	6	MEAN	71.1
STATION	BARROW	SD	52.9
VARIABLE	WIND DIR		

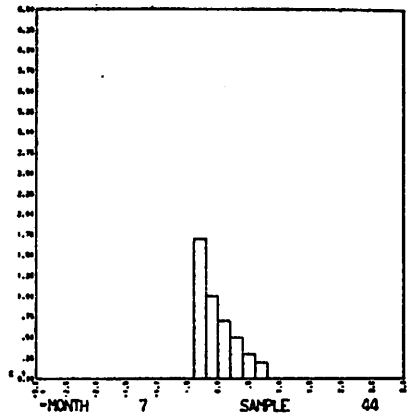

MONTH	7	SAMPLE	44
PATTERN	6	MEAN	-.3
STATION	BARROW	SD	3.0
VARIABLE	T-DEP		

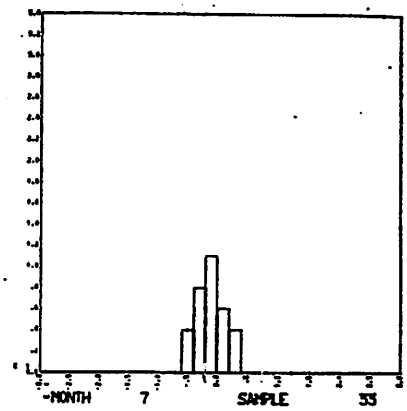

MONTH	7	SAMPLE	33
PATTERN	6	MEAN	-1.2
STATION	BARTER	SD	2.5
VARIABLE	T-DEP		

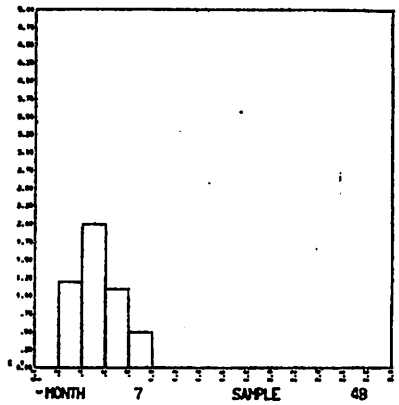

MONTH	7	SAMPLE	48
PATTERN	6	MEAN	5.4
STATION	BARROW	SD	1.9
VARIABLE	WIND-1		

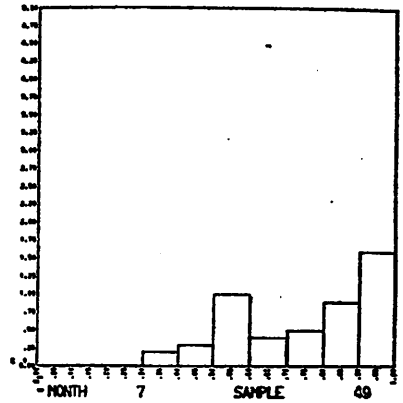

MONTH	7	SAMPLE	49
PATTERN	6	MEAN	8.0
STATION	BARROW	SD	1.9
VARIABLE	CLOUD		

Figure 49: Histograms for July: CP6

cyclonic curvature of CP6 is associated with measurable precipitation in 34% of cases at Barrow, yielding 8% of the July-August total. 8.0 tenths sky coverage and 1.8°C dew point depressions highlight the moist, marine aspects of this pattern. Note that CP6 is another pattern with easterly surface winds at Barrow, and the mean speed there is 5.4 ms^{-1}, third-highest for the month. It is worthwhile to point out that CP6 and CP15 often occur in the inter-CP transition sequences with Pacific lows moving northward along the west coast. Although one expects similar large-scale air mass advection for two such patterns, we see that CP15 has positive departures while CP6's are negative. It appears that the local-scale advection of air from tundra or ocean is paramount in determining the summer temperature departures.

CP8 occurs on 7% of days in July and is not regularly associated with the west coast storm trajectory. This pattern has a low over east-central Alaska (Figure 50). CP8 winds come from almost due north over Barrow as the air circulates about the low pressure cell. Again the local flow direction dominates the temperature conditions, as indicated by mean departures of -2.5°C at Barrow and -3.0°C at Barter Island. The scatter on these histograms is particularly small. Barrow dew point depressions are at a minimum for CP8 (0.9°C), emphasizing the advection of moisture off the sea by the notherly winds. CP8 also brings cloudy skies and frequent precipitation (37% of cases) to Barrow.

The coolest major CP in July is CP14 (Figure 51), with a high pressure cell in the Chukchi Sea bringing northwesterly surface geostrophic flow over the Beaufort Sea coast. Surface winds at Barrow are also northwesterly in July. The mean temperature departures at Barrow and Barter Island are -3.2°C and -2.6°C, respectively, which translate to actual temperatures only 0.5 to 1.8°C above freezing. The local marine environment of ice and open water is probably responsible for these temperature data, because the surface air parcels with long trajectories over the ocean are cooled by turbulent enthalpy exchange, while the ocean warms only slightly because of its larger heat capacity. CP14's relatively small dew point depression (1.4°C) also indicates marine influences. The small standard deviations of the temperature departure distributions imply a near-constant cold source for the air, which is provided by the ice-covered ocean with a surface temperature near 0°C. CP14 has the lowest mean wind speed of all July CP's (3.9 ms^{-1} at Barrow), so even in summer the ridges from the west bring calmer conditions. Despite the anticyclonic curvature of the streamlines, 30% of CP14 cases had measurable precipitation at Barrow during July-August. The CP14 summer total amounts to 2% of the seasonal catch.

CP4 occurs on about 5% of July days, and is the warmest pattern at Barrow (+2.0°C). As in winter, the surface winds are easterly (Figure 52). Mean sky cover is a relatively low 6.9 tenths, probably associated with the large-scale flow from the dry interior of Alaska and the lack of strong cyclonic curvature near Barrow. Precipitation accompanies 21% of the CP4's, accounting for only 3% of the July-August catch at Barrow. The mean wind speed is above the overall July average at 5.5 ms^{-1}, again illustrating the relative strength of easterly flow patterns.

As in June, the CP21 temperature departures are positive (+0.6°C) at Barrow and negative (-1.8°C) at Barter Island, indicating the importance of off-tundra flow in the former case and off-ocean flow in the latter (Table XXXVIII). This pattern occurs on 4% of July days, and brings easterly surface winds to Barrow at 5.3 ms^{-1}.

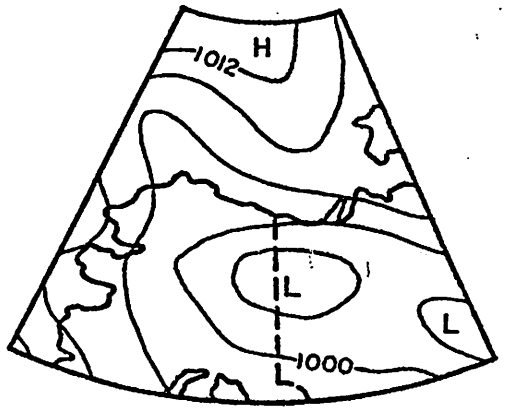

CP8

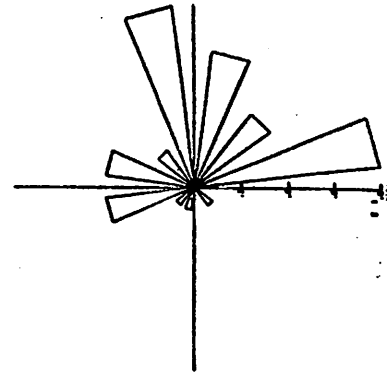

MONTH 7 SAMPLE 59
PATTERN 8 MEAN 8.7
STATION BARROW SD 75.1
VARIABLE WIND DIR

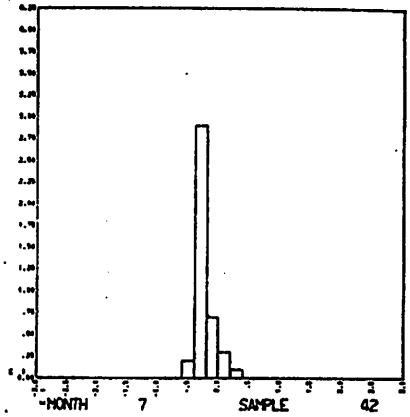

MONTH 7 SAMPLE 42
PATTERN 8 MEAN -2.5
STATION BARROW SD 1.7
VARIABLE T-DEP

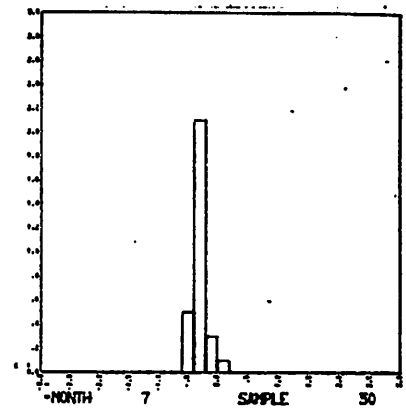

MONTH 7 SAMPLE 50
PATTERN 8 MEAN -3.0
STATION BARTER SD 1.3
VARIABLE T-DEP

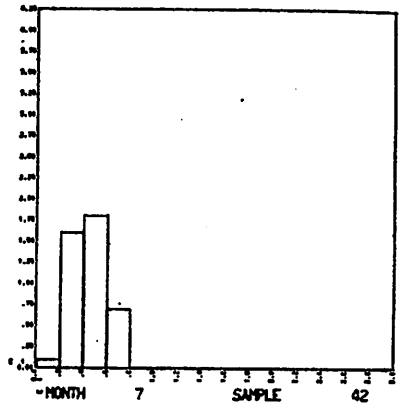

MONTH 7 SAMPLE 42
PATTERN 8 MEAN 4.6
STATION BARROW SD 1.3
VARIABLE WIND-1

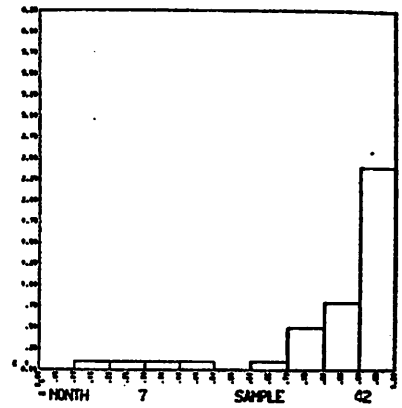

MONTH 7 SAMPLE 42
PATTERN 8 MEAN 8.9
STATION BARROW SD 2.0
VARIABLE CLOUD

Figure 50: Histograms for July: CP8

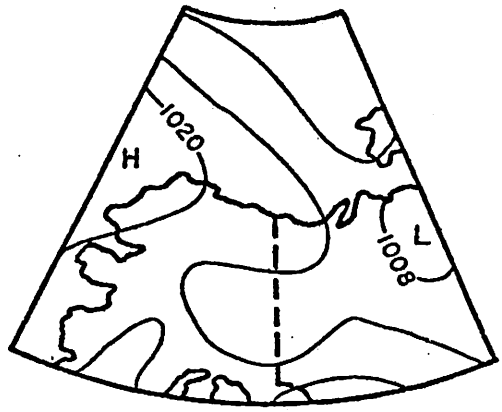

CP14

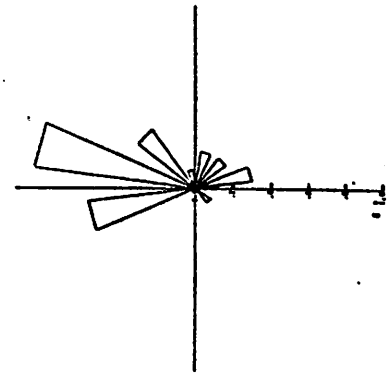

MONTH	7	SAMPLE	28
PATTERN	14	MEAN	307.7
STATION	BARROW	SD	66.4
VARIABLE	WIND DIR		

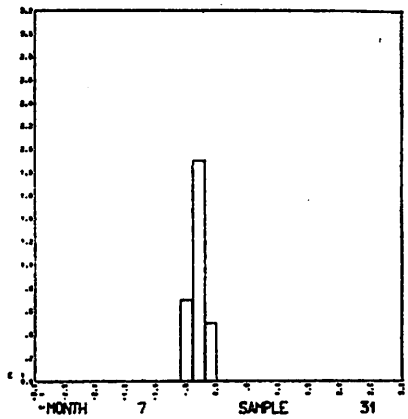

MONTH	7	SAMPLE	31
PATTERN	14	MEAN	-3.2
STATION	BARROW	SD	1.2
VARIABLE	T-DEP		

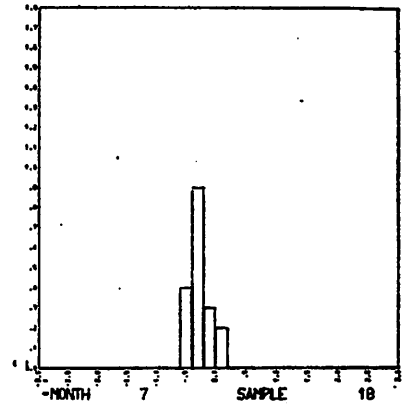

MONTH	7	SAMPLE	18
PATTERN	14	MEAN	-2.6
STATION	BARTER	SD	1.6
VARIABLE	T-DEP		

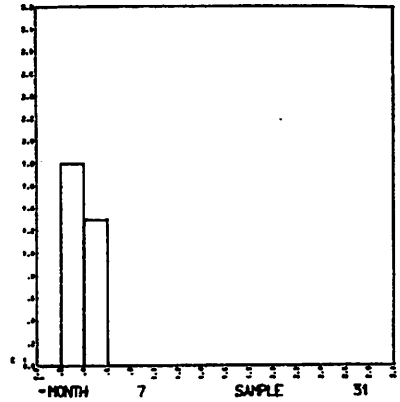

MONTH	7	SAMPLE	31
PATTERN	14	MEAN	3.9
STATION	BARROW	SD	1.0
VARIABLE	WIND-1		

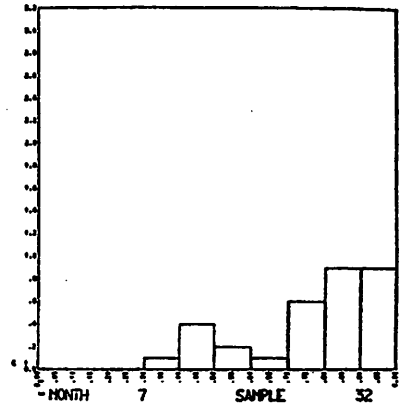

MONTH	7	SAMPLE	32
PATTERN	14	MEAN	8.2
STATION	BARROW	SD	1.8
VARIABLE	CLOUD		

Figure 51: Histograms for July: CP14

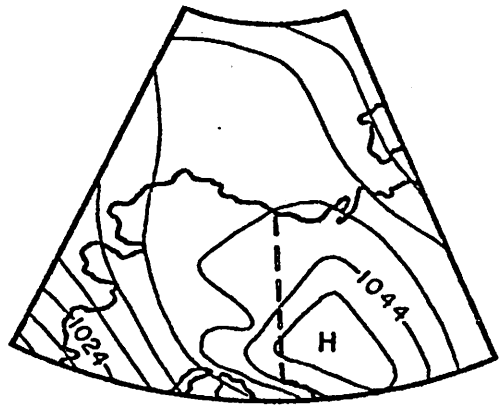

CP4

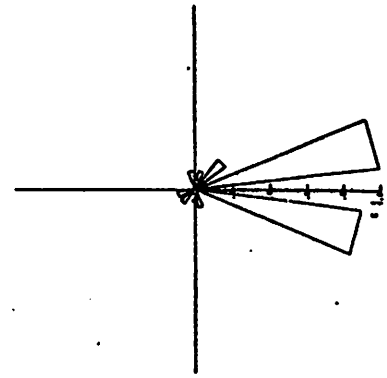

MONTH	7	SAMPLE	26
PATTERN	4	MEAN	88.9
STATION	BARROW	SD	47.4
VARIABLE	WIND DIR		

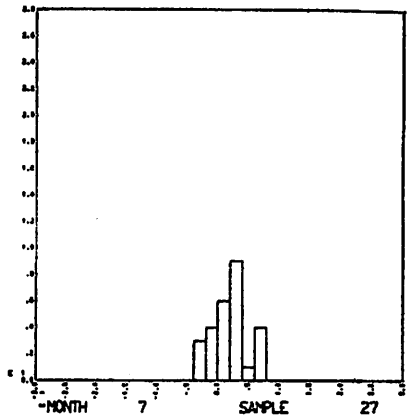

MONTH	7	SAMPLE	27
PATTERN	4	MEAN	2.0
STATION	BARROW	SD	3.0
VARIABLE	T-DEP		

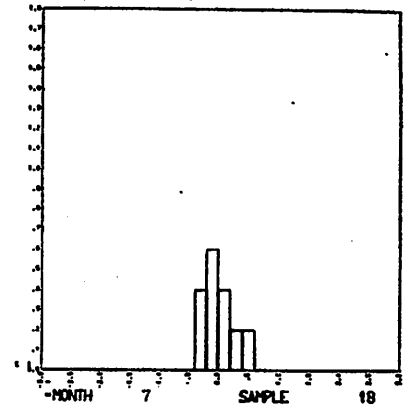

MONTH	7	SAMPLE	18
PATTERN	4	MEAN	.2
STATION	BARROW	SD	2.6
VARIABLE	T-DEP		

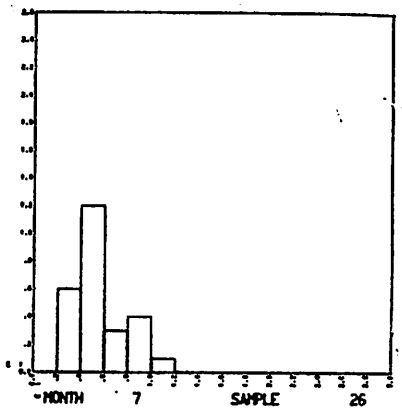

MONTH	7	SAMPLE	26
PATTERN	4	MEAN	5.5
STATION	BARROW	SD	2.2
VARIABLE	WIND-1		

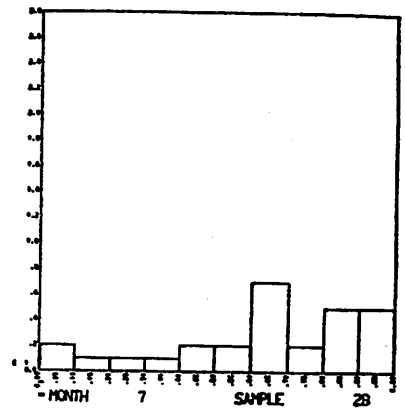

MONTH	7	SAMPLE	28
PATTERN	4	MEAN	6.9
STATION	BARROW	SD	2.7
VARIABLE	CLOUD		

Figure 52: Histograms for July: CP4

The major summer pressure patterns are more numerous and varied than those of winter. The overwhelming winter dominance of easterly surface winds gives over to a bi-modal distribution in summer, with frequent east-northeasterly and southwesterly winds. CP's 2, 5, 6, and 15 are frequent in summer and occur in transitional sequences which indicate the passage of cyclonic storms up the west coast of Alaska and into the Beaufort Sea. The onset of this regime may depend critically on the date at which the Pacific high pressure cell establishes its more-northerly summer position. It is worth emphasizing that no major summer CP has a mean wind direction in the southeast quadrant, which is the most direct path from the interior of the state to Barrow. In general, the agreement is quite good between observed surface wind directions and the expected flow based on the CP synoptic maps.

Temperature departures appear to be dominated by the local airflow direction. Winds from the ocean (WSW through ENE) at Barrow are associated with temperature departures between 1°C and 3°C below normal. Winds between E and SW bring positive departures in the range +1°C to +2°C.

Overall July sky cover is heavy, with a mean of 8 tenths. CP1 and CP4, the two major winter patterns which occur on over 5% of summer days, have mean values one to two tenths below the other patterns in July. These two CP's are also associated with rather infrequent precipitation in July. The major summer precipitation patterns are CP's 2, 15, and 5, which jointly account for 64% of the July-August precipitation total. Measurable precipitation is recorded at Barrow in about 50% of cases for each of these three patterns. CP's 6 and 8 are also substantial contributors, bringing the joint precipitation of CP's 2, 15, 5, 6, and 8 to 79% of the July-August total. It is well to note that the summer total for this group (813.3 mm during 1955-1974) represents more than 30% of the 20-year annual total at Barrow. These statistics serve to emphasize the importance of the brief summer circulation season, when the west-coast cyclone path dominates.

Relatively high mean wind speeds tend to be associated with the easterly patterns in summer, although surface geostrophic wind calculations (Moritz, 1977) show that the westerlies should be slightly stronger at this season. It is plausible that a sea-breeze type of pressure gradient exists quasi-permanently along the Beaufort Sea coast in summer, but is not recorded by the sparse synoptic station network. Such a gradient should form due to heating contrasts between the tundra surface and the sea, and would servce to increase the magnitude of easterlies and decrease the westerlies, so long as the winds remained roughly geostrophic.

Autumn

The transition from summer pressure patterns to the winter regime occurs rapidly during August-September (Figures 23 and 24). CP's 1, 3, 4, 7, and 9 increase in frequency while CP's 2, 5, 6, 8, and 15 decrease over this period. As in June, the interdiurnal variability of temperature, dew point depression and sky cover are small (Table III), and the average monthly temperature is near the freezing point. At this season, however, ocean surface layers and freezing sea ice act as heat sources, buffering the cooling effect of the negative surface net radiation.

The September weather characteristics are shown in Table XXXIX. CP1 resumes its cominant role, occurring in 26% of cases (Figure 53). As in all other seasons, CP1 brings east-northeasterly winds, negative temperature departures at both stations, relatively strong winds and infrequent measurable precipitation. The mean CP1 wind speed (6.5 ms^{-1} at Barrow) is the highest of all September patterns. CP-sky cover associations were not significantly different from random in September (Table XXXIII) because all patterns have nearly overcast skies. However, the precipitation differences were highly significant, and CP1 figures prominently in the χ^2 test results. Depsite its 26% frequency of occurrence, CP1 contributed only 12% of the September precipitation catch at Barrow, with measurable precipitation in 25% of cases. Five of the major September CP's had measurable precipitation in over 50% of their occurrences, illustrating once again that CP1 is basically a dry circulation pattern, in all seasons. CP1's mean temperature departure of -1.5°C makes it the coolest of all September patterns at Barrow.

CP4 is the second-most frequent pattern in September, accounting for 14% of the daily pressure grids. Table XXXIX shows that the weather characteristics of CP4 are much the same in September as in other months. Barrow surface winds are from the east, averaging 5.2 ms^{-1}, or about 0.5 ms^{-1} below the monthly normal. Mean temperature departures at Barrow and Barter Island are very slightly above normal, with considerable scatter in their distributions. CP4 is also the driest September pattern, with measurable precipitation in only 16% of cases.

CP6 has 7% frequency of occurrence in September, and is associated with surface easterlies at Barrow (Figure 54). Temperature departures of +1.3°C at Barrow and +1.5°C at Barter Island make CP6 a warming pattern. This weather characteristic represents a change from summer conditions, when CP6 had negative mean temperature departures. One possible explanation is that during September the surface temperature of near-shore sea water is not much different than the local tundra surface temperature near the coast. The latter surface cools faster because conduction cannot penetrate the medium as rapidly as convection (in the ocean), and the energy losses at the surface are thus confined to a shallow layer of soil. Local temperature advection should be relatively unimportant when the surface temperature is spatially homogeneous. However, as the Arctic region cools relative to mid-latitudes in the fall, air mass contrasts again become important on a larger scale. Since CP6 usually represents a Pacific cyclone which moves up the west coast of Alaska and influences the Beaufort Sea area, we would expecte the positive departures of temperature. If this argument is correct, the same kind of situation should obtain in June, when the tundra and ocean have about equal surface temperatures. The CP6 temperature departures at Barrow at 0°C in June, -0.3°C in July, and +1.3°C in September. The corresponding Barter Island data are +0.9°C, -1.2°C and +1.5°C. The signs of these departures are consistent with the argument given above. Rather strong winds (6.3 ms^{-1}) accompany CP6 occurrences in September at Barrow. However, the sea-breeze heating contrasts should be gone by this time, as the tundra becomes snow-covered and the ocean surface approaches the freezing point. During July it was the easterly winds which were strongest, but In September, CP's 5 (6.1 ms^{-1}) and 10 (6.0 ms^{-1}) have strong mean wind speeds from the west and southeast, respectively. Some other mechanism besides the sea-breeze must, then, be responsible for the relatively high mean wind speeds in September. Kovacs and Mellor (1974) note that the fall storms

TABLE XXXIX

SEPTEMBER CP WEATHER CHARACTERISTICS

CP	$\overline{dT1}$ (°C)	$\overline{dT2}$ (°C)	$\overline{WD}$ (°)	$\overline{U}$ (m/s)	$\overline{SC}$ (1/10)	$\overline{dT_D}$ (°C)	r* (mm)	%-1 (%)	%-2 (%)
1	-1.5	-1.1	75	6.5	9.4	0.8	36.8	12	25
2	+1.2	+2.4	242	5.0	9.5	1.3	23.4	8	50
3	-1.5	-2.0	42	4.9	9.5	1.1	7.9	3	42
4	+0.4	+0.1	92	5.2	8.4	0.9	11.4	4	16
5	-0.5	-0.4	270	6.1	9.6	0.9	20.8	7	54
6	+1.3	+1.5	90	6.3	9.4	0.8	64.8	22	60
7	-1.4	-3.0	357	4.8	8.6	0.8	7.9	3	36
8	-0.6	-1.0	345	5.1	9.5	0.9	43.2	15	66
10	+2.5		148	6.0	9.0		14.2	5	40
15	+1.9	+2.0	181	5.9	9.0	0.5	15.0	5	69

*Precipitation data are for season V (September).

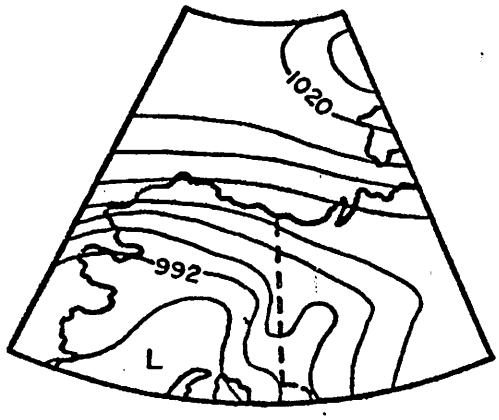

CP1

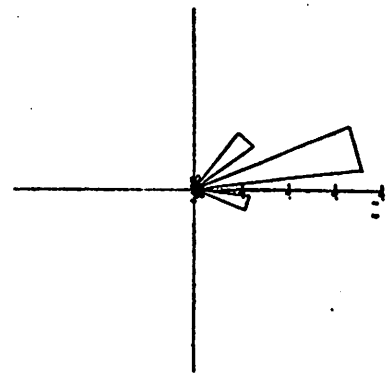

MONTH	9	SAMPLE	150
PATTERN	1	MEAN	75.4
STATION	BARROW	SD	36.5
VARIABLE	WIND DIR		

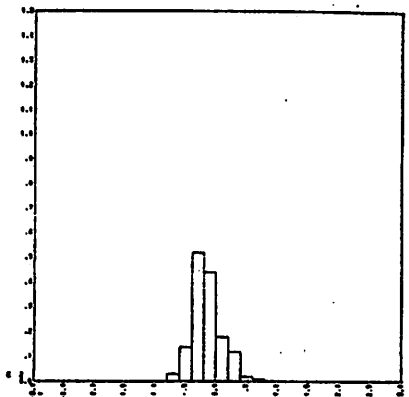

MONTH	9	SAMPLE	146
PATTERN	1	MEAN	-1.5
STATION	BARROW	SD	2.4
VARIABLE	T-DEP		

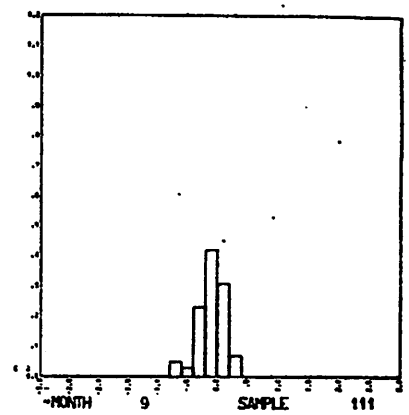

MONTH	9	SAMPLE	111
PATTERN	1	MEAN	-1.1
STATION	BARTER	SD	2.2
VARIABLE	T-DEP		

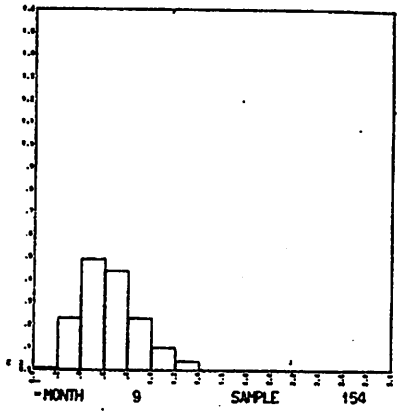

MONTH	9	SAMPLE	154
PATTERN	1	MEAN	6.5
STATION	BARROW	SD	2.5
VARIABLE	WIND-1		

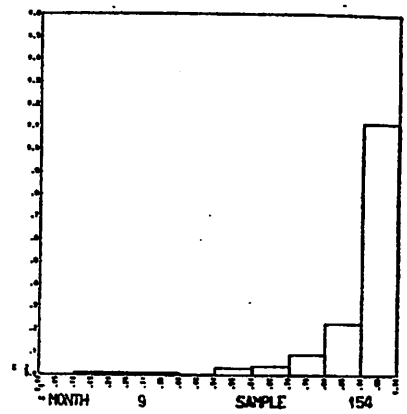

MONTH	9	SAMPLE	154
PATTERN	1	MEAN	9.4
STATION	BARROW	SD	1.3
VARIABLE	CLOUD		

Figure 53: Histograms for September: CP1

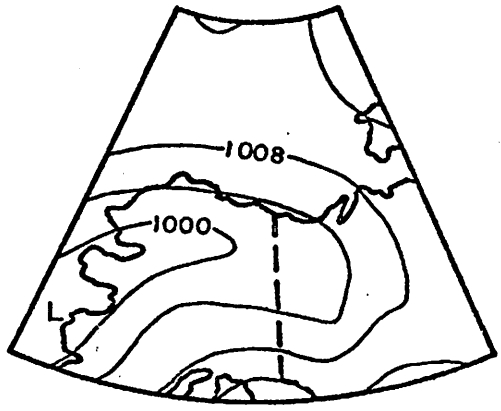

CP6

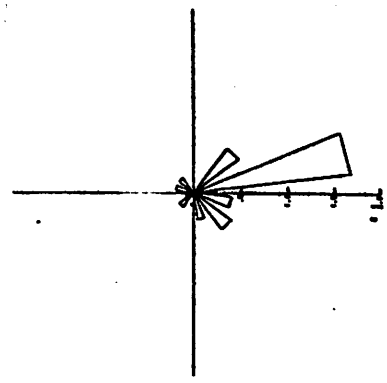

MONTH 9 SAMPLE 42
PATTERN 6 MEAN 89.5
STATION BARROW SD 62.7
VARIABLE WIND DIR

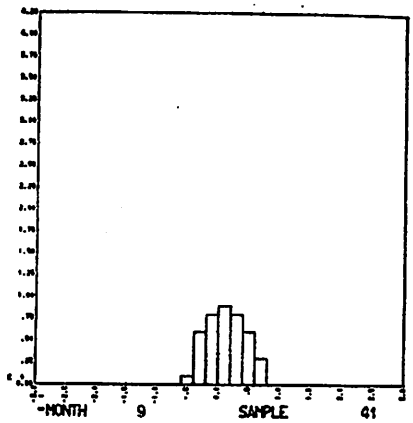

MONTH 9 SAMPLE 41
PATTERN 6 MEAN 1.3
STATION BARROW SD 3.1
VARIABLE T-DEP

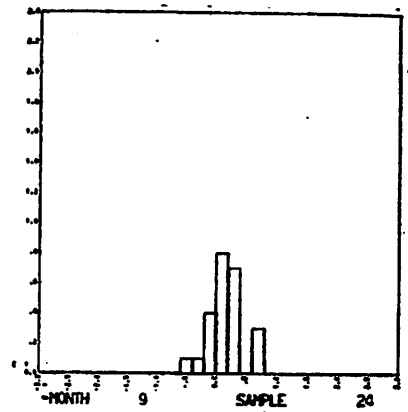

MONTH 9 SAMPLE 24
PATTERN 6 MEAN 1.5
STATION BARTER SD 3.1
VARIABLE T-DEP

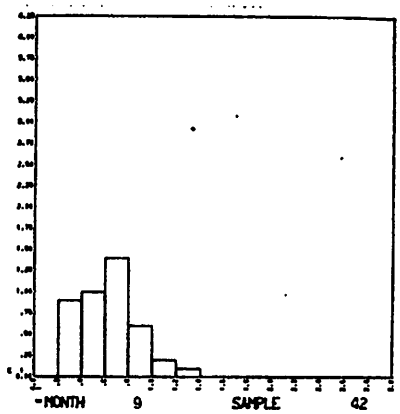

MONTH 9 SAMPLE 42
PATTERN 6 MEAN 6.3
STATION BARROW SD 2.3
VARIABLE WIND-1

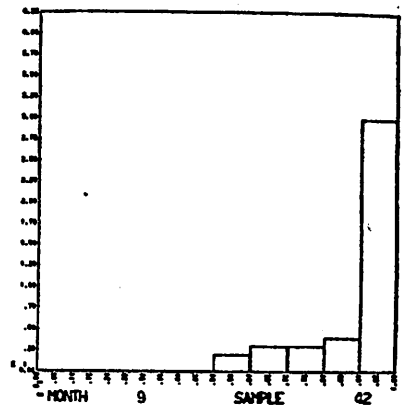

MONTH 9 SAMPLE 42
PATTERN 6 MEAN 9.4
STATION BARROW SD 1.2
VARIABLE CLOUD

Figure 54: Histograms for September: CP6

are usually the most severe on the Beaufort Sea coast, and indeed all three of the CP's metnioned above are associated with low pressure systems in the vicinity of the Beaufort Sea.

CP6 is the most important precipitation pattern in September, supporting the idea of its frequent Pacific origin. 60% of CP6 cases brought measurable precipitation to Barrow, accounting for 22% of the monthly catch. The former figure is substantially larger than in July, when only 34% of CP6 patterns had precipitation. As noted above, however, these cyclonic patterns tend to be stronger in the fall, and a more-intense circulation pattern should bring more precipitation, when the flow is cyclonic. Recall from Chapter IV (Table XII) that the CP6 mean pressure intensity index s_p nearly doubles between July and October, illustrating the strengthening patterns in fall.

CP2 (Figure 55) occurs on 6% of September days with mean surface winds from southwest at Barrow. As in all other seasons, CP2 temperature departures are positive at Barrow (+1.2°C) and Barter Island (+2.4°C), and are larger than the corresponding August values. Average wind speeds are slightly below the seasonal normal at Barrow for CP2, and mean sky cover is near ten tenths. 50% of CP2 occurrences have measurable precipitation at Barrow, much like the July statistic (46%). Overall CP2 continues to exhibit the same weather characteristics as in other seasons. The extremely high temperature departures and wind speeds of winter become a CP2 characteristic in November.

CP8 is the next major pattern, with 6% frequency in September (Figure 56). The northerly surface winds are still present but temperature departures are relatively modest at Barrow (-0.8°C) and Barter Island (-1.0°C). These data support the contention that local temperature advection from the ice or tundra becomes less important as summer turns to winter. CP8's frequency of measurable precipitation rises to 66% in September, again indicating the correspondence between cyclonic patterns and autumn rain or snow. The mean CP8 wind speed is rather unremarkable at 5.1 ms^{-1}, but this is an increase of 0.5 ms^{-1} since July. As with CP6, this increase suggests more intense cyclonic patterns in the fall.

CP3 re-enters the circulation picture in September after its summer frequency minimum. From Table XXXIX we see that this pattern establishes some of its major winter weather characteristics by September, including frequent northerly surface winds, negative temperature departures at both stations, and relatively low wind speeds. However, we note that 42% of the CP3 cases produced measurable precipitation at Barrow, in contrast with only 11% in January. Also, CP3 mean sky cover is over nine tenths in September, illustrating the non-significance of CP-sky cover associations at this season.

The last major September pattern is CP5, with 5% frequency of occurrence (Figure 57). CP5 surface winds are westerly again in September, but the mean temperature departures are only -0.5°C at Barrow and -0.4°C at Barter Island, compared with respective values of -2.1°C and -1.4°C in July. It appears that CP5's summer effects were also due to local off-ice temperature advection, and by September the large-scale air mass properties become more important. Recall, for example, that CP5 brings above-average temperatures in January. The intermediate temperature departures in September, then, represent the changing contributions of local vs. synoptic scale advection effects as the local surface

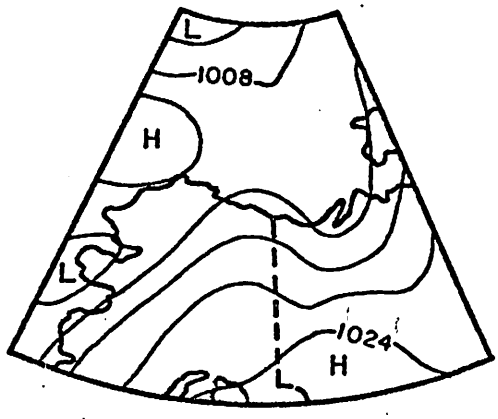

CP2

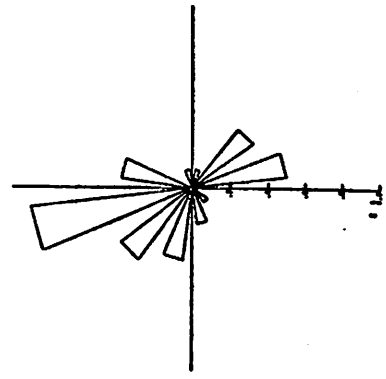

MONTH 9 SAMPLE 36
PATTERN 2 MEAN 242.1
STATION BARROW SD 90.4
VARIABLE WIND DIR

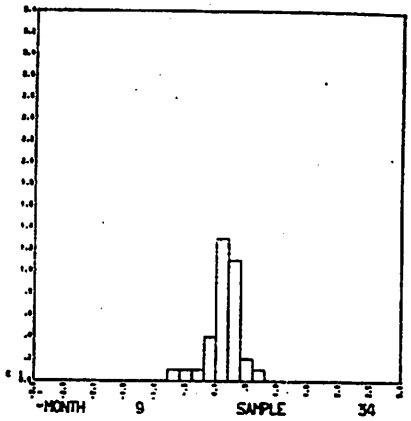

MONTH 9 SAMPLE 34
PATTERN 2 MEAN 1.2
STATION BARROW SD 2.6
VARIABLE T-DEP

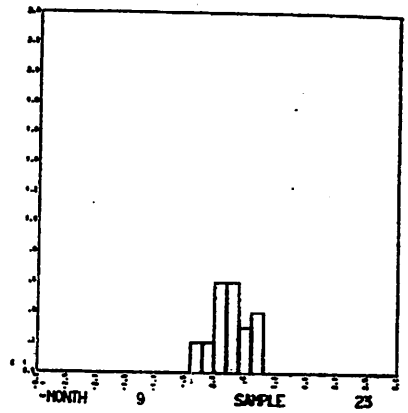

MONTH 9 SAMPLE 25
PATTERN 2 MEAN 2.4
STATION BARTER SD 2.9
VARIABLE T-DEP

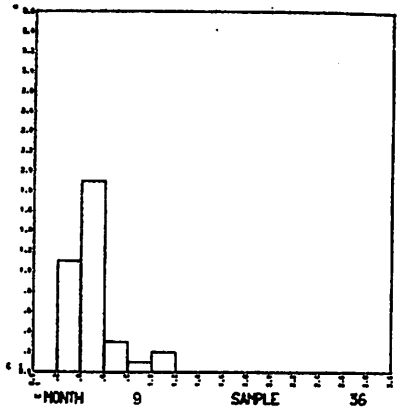

MONTH 9 SAMPLE 36
PATTERN 2 MEAN 5.0
STATION BARROW SD 2.0
VARIABLE WIND-1

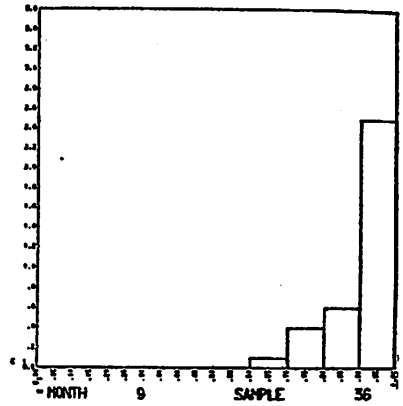

MONTH 9 SAMPLE 36
PATTERN 2 MEAN 9.5
STATION BARROW SD .8
VARIABLE CLOUD

Figure 55: Histograms for September: CP2

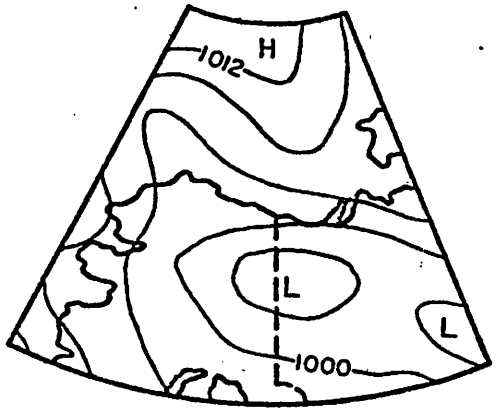

CP8

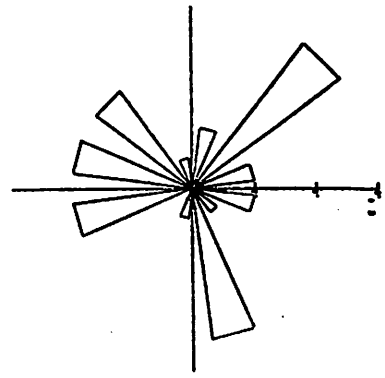

MONTH	9	SAMPLE	32
PATTERN	8	MEAN	344.8
STATION	BARROW	SD	115.9
VARIABLE	WIND DIR		

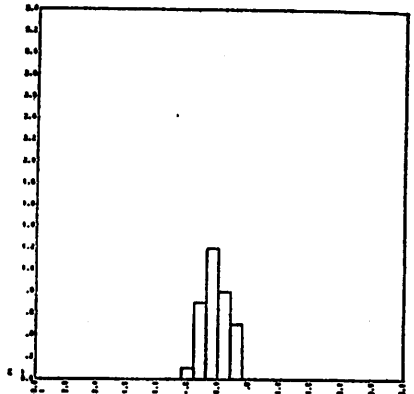

MONTH	9	SAMPLE	33
PATTERN	8	MEAN	-.6
STATION	BARROW	SD	2.1
VARIABLE	T-DEP		

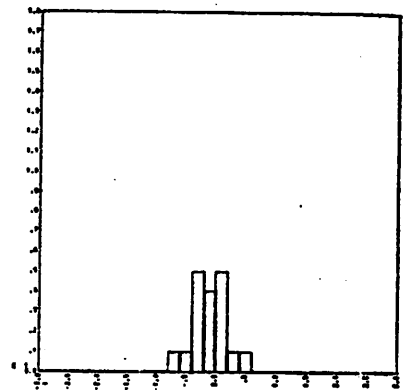

MONTH	9	SAMPLE	18
PATTERN	8	MEAN	-1.0
STATION	BARTER	SD	2.6
VARIABLE	T-DEP		

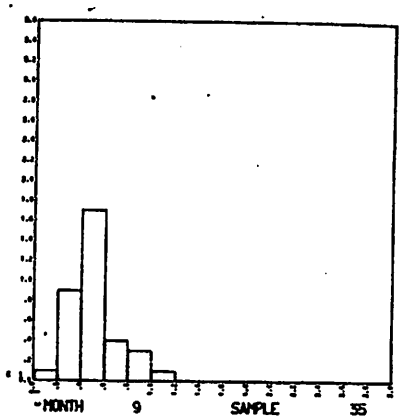

MONTH	9	SAMPLE	35
PATTERN	8	MEAN	5.1
STATION	BARROW	SD	1.9
VARIABLE	WIND-1		

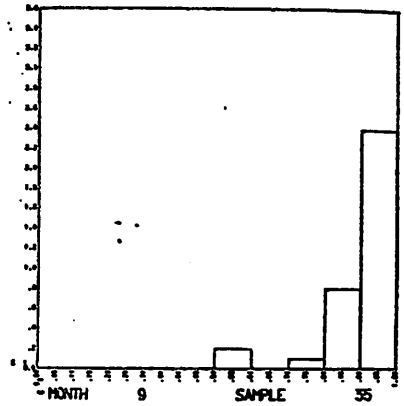

MONTH	9	SAMPLE	35
PATTERN	8	MEAN	9.5
STATION	BARROW	SD	1.0
VARIABLE	CLOUD		

Figure 56: Histograms for September: CP8

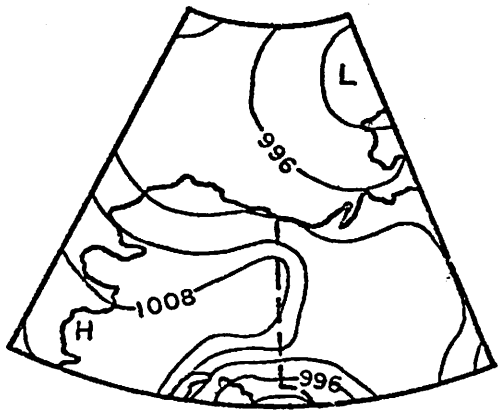

CP5

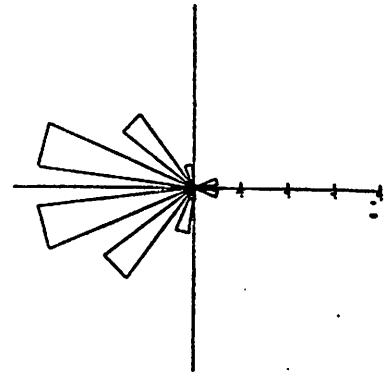

MONTH 9 SAMPLE 28
PATTERN 5 MEAN 269.7
STATION BARROW SD 50.0
VARIABLE WIND DIR

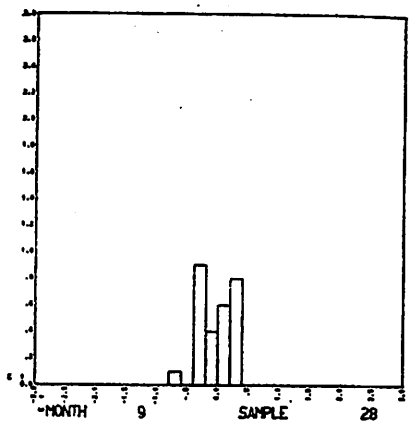

MONTH 9 SAMPLE 28
PATTERN 5 MEAN -.5
STATION BARROW SD 2.7
VARIABLE T-DEP

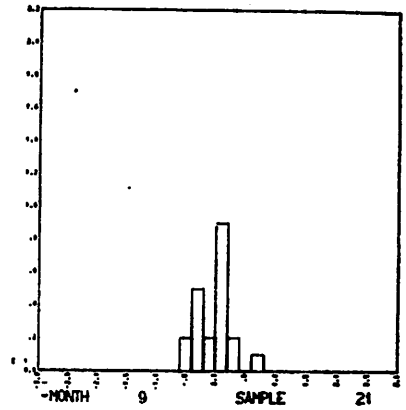

MONTH 9 SAMPLE 21
PATTERN 5 MEAN -.4
STATION BARTER SD 2.8
VARIABLE T-DEP

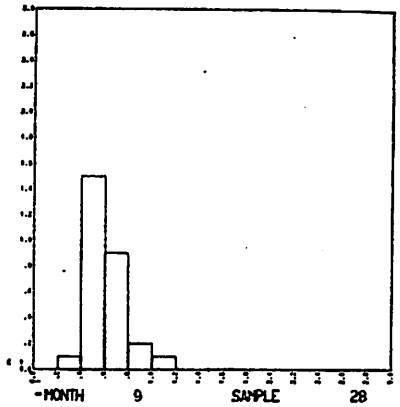

MONTH 9 SAMPLE 28
PATTERN 5 MEAN 6.1
STATION BARROW SD 1.8
VARIABLE WIND-1

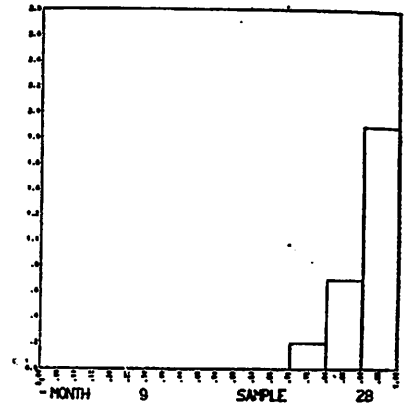

MONTH 9 SAMPLE 28
PATTERN 5 MEAN 9.6
STATION BARROW SD .6
VARIABLE CLOUD

Figure 57: Histograms for September: CP5

properties change. The Barrow CP5 wind speed of 6.1 ms^{-1} is intermediate between the July value (5.0 ms^{-1}) and the January mean speed (6.9 ms^{-1}). 54% of September CP5 cases brought measurable precipitation to Barrow, accounting for 7% of the monthly total.

Two less-frequent fall patterns deserve mention because of their interesting weather characteristics. CP7 (ridge from the west, low to the northeast) establishes its winter characteristics in September, including negative mean temperaure departures at Barrow and Barter Island, and light winds from the north. CP15, with a low pressure cell in the Chukchi Sea area, brings above-normal temperatures, southerly winds at 5.9 ms^{-1} and precipitation in 69% of cases. All of these characteristics agree with the properties of other patterns which are associated with the northward movement of Pacific cyclonic storms.

September is a month of transition on the Beaufort Sea coast, as mean temperature falls rapidly, often ice begins to form on the lakes and sea, and the tundra gets its first snow cover. The winter circulation patterns begin to dominate after their brief summer minima. The variances of daily series of temperature departures, dew point depressions and sky cover are substantially reduced from summer. Pressure patterns associated with the northward incursion of Pacific storms (CP's 2, 6, 10 and 15) bring positive temperature departures and surface winds between easterly and southwesterly at Barrow. Major winter patterns, on the other hand, represent the progressive "cutting off" of the regional surface circulation from events south of the Brooks Range (CP's 1, 3, 4 and 7), and lead to negative temperature departures and surface winds between northwesterly and east-northeasterly at Barrow. Mean sky cover is more than eight tenths for all of the major patterns in September. The summer patterns, including CP's 2, 5, 6, 8, and 15 are most frequently associated with precipitation while the winter patterns are among the least-frequent precipitators. The implication is that the northward transport of moisture and cyclonic vorticity at the surface (which characterize the summer regime) lead to precipitation occurrence in September. Since the weather characteristics of the major winter and summer CP's do not generally vary from one season to the next, except for CP6, we would expect an early onset of winter weather conditions to occur with an early transition to the winter circulation regime and vice versa. This transition occurs when the low pressure centers from the north Pacific begin to move south of Alaska, with ridge and high pressure conditions dominating along the Beaufort Sea coast region.

Summary

In Chapter V we showed that the characteristic pressure patterns can be distinguished by their weather characteristics. We have seen that some of these characteristics can be related to physical processes in a meaningful way by analysis of the CP synoptic maps, transition sequences, and the associations between the several different weather characteristics for a given CP. The major points which result from this analysis are summarized below.

Winter temperature departures are more variable on a daily basis than are those of any other season. This is due in large measure to the existence of heat sources which can warm the air in our region under favorable circulation conditions. The large temperature difference between the Arctic Slope and the

north Pacific region in winter leads to spectacular warmings on the Beaufort Sea coast, when cyclonic systems advect the air northward. The vertical temperature inversion represents a second heat reservoir, which warms the air when winds become strong enough to overcome the vertical stability and advect air of high potential temperature downward into the surface layer. Both the horizontal and vertical warming processes appear to operate when CP2 occurs in winter and, less frequently, with CP's 6 and 10. All of these patterns bring large positive temperature departures, relatively cloudy skies, high winds and frequent precipitation. During the Arctic winter the surface net radiation is negative. When the region is cut off from significant advection of air from the south, the radiative processes tend to cool the surface and thus the lowest layer of air. When the winds are light the cooling is confined to a shallow layer because of vertical stability. These conditions occur when CP's 3 and 7 occur, in association with light, northerly winds, relatively clear skies, and negative temperature departures. In contrast to the cyclonic, warming patterns, CP's 3 and 7 are associated with an eastward extension of the Siberian high pressure cell, which forms a ridge over the Beaufort Sea coast. This regime leads to a minimum of surface air mass exchange between the Arctic Slope and the north Pacific region. These coolings, while not as extreme as the CP2 warmings, are much more frequent. The dominant winter mode of circulation is CP1 with a low to the south and high to the north. The high winter frequency of this pattern leads to weather characteristics not far from the monthly normal values. Exchange of air between the Pacific region and the Beaufort Sea coast is intermediate between CP2 and CP's 3 and 7, but appears to be closer to the latter regime. In summer, the temperature departures are positive or negative as the local winds are from the tundra or the sea, respectively. These departures are thus largely independent of the macroscale air mass trajectories, at least insofar as the resolution of our statistics allows. At Barrow the winds between west and east-northeast bring negative departures, while the other directions bring positive departures. The temperature characteristics are largely similar at Barter Island, except for CP's 21 and 15, where the surface geostrophic flow has the opposite direction with respect to the sea tundra boundary than at Barrow. During the transition seasons, the temperature departures are generally smaller on interdiurnal time scales than for winter or summer. Also, the physical processes appear to be intermediate, with effects of both local and large-scale advection present.

The wind directions at Barrow are in general agreement with the CP synoptic map isobars in the majority of cases. As one might expect, wind direction is the most consistent characteristic of the CP's from season to season.

Barrow wind speeds show significant inter-CP differences in all seasons. In winter the ridge patterns (CP's 3 and 7) bring low wind speeds, while the cyclonic storms from the Pacific bring quite strong surface winds. These strong winds would be expected to develop when such intense baroclinicity is present in the surface layers. During the spring transition season most of the patterns have wind speeds around 5 ms^{-1}, but CP1 is one to two ms^{-1} faster. This increase occurs at the same time the pressure pattern intensity index is falling sharply for CP1, indicating weaker geostrophic flow. The implication is that the synoptic station network is inadequate to define the true pressure gradient near the coast. This problem continues into the summer, when sea-breeze effects are probably present, as indicated by strong easterly patterns and weak westerly winds. Even during summer the patterns with northerly flow tend to have low mean wind speeds. In the autumn the cyclonic storms begin to become more intense, leading to higher winds.

Precipitation is primarily a function of the vertical motion field and the humidity of the air. During winter the patterns with advection from the Pacific are cyclonic in nature, implying positive vertical motions near Barrow, and bring moist, marine air into the region. Thus CP2 is associated with measurable precipitation in over half of its occurrences. However, the overall high frequency of CP1 and the generally small precipitation totals for the winte months make CP1 the major winter precipitation pattern. By contrast, in summer the west coast cyclonic patterns are most frequent, and the vast majority of the annual precipitation falls (June to September) in association with those patterns.

Several relationships between the weather characteristics and pressure patterns suggest useful applications. As mentioned earlier, the establishment of the Pacific high pressure cell in its summer position should usher in the summer regime dominated by CP2. If monthly forecasts of the pressure field can be made, by numerical, analog or other means, then a forecast involving the early displacement of the Pacific high in spring implies an early onset of positive temperature departures, offshore winds, and, possibly, a lighter-than-normal ice year on the coast. The occurrence of high winds with winter incursions of cyclones implies that the near-shore ice in the region may be subject to "false freezeups" and subsequent disruption by these storms before, say, January or February. One such case has been documented for December, 1973 (Shapiro, 1976). The wind speeds associated with these storms might then be used as baseline environmental data on which to base design criteria for structures in the ice zones. The general seasonal character of the pressure patterns, and their associated weather statistics should also be useful as an introduction for forecasters in the region. The major application of the data should be as an information resource for planning and decision-making involving the Beaufort Sea coastal region. Development of the petroleum resources in the area is taking place on land and is planned in the offshore zones. The statistical data on the pressure patterns and their characteristics should aid any analysis which requires information on the weather and climate of the region.

CHAPTER SEVEN

CONCLUSION

Introduction

In Chapter One we stated three basic objectives for this study:

1) Determine the predominant spatial and temporal modes of the regional surface pressure field.

2) Analyze and test the significance of relationships between pressure pattern groups and coastal weather/climate.

3) Synthesize the pressure patterns and meteorological information to characterize the regional synoptic climatology.

The major results and the degree to which these objectives have been achieved are summarized in the following section. Recommendations for further study conclude the chapter.

Results

Daily pressure grids over the Alaska region for 1946 to 8/1974 were classified into 21 discrete characteristic pressure pattern types. Over 95% of the daily grids passed the objective pressure pattern similarity tests with at least one of the CP's. The features of circulation on the CP synoptic maps compare favorably with important features identified by previous workers. The most frequent patterns are those with low pressure to the southwest, south, or southeast in the grid sector, and highs or ridges to the north. Analyses of daily surface pressure charts in relation to the synoptic catalog of nominal pressure pattern types showed that some variation in qualitative features of the pressure field is to be expected among individual cases for a single CP. Such variation is due to the range of SCORES which can meet the pattern-similarity criteria. However, the patterns were generally well-defined with respect to location of major features of circulation (lows, highs, troughs, and ridges) in the grid sector and the geostrophic flow directions on the Beaufort Sea Coast.

The time series of nominal pressure patterns was analyzed for seasonal changes. In winter (mid-September to mid-May) CP1 dominates the surface circulation, with lows to the south and highs to the north. CP's 3, 4, 7, and 9 are also important in winter, and have highest pressure somewhere near the northern coast with lower pressures to the southwest, south or southeast. A pronounced shift in mean monthly pressure pattern frequencies occurs from mid-May through June, characterized by more-frequent occurrence of CP's 2, 5, 6, 8, 10, 14, 15, and 21, and a corresponding decrease in the main winter CP's. The summer regime consists of the former patterns, and is well-developed during July through late August. This regime has frequent low pressure features over the central, western and northern portions of the grid sector. To the south, the Pacific High often extends northward as a ridge over the Gulf of Alaska at this season. The summer regime has a greater variety of patterns than does the winter regime. A second transition occurs from late August to mid-September, when the winter patterns begin to dominate again. During January, CP's 2 and 4 undergo a one-month frequency increase, leading to small kinks in the seasonal temperature

curves at Barrow and Barter Island. This phenomenon is similar to, but less-pronounced than, the Antarctic coreless winter, and is caused by increased temperature advection from the Pacific region when the two patterns occur.

On the interdiurnal time scale, persistence is the most important characteristic of the pressure pattern time series. All CP's persist significantly more often than at random. Nonpersistence transition probabilities were generally too small to be of forecasting value, but were nonetheless highly-significant in a statistical sense. Persistence was most pronounced for CP1 and the winter regime in general. Non-persistence transitions indicated an eastward progression of low pressure features through the southern grid sector in winter. Beaufort Sea highs and ridges often tend to be displaced south or southeastward at this season..... In spring the southwest lows often move over central Alaska rather than skirting the state to the south, while in summer Pacific cyclone systems move northward along the west coast and into the Arctic Basin.

Coastal weather data are serially correlated on a day to day basis in the region, leading to reductions in the per-month degrees of freedom for the series. Nonetheless, daily temperature departures, wind speeds, and wind directions all showed highly-significant associations with the CP categories in all months. Weather characteristics which had significant inter-CP differences in some, but not all, months include daily sky cover, dew point depression, and precipitation amount. These tests demonstrate conclusively that a part of the variance in the weather data series is due to the characteristic pressure patterns as defined by the objective algorithms in Chapter Three.

Although any study of this size cannot completely characterize all aspects of a regional synoptic climatology, several important features were identified by our methods. In all seasons, the surface wind directions are largely determined by the prevailing surface pressure pattern on the Beaufort Sea Coast. Generally good agreement was found between the Barrow surface wind directions and the geostrophic directions on the CP synoptic maps. Daily temperature departures have three major regimes through the year. In winter the overall variance of temperature is largest. Screen temperatures are determined primarily by the surface net radiation and the three-dimensional advection of temperature by the circulation. Thus, extreme warmings are associated with influx of moist Pacific air, high wind speeds and relatively heavy cloud cover when CP2 occurs. By contrast, CP's 3 and 7 bring cold, clear, dry air from the central Arctic, and cut off the Pacific influences at the surface. The normal winter pattern, CP1, lies between these two extremes with an intermediate rate of temperature advection from the south, on average. CP's temperature departures are, however, substantially closer to those of CP3 and CP7 than to those of CP2, which is a relatively rare pattern in winter. These relationships lead to a right-skew distribution of screen temperatures in winter. During the spring transition in the large-scale surface temperature contrasts between the North Pacific heat source and the Beaufort Sea Coast are at an annual minimum, leading to a minimum in the variance of daily temperature departures. In some cases, notably CP6, the positive effects of large-scale advection from the south begin to be balanced by local ocean/tundra heating differences. In summer, these local contrasts are paramount, leading to positive temperature departures with offshore flow and negative departures for onshore winds. Since the surface winds are largely determined by the synoptic pressure patterns, there is a good discrimination of CP's based on their mean temperature departures in summer. CP's 2, 4, 10, 15 and 21 have southerly components to their

mean wind directions, bringing positive temperature departures and relatively large dew point depressions to Barrow in summer. By contrast, CP's 1, 5, 6, 8, and 14 have wind directions between west and east-northeast at Barrow, bringing negative temperature departures up to -3°C and near-saturated air.

Winter winds are highest when the low pressure cells penetrate from the Pacific, as one might expect from the intense baroclinity which drives these systems. During spring and summer the easterly patterns are generally the windiest, indicating a nearly-geostrophic thermal monsoon effect, created by the juxtaposition of freezing ocean and heated tundra. In all seasons the lightest winds are associated with the ridges from the west (CP's 3, 7, 14).

Precipitation occurs mainly in summer, especially in association with the west-coast cyclone transition sequences. In winter the infrequent incursions of Pacific storms bring the heaviest falls, but overall totals are relatively small. Patterns with ridges out of the west over the Beaufort Coast are extremely dry in winter. In general, patterns with cyclonically-curved isobars near the coast are much more effective sources of precipitation than the anticyclonic patterns.

Many associations between pressure patterns and weather on the Beaufort Sea Coast can be explained by arguments based on surface geostrophic flow, large-scale air mass trajectories (from transition sequences), and local surface conditions. The latter conditions include surface net radiation, surface type, and the local vertical stability of the air column at each season. Extreme weather conditions, particularly in winter, fit nicely into this framework, using the characteristic pressure patterns as representatives for the surface circulation type. The pressure patterns and their climatology should serve as a useful introduction to forecasters coming into the region. This information can also be utilized as baseline enviromental data with applications for offshore petroleum development in the region.

Further Work

The characteristic pressure patterns defined in Chapter Three were generally found to represent the important qualitative features of circulation on the individual synpotic maps comprising their CP groups. However, some of the weather characteristic distributions (e.g. temperature departures for CP's 4, 5, and 9 in winter) have a great deal of scatter. Case studies of CP occurrences with different weather characteristics should lead to a better definition of the features of circulation which are most important in determining weather, but which are unresolved by our classification techniques.

Several interesting physical processes were inferred from the CP-weather characteristic associations in Chapter Six. Physical modelling studies and direct measurements could substantiate and expand these inferences in several cases. For instance, computation of three-dimensional trajectories and analysis of time series of Beaufort Coast atmospheric soundings during the winter CP2 warming events would help define the relative contributions of local processes, horizontal temperature changes. Also, mesoscale pressure and wind measurements on transects across the ocean-tundra boundary in summer would lead to further evaluation of sea-breeze or monsoon effects at this season.

Finally, a variety of special problems, including interannual climate variability, Beaufort Coast ice forecasting, and weather-dependent coastal

operations of all kinds can be studied using the CP's and their weather characteristics as a point of departure. For example, Barnett (1976) has classified the ordinal "severity" of navigation season sea ice conditions along the coast for 1956-1975. The synoptic catalog could be analyzed to determine whether or not certain CP's are more or less frequent during years with given ice conditions. If significant CP-ice relationships exist, they should lead to a better understanding of the large-scale links between atmospheric processes and sea ice conditions.

BIBLIOGRAPHY

Alder, H.L. and E.B. Roessler, 1972: Introduction to Probability and Statistics. W.H. Freeman and Co., San Francisco, 373 pp.

Badgley, F.I., 1966: Heat Budget at the Surface of the Arctic Ocean. In: Proceedings of the Symposium on the Arctic Heat Budget and Atmospheric Circulation, J.O. Fletcher (ed.). Rand Corp., Santa Monica, California, pp. 267-278.

Barnett, D., 1976: A Practical Method of Long-Range Ice Forecasting for the North Coast of Alaska, Part I. United States Navy, Fleet Weather Facility, Technical Report 1, 16 pp.

Barry, R.G. and A.H. Perry, 1973: Synoptic Climatology. Methuen, London, 555 pp.

Barry, R.G., 1974: Further Climatological Studies of Baffin Island, Northwest Territories. Environment Canada, Ottawa, Inland Waters Technical Bulletin 65, 54 pp.

Barry, R.G., R.S. Bradley and L.F. Tarleton, 1977: The Secular Climatic History of the Rocky Mountain Area. Final Report NSF GA-40256, University of Colorado, Institute of Arctic and Alpine Research, Boulder, 294 pp.

Baur, F., 1939: Das Klima der bisher erforschen Tiele der Arktis. Arktis, 2, pp. 77-78.

Bilello, M.A., 1966: Survey of Arctic and Subarctic Temperature Inversions. U.S. Army CRREL, Technical Report 161, 35 pp.

Bjerknes, J., 1937: Theorie der Aussertropischen Zyklonenbildung. Meteorologische Zeitschrift, 54, pp. 462-466.

Bjerknes, J. and J. Holmboe, 1944: On the Theory of Cyclones. Journal of Meteorology, 1, pp. 1-22.

Blasing, T.J., 1975: A Comparison of Map-Pattern Correlation and Principal Component Eigenvector Methods for Analyzing Climatic Anomaly Patterns. Fourth Conference on Probability and Statistics, American Meteorological Society, Boston, pp. 96-101.

Bodhurtha, F.T., Jr., 1952: An Investigation of Anticyclogenesis in Alaska. Journal of Meteorology, 9, pp. 118-125.

Bolin, B., 1950: On the Influence of the Earth's Orography on the Westerlies. Tellus, 2, pp. 184-195.

Bryson, R.A. and W.P. Lowry, 1955: Synoptic Climatology of the Arizona Summer Precipitation Singularity. Bulletin of the American Meteorological Society, 36, pp. 329-339.

Bryson, R.A. and J.F. Lahey, 1958: The March of the Seasons. Final Report, Contract AF 19-(604)-992, Department of Meteorology, University of Wisconsin, Madison, 41 pp.

Charney, J.G. and A. Eliassen, 1949: A Numerical Method for Predicting the Perturbations of the Middle Latitude Westerlies. Tellus, 1, pp. 38-55.

Cochran, W.G., 1954: Some Methods for Strengthening the Common χ^2 Tests. Biometrics, 10, pp. 417-451.

Dickey, W.W., 1961: A Study of a Topographic Effect on Wind in the Arctic. Journal of Meteorology, 18, pp. 790-803.

Dingman, S.L., R.G. Barry, G. Weller, C. Benson, E. LeDrew, and C. Goodwin, in press: Climate, Snow Cover, Microclimate and Hydrology. In: An Arctic Ecosystem: The Coastal Tundra at Barrow, Alaska, J. Brown, P.C. Miller, L.L. Tieszen, and F.L. Bunnell (eds.). Dowden, Hutchinson and Ross, Inc., Stroudsburg, Pennsylvania, Chapter 2.

Durst, C.S., 1951: Climate: the Synthesis of Weather. In: Compendium of Meteorology, T.F. Malone (ed.). American Meteorological Society, Boston, pp. 967-975.

Dzerdzeevskii, B.L., 1945: Tsirkuliatsionnye Skhemy v Troposfere Tsentral' noi Arktiki. In: Izdatel' stvo Akad. Nauk.

Fahl, C.B., 1975: Mean Sea Level Pressure Patterns Relating to Glacier Activity in Alaska. In: Climate of the Arctic, G. Weller and S. Bowling (eds.). Geophysical Institute, Fairbanks, Alaska, pp. 339-346.

Fletcher, J.O., 1969: Ice Extent on the Southern Ocean and its Relation to World Climate. Rand Corp., Santa Monica, California, 111 pp.

Fliri, F., 1965. Uber Signifikanzen Synoptisch-Klimatologischer Mittelwerte in Verschiedenen Alpinen Wetterlagensystemen. Carinthia II, Vienna, Sonderheft, 24, pp. 36-48.

Godske, C.L., 1959: Information, Climatology and Statistics. Geografiska Annaler, 41, pp. 85-93.

Godske, C.L., 1966: Methods of Statistics and Some Applications to Climatology. In: Statistical Analysis and Prognosis in Meteorology. W.M.O., Geneva, Technical Note 71, pp. 9-86.

Hare, F.K., 1955: Dynamic and Synoptic Climatology. Annals of the Association of American Geographers, 45, pp. 152-162.

Hare, F.K., 1960: The Westerlies. Geographical Review, 50, pp. 345-367.

Hare, F.K., 1968: The Arctic. Quarterly Journal of the Royal Meteorological Society, 94, pp. 439-459.

Hesselberg, T. and T.W. Johannessen, 1958: The Recent Variations of the Climate at the Norwegian Arctic Stations. In: Proceeding, Part 1, Meteorology Section, Polar Atmosphere Symposium, Pergamon Press, New York, pp. 18-29.

Holmgren, B. and G. Weller, 1974: Local Radiation Fluxes over Open and Freezing Leads in the Polar Pack Ice. AIDJEX Bulletin, 27, pp. 149-166.

Holton, J.R., 1972: An Introduction to Dynamic Meteorology. Academic Press, New York, 319 pp.

Jenne, R.L., 1975: Data Sets for Meteorological Research. National Center for Atmospheric Research, Boulder, Colorado, Technical Note TN IA-111, 172 pp.

Keegan, T.J., 1958: Arctic Synoptic Activity in Winter. Journal of Meteorology, 15, pp. 513-521.

Kellogg, W.W., 1975: The Poles: A Key to Climate Change. In: Climate of the Arctic, G. Weller and S. Bowling (eds.). Geophysical Institute, Fairbanks, Alaska, pp. v-vii.

Kirchhofer, W., 1973: Classification of European 500 mb Patterns. Swiss Meteorologische Institut, Zurich, Arbeits 3, 16 pp.

Klein, W.H., 1957: Principal Tracks of Cyclones and Anticyclones in the Northern Hemisphere. U.S. Weather Bureau, Washington, D.C., Research Paper 40, 22 pp.

Klein, W.H. and J.S. Winston, 1958: Geographical Frequency of Troughs and Ridges on Mean 700 mb Charts. Monthly Weather Review, 86, pp. 344-358.

Kovacs, A. and M. Mellor, 1974: Sea Ice Morphology and Ice as a Geologic Agent in the Southern Beaufort Sea. In: The Coast and Shelf of the Beaufort Sea, J.C. Reed and J.E. Sater (eds.). Arctic Institute of North America, Washington, D.C., pp. 113-162.

Krebs, S. and R.G. Barry, 1970: The Arctic Front and the Tundra-Taiga Boundary in Eurasia. Geographical Review, 60, pp. 548-554.

LeDrew, E.F., 1976: Physical Mechanisms Responsible for the Major Synoptic Systems in the Eastern Canadian Arctic in the Winter and Summer of 1973. University of Colorado, Institute of Arctic and Alpine Research, Occasional Paper 22, 205 pp.

Lund, I.A., 1963: Map-Pattern Classification by Statistical Methods. Journal of Applied Meteorology, 2, pp. 56-65.

Mardia, K.V., 1972: Statistics and Directional Data. Academic Press, New York, 187 pp.

Maxwell, A.E., 1975: Analysing Qualitative Data. Halstead Press, Philadelphia, 123 pp.

Maykut, G.A. and P.E. Church, 1973: Radiation Climate of Barrow, Alaska, 1962-66. Journal of Applied Meteorology, 12, pp. 620-628.

Moritz, R.E., 1977: On a Possible Sea Breeze Circulation near Barrow, Alaska. Arctic and Alpine Research, 9, pp. 427-431.

Namias, J., 1958: The General Circulation of the Lower Troposphere over Arctic Regions and its Relations to the Circulation Elsewhere. In: Proceedings, Part 1, Meteorology Section, Polar Atmosphere Symposium, Pergamon Press, New York, pp. 45-61.

NOAA, 1975: Local Climatological Data, Annual Summary with Comparative Data, Barter Island, Alaska. U.S. Dept. of Commerce, National Climatic Center, Asheville, North Carolina, 4 pp.

NOAA, 1976a: Local Climatological Data, Annual Summary with Comparative Data, Barrow, Alaska. U.S. Dept. of Commerce, National Climatic Center, Asheville, North Carolina, 4 pp.

NOAA, 1976b: Local Climatological Data, Annual Summary with Comparative Data, Barter Island, Alaska. U.S. Dept. of Commerce, National Climatic Center, Asheville, North Carolina, 4 pp.

O'Connor, J.F., 1961: Mean Circulation Patterns based on 12 years of Recent Northern Hemispheric Data. Monthly Weather Review, 89, pp. 211-228.

Palmen, E., 1951: The Role of Atmospheric Disturbances in the General Circulation. Quarterly Journal of the Royal Meteorological Society, 77, pp. 337-354.

Palmen, E. and C. Newton, 1969: Atmospheric Circulation Systems: Their Structure and Physical Interpretation. Academic Press, New York, 603 pp.

Panofsky, H.A. and G.W. Brier, 1968: Some Applications of Statistics to Meteorology. College of Earth and Mineral Sciences, Pennsylvania State University, University Park, Pennsylvania, 224 pp.

Petterssen, S., 1950: Some Aspects of the General Circulation of the Atmosphere. Centenary Proceedings of the Royal Meteorological Society, pp. 120-155.

Putnins, P., 1966: Sequences of Baric Weather Patterns over Alaska. Studies on the Meteorology of Alaska, 1st Interim Report, ESSA, Washington, D.C., 81 pp.

Putnins, P., 1967: Extremely Cold Weather Spells in Alaska. Studies on the Meteorology of Alaska, 2nd Interim Report, ESSA, Washington, D.C., 53 pp.

Putnins, P., 1969: Weather Situations in Alaska During the Occurrence of Specific Baric Weather Patterns. Studies on the Meteorology of Alaska, Final Report, ESSA, Washington, D.C., 267 pp.

Reed, J.C., 1974: Preface. In: The Coast and Shelf of the Beaufort Sea, J.C. Reed and J.E. Sater (eds.). Arctic Institute of North America, Arlington, Virginia, pp. 3-5.

Reed, R.J., 1959: Arctic Weather Analysis and Forecasting. Department of Meteorology and Climate, University of Washington, Seattle, Occasional Report 11, 78 pp.

Reed, R.J. and B.J. Kunkel, 1960: The Arctic Circulation in Summer. Journal of Meteorology, 17, pp. 489-506.

Reimnitz, E. and P.W. Barnes, 1974: Sea Ice as a Geologic Agent on the Beaufort Sea Shelf of Alaska. In: The Coast and Shelf of the Beaufort Sea, J.C. Reed and J.E. Sater (eds.). Arctic Institute of North America, Arlington, Virginia, pp. 301-353.

Sabin, R.C., 1974: Computer Map Typing-Optimizing the Correlation Coefficient Threshold. 12th Weather Squadron Technical Paper, U.S. Air Force, Ent Air Force Base, Colorado, 16 pp.

Sater, J.E. (ed.), 1969: The Arctic Basin. Arctic Institute of North America, Washington, D.C., 337 pp.

Sater, J.E., J.E. Walsh, and W.I. Wittman, 1974: Impingement of Sea Ice on the North Coast of Alaska. In: The Coast and Shelf of the Beaufort Sea: Proceedings of a Symposium on Beaufort Sea Coast and Shelf Research, J.C. Reed and J.E. Sater (eds.). Arctic Institute of North America, Arlington, Virginia, pp. 85-105.

Scholefield, P.R., 1973: Comparing Correlations Between Weather Maps with Similar Isobaric Configurations but Varying Pressure Intensities. 12th Weather Squadron Technical Paper, U.S. Air Force, Ent Air Force Base, Colorado, 5 pp.

Schwerdtfeger, W., 1975: Mountain Barrier Effect on the Flow of Stable Air North of the Brooks Range. In: Climate of the Arctic, G. Weller and S. Bowling (eds.). Geophysical Institute, Fairbanks, Alaska, pp. 204-208.

Selkregg, L.L., 1974: Arctic Climate. In: Alaska Regional Profiles. Arctic Region, Arctic Environmental Information and Data Center, Anchorage, Alaska, pp. 10-25.

Sellers, W.D., 1965: Physical Climatology. University of Chicago Press, Chicago, 272 pp.

Shortley, G. and D. Williams, 1971: Elements of Physics. Prentice-Hall, Englewood Cliffs, New Jersey, 947 pp.

Siegel, S., 1956: Nonparametric Statistics for the Behavioral Sciences. McGraw-Hill, New York, 312 pp.

Shapiro, L.H., 1976: A Preliminary Study of Ridging in Landfast Ice at Barrow, Alaska, Using Radar Data. In: Proceedings of the Third International Conference on Port and Ocean Engineering Under Arctic Conditions, 11 August 1975. Institute of Marine Science, University of Alaska, Fairbanks, Vol. 1, pp. 417-425.

Smagorinsky, J., 1953: The Dynamical Influence of Large-Scale Heat Sources and Sinks on the Quasi-Stationary Mean Motions of the Atmosphere. Quarterly Journal of the Royal Meteorological Society, 79, pp. 342-366.

Streten, N.A., 1974: A Satellite View of Weather Systems over the North American Arctic. Weather, 29, pp. 369-380.

Study of Man's Impact on Climate, 1971: Inadvertent Climate Modification. MIT Press, Cambridge, Massachusetts, 308 pp.

Sutcliffe, R.C., 1951: Mean Upper Contour Patterns of the Northern Hemisphere - the Thermal-Synoptic Viewpoint. Quarterly Journal of the Royal Meteorological Society, 77, pp. 435-440.

Thom, H.C.S., 1966: Some Methods of Climatological Analysis. W.M.O., Geneva, Technical Note 81, 53 pp.

Thom, H.C.S., 1970: The Analytical Foundations of Climatology. Archiv für Meteorologie, Geophysik und Bioklimatologie, Ser. B, 18, pp. 205-220.

U.S. National Academy of Science, 1975: Understanding Climatic Change, a Program for Action. U.S.N.A.S., Washington, D.C., 239 pp.

U.S. Weather Bureau, 1946: Normal Weather Maps, Northern Hemisphere Sea Level Pressure. U.S. Dept. of Commerce, Washington, D.C.

Van Loon, H., 1967: The Half-Yearly Oscillations in Middle and High Southern Latitudes and the Coreless Winter. Journal of Atmospheric Science, 24, pp. 472-486.

Van Loon, H., 1972: Temperature in the Southern Hemisphere. In: Meteorology of the Southern Hemisphere, Meterological Monographs, 13, pp. 25-54.

Vowinckel, E. and S. Orvig, 1962: Relation Between Solar Radiation Income and Cloud Type in the Arctic. Journal of Applied Meteorology, 1, pp. 552-559.

Vowinckel, E. and S. Orvig, 1967: The Inversion over the Polar Ocean. In: W.M.O.-S.C.A.R.-I.C.P.M. Symposium on Polar Meteorology, W.M.O., Geneva, Technical Note 87, 39-59.

Vowinckel, E. and S. Orvig, 1970: The Climate of the North Polar Basin. In: World Survey of Climatology, 14, Elsevier, Amsterdam, pp. 129-251.

Walsh, J.E., 1977: Measurements of the Temperature, Wind and Moisture Distribution Across the Northern Coast of Alaska. Arctic and Alpine Research, 9, pp. 175-182.

Watson, C.E., 1968: The Climate of Alaska. In: Climates of the States, 2, NOAA, Washington, D.C., pp. 481-501.

Weaver, D.F., 1970: Radiation Regime over Arctic Tundra and Lake, 1966. Scientific Report, Department of Atmospheric Science, University of Washington, Seattle, 112 pp.

Weller, G. and B. Holmgren, 1974: The Microclimates of the Arctic Tundra. Journal of Applied Meteorology, 13, pp. 854-862.

Weller, G. and S. Bowling (eds.), 1975: Climate of the Arctic. Geophysical Institute, Fairbanks, Alaska, 436 pp.

Wexler, H., 1958: The "Kernlose" Winter in Antarctica. Geophysics, 6, pp. 577-595.

Wilson, C., 1967: Climatology of the Cold Regions, Part a. U.S. Army CRREL, Hanover, New Hampshire, Report I-A3a, 141 pp.

Wonnacott, T.H. and R.J. Wonnacott, 1969: Introductory Statistics. Wiley and Sons, New York, 403 pp.

World Meteorological Organization, 1975: The Physical Basis of Climate and Climate Modeling. W.M.O.-I.C.S.U., Geneva, 265 pp.

INSTITUTE OF ARCTIC AND ALPINE RESEARCH
OCCASIONAL PAPERS

Numbers 1 through 5, and 9, 11, 12, 17, and 23 are out of print. A second edition of Number 1 is available from the author. Numbers 2, 3, 4, 5, 9, and 11 are available from National Technical Information Service, U.S. Department of Commerce. For details, please write to INSTAAR.

6. *Guide to the Mosses of Colorado.* By W. A. Weber. 1973. 48 pp. Order from the author, University of Colorado Museum, Boulder, Colorado 80309. $2.50.
7. *A Climatological Study of Strong Downslope Winds in the Boulder Area.* By W.A.R. Brinkmann. 1973. 228 pp. Order from the author, Institute for Environmental Studies, University of Wisconsin, 1225 West Dayton Street, Madison, Wisconsin 53706.

†8. *Environmental Inventory and Land Use Recommendations for Boulder County, Colorado.* Edited by R.F. Madole. 1973. 228 pp. 7 plates. $6.00.

†10. *Simulation of the Atmospheric Circulation Using the NCAR Global Circulation Model With Present Day and Glacial Period Boundary Conditions.* By J.H. Williams. 1974. 328 pp. $4.75.

†13. *Development of Methodology for Evaluation and Prediction of Avalanche Hazard in the San Juan Mountains of Southwestern Colorado.* by R.L. Armstrong, E.R. LaChapelle, M.J. Bovis, and J.D. Ives. 1975. 141 pp. $4.75.

†14. *Quality Skiing at Aspen, Colorado: A Study in Recreational Carrying Capacity.* By C. Crum London. 1975. 134 pp. 3 plates. $5.50.

†15. *Palynological and Paleoclimatic Study of the Late Quaternary Displacements of the Boreal Forest-Tundra Ecotone in Keewatin and Mackenzie, N.W.T., Canada.* By H. Nichols. 1975. 87 pp. $4.00.

†16. *Computer Techniques for the Presentation of Palynological and Paleoenvironmental Data.* By M. Eccles, M. Hickey, and H. Nichols. 1979. 140 pp. $6.00.

†18. *Century of Struggle Against Snow: A History of Avalanche Hazard in San Juan County, Colorado.* By B.R. Armstrong. 1976. 97 pp. 11 plates. $4.50.

†19. *Avalanche Release and Snow Characteristics, San Juan Mountains, Colorado.* Edited by R.L. Armstrong and J.D. Ives. 1976. 256 pp. 7 plates. $7.50.

†20. *Landslides Near Aspen, Colorado.* C.P. Harden. 1976. 61 pp. 5 plates. $3.75.

†21. *Radiocarbon Date List III. Baffin Island, N.W.T., Canada.* By J.T. Andrews. 1976. 50 pp. $2.50.

†22. *Physical Mechanisms Responsible for the Major Synoptic Systems in the Eastern Canadian Arctic in the Winter and Summer of 1973.* By E.F. LeDrew. 1976. 205 pp. $4.50.

†24. *Avalanche Hazard in Ouray County, Colorado, 1877-1976.* By B.R. Armstrong. 1977. 125 pp. 32 plates. $4.50.

†25. *Avalanche Atlas, Ouray County, Colorado.* By B.R. Armstrong and R.L. Armstrong. 1977. 132 pp. 34 plates. $6.00.

†26. *Energy Budget Studies in Relation to Fast-ice Breakup Processes in Davis Strait: Climatological Overview.* R.G. Barry and J.D. Jacobs with others. 1978. 284 pp. $7.00.

†27. *Geoecology of Southern Highland Peru: a Human Adaptation Perspective.* By B.P. Winterhalder and R.B. Thomas. 1978. 91 pp. $6.00.

†28. *Tropical Teleconnection to the Seesaw in Winter Temperatures between Greenland and Northern Europe.* By G.A. Meehl. 1979. 110 pp. $4.00.

†29. *Radiocarbon Date List IV. Baffin Island, N.W.T., Canada.* By G.H. Miller. 1979. 61 pp. $4.00.

†30. *Synoptic Climatology of the Beaufort Sea Coast of Alaska.* By R.E. Moritz. 1979. 176 pp. $6.00.

†31. *The North Pacific Oscillation and Eigenvectors of Northern Hemisphere Atmospheric Circulation during Winter.* By J.C. Rogers. 1979. (In preparation.)

†32. *Modeling of Air Pollution Potential for Mountain Resorts.* by D.E. Greenland. 1979. (In preparation.)

†Order from INSTAAR, University of Colorado, Boulder, Colorado 80309. Orders by mail add $1.00 per title.

Occasional Papers are a miscellaneous collection of reports and papers on work performed by INSTAAR personnel and associates. Generally, these papers are too long for publication as journal articles, or they contain large amounts of supporting data that are normally difficult to publish in the standard literature.